Gene Therapy for Duchenne Muscular Dystrophy: Engineering microdystrophin expressing cassettes from recombinant adeno-associated virus for improved clinical efficacy

Nertiyan Elangkovan

Thesis submitted for the degree of Doctor of Philosophy

Royal Holloway, University of London

May 2021

UNIVERSITY OF LONDON

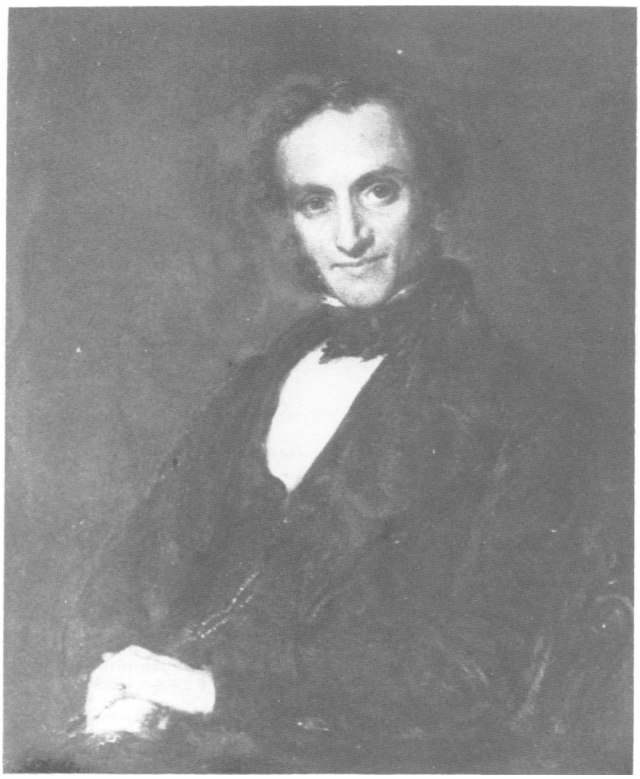

Edward Meryon (1807-1880) (MD, FRCP). First to describe muscular dystrophy.[1]

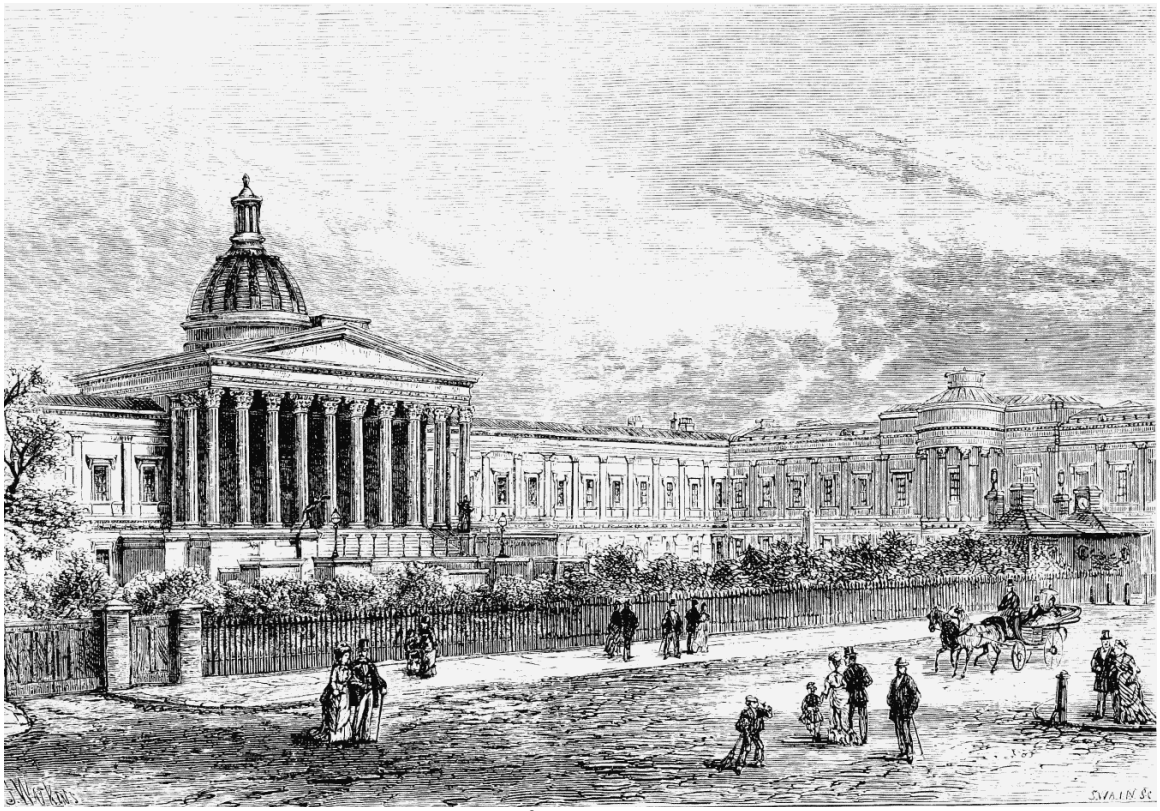

University College, Gower Street, London[2]. Meryon enrolled as a medical student at London University (now University College) in 1829 [3].

[1] Image from (Emery & Emery, 1993).
[2] Image from British History Online (Walford, 1878).
[3] (Angelini, 2009)

TO MY PARENTS

who gifted me the life

AND TO MY MOTHER

for making everything possible

Declaration of Authorship

I, Nertiyan Elangkovan hereby declare that this thesis and the work presented in it is entirely my own. Where I have consulted the work of others, this is always clearly stated. No part of this thesis has been submitted for any other degree at this or any other university.

Signed: 

Date: 12 May 2021

Acknowledgement

First of all, I would like to express my sincere gratitude to Professor George Dickson for his great leadership and expertise in the field of genetic therapy for muscular dystrophy. I came to Royal Holloway in 2016 to study for a Masters by Research, at which point I never thought I would stay for another three years doing a PhD. It is George who inspired me a lot and made me decide that I wanted to further my career in the field of gene therapy and I wanted to do so under his supervision. George, I would not have come this far without you and I will always be grateful for everything you have done to ensure my smooth journey as a graduate research student. You are the best mentor I have ever had. My time at Royal Holloway as a research student have been the most exciting one in my life so far.

I am extremely indebted to Dr Linda Popplewell and Dr Caroline Le Guiner (University of Nantes) for their valuable mentoring and encouragement extended to me. This research project would have been impossible for me to complete without their ongoing support and guidance. Collaborators for this project include Dr Caroline Le Guiner and Audrey Bourdon from University of Nantes. Audrey, thank you for all the help you have offered including sending samples and explaining some protocols to me. I enjoyed collaborating with both Caroline and you, and it has been a very motivating experience to me to have multiple talented people working with me.

I would also like to express my sincere appreciation to my parents, Mr Elangkovan and Dr Vijayaletchumy for believing in me and encouraging me to pursue my dreams. This journey as a graduate student would have been impossible without their moral and financial support. A very special thanks to my mum for everything she has done for me. Mum, I would not have come this far in life without you. Thank you. To my brother whom I called almost fifteen times a day when I was writing this thesis, thank you for always being a great source of inspiration and a great friend.

Some friends change your life and I am extremely blessed to have such friends around me that have truly been there for me and have always encouraged and motivated me to do better. Irsyad, Mariana and Luis: I love you guys. Luis, when things were really tough, you were there for me, I am forever grateful for that.

I would also like to express my deepest appreciation to every member of the Dickson and Popplewell lab that have either been involved in my research directly or indirectly. I apologise for not individually listing everyone here, but I am very thankful to everyone for welcoming me into the team four years ago and for all the help and support that enabled me to complete my work on time.

- Dr Alberto Malerba, thank you for being a great colleague and friend throughout my PhD years. Thank you for all your guidance, help and mentorship.
- Dr Ngoc Lu-Nguyen, thank you for your help in all the electrophysiology experiments described in this thesis.
- Dr Shan Herath, thank you for spending so much time with me guiding me through the AAV production, purification and quantification workflow.
- Dr Penelope Smith, thank you for always being such a friendly team member, helping me with all the reagent and material orders and assisting me with all the questions I had throughout these four years.
- Emma and Nikki, thank you for taking great care of all the animals including my mice in the husbandry and thank you for always being great colleagues to work with.

Also not forgetting some of the past postdoctoral researchers in the lab that have inspired me a lot to be a hardworking scientist: Dr Susan Jarmin, Dr Betty Kao, Dr Anita Le Heron and Dr Hayder Abdul-Razak; thank you. It is a relatively small world and this is even more true for the AAV gene therapy community. I met Susan in Chicago and Hayder in Barcelona in the annual conferences when I had no idea they were going: always a pleasant surprise to see a familiar face at the poster exhibition areas and I hope I will meet many more in future.

Last but not least, I am extremely grateful to Royal Holloway, University of London for providing me the Science Excellence Scholarship to carry out my PhD and for the funding received from Genethon, France. Thank you.

It was 12 a.m. when the nation went into a lockdown. Not a single person on the streets. It felt strange. This was not the London I knew.

23 March 2020

I PAY TRIBUTE TO ALL COVID-19 WARRIORS AROUND THE WORLD.

Abstract

Duchenne muscular dystrophy (DMD) is an X-linked, muscle wasting disease that affects 1 in 5000 males. Affected individuals become wheelchair bound by the age of twelve and eventually die in their third decade due to respiratory and cardiac complications. The disease is caused by mutations in the *DMD* gene that codes for dystrophin. Dystrophin is a structural protein that maintains the integrity of muscle fibres and protects them from contraction-induced damage. The absence of dystrophin compromises the stability and function of the muscle fibres, eventually leading to muscle degeneration. So far, there is no effective treatment for deteriorating muscle function in DMD patients. A promising approach for treating this life-threatening disease is gene transfer to restore dystrophin expression using a safe, non-pathogenic virus called adeno-associated virus (AAV). Whilst microdystrophin gene transfer using AAV shows extremely impressive therapeutic success so far in large animal models of DMD, translating this advanced therapy medicinal product from bench to bedside still require a few optimization steps. One such area is transgene potency to achieve therapeutic level of expression. This can be achieved in a dose-dependent manner but there is a positive correlation of vector dose and undesirable immune response, which eventually reduces the transgene expression. Here we attempt to use an engineered intron in the recombinant AAV expression cassette to increase the microdystrophin transgene expression by several fold. We have established proof-of-principle in an *in vitro* model showing the ability of the engineered intron - R6K-RNA-OUT to increase the microdystrophin transgene expression by four-fold. We experienced several hurdles translating this finding into *in vivo* settings, but we have identified several key areas that require addressing. If successful *in vivo*, this would reduce the AAV vector dose required in the treatment, making the therapy safer due to decreased toxicity and at the same time, reduces the cost of therapy. This could potentially overcome some hurdles that have emerged in preclinical studies of DMD and clinical trials of other genetic diseases utilizing this viral vector.

Table of contents

Declaration of Authorship 4
Acknowledgement 5
Abstract 7
List of tables 12
List of figures 13
List of abbreviations 20
Chapter 1 Introduction 23
1.1 Duchenne muscular dystrophy 23
1.1.1 Disease history and condition 23
1.1.2 *DMD* gene and dystrophin 30
1.1.3 Animal models of DMD 38
1.2 Treatment strategies for DMD 41
1.2.1 An overview of DMD therapies and novel experimental approaches 41
1.2.2 Antisense-mediated modulation of exon splicing (exon skipping) 44
1.2.3 Stop codon readthrough (SCR) or translational read-through 52
1.2.4 Other dystrophin-restoration therapies in progress 54
1.2.5 Microdystrophin gene replacement therapy for DMD 56
1.3 Adeno-associated virus (AAV) as a gene delivery vector 63
1.3.1 AAV journey from bench to bedside 63
1.3.2 Genetics, biology and structure of AAV 64
1.3.3 Diversity and tropism of AAVs and derived rAAV vectors 67
1.3.4 Replication-defective recombinant AAV as a gene transfer vector 73
1.4 Safety and effectiveness of rAAV-mediated gene therapy. 74
1.4.1 Immunogenicity 75
1.4.2 Genotoxicity 78
1.4.3 Persistence 79
1.4.4 Potency and efficacy 80
1.5 Enhancing transgene potency using a regulatory element 85
1.5.1 Enhancing transgene expression from rAAV vectors using engineered intron 85
1.5.2 Statement of aims 88
Chapter 2 Materials and methods 91
2.1 Molecular biology 91
2.1.1 R6K-RNA-OUT synthesis 91

2.1.2 Cloning of R6K-RNA-OUT in human and mouse codon optimized rAAV-Spc5.12-MD1 vector plasmids 92
2.1.3 Minimisation of p-mMD1 93
2.1.4 Cloning of R6K-RNA-OUT intron into minimised p-mMD1 vector plasmid 95
2.2 Microbiology 97
2.2.1 Transformation of TOP10 chemically competent *E. coli* 98
2.2.2 Miniprep/ starter cultures and glycerol stocks 98
2.2.3 Maxiprep cultures 98
2.2.4 Gigaprep cultures 98
2.3 DNA and RNA assays 99
2.3.1 Plasmid DNA purification 99
2.3.2 RNA extraction and reverse transcription (RT) 100
2.3.3 Polymerase chain reaction (PCR) 102
2.3.4 Gel electrophoresis 104
2.3.5 Restriction digest 104
2.3.6 Gel extraction 104
2.4 Mammalian cell culture 105
2.4.1 Human Embryonic Kidney 293T (HEK293T) 105
2.4.2 H2kb.mdx transgenic mice myoblast 105
2.4.3 C2C12 mouse myoblast cell line 106
2.5 Transient transfection 106
2.5.1 Human Embryonic Kidney 293T (HEK293T) 106
2.5.2 H2kb.mdx transgenic mice myoblast 106
2.5.3 C2C12 mouse myoblast cell line 107
2.6 Total protein assays 108
2.6.1 Total protein extraction and quantification from cell and tissue samples 108
2.6.2 Western blot analysis 109
2.7 Adeno-associated virus (AAV) production, purification and quantification 111
2.8 Infectious centre assay 117
2.9 *In vivo* gene delivery 118
2.9.1 Animal husbandry 118
2.9.2 Plasmid DNA electrotransfer 118
2.9.3 Intramuscular AAV delivery 119
2.9.4 Muscle electrophysiology 121

2.9.5 Muscle harvest and processing 122
2.9.6 Immunohistochemistry and histology 122
2.9.7 Percentage microdystrophin-positive fibers calculation 123
2.9.8 Haematoxylin and eosin staining 123
2.9.9 Percentage centronucleated fibers (CNFs) calculation 123
2.10 Statistical analysis 124
2.11 Bioinformatics analysis 124
2.12 Graphics and illustrations 124
Chapter 3 Evaluating expression levels from microdystrophin gene constructs harbouring R6K-RNA-OUT (RRO) sequence elements 125
3.1 Introduction 125
3.2 Results 131
3.2.1 Synthesis of RRO-intron 131
3.2.2 Codon optimisation did not introduce CpG islands to the transgene sequence 132
3.2.3 Characterisation of initial plasmids used in cloning: Restriction digest using multiple restriction enzymes shows integrity of purified rAAV-Spc5.12-MD1 plasmids 137
3.2.4 Plasmid cloning of RRO elements into the AAV expression cassettes harbouring codon-optimized MD1 genes. 140
3.2.5 Testing of microdystrophin constructs in an *in vitro* model to evaluate transgene expression level and splicing activity. 148
3.3 Discussion 157
3.4 Supplementary data 165
3.5 Appendix for Chapter 3 166
3.5.1 Sequence of Spc5.12 promoter 166
3.5.2 Sequence of mMD1 166
3.5.3 Sequence of hMD1 167
3.5.4 Sequence of SV40 polyadenylation signal 167
3.5.5 Sequence of 5' AAV2 ITR 167
3.5.6 Sequence of 3' AAV2 ITR 167
3.5.7 Sequence of 585 RRO 168
3.5.8 Sequence of 456 RRO 168
Chapter 4 Evaluating the functionality of the new microdystrophin expression plasmid constructs in a muscle tissue model 169
4.1 Introduction 169
4.2 Results 174

4.2.1 Testing of microdystrophin constructs in an *in vitro* muscle model to evaluate transgene expression level 174
4.2.2 Electro-transfer of p-mMD1 and p-585mMD1 plasmids in muscle tissue of *mdx* mice model to evaluate transgene expression level *in vivo* 178
4.3 Discussion 202
Chapter 5 Evaluating AAV/mMD1 and AAV/585mMD1 *in vivo* via intramuscular delivery of the vectors 205
5.1 Introduction 205
5.2 Results 208
5.2.1 AAV production and quantification 208
5.2.2 Intramuscular injection of AAV vector in *mdx* mice model to evaluate transgene expression level *in vivo* and functional outcomes. 215
5.2.3 AAV9/585mMD1 were less infectious than AAV9/mMD1 242
5.2.4 Generation of minimised versions of mMD1 and 585mMD1 constructs that are within the AAV packaging capacity 245
5.2.5 Enhancement of microdystrophin expression *in vitro* following addition of engineered intron into mini MD1 cassette. 250
5.3 Discussion 254
5.4 Appendix 262
Chapter 6 Conclusion and future work 264
6.1 Summary of research findings 264
6.2 Significance of this work 267
6.3 Future work 268
6.3.1 Evaluation of the infectivity of the minimised constructs 269
6.3.2 Systemic delivery of the AAV vectors to evaluate transgene expression level and tissue specificity 270
6.3.3 The use of dystrophin-deficient rat model to evaluate cardiac phenotype rescue 271
6.3.4 The hunt for a more muscle specific AAV serotype 272
References 274

List of tables

Table 1.1 Clinical signs of DMD and BMD. [Page 37]

Table 1.2 Clinical manifestations and histopathology of dystrophin-deficient mice, dogs and humans. [Page 38]

Table 1.3 Active microdystrophin gene transfer clinical trials for DMD using AAV in the United States [Page 60]

Table 1.4 Clinical trial history and early data on outcomes of the AAV-microdystrophin trials [Page 61]

Table 1.5 Glycan receptor and co-receptors for AAV serotypes 1-9. [Page 69]

Table 1.6 Overview of tissue and species tropism of rAAV gene therapy vector serotypes currently utilized in pre-clinical and clinical applications. [Page 70]

Table 5.1 Quantification of titre values of AAV9/mMD1 and AAV9/585mMD1 [Page 214]

Table 5.2 Infectious centre assay (ICA) of AAV9/mMD1 and AAV9/585mMD1 [Page 243]

List of figures

Figure 1.1 Duchenne's first DMD patient, Joseph Sarrazin. [Page 24]

Figure 1.2 Gowers' sign. [Page 25]

Figure 1.3 Progression of cardiomyopathy in DMD patients. [Page 26]

Figure 1.4 Survival of DMD patients following interventional strategies. [Page 27]

Figure 1.5 Three main types of muscle tissues in human body. [Page 29]

Figure 1.6 DMD exons and coding domain structures. [Page 30]

Figure 1.7 Full length dystrophin. [Page 31]

Figure 1.8 Dp427m and the binding partners forming dystrophin-associated protein complex (DAPC). [Page 33]

Figure 1.9 Full length dystrophin (DP427m) and dystrophin-associated protein complex (DAPC). [Page 34]

Figure 1.10 Animal models developed for DMD. [Page 39]

Figure 1.11 Altered cellular pathways in DMD and therapeutic opportunities. [Page 42]

Figure 1.12 Mechanism of intron splicing. [Page 44]

Figure 1.13 Exon-skipping strategy. [Page 46]

Figure 1.14 Modifications made to AONs. [Page 48-49]

Figure 1.15 Clinically relevant miniaturised dystrophin constructs. [Page 59]

Figure 1.16 AAV genome. [Page 64]

Figure 1.17 AAV life cycle. [Page 66]

Figure 1.18 Distribution of AAV genome in human and non-human primate tissues. [Page 68]

Figure 1.19 Proposed model of transport of AAV in the cell. [Page 71]

Figure 1.20 Model of therapeutic efficacy based on capsid dose following systemic AAV vector delivery. [Page 81]

Figure 1.21 Addition of engineered intron into rAAV cassette enhances transgene expression. [Page 87]

Figure 1.22 R6K-RNA-OUT intron. [Page 88]

Figure 1.23 RNA-OUT mechanism. [Page 89]

Figure 2.1 Minimisation strategy of p-mMD1 and p-585mMD1 to produce p-mini MD1 and p-mini 585MD1 respectively. [Page 94]

Figure 2.2 Schematic of the synthesised fragment for subsequent cloning into mini MD1 vector plasmid. [Page 95]

Figure 2.3 Cloning of R6K-RNA-OUT intron into p-mini MD1. [Page 96]

Figure 2.4 Helper plasmid pDP9rs. [Page 113]

Figure 2.5 Iodixanol gradients before (left) and after (right) ultracentrifugation for purification of rAAV. [Page 114]

Figure 3.1 Components of RRO intron. [Page 126]

Figure 3.2: Schematic representation of microdystrophin-1 (MD1) used in this study. [Page 128]

Figure 3.3 Plasmid vector carrying AAV-MD1 gene expression cassette. [Page 129]

Figure 3.4 Components of 456 bp R6K-RNA-OUT (456 RRO). [Page 131]

Figure 3.5 Bioinformatic prediction of CpG islands in wild-type human dystrophin gene. [Page 133]

Figure 3.6 Bioinformatic prediction of CpG islands in mouse codon-optimised mMD1 gene sequences. [Page 134]

Figure 3.7 Bioinformatic prediction of CpG islands in human codon-optimised mMD1 gene sequences. [Page 135]

Figure 3.8 Bioinformatic prediction of CpG islands in 585 RRO intron sequence. [Page 136]

Figure 3.9 Restriction enzyme digest profile of mouse-codon optimized pAAV-Spc5.12-MD1. [Page 138]

Figure 3.10 Restriction enzyme digest profile of human-codon optimized pAAV-Spc5.12-MD1. [Page 139]

Figure 3.11 Cloning of the 456 RRO element into MD1 plasmids. [Page 141]

Figure 3.12 PCR screening to identify plasmids harbouring the 465bp RRO in the correct orientation. [Page 142]

Figure 3.13 Transcription units generated following cloning of the 585bp and 465bp RRO elements into mMD1 and hMD1 AAV plasmids. [Page 144]

Figure 3.14 Restriction enzyme digest profile of mouse-codon optimized p-456mMD1 and p-585mMD1. [Page 145]

Figure 3.15 Conventional Sanger sequencing suggests that a small deletion may potentially exist in the 5'-ITR of hMD1 plasmid. [Page 147]

Figure 3.16 Total RNA analysis following transient transfection of HEK293T with the codon optimised MD1 plasmid constructs. [Page 149]

Figure 3.17 Total RNA analysis evaluating splicing of RRO following transient transfection of HEK293T with codon optimised MD1 constructs. [Page 150]

Figure 3.18 Western blot analysis following transient transfection of HEK293T with codon optimised MD1 constructs. [Page 152]

Figure 3.19 Western blot analysis following transient transfection of HEK293T with codon optimised MD1 constructs. [Page 156]

Supplementary figure 3.1 Total RNA analysis following transient transfection of HEK293T with the human codon optimised hMD1 and 585hMD1 constructs. [Page 165]

Figure 4.1 Electrotransfer of plasmid DNA in tibialis anterior (TA) muscle of mdx mice. [Page 172]

Figure 4.2 Mouse muscle anatomy. [Page 173]

Figure 4.3 Western blot analysis following transient transfection of C2C12 cells with p-mMD1 and p-585 mMD1. [Page 176]

Figure 4.4 Tissue collection (TA muscle) and processing following treatment. [Page 181]

Figure 4.5 Western blot analysis of expression of microdystrophin in mdx TA muscle following in vivo plasmid electrotransfer. [Page 184]

Figure 4.6 Immunohistochemistry analysis of expression of microdystrophin in mdx TA muscle following in vivo plasmid electrotransfer (representative image of a saline treated TA). [Page 187]

Figure 4.7 Immunohistochemistry analysis of expression of microdystrophin in mdx TA muscle following in vivo plasmid electrotransfer (representative image of a p-mMD1 treated TA). [Page 189]

Figure 4.8 Immunohistochemistry analysis of expression of microdystrophin in mdx TA muscle following in vivo plasmid electrotransfer (representative image of a p-585 mMD1 treated TA). [Page 191]

Figure 4.9 Percentage microdystrophin positive fibers analysis in mdx TA muscle following in vivo plasmid electrotransfer. [Page 194]

Figure 4.10 Electrophysiological evaluation of specific force generation in untreated C57/BL10 wild-type and mdx TA muscles following in vivo plasmid electrotransfer. [Page 197]

Figure 4.11 Electrophysiological evaluation of loss of force following repetitive eccentric contractions in untreated C57/BL10 wild-type and mdx TA muscles following in vivo plasmid electrotransfer. [Page 199]

Figure 4.12 Evaluation of TA length, mass and cross sectional-area (CSA) of mdx TA muscles following in vivo plasmid electrotransfer. [Page 200]

Figure 5.1 rAAV purification using iodixanol gradient. [Page 209]

Figure 5.2 Quantification of rAAV titres using qPCR. [Page 211]

Figure 5.3 Western blot analysis of expression of microdystrophin in mdx TA muscle following IM injection with either saline, AAV9/mMD1 or AAV9/585mMD1 at two doses. [Page 219]

Figure 5.4 Immunohistochemistry analysis of expression of microdystrophin in mdx TA muscle following IM injection with either saline, AAV9/mMD1 or AAV9/585mMD1 at two doses. [Page 222]

Figure 5.5 Percentage microdystrophin positive fibers analysis in mdx TA muscle following IM injection with either saline, AAV9/mMD1 or AAV9/585mMD1 at two doses. [Page 225]

Figure 5.6 Electrophysiological evaluation of specific force generation in untreated C57/BL10 wild-type and mdx TA muscles following IM injection with either saline, AAV9/mMD1 or AAV9/585mMD1 at two doses. [Page 229]

Figure 5.7 Electrophysiological evaluation of loss of force following repetitive eccentric contractions in untreated C57/BL10 wild-type and mdx TA muscles following IM injection with either saline, AAV9/mMD1 or AAV9/585mMD1 at two doses. [Page 231]

Figure 5.8 Evaluation of TA length, mass and cross sectional-area (CSA) of mdx TA muscles following IM injection with either saline, AAV9/mMD1 or AAV9/585mMD1 at two doses. [Page 234]

Figure 5.9 Centronucleation (CN) analysis in mdx TA muscle following IM injection with either saline, AAV9/mMD1 or AAV9/585mMD1 at two doses. [Page 237]

Figure 5.10 Haematoxylin and eosin (H&E) histopathology evaluation of mdx TA muscle following IM injection with either saline, AAV9/mMD1 or AAV9/585mMD1 at two doses. [Page 240]

Figure 5.11 Minimisation strategy of p-mMD1 and p-585mMD1 to produce p-mini MD1 and p-mini 585MD1 respectively. [Page 246]

Figure 5.12 Restriction enzyme digest profile of mini MD1 and mini 585MD1 plasmids. [Page 248]

Figure 5.13 Western blot analysis following transient transfection of HEK293T with mini MD1 and mini 585MD1 plasmids. [Page 251]

Figure 5.14 Proposed mechanism of microdystrophin expression in AAV9/mMD1 and AAV9/585mMD1 treated cells. [Page 257]

Figure 5.15 Recombination events generate intact vector genomes from fragmentary vector genomes in oversized 585mMD1 construct. [Page 260]

List of abbreviations

AAP	assembly-activating protein
AAV	Adeno-associated virus
AON	antisense oligonucleotide
B4GALNT2	β1,4 N-acetylgalactosaminyltransferase 2
BLAST	Basic Local Alignment Search Tool
BMD	Becker muscular dystrophy
BMP	bone morphogenetic protein
Cas	CRISPR-associated
CAV	caveolar endocytosis
CCP	clathrin-mediated endocytosis
CLIC/GEEC	clathrin-independent carriers/GPI-enriched endocytic compartment
CNF	centrally nucleated fibers
CNS	central nervous system
CRISPR	clustered regularly interspaced palindromic repeats
CSA	cross sectional area
DAPC	dystrophin-associated protein complex
DGC	dystrophin-associated glycoprotein complex
DMD	Duchenne muscular dystrophy
DMEM	Dulbecco's modified Eagle's medium
DSB	double-strand break
ECG	electrocardiogram
ECM	extracellular matrix
EE	early endosome
EGFR	epidermal growth factor receptor
EMA	European Medicines Agency
eMYHC	embryonic myosin heavy chain
ERS	exon recognition sequence
FBS	Foetal Bovine Serum
FDA	Food and Drug Administration
FGFR1	fibroblast growth factor receptor 1
GC	glucocorticosteroid

H&E	haematoxylin and eosin
HCC	hepatocellular carcinoma
HDAC	histone deacetylase
HDR	homology directed repair
HGFR	hepatocyte growth factor receptor
HR	homologous recombination
HSPG	heparan sulfate proteoglycan
ICA	infectious centre assay
IGF1	insulin-like growth factor 1
IM	intramuscular
iPSC	induced pluripotent stem cell
ITR	inverted terminal repeat
IV	intravascular
LE	late endosome
MHC	major histocompatibility complex
MMP	matrix metalloproteinase
MN	meganuclease
MTM1	myotubularin
NF-κB	nuclear factor-κB
NHEJ	nonhomologous end joining
nNOS	neuronal nitric oxide synthase
NO	nitric oxide
NOS	nitric oxide synthase
NPC	nuclear pore complex
ORF	open reading frame
PCR	polymerase chain reaction
PDE5	phosphodiesterase 5
PDGFR	platelet-derived growth factor receptor
PI3	phosphatidylinositol-3
PLA2	phospholipase A2
PNRE	perinuclear recycling endosome
rAAV	recombinant AAV
RD	rhabdomyosarcoma
ROS	reactive oxygen species

SEM	standard error of the mean
TALEN	transcription activator-like effector nuclease
TGFβ	transforming growth factor-β.
TGN	trans-Golgi network
XLMTM	X-linked myotubular myopathy
ZFN	zinc finger nuclease

Chapter 1 Introduction

1.1 Duchenne muscular dystrophy

1.1.1 Disease history and condition

Duchenne muscular dystrophy (DMD) is a lethal, muscle wasting disease that affects 1 in 5000 male births (Le Guiner *et al.*, 2017). The disease was originally described by Edward Meryon (1807-1880) and is a muscle disease that causes the integrity of the sarcolemma to be compromised (Emery, 2002). Meryon followed cases of nine boys in three different families and noted some of the clinical descriptions of the progressive muscle wasting such as enlargement of calf muscles (Angelini, 2009). The disease was later further characterised by Guillaume B.A. Duchenne (de Boulogne) (1806-1875) as he performed a complete study of his first patient (Figure 1.1) believed to be affected by "progressive muscular atrophy with degeneration" (which was later named Duchenne muscular dystrophy) (Angelini, 2009).

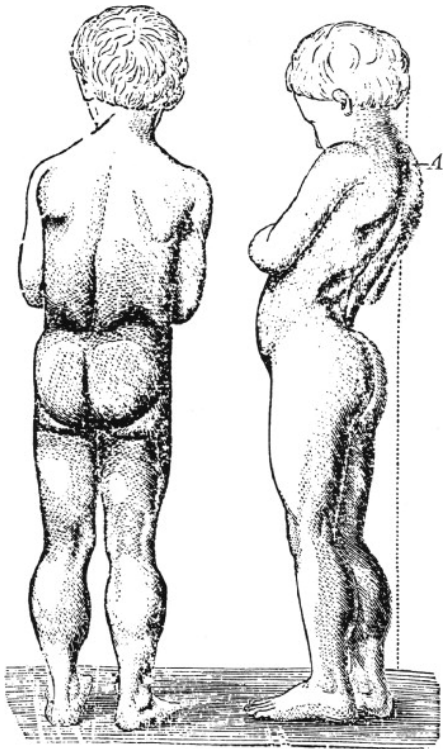

Figure 1.1 **Duchenne's first DMD patient, Joseph Sarrazin**. Note the scoliosis and enlarged calves, some of the clinical characteristics of Duchenne patients. Image from Angelini, 2009.

As Duchenne conducted further pathological studies, he changed the initial description of the disease to "pseudo-hypertrophic muscular paralysis" or "myo-sclerotic paralysis" (Angelini, 2009). Sir William Richard Gowers later completed the clinical picture of DMD by reporting the inherited nature of the disease, the preferred bias towards males and the characteristic way in which patients rise from the floor to the standing position (to this day called the Gower's sign) (Gower, 1879) (Figure 1.2). To quote from Gower's paper: "He helps himself in a very peculiar way – by putting his hands upon his knees, and grasping his thighs higher and higher, and so by…climbing up his thighs he pushes his trunk up."

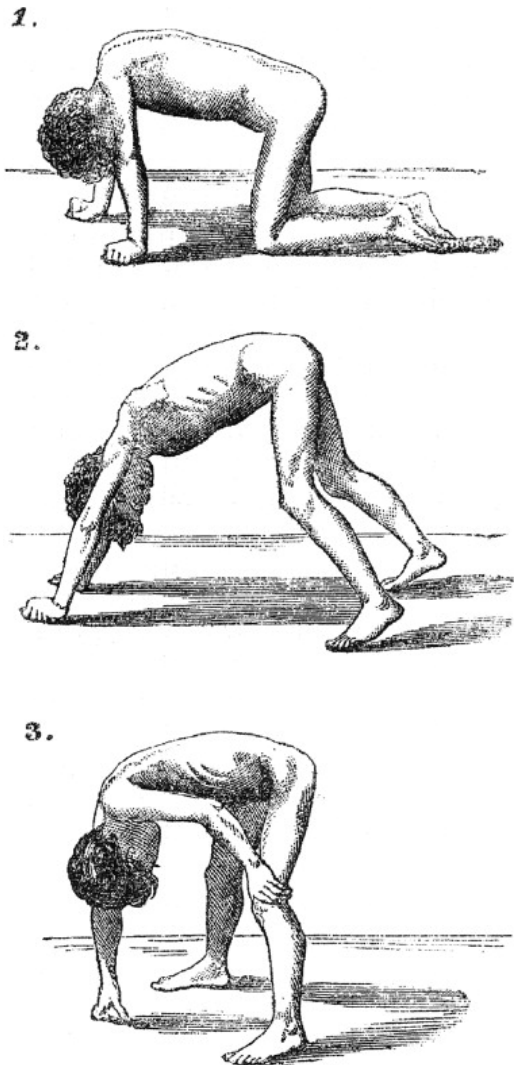

Figure 1.*2* **Gowers' sign.** A peculiar way of patients (often with neuromuscular conditions) rising from the floor by 'climbing up their knees and thighs' to the standing position (Gower, 1879). Original image published in Gower, 1879.

By positional cloning Koenig *et al.* later mapped the *DMD* gene associated with the defect to the short arm of the X-chromosome (Koenig *et al.*, 1987). Then via expression studies in bacteria and antibody production, the product of the *DMD* gene was identified as a 427kD muscle protein called dystrophin (Koenig, Monaco and Kunkel, 1988) that is expressed in skeletal, cardiac and smooth muscle cells, and in the CNS. The progressive X-linked disease is degenerative in nature and patients become wheelchair bound in their teens. In addition to respiratory insufficiency, cardiomyopathy contributes significantly to the early death in DMD patients (Figure 1.3) (Kamdar and Garry, 2016).

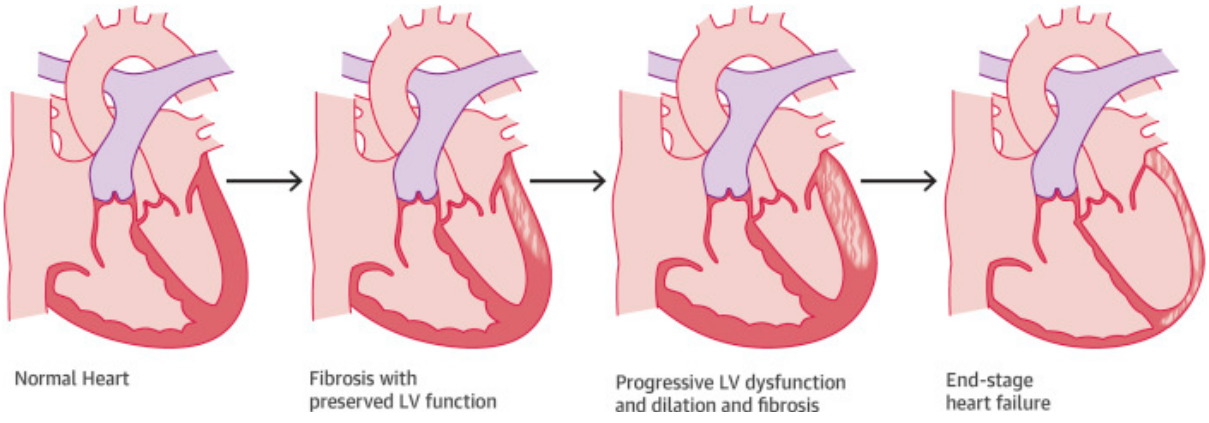

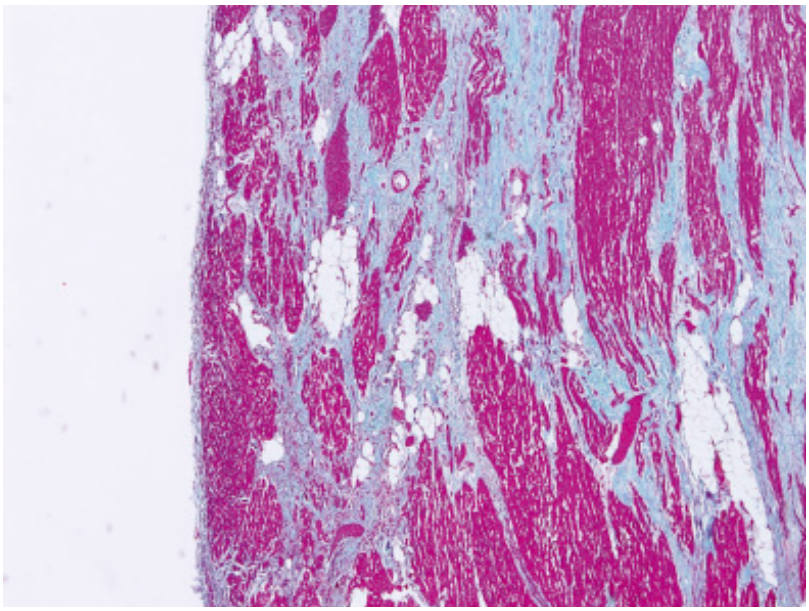

Figure 1.3 **Progression of cardiomyopathy in DMD patients**. (Top) Patients are born with structurally normal hearts, however progressive fibrosis is seen over time followed by left ventricular (LV) dysfunction. Cardiac function is compromised and as a result, patients suffer from end-stage heart failure. (Bottom) Masson trichrome stain of the basal posterior wall of the left ventricle in a patient with DMD. Subepicardial fibrotic replacement of the myocardium is shown in blue. (Kamdar and Garry, 2016). Images from Kamdar and Garry, 2016.

DMD patients used to die in their second decade of life till the 1990s (Figure 1.4). The use of respiratory and cardiac support however have contributed to the survival of patients to mid-30s (Blake *et al.*, 2012; Chamberlain and Chamberlain, 2017).

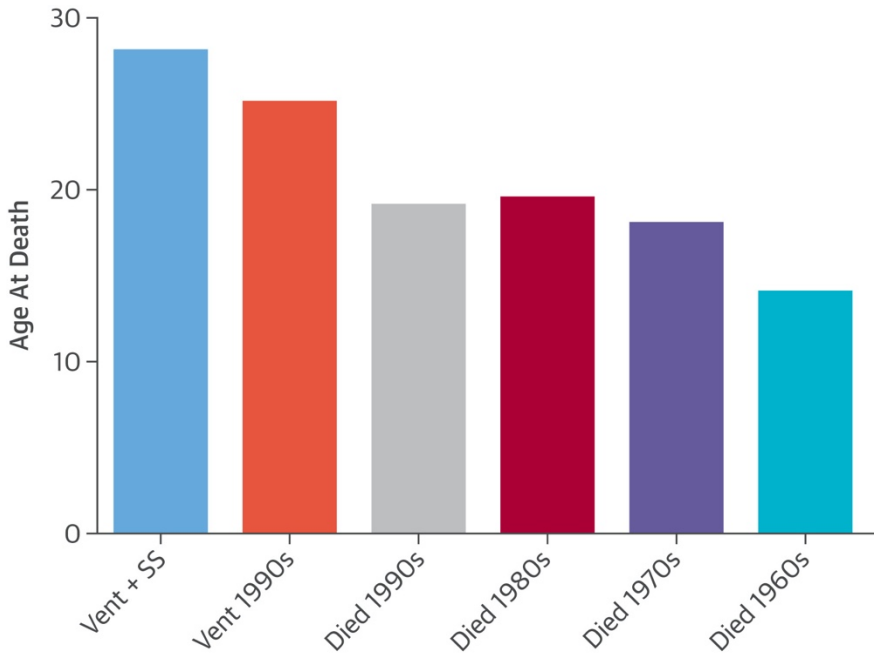

Figure 1.4 **Survival of DMD patients following interventional strategies**. Mean age of death increased from 14.4 years in the 1960s to 25.3 years in 1990s following ventilation (vent) as an intervention strategy (Eagle et al, 2002). Spinal stabilisation surgeries (SS) further increased survival of patients with DMD (Kamdar and Garry, 2016). Image adapted from (Kamdar and Garry, 2007). Data presented here was originally published in Eagle et al, 2002.

A combination of physiotherapy and corticosteroids have also helped to improve the quality of life of patients, nevertheless these palliative treatments are not a cure. Survival of patients into their fourth decade is rare (Birnkrant et al, 2018; Vandewalle et al, 2018).

In addition to the progressive skeletal and cardiac muscle pathology observed in DMD patients which is a hallmark of the disease, DMD patients can be diagnosed with cognitive and behavioural problems: cognitive impairment (IQ < 70) (30%), reading deficits similar to phonological dyslexia (40%), attention-deficit/hyperactivity disorder (ADHD) (32%), anxiety disorder (27%), autism spectrum disorders (ASD) (15%), epilepsy (6.3%), and obsessive-compulsive disorder (OCD) (4.8%) in patients with DMD (Doorenweerd et al, 2017). Whilst there are currently no longitudinal studies that investigate the progressive nature of the cognitive pathology seen in DMD patients, there are studies that suggest progression of cognitive pathology with age; for example, studies by (Yoshioka et al, 1980) reported more severe cerebral atrophy in older DMD patients.

As DMD patients survive into adulthood due to the interventional strategies and corticosteroid regiment employed as standard of care (Figure 1.4), they often suffer from gastrointestinal or nutritional complications that include weight gain or loss, dietary or nutrient imbalance, fluid imbalance, low bone density, swallowing dysfunction, and mandibular contracture (Birnkrant et al, 2018). Fluctuations in weight is often caused by the glucocorticoid treatment and decreased energy expenditure due to immobility (Vandewalle et al, 2018); however, other phenotypes observed such as swallowing dysfunction and life-threatening constipation (Lo Cascio et al, 2016) may be caused by defects in smooth muscles lining the digestive tract, suggesting the relevance of functional dystrophin protein in smooth muscles (Figure 1.5).

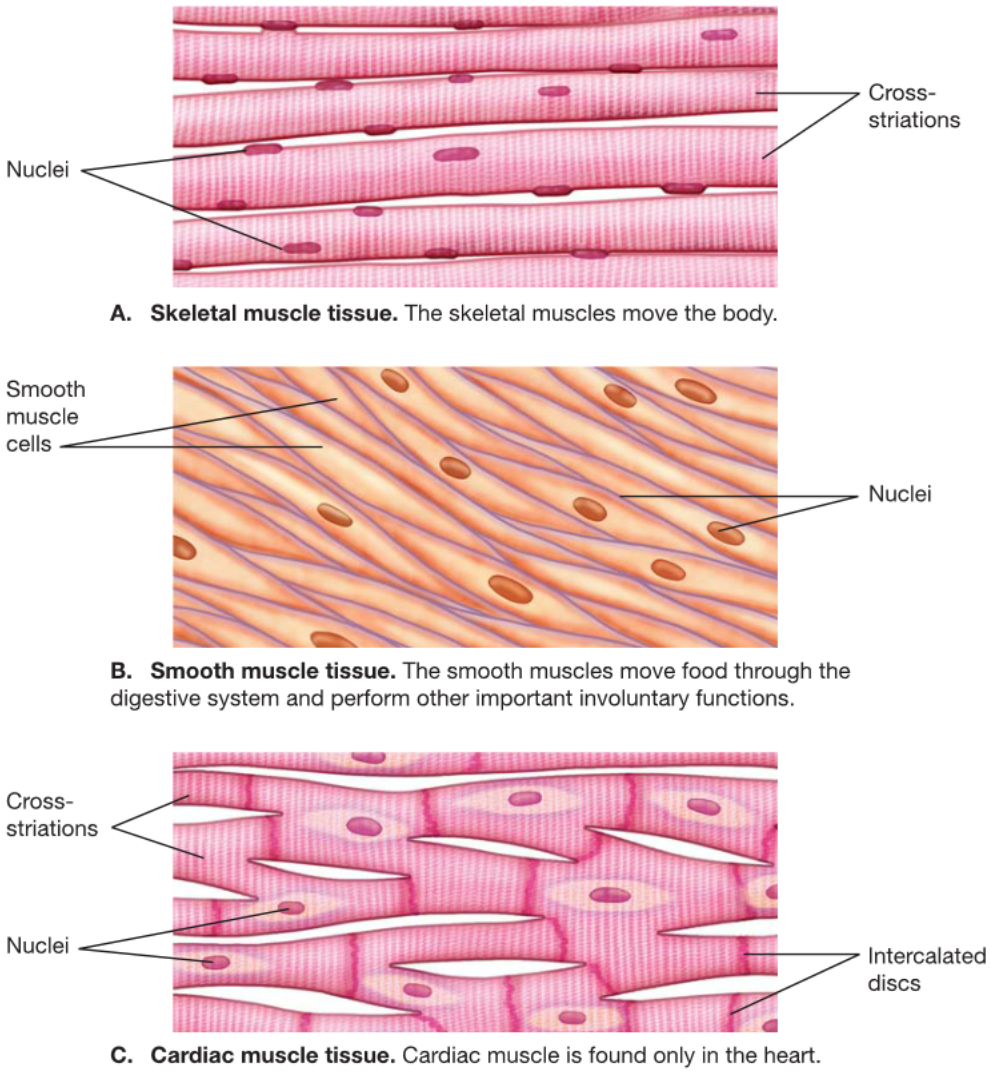

Figure 1.5 **Three main types of muscle tissues in human body**. Skeletal muscle myofibres are striated and multinucleated, occur in a number of fibre types (slow, fast, etc) and are involved in voluntary movements of the body. Smooth muscle cells are mononucleated, spindle-shaped and have no striations; and are involved in involuntary functions such as moving food, urine, secretions, as well as controlling the diameter of respiratory passages and blood vessels. Cardiac muscle cells (cardiomyocytes) are only found in the walls of the heart and contains striations and intercalated discs. Cardiomyocytes are branched and can be either mononucleated or binucleated and are involved in involuntary pumping of the heart. Note that the nuclei of skeletal myofibres are located at the periphery of the cell, whilst smooth muscles and cardiac muscle are centrally nucleated (Provost-Craig, Rose and Hall, 2013). Figure from Provost-Craig, Rose and Hall, 2013.

1.1.2 *DMD* gene and dystrophin

The *DMD* gene is the largest protein-coding gene in the human genome, covering over 2.6 million base pairs with 79 exons (van Deutekom and van Ommen, 2003). Multiple dystrophin isoforms are expressed from the *DMD* gene in a tissue specific manner (Figure 1.6). The large size of the gene makes it prone to mutations such as deletions (about 60%), duplications (about 6%), translocations and point mutations which disrupts the reading frame and eventually causes abnormal dystrophin to be synthesised (Koenig et al, 1989; van Deutekom and van Ommen, 2003).

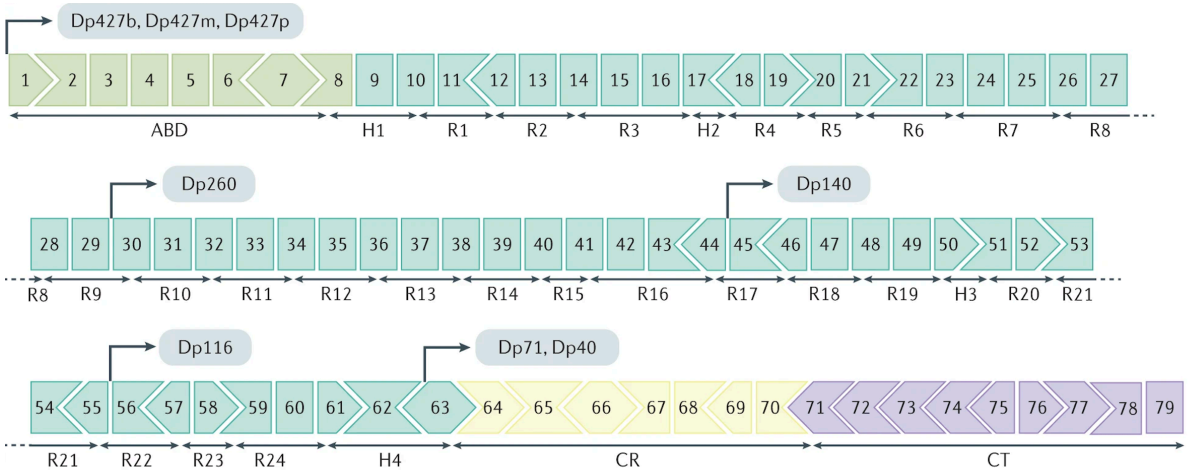

Figure 1.6 ***DMD* exons and coding domain structures**. The *DMD* gene is ~2.4 Mb long and consists of eight promoters and 79 exons. Exon map of *DMD* gene above shows 79 exons fitting together to form the normal open reading frame of dystrophin. The protein domains coded by the exons are shown under the exons. ABD: actin-binding domain; H: hinge; R: rod, CR: cysteine-rich domain; CT: C-terminal domain. The full-length tissue-specific dystrophin (Dp427) is expressed in the brain (Dp427b), skeletal muscle (Dp427m) and cerebellar Purkinje cells (Dp427p) based on the tissue-specific promoters that drive the expression. Dp427m expressed in the muscles forming full-length dystrophin is the main muscle isoform. Other shorter non-muscle dystrophin isoforms (Dp260, Dp140, Dp116 and Dp71) and their promoters are shown in the diagram. Alternative splicing at 3' end and alternative polyadenylation produces Dp40 (the shortest dystrophin isoform) (Duan et al, 2021). Image adapted from Duan et al, 2021.

Full length dystrophin (Dp427) (Figure 1.7) is a sarcolemmal cytoskeletal protein that links via the dystrophin-associated protein complex (DAPC) to the extracellular matrix (ECM) (Davies and Nowak, 2006). Dystrophin is widely expressed in skeletal and cardiac muscle and a small amount in the brain (Fairclough, Wood and Davies, 2013). Dystrophin is also expressed in smooth muscles (Lionarons et al, 2019). (Davies and Nowak, 2006) The dystrophin protein contains an actin binding domain (which is also the N-terminal domain), a rod domain made of spectrin repeats (labelled R1-R24), four hinges (labelled H1-H4), a cysteine-rich domain (CRD) and a carboxy-terminal domain (CTD) (Fairclough, Wood and Davies, 2013) (Figures 1.7 and 1.8).

Figure 1.7 **Full length dystrophin**. The dystrophin protein contains an actin binding domain (which is also the N-terminal domain), a rod domain made of spectrin repeats (labelled R1-R24), four hinges (labelled H1-H4), a cysteine-rich domain (CRD) and a carboxy-terminal domain (CTD) (Fairclough, Wood and Davies, 2013). Figure adapted from Fairclough, Wood and Davies, 2013.

Spectrin per se is a component of the cytoskeleton in red blood cells that is important for cell flexibility and also has a function as scaffold protein for other proteins (Grum *et al.*, 1999). The occurrence of spectrin repeats (tandem, antiparallel coiled-coil repeats) in the rod domain of dystrophin is thought to contribute to cellular protection from stress generated during muscle contraction and muscle stretch as spectrin provides mechanical support (Grum et al, 1999; Davies and Nowak, 2006). A significant reduction of stiffness (almost fourfold) is observed in cells that lack dystrophin compared to healthy control, confirming the structural role of dystrophin in reinforcing the myofibre (Pasternak, Wong and Elson, 1995). The spectrin repeats between hinges 2 and 3, together with the N-terminal domain of dystrophin have actin binding activity (Hemmings,

Kuhlman and Critchley, 1992; Fairclough, Wood and Davies, 2013). The distance between the two actin binding domains is crucial in protecting the filamentous F-actin from depolymerising (Rybakova and Ervasti, 1997). 24 actin monomers forming F-actin interact with one dystrophin monomer and the dystrophin-glycoprotein complex does not bind globular G-actin (Rybakova and Ervasti, 1997).

In striated muscle, the full-length dystrophin (Dp427m) interacts with multiple binding partners as shown in Figure 1.8. The structural role that Dp427m plays by linking the cytoskeleton to the ECM allows the transmission of force from the contractile elements in the cell to extracellular structures, at the same time maintaining the integrity of the muscle fibers and the sarcolemma (Douglas and Wood, 2013). A simplified illustrated version of Figure 1.8 is shown as Figure 1.9.

Two of the key hypotheses proposed for the role of dystrophin in skeletal muscle are the (i) structural hypothesis (Petrof et al, 1993) and (ii) ion channel hypothesis (Carlson, 1998; Allard, 2006; Chan, Head and Morley, 2007). The structural hypothesis states that the primary role of the dystrophin is to provide reinforcement to the sarcolemma, protecting it from contraction-induced damage (Petrof et al, 1993). The ion channel hypothesis on the other hand argues that the lack of dystrophin disrupts the ion channel function rather than contributing to membrane fragility (Chan, Head and Morley, 2007). The channelopathy arises from the influx of Ca^{2+} and the chronic intracellular Ca^{2+} overload causes fiber damage through the activity of proteases and reactive oxygen species (Carlson, 1998; Allard, 2006; Chan, Head and Morley, 2007; Whitehead, Yeung and Allen, 2005).

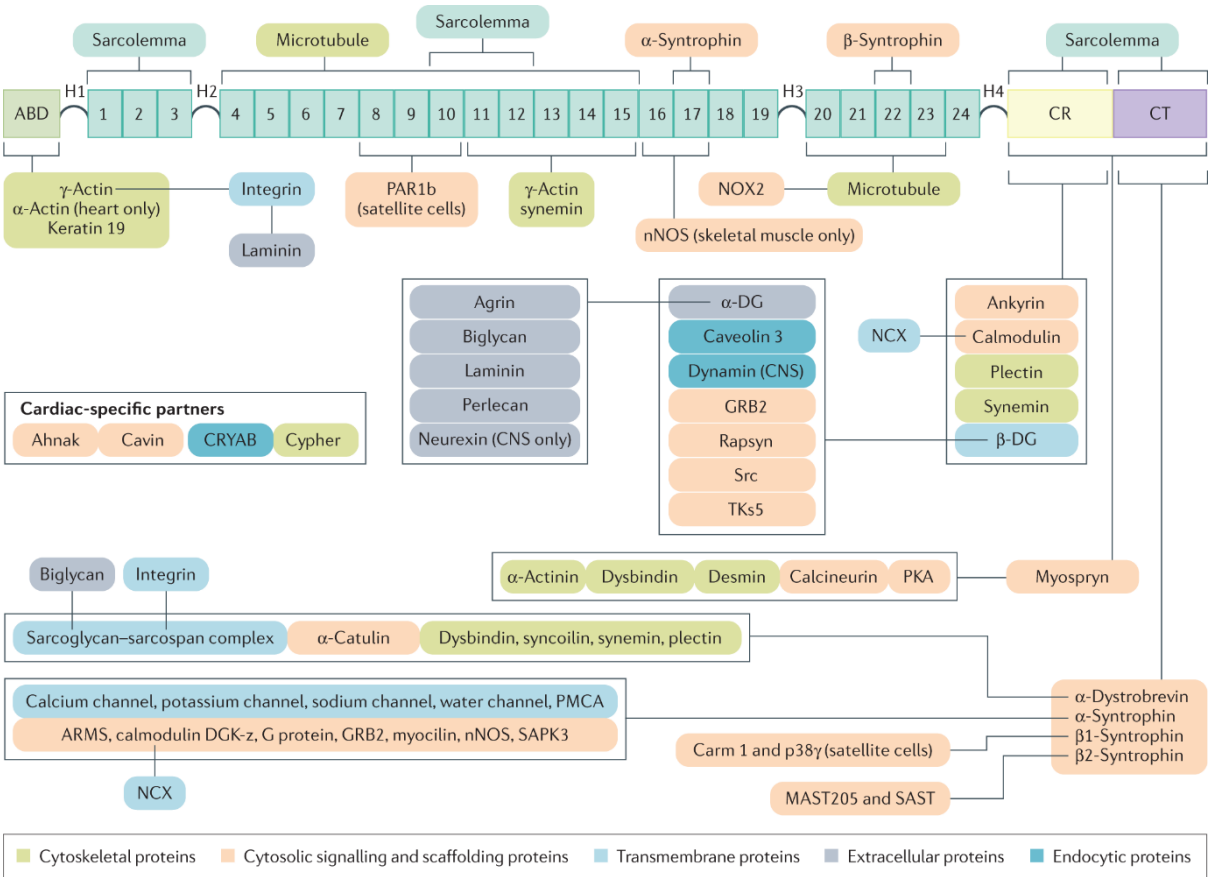

Figure 1.8 **Dp427m and the binding partners forming dystrophin-associated protein complex (DAPC).** The multiple dystrophin binding partners are categorized as cytoskeletal proteins, transmembrane proteins, extracellular proteins, cytosolic signalling and scaffolding proteins, endocytic proteins, and cardiac-specific interacting proteins. Together, these proteins form a complex called DAPC. ABD, actin-binding domain; CNS, central nervous system; CR, cysteine-rich domain; CT, C-terminal domain; DG, dystroglycan; NCX, sodium-calcium exchanger; nNOS, neuronal nitric oxide synthase; NOX2, NADPH oxidase 2; PMCA, plasma membrane calcium ATPase (Duan et al, 2021). Image adapted from Duan et al, 2021.

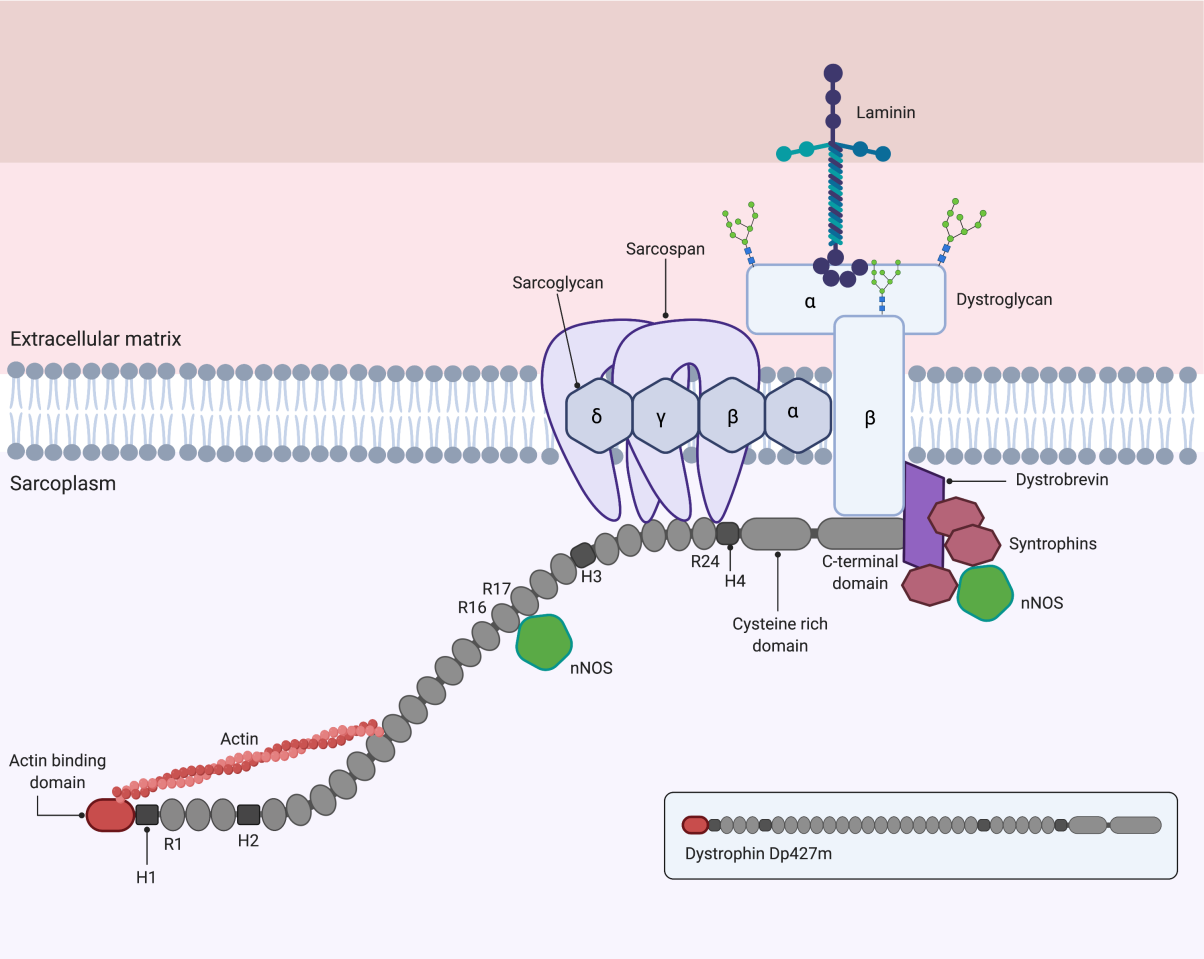

Figure 1.9 **Full length dystrophin (DP427m) and dystrophin-associated protein complex (DAPC)**. The dystrophin protein contains an N-terminal domain (that binds F-actin), rod domain made of spectrin-like repeats (labelled R1-R24), four hinge regions (labelled H1-H4), a cysteine-rich domain (CRD) and a carboxy-terminal domain (CTD). Dystrophin is attached to the DAPC via the cysteine-rich domain (which bind dystroglycan) and C terminus (which bind syntrophins and dystrobrevin), linking the internal cytoskeleton and extracellular matrix (Davies and Nowak, 2006; Fairclough, Wood and Davies, 2013). 11 main proteins make up the DAPC: dystrophin, the dystroglycan subcomplex (α-dystroglycan and ß-dystroglycan), the sarcoglycan subcomplex (α-sarcoglycan, ß-sarcoglycan, γ-sarcoglycan and δ-sarcoglycan), sarcospan, syntrophin, dystrobrevin and neuronal nitric oxide synthase (nNOS).

Syntrophins recruits multiple proteins to the DAPC (shown in Figure 1.8) as well as neuronal nitric oxide synthase (nNOS) to the sarcolemma (Allen, Whitehead, and Froehner, 2016). The rod domain of dystrophin (R16-R17) also contains nNOS binding domain that localises nNOS at the sarcolemma. This enables immediate diffusion of nitic oxide into the blood vessels to promote vasodilation in contracting muscles, allowing sufficient blood perfusion (Duan, 2018). The delocalisation of nNOS due to absence of functional dystrophin causes (i) functional ischaemia and (ii) nitrosative stress that damages cells, compromising force production in the muscle (Duan, 2018).

The DAPC consists of multiple transmembrane, cytoplasmic and extracellular proteins and in DMD patients, the absence of functional dystrophin destabilises the DAPC (Ervasti *et al.*, 1990; Yoshida and Ozawa, 1990). Cell signalling mediated by the dystrophin-glycoprotein complex are also disrupted due to the loss of dystrophin (Rando, 2001). Many proteins found within the DAPC including alpha-dystrobrevin, sarcoglycan, dystroglycan, and sarcospan are essential components in cellular signalling that maintains healthy muscle function and development (Abdul-Razak, Malerba and Dickson, 2016). The complex interactions between dystrophin and various signalling and scaffolding proteins either directly or indirectly are shown in Figure 1.8.

In the absence of functional dystrophin in skeletal and cardiac muscle, the muscle cell plasma membrane integrity is affected, making the muscle fibres prone to damage induced by contraction, eventually leading to progressive muscle wasting in patients (Ennen, Verma and Asakura, 2013). This hypothesis is supported by two main observations: (i) sarcolemmal tears (also referred to as 'delta lesions') have been observed in muscle samples of DMD patients visualised by electron microscopy (Mokri and Engel, 1998) and (ii) sarcolemmal rupture causes leaking of biomarker such as creatine kinase (muscle enzyme) into the blood (Duan et al, 2021).

A less severe form of dystrophinopathy is called Becker muscular dystrophy (BMD) (Koenig, Monaco and Kunkel, 1988) (Table 1.1). Like DMD, BMD is also caused by mutations in the same X-linked gene, however the disease is much milder than DMD where the age of onset of BMD can be as late as 30 or 40 years (England *et al*, 1990). The transcript reading frame downstream of the mutation is not disturbed in BMD but the aberrant transcript codes for shorter dystrophin that is partially functional, with reduced expression (van Deutekom and van Ommen, 2003).

In patients with deletion mutations, the 'reading frame' hypothesis suggests that semi-functional, internally deleted dystrophin protein is produced in BMD patients giving rise to a less severe form of dystrophinopathy (Koenig et al, 1989). Size of the deletion is not related to disease severity, and in one case studies have revealed that a 61-year old BMD patient was still ambulant even though 46% of the coding information was lost in the deletion in his *DMD* gene (England *et al*, 1990). On the other hand, the 'reading frame' hypothesis suggests that in DMD patients the reading frame downstream of mutations is disrupted. This leads to translation termination and a truncated protein that is non-functional and unstable causing the more severe form of dystrophinopathy (Koenig et al, 1989) (Table 1.1). An analysis of 258 independent deletion mutations at the DMD/BMD locus revealed that there was a correlation between phenotype and type of deletion mutations in 92% of cases; and in fact, many "in-frame" deletions of the *DMD* gene are not detected as the individuals with such mutations are either asymptomatic or exhibit non-DMD/non-BMD clinical features (Koenig et al, 1989). This finding was not only intriguing suggesting size of deletions in the *DMD* gene are not necessarily related to severity of the disease, but also revealed the possibility of manipulating the large *DMD* gene as a strategy to restore muscle function in affected patients, a proposition which has been exploited and is discussed below (Section 1.2.5).

Table 1.1 Clinical signs of DMD and BMD.

	DMD	BMD
Motor function	Independent ambulation achieved, but lost before age of 13 years	Independent ambulation achieved, variable progression
Cardiomyopathy	Severe	Severe
Respiratory impairment	Severe	Not frequent
Rigid spine	Absent	Absent
Disease course	Progression of motor, cardiac, and respiratory signs	Progressive with substantial variability
Increased creatine kinase	Severe	Severe
Other signs	Mental retardation in 30%	None

Table adapted from Mercuri and Muntoni, 2013.

1.1.3 Animal models of DMD

It is estimated that there are currently about 60 different animal models for DMD, some spontaneous and some generated, but the *mdx* mouse has been the most used in DMD research (Table 1.2 and Figure 1.10) (McGreevy *et al*., 2015). Dog models are also becoming increasingly popular in the field (Echigoya *et al*., 2017; Le Guiner *et al*., 2017) and with more severe phenotypes compared to the *mdx* mouse providing better model of human DMD (McGreevy *et al*., 2015). In addition, the dog models seem to provide more relevant data regarding potential immune responses against different adeno-associated virus (AAV) serotypes used in delivering therapeutic gene (Chamberlain and Chamberlain, 2017).

Table 1.2 Clinical manifestations and histopathology of dystrophin-deficient mice, dogs and humans.

	***mdx* Mice**	**Dogs**	**Human**
Clinical manifestations			
Birth body weight	= normal	= normal	= normal
Grown-up body weight	≥ normal	< normal	< normal
Clinical course	Mild, non-progressive	Severe, progressive	Severe, progressive
Lifespan	= 75% of normal	= 25% of normal	= 25% of normal
Neonatal death	Rare	~ 25% of affected dogs	Rare
Age at first symptom	≥ 15 months	Birth to 3 months	2 to 4 years
Loss of ambulation	Not seen in the mice model	Not a clinical feature in young dog model	Common at early teenage
Muscle wasting	Minimal until ≥ 15 months	Progressive	Progressive
ECG abnormality	Frequent	Frequent	Frequent
Cardiomyopathy	≥ 20 months; dilated (female) and hypertrophic (male)	Detectable at 6 months by echocardiography	Evident at 16 years
Cognitive and CNS defects	Mild	No information available	One third of affected individuals
Histopathology			
At birth	Minimal	Minimal	Minimal
Acute necrosis	2 to 6 weeks	None	None
Limb muscle fibrosis	Minimum in adult	Extensive and progressive	Extensive and progressive
Muscle regeneration	Robust	Poor	Poor

CNS: Central nervous system; ECG: electrocardiogram. Table adapted from McGreevy et al., 2015.

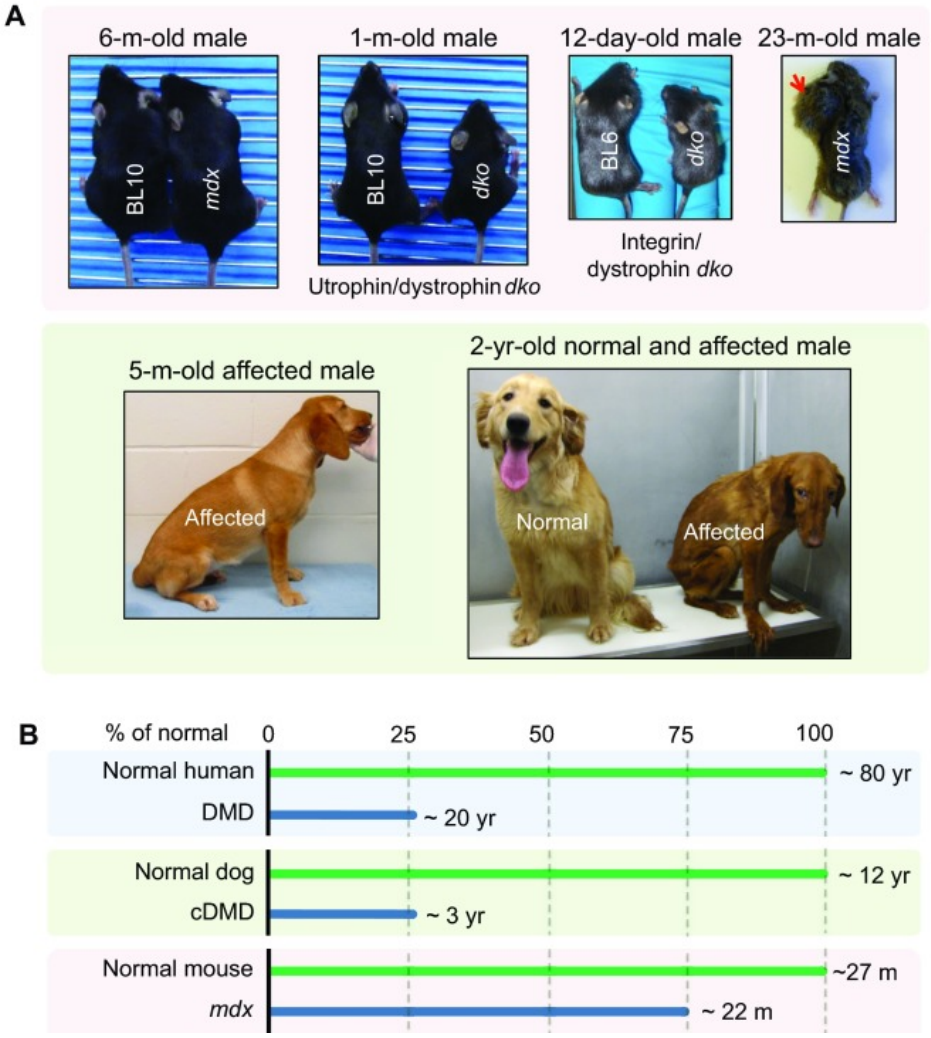

Figure 1.10 **Animal models developed for DMD**. (A) The younger *mdx* mouse model does not show many symptoms, but symptoms begin to appear when the mouse ages (see 23-m-old photo). The red arrow indicates tumor growth, as older *mdx* mouse tend to develop rhabdomyosarcoma (rare cancer specifically in skeletal muscle tissue). The utrophin/dystrophin double knockout *dko* mice tend to show more severe symptoms and are smaller than the control BL10 and BL6 mice. Utrophin is a dystrophin related protein that is found in fetal and regenerating muscle, as well as in neuromuscular junction of adult muscle (Tinsley et al., 1992). Utrophin and dystrophin have conserved structure with higher sequence similarity in the C- and N- terminus, however, the utrophin gene is about one third in length compared to that of dystrophin (Pozzoli et al., 2002). The dog model also portrays severe clinical symptoms over time and they are reluctant to exercise. (B) Lifespan of healthy and affected humans, dogs and mice (McGreevy et al., 2015[used throughout the legend]). Figure adapted from McGreevy et al., 2015.

The dystrophin-deficient rats (*Dmd*^{mdx}) are another addition to the small animal models in DMD research, and they closely resemble the pathological phenotype of DMD patients (Ouisse et al, 2019). *Dmd*^{mdx} also display a more severe cardiac phenotype mimicking the dilated cardiomyopathy observed in human patients (Larcher et al, 2014). Whilst the rat model is another small animal model, it is ten times bigger than the *mdx* mice model and thus can better represent the disease phenotype; at the same providing the advantage over large animal models such as dogs that are often expensive and difficult to handle (Larcher et al, 2014).

The availability of animal models for DMD has enabled systematic testing of many experimental treatment strategies that have been developed over the years, some of which have successfully passed clinical trials and are currently being marketed (discussed in section 1.2 below).

1.2 Treatment strategies for DMD

1.2.1 An overview of DMD therapies and novel experimental approaches

Currently, there is no cure for DMD. However, many therapeutic strategies are being tested in clinical trials. DMD is a complex disease, where the lack of dystrophin triggers a series of cellular events that eventually compromise muscle function (Bushby et al, 2010). A schematic summary of these altered cellular pathways in DMD and the therapeutic opportunities they afford is shown in Figure 1.11.

So far, glucocorticosteroids (GCs) such as prednisone and deflazacort are the widely used standard of care drugs for DMD patients (Matthews et al, 2016). Whilst the use of GCs does not cure the disease, the ambulation of patients has been prolonged and GCs have contributed to the extension of life expectancy of patients into their fourth decade (Bushby et al, 2010). It is important to note that GCs come with many undesirable metabolic side effects such as osteoporosis, hyperglycemia, poor wound healing, increased risk for infections, insulin resistance and weight gain (Bushby et al, 2010; Vandewalle et al, 2018). Vamorolone (a safer anti-inflammatory drug) is currently in human trials to provide an alternative to the current standard of care for DMD patients using GCs (Conklin et al, 2018).

As the lack of functional dystrophin contributes to DMD pathology, restoring dystrophin would be the most obvious therapeutic approach; and primary therapies in DMD aim to restore dystrophin by either restoring the reading frame of dystrophin or replacing lost dystrophin. Three main strategies of restoring the reading frame of dystrophin are via exon skipping, stop codon readthrough and genome editing. These strategies are discussed in detail in Sections 1.2.2, 1.2.3 and 1.2.4 respectively. Microdystrophin gene therapy is a promising strategy to directly introduce a recombinant dystrophin gene, or mini- or micro-gene and thus restore lost dystrophin with a functional replacement (discussed in detail in Section 1.2.5).

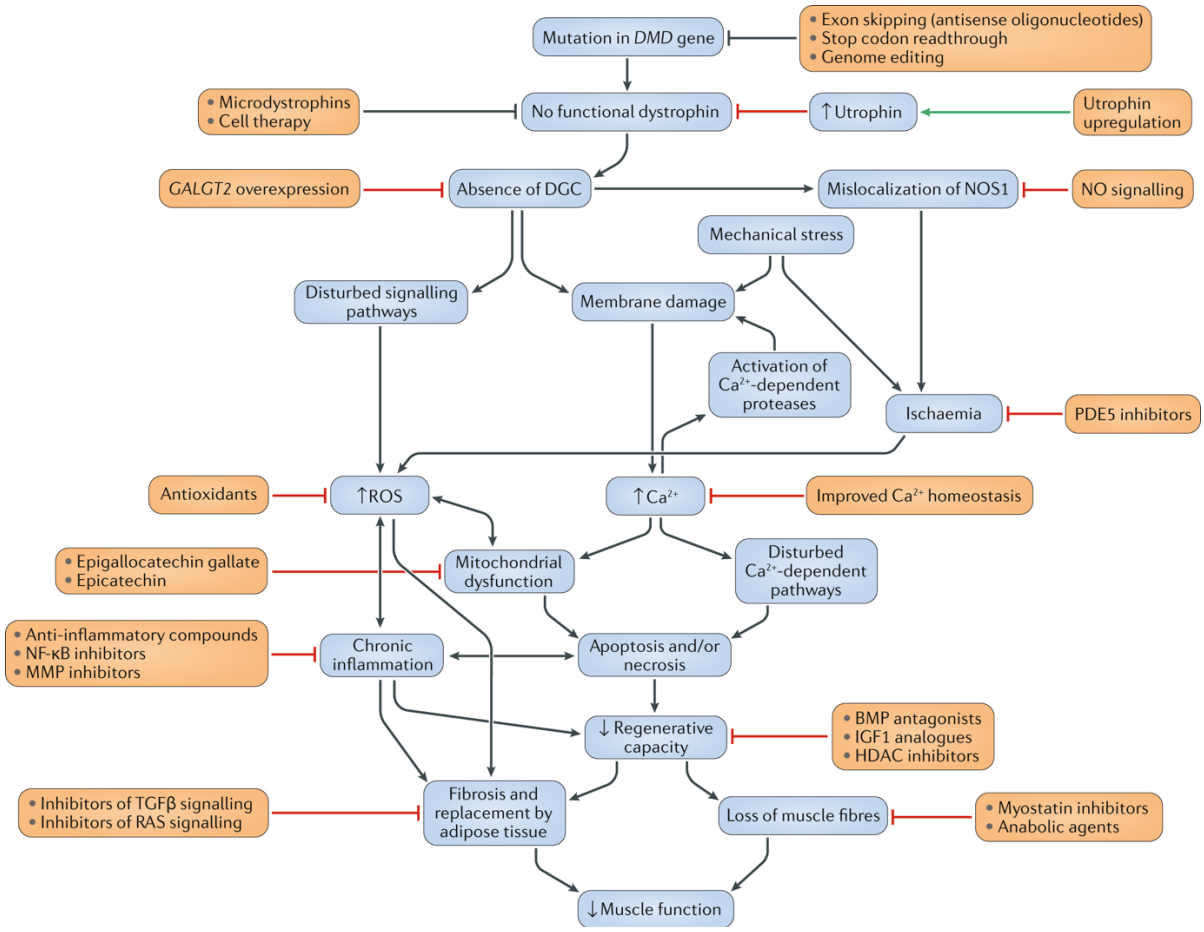

Figure 1.11 **Altered cellular pathways in DMD and therapeutic opportunities**. Many cellular pathways are disturbed as a result of lack of dystrophin. Primary therapies (black arrows) aim to restore dystrophin by either restoring the reading frame of dystrophin or replacing lost dystrophin. Secondary therapies aim to target the cellular pathways that are affected by either inhibition (red arrows) or upregulation (green arrow) (Verhaart & Aartsma-Rus, 2019). BMP, bone morphogenetic protein; DGC, dystrophin-associated glycoprotein complex; GALGT2, the gene encoding ß1,4 N-acetylgalactosaminyltransferase 2 (also known as B4GALNT2); HDAC, histone deacetylase; IGF1, insulin-like growth factor 1; MMP, matrix metalloproteinase; NF-κB, nuclear factor-κB; NO, nitric oxide; NOS1, nitric oxide synthase; PDE5, phosphodiesterase 5 (also known as cGMP-specific 3′,5′-cyclic phosphodiesterase); ROS, reactive oxygen species; TGFß, transforming growth factor-ß. Image from Verhaart & Aartsma-Rus, 2019.

DMD is a complex disease with many clinical complications that affect multiple systems in the body (Bushby et al, 2010). As such, some therapies can be targeted to address the secondary pathology of DMD (shown in Figure 1.11). Many secondaries therapies targeting fibrosis, regeneration, inflammation, muscle growth, calcium homeostasis, vasodilation, cardiomyopathy, mitochondria biogenesis, osteoporosis, puberty delay and utrophin upregulation are not discussed in detail here, but the author refers interested reader to an excellent, comprehensive review by Verhaart and Aartsma-Rus (2019). Whilst many therapies targeting secondary pathology are in human clinical trials, not all of them have been successful. As such, the respective trials have been terminated (reviewed in Verhaart & Aartsma-Rus, 2019).

1.2.2 Antisense-mediated modulation of exon splicing (exon skipping)

In eukaryotic genomes, segments of DNA that code for proteins called genes are composed of exons and introns. Following synthesis of pre-mRNA during transcription, splicing occurs (Figure 1.12) to remove introns in between exons, joining together two neighbouring exons. The final series of exons spliced together forms the coding sequence mRNA for a particular protein that is produced during translation.

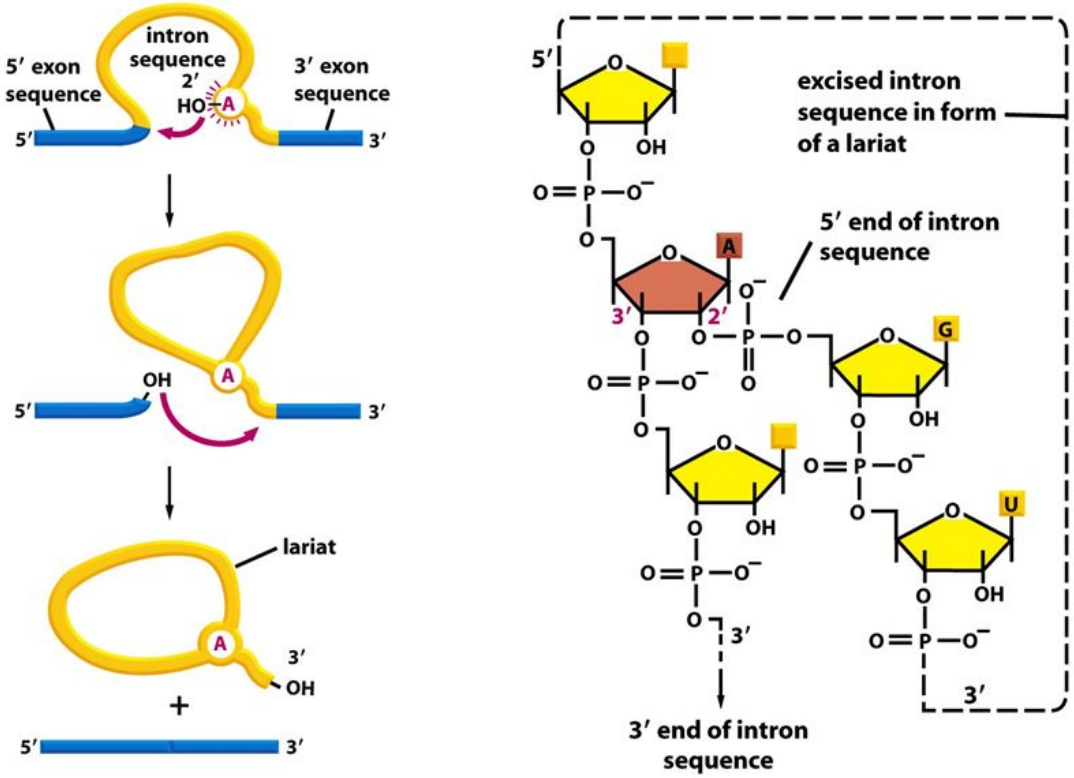

Figure 1.12 **Mechanism of intron splicing**. The splicing process to remove an intron in the pre-mRNA involves two successive trans-esterification reactions. In the first step, the 2' OH of a specific adenine nucleotide near the 3' end of the intron attacks the 5' splice site of the intron; breaking the sugar-phosphate bond leaving an OH at the 3' of the first exon. In the process, the cut 5' end of the intron forms a 2'-5' phosphodiester bond with the adenine that initiated the attack; creating an intron-3' exon intermediate in the form of a lariat. In the second step, the 3' OH of the first exon attacks the 3' splice site of the intron, releasing the lariat (intron) and joining the two exons together forming a continuous coding sequence. The lariat is rapidly degraded (Alberts et al, 2008). Figure adapted from Alberts et al, 2008.

DMD can arise due to a range of mutations, for example, small and large deletions, duplications, point mutations producing nonsense and missense codons, and mutations involving creation of cryptic splice site. However, the majority of cases arise from so-called frame-shifting mutations, most often large gene deletions, which alter the translational reading frame in the resultant mRNA and result in the absence of dystrophin (Sherratt *et al.*, 1993; Flanigan et al, 2009). However, even in these circumstances, a small proportion of skeletal muscle fibres called 'revertant fibres' express dystrophin using a frame-restoring mechanism, where out-of-frame exons next to the deleted ones from the genome are skipped during maturation of pre-mRNA to mRNA (Sherratt *et al.*, 1993). This has been confirmed by biopsies from DMD patients that have been shown to be positive for dystrophin although dystrophin is expressed at a low level (Nicholson, 1993). In addition, Matsuo and colleagues revealed that deletion internal to a specific exon causes the exon to be skipped, resulting in an abnormally spliced mRNA (Matsuo *et al.*, 1991). Molecular analysis of the *DMD* gene of a Japanese DMD patient showed a deletion of 52 base pairs from exon 19 caused the exon to be skipped during transcription, joining exon 18 and exon 20 together (Matsuo *et al.*, 1991).

As such, even though non-functional dystrophin protein is produced in DMD patients with mutations in the *DMD* gene, in some patients, the reading frame can be restored to produce a partially functional dystrophin protein (van Deutekom and van Ommen, 2003) (Figure 1.13). In devising treatment strategies for DMD, the restoration of the reading frame is achieved by targeting modulation of exon splicing in the mutant pre-mRNA in a sequence-specific manner using antisense oligonucleotides (AONs), that are short stretches of synthetic nucleic acids that bind to target sequences via Watson-Crick base pairing (van der Bent et al, 2018). The aim is to exclude a specific frame-shifting exon and favour splicing patterns which produce BMD-like mRNAs and dystrophin protein variants (one such example is shown in Figure 1.13). Such antisense sequences can be delivered either as synthetic nucleic acid materials or via expression from gene constructs (Dickson, Hill & Graham, 2002; Graham et

al, 2004; Waldrop et al, 2020). It is important to note that the specific sequences targeted by this type of treatment strategy for DMD is mutation-dependant and is only applicable to a small subset of the DMD patients; for example, exon 51 skipping is applicable to 13-14% of DMD patients (Aartsma-Rus *et al*, 2009).

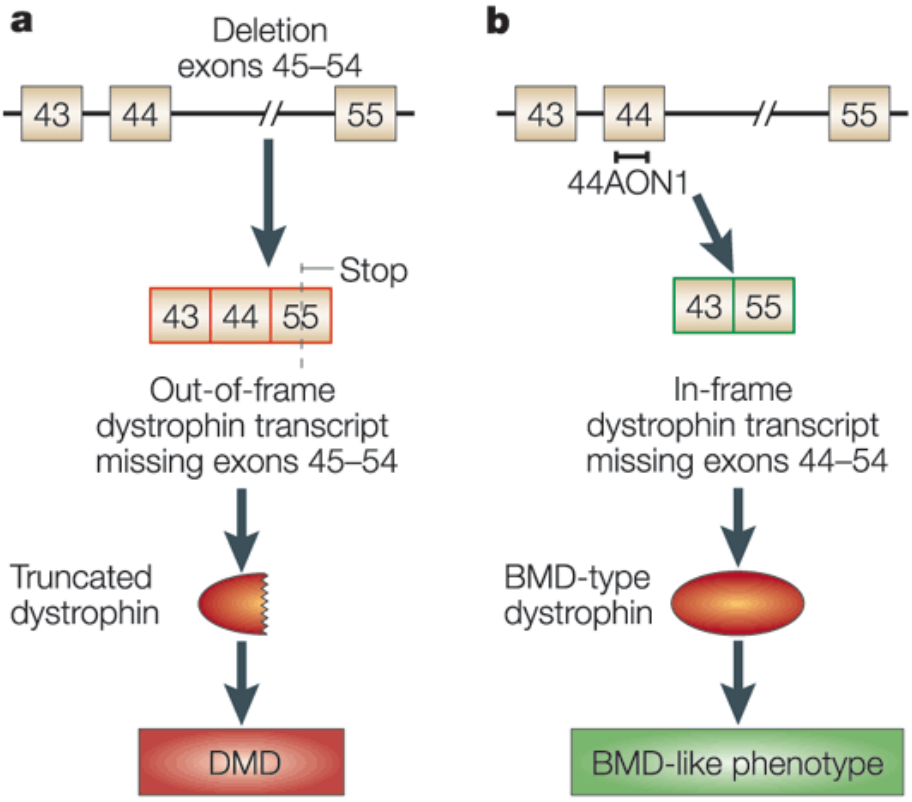

Figure 1.13 **Exon-skipping strategy**. (a) In DMD patient with deletion of exons 45-54, the dystrophin transcript becomes out-of-frame. This is because exons 44 and 55 are not in-frame as illustrated in Figure 1.6. As a result, truncated dystrophin is produced and the patient suffers from DMD. (b) When an antisense oligonucleotide (AON) internal to exon 44 is introduced, the exon is skipped and the resulting transcript is in-frame, producing shorter, BMD-type dystrophin. As a result, the patient exhibits a milder BMD-like phenotype (van Deutekom and van Ommen, 2003). Image from van Deutekom and van Ommen, 2003.

Delivery of nucleic acids as therapeutics comes with the limitation of being prone to rapid degradation by endonucleases. As such, many modifications can be made to synthetic oligonucleotide therapeutics to prevent them from being degraded by such endonucleases, as well as improving affinity for the target sequence and reducing toxicity of the AONs themselves (van der Bent et al, 2018 [used throughout this paragraph]). In addition, in the case of exon skipping which is a steric blocking technique, the AON/RNA duplex should be resistant to RNAse H, which degrades RNA bound in RNA/DNA heteroduplexes (Douglas and Wood, 2013). Some of the common modifications made to AONs are sugar modifications such as 2′ hydroxyl methylation (2′OMe) or methoxyethylation (MOE), use of phosphorothioate (PS) linkages in the backbone or constraints such as the 2′-O, 4′-C methylene bridge in locked nucleic acids (LNA) (Figure 1.14). Other chemistries that include uncharged variations on the regular structure of oligonucleotides; for example, phosphorodiamidate morpholino (PMO) and peptide nucleic acid (PNA) (Figure 1.14).

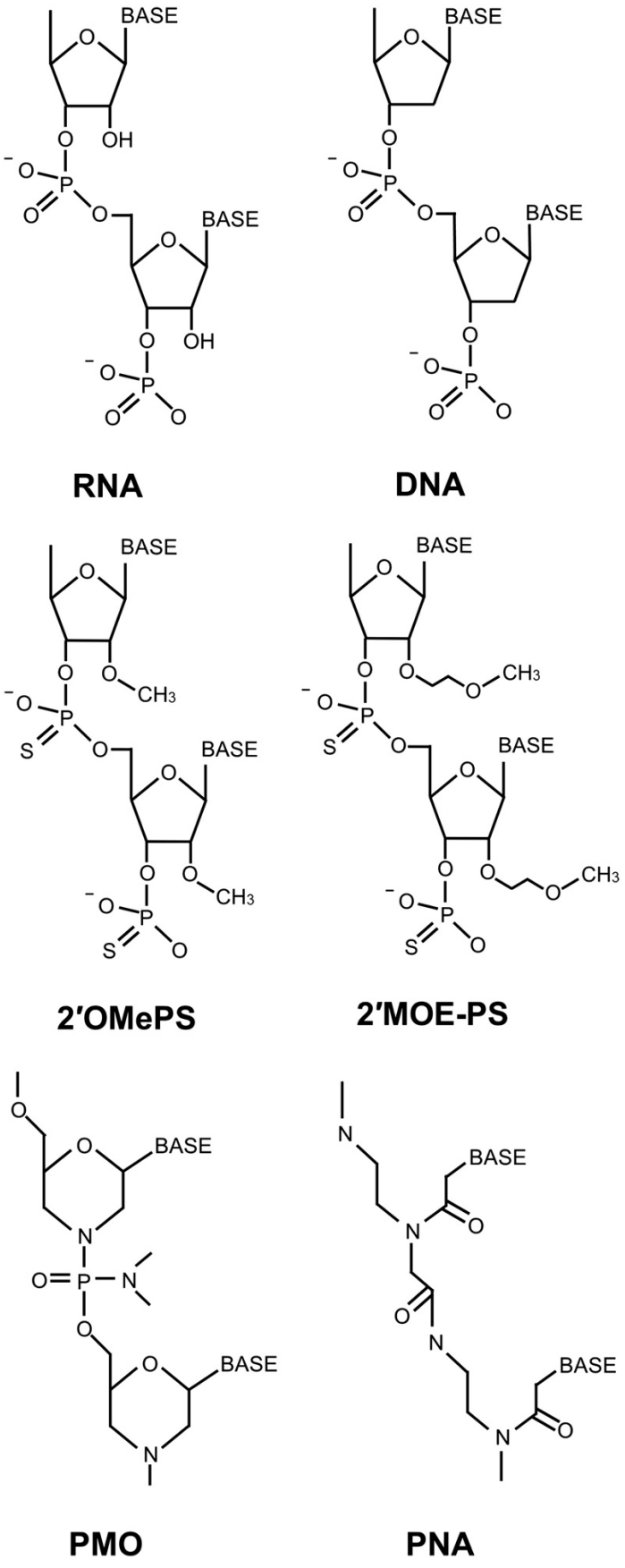

Figure continued on next page.

Figure continued from previous page.

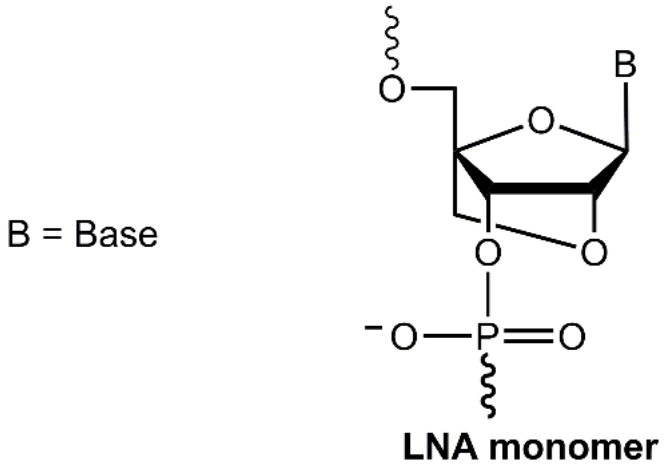

Figure 1.14 **Modifications made to AONs**. AONs require several features to be effective therapeutics in exon skipping: high-specificity to the target binding site, chemistry that enables cellular uptake, single-stranded stability, resistance to endonucleases and RNAse H, reduced toxicity and effective tissue specificity. Structures of RNA and DNA are shown as reference. 2′OMePS modifications are based on RNA but a non-bridging oxygen atom of the phosphate is substituted with a sulphur atom, making a phosphorothioate. The hydrogen of the 2′hydroxyl group is also substituted for a methyl group. 2′MOE-PS is similar to 2′OMePS but has a methoxyethyl group instead of a methyl group. PMOs have a six-membered morpholine ring moiety replacing the ribose and the rings are joined together by phosphorodiamidate linkages, having no charge on their backbone. PNAs also carry no charge on their backbone and have similar pharmacokinetic profiles to PMOs, but with different backbone with peptide linkages between N- (2-aminoethyl) glycine units. The absence of electrical charge on the backbone reduces the off-target interactions of the AON molecules but at the same time prevents them from forming electrostatic interactions with delivery vectors. As such, these AONs can be conjugated to delivery moieties such as cell penetrating peptides (Douglas and Wood, 2013 [used throughout]). LNA contains constraints such as the 2′-O, 4′-C methylene bridge, in which the ribose sugar moiety is locked by an oxymethylene bridge connecting the C2′ and C4′ carbon atoms that provides high resistance to enzymatic degradation (Poongavanam et al, 2014). Figure adapted from Douglas and Wood, 2013 and Poongavanam et al, 2014.

One antisense oligonucleotide therapy targeting exon 51 has been approved by the Food and Drug Administration (FDA); however, the drug (Eteplirsen or Exondys 51) had a very modest treatment outcome (0.4% increase in dystrophin level after 48 weeks and 0.9% increase after 180 weeks of treatment) (Charleston et al, 2018). Another AON with different chemistry targeting exon 51 (Drisapersen) was stopped from development as it failed to secure FDA authorisation and demonstrated very low clinical benefits and significant toxicities (Aartsma-Rus and Krieg, 2017). Whilst the exact mechanism behind why the drug failed is not known, high doses of the drug with 2′-OMePS AON chemistry and the route of delivery subcutaneously might have contributed to the life-threatening toxicity (Le et al, 2017; Hilhorst et al, 2019). Another drug, Nusinersen (Spinraza) with similar 2′-OMePS chemistry delivered intrathecally for treatment of spinal muscular atrophy (SMA) had been effective and approved by the FDA; where the delivery method intrathecally may have resulted in better delivery efficiency of the drug to the central nervous system (van der Bent et al, 2018). In addition, many preclinical studies have also reported higher efficiency of exon skipping using AONs with PMO chemistry (such as Eteplirsen) compared to 2′-OMePS chemistry (such as Drisapersen) (Lu, Cirak and Partridge, 2014), and as such the chemistry of the AONs could also explain why Eteplirsen worked better in patients compared to Drisapersen even though they both target the same exon (exon 51). The next AON therapy that was approved by the FDA recently is Golodirsen or VyonDys53 (PMO chemistry) that targets exon 53; and is applicable to approximately 7.7% of DMD patient population (Frank et al, 2020). Golodirsen was well tolerated and the treatment resulted in dystrophin production and correct localisation of the protein to the sarcolemma (Frank et al, 2020). Viltolarsen (NS-065) (Watanabe et al, 2018) targeting exon 53 (PMO chemistry) was also approved by the FDA in 2020. Casimersen (Amondys 45) (PMO chemistry) targeting exon 45 was approved by the FDA in February 2021 (Shirley, 2021). Other exon skipping therapies targeting exon 45 (DS-5141b) and exon 51 (SRP-5051 and Suvodirsen) are currently in clinical trials (Verhaart & Aartsma-Rus, 2019).

DMD exon 2 is one of the most commonly duplicated exons resulting in formation of incorrect dystrophin protein (Waldrop et al, 2020). In duplication mutation of the *DMD* gene, exon skipping has a potential to restore the reading frame for production of full-length dystrophin. This strategy is currently being investigated by Audentes Therapeutics, where an AAV vector is used to deliver four copies of a modified U7 small nuclear RNA (snRNA) that contains antisense sequences targeting the splice donor (2 copies) and splice acceptor (2 copies) of the *DMD* exon 2 (Waldrop et al, 2020; NCT04240314). Three-month post-infusion data in the first 2 subjects treated with vector dose of 3.0×10^{13} vector genome per kilogram of body weight (vg/kg) showed expression of apparently full-length dystrophin protein and stable or improved functional outcome (Waldrop et al, 2020). The study is ongoing.

As a treatment strategy targeting the secondary pathology of DMD, the antisense technology can also be used to induce exon skipping of the myostatin pre-mRNA that destroys the reading frame and knocks down myostatin (Lu-Nguyen et al., 2017). Myostatin is a growth factor that negatively regulates skeletal muscle growth and differentiation (Guo et al., 2009; Lu-Nguyen et al., 2017). In the absence of myostatin, enhanced muscle regeneration and reduced fibrosis are observed in the mdx mouse (Li, Kollias and Wagner, 2008). This approach however remains controversial as muscle hypertrophy could potentially led to postural instability and joint contractures (Kornegay et al, 2012) which have been observed in golden retriever muscular dystrophy (GRMD) dogs (DMD dog model) (Kornegay et al, 2016). Also, clinical trials in DMD patients using monoclonal antibodies which block myostatin have been conducted without success (six trials so far and none demonstrated functional efficacy) (Wagner, 2020).

1.2.3 Stop codon readthrough (SCR) or translational read-through

Nonsense mutations cause appearance of stop codons and result in pre-mature translation termination and production of truncated often unstable protein products. In DMD patients with nonsense mutations, the appearance of premature stop codons due to mutations causes truncated, non-functional dystrophin polypeptides to be produced which are likely to be unstable (Bushby et al., 2014). One treatment strategy for such nonsense mutation is called premature termination codons (PTCs) suppression or stop-codon readthrough. PTC suppression was originally described in 1996 as a treatment strategy for cystic fibrosis caused by nonsense mutations in the *CFTR* gene (Howard, Frizzell and Bedwell, 1996).

Stop-codon readthrough refers to the phenomenon that a ribosome fails to recognise stop codon and continues translating through into the otherwise untranslated region (UTR) of a transcript. This 'readthrough' of the ribosome will result in possibly a random addition of amino acid where the premature stop codon is encountered. This strategy is based on the class of antibiotic called aminoglycosides that bind to the ribosomal decoding centre (Recht, Douthwaite and Puglisi, 1999). The ribosomal decoding centre has proofreading function by monitoring the codon-anticodon interactions between the mRNA and tRNA to ensure that only cognate aminoacyl-tRNAs are correctly accommodated into the peptidyl transferase centre, where peptide bond is formed (Keeling et al, 2014). Aminoglycosides have high affinity to the bacterial decoding center which causes misincorporation of near-cognate aminoacyl-tRNAs at both sense and stop codons, leading to extensive translational misreading, eventually inhibiting protein synthesis at higher concentrations (Keeling et al, 2014). The eukaryotic ribosomal RNA (rRNA) sequence differs from prokaryotic rRNA sequence by two nucleotides and this reduces the affinity of aminoglycosides for eukaryotic ribosomal decoding centre (Lynch and Puglisi, 2001; Recht, Douthwaite and Puglisi, 1999). Whilst aminoglycosides do not seem to induce significant misreading at sense codons in eukaryotes, a subset of them have been shown to bind to eukaryotic ribosomes resulting in misincorporation of near-cognate

aminoacyl-tRNAs when a premature termination codon is encountered (Keeling et al, 2014). One such aminoglycoside that has been tested in the treatment of DMD is gentamicin (Barton-Davis *et al.*, 1999), which failed in terms of reproducibility (Dunant *et al.*, 2003). This is possibly due to the fact that the incorporation of an amino acid when a premature stop codon is encountered is a totally random process, which may result in only a small proportion of 'functional' protein to be produced.

A non-glycoside compound, PTC124, now known as Translarna (Ataluren) was developed by PTC Therapeutics as a drug that supresses premature termination by incorporating a random amino acid when a premature stop codon is encountered, and have shown partial functional rescue in DMD mice model (*mdx* mice) (Welch et al., 2007). PTC124 is a compound discovered by PTC Therapeutics as a 'nonsense suppression agent' following high-throughput screening of ~800,000 compounds (Welch et al., 2007). Ataluren was subsequently tested in humans and has shown safety, tolerability and meaningful differences in clinical endpoints (although the primary clinical endpoint of a significant increase in 6-minute walk test distance between placebo and treatment groups was never met) (Bushby et al., 2014; McDonald et al., 2017). This subsequently led to the conditional approval of Ataluren by the European Medicines Agency (EMA). Despite several applications however, the FDA have yet to approve the drug (Verhaart & Aartsma-Rus, 2019).

1.2.4 Other dystrophin-restoration therapies in progress

Myoblast transplantation is another treatment strategy that has been studied for several decades (Watt et al, 1982) and aims to restore dystrophin in DMD patients by transplanting normal muscle precursor cell via intramuscular injections (Skuk et al, 2006). The myoblasts are derived from healthy donors and passaged in culture before injected into patients, with immunosuppression (Skuk et al, 2004). Whilst these studies provided proof-of-principle, the treatment efficiency remains poor as dystrophin-positive fibers were only found very close to injection sites (Skuk et al, 2006). Currently, one phase I/II clinical trial is recruiting to investigate this approach (NCT02196467).

Genome editing enables mutations to be corrected at the DNA level for the production of functional dystrophin protein (Chamberlain and Chamberlain, 2017). The clustered regularly interspaced palindromic repeats (CRISPR)-associated protein 9 [CRISPR/Cas9] nuclease is used to make double-strand break (DSB) at specific DNA sequences. The cellular DNA repair mechanism is then activated to repair the DBS either via nonhomologous end joining (NHEJ) or homology directed repair (HDR) (Kupatt et al, 2021). NHEJ pathway is more error prone as it introduces small insertions or deletions as ligation of the DNA break happens; which can be used to (i) disrupt genomic sequences or (ii) induce targeted deletions where DSBs are introduced at each end of the target sequence which is deleted as NHEJ mediates joining of the ends (Prakash, Moore and Yáñez-Muñoz, 2016). HDR on the other hand is a more precise pathway, where a homologous donor template is used to repair the lesion to restore the original sequence; however, this approach is not widely used as this is an uncommon event especially in post-mitotic cells (Lim, Yoon & Yokota, 2018).

If larger deletions of the *DMD* gene are involved, then truncated, functional dystrophin protein will be produced (Chamberlain and Chamberlain, 2017). Whilst many proof-of-principles studies *in vitro* and in *mdx* mouse model has been successful in restoring functional, truncated dystrophin (Long et al, 2014; Long et al, 2016; Tabebordbar et al, 2016; Nelson et al, 2016); the gene editing

approach has multiple disadvantages such as: (i) very low efficiency in deleting multiple exons, (ii) lack of efficiency in delivering the CRISPR-Cas9 system *in vivo,* (iii) possible need for repeated treatments, and (iv) safety concerns regarding off-target effects of Cas9 activity (Verhaart & Aartsma-Rus, 2019). There are no clinical trials so far using genome editing approach for DMD.

1.2.5 Microdystrophin gene replacement therapy for DMD

Many current treatment strategies for DMD are symptomatic rather than curative, where focus is put on improving quality of lives of patients (Lu-Nguyen *et al*., 2017). Gene therapy is a treatment strategy that involves the delivery of nucleic acid into target cell to either regulate gene expression of a target gene, replace a faulty gene or reduce the expression of faulty proteins (Nonnenmacher and Weber, 2012). The biggest challenge in devising gene transfer therapy for DMD is the size of the gene, where in the case of the Dp427 isoform of dystrophin, the *DMD* gene is transcribed to an mRNA of 14kb which contains the ORF of ~ 11.5 kb long. Since the discovery of the full coding sequence of the *DMD* gene, replacing the defective gene has been one of the treatment strategies that was planned. The conventional strategies using adenoviral vectors (Chen *et al.*, 1997; Kochanek *et al.*, 1996) and herpes simplex viral vectors provided advantage of delivering the full-length cDNA dystrophin construct, however the potential is limited to newborn and regenerating muscle (Akkaraju *et al.*, 1999; Huard *et al.*, 1997). In addition, viral cytotoxicity reduces the attractiveness of herpes simplex virus as a gene therapy vector (Huard *et al.*, 1997). Adenoviral vectors have a limited insert capacity of 8 kb, however the newer helper-dependent adenoviral vectors can package up to 28.2 kb of non-viral DNA (Stefan *et al.*, 1996). More importantly, the strong immunotoxicity of adenoviral vectors limited the use of this vector (van Deutekom and van Ommen, 2003). Another approach of transferring full-length dystrophin cDNA into cells is by using plasmid vectors but the efficiency was very limited (Lu *et al.*, 2003; Romero et al, 2004). In order to overcome the inefficiency, other methods such as (i) injection of plasmid followed by electroporation (Murakami *et al.*, 2003), (ii) microbubble ultrasound (Lu *et al.*, 2003) and (iii) electrotransfer (Gollins *et al.*, 2003) have to be used to enhance transfection. The plasmid gene delivery method proved to be very inefficient for *in vivo* muscle gene therapy (Duan, 2008).

In 1990, the Davies lab reported a very intriguing finding where in one subset of deletions that causes mild BMD, a central part of dystrophin with 5106 bp coding sequence (almost half of the coding sequence) was removed and one patient was still ambulant at 61 years (England *et al.*, 1990). This suggests that a full-length dystrophin is not required in developing gene replacement therapy and a smaller gene construct is sufficient to replace the large sized dystrophin in patients lacking functional dystrophin (England *et al.*, 1990).

Studies using transgene mice to identify the dystrophin regions essential for sarcolemmal integrity showed that deletion of the N-terminal domain and a significant portion of the rod domain resulted in reduction in force generation similar to dystrophin-deficient *mdx* mice, but still protected the mice from contraction-induced injury, partially preventing dystrophy (Warner *et al.*, 2002). On the other hand, deletion of the cysteine rich domain resulted in severe dystrophy suggesting that this domain has essential function in linking dystrophin to the ECM (Rafael *et al.*, 1996). The C-terminal domain is not essential for dystrophin function and an alternatively spliced variant of dystrophin without the C-terminal domain still showed normal muscle function and assembly of the DAPC (Crawford, 2000). These systematic studies of dystrophin domains combined with observations in mildly affected BMD patients resulted in generation of microdystrophins (early generation microdystrophins lacked the C-terminal and up to 20 spectrin-repeats) that were highly effective in reversing the disease phenotype in *mdx* mice model (Ramos et al, 2019).

Transfer of recombinant miniaturised-dystrophin cDNA using adenovirus and retrovirus has achieved some success. However, these vectors have proven to be not ideal due to immunogenicity and inefficiencies in transducing mature myofibres (Fabb *et al.*, 2002). About 50% of the human population also test positive for neutralizing antibodies against adenovirus, further reducing the attractiveness of the viral vector as a gene delivery vehicle (Foy and Grayston, 1976).

The discovery of the very desirable non-pathogenic virus called adeno-associated virus (AAV) in 1965, followed by the building of first recombinant AAV by the Muzyczka laboratory in 1984 propelled the gene therapy field forward (Hermonat and Muzyczka, 1984) (AAVs are discussed in detail in Section 1.3). Whilst AAVs possess many desirable qualities for use in muscle gene therapy, the small virus is only capable of packaging transgenes of limited size (~4.7kb) (Kotterman and Schaffer, 2014). The truncated dystrophin genes packaged into an AAV shows stable gene expression when expressed in *mdx* mice, leading to normal muscle phenotype (Wang, Li and Xiao, 2000). There was no difference observed between normal muscle and muscle expressing the smallest dystrophins, demonstrating that micro-dystrophins are capable of reversing the disease pathology (Harper *et al.*, 2002). A huge breakthrough in the field was also observed recently where DMD dog model injected with rAAV expressing canine microdystrophin, appear 'disease-free' after two years, showing great potential of the therapy in humans (Le Guiner *et al.*, 2017). As a result, multiple variants of mini-/ micro-dystrophins with clinical potential have been generated (Wang et al., 2000; Harper et al., 2002; Hakim et al., 2017; Le Guiner et al., 2017) (Figure 1.15).

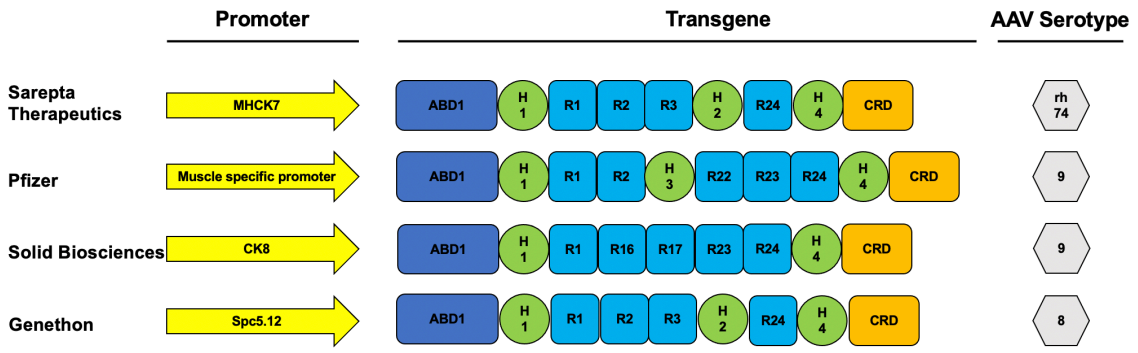

Figure 1.15 **Clinically relevant miniaturised dystrophin constructs**. The promoters utilised in the therapeutic constructs are shown by yellow arrows. These promoters are shown to be muscle and heart specific and will preferentially express the transgene in those tissues. The transgene of all the constructs contain the coding sequence for protein domains that are clinically relevant and functional, discovered by generation of multiple microdystrophin constructs and testing them in *mdx* mice model, followed by analysis of skeletal muscle pathophysiology (Ramos et al, 2019). The AAV serotype of choice is also based on tissue tropism, where they are muscle and heart tropic. Clinical constructs for Sarepta Therapeutics, Pfizer, Solid Biosciences and Genethon adapted from Wang et al., 2000; Harper et al., 2002; Hakim et al., 2017 and Le Guiner et al., 2017 respectively. ABD: Actin-binding domain; H: hinge; R: rod; CRD: cysteine-rich domain; CTD: C-terminal domain.

Large animal models of DMD have shown significant improvements following systemic delivery of engineered micro-dystrophin using AAV, leading to human clinical trials (Le Guiner et al., 2017) (Table 1.3). The successful single-dose gene-replacement therapy in humans for Spinal Muscular Atrophy (SMA) using AAV with dosage up to 2.0×10^{14} vg per kilogram, has provided proof-of-principle for systemic gene transfer using AAV (Mendell *et al.*, 2017). Three clinical trials of DMD gene therapy using AAV-microdystrophin vectors are currently ongoing in the United States by Nationwide Children's, Pfizer and Solid Biosciences (Table 2); each with a slightly different mini-/ micro-dystrophin constructs (Figure 1.15). Clinical trial in Europe was recently initiated by Genethon (Trial number 2020-002093-27) and the first patient was dosed in April 2021. It is also worth noting that unlike exon skipping and stop-codon readthrough, this gene

addition therapy strategy is applicable to all DMD patients regardless of the mutations they carry in the *DMD* gene.

Table 1.3 Active microdystrophin gene transfer clinical trials for DMD using AAV in the United States (US)

	Nationwide Children's NCT03375164 NCT03769116	**Pfizer** NCT03362502	**Solid Biosciences** NCT03368742
Phase	1/2	1b	1/2
Intervention	**AAVrh74.MHCK7.micro-Dystrophin** Recombinant AAV carrying a micro-dystrophin gene and promoter	**PF-06939926** Recombinant AAV9 carrying a human mini-dystrophin gene and a human muscle specific promoter	**SGT-001** Recombinant AAV9 containing a micro-dystrophin gene and a muscle-specific promoter
Age range	3 months – 7 years	5 years – 12 years	4 years – 17 years
Total number	12 boys	12 boys	16 boys
Mutation	DMD gene mutation between exons 18-58	None specified	None specified
Ambulation	Ambulatory	Ambulatory	Ambulatory and non-ambulatory
Corticosteroid use	No requirement however the dosage of steroids can be adjusted depending on T cell response to AAV or microdystrophin	On stable steroid for 6 months	On stable steroid for 6 months
Route of delivery and frequency	Single intravenous infusion in arm (one hour infusion)	Single intravenous infusion	Single intravenous infusion
Length of trial	Follow-up for 2 years	Follow-up for 5 years	Follow-up for 2 years

Table adapted from (Parent Project Muscular Dystrophy (PPMD), 2017) and updated using data from PPMD 2019 Conference presentations by Genevieve Laforet (Solid Biosciences), Michael Binks (Pfizer) and Doug Ingram (Sarepta).

Some encouraging data have emerged from the clinical trials in the US, notably from Nationwide Children's and Pfizer (Table 1.4). These data provide proof-of-principle that AAV gene transfer to target the human muscle is possible from a clinical and manufacturing perspective.

Table 1.4 Clinical trial history and early data on outcomes of the AAV-microdystrophin trials [4].

Intervention	Clinical trial history	Outcome evaluation
SGT-001 (Solid Biosciences) NCT03368742	• Low dose of $5x10^{13}$ vg/kg was administered in the first cohort of phase 1/2 IGNITE-DMD trial. First patient suffered serious adverse effect (SAE) which was resolved. • Age matched dose escalation study has been initiated with a higher dose of $2x10^{14}$ vg/kg. Patient in the treatment group suffered SAE which was resolved with an increase in oral glucocorticoids. • Patients are currently being enrolled.	Very low amount of microdystrophin (less than 5% of normal dystrophin) was present in muscle biopsies (Verhaart & Aartsma-Rus, 2019). After an FDA clinical halt (due to safety concerns) was released, patient dosing continued with modified manufacturing and trial protocols. No subsequent SAEs reported.
PF06939926 (Pfizer) NCT03362502	• $1x10^{14}$ vg/kg was administered in the first cohort of Phase 1b study. • Patients in the second cohort of the dose escalation study received $3x10^{14}$ vg/kg. • Two patients suffered SAE but was resolved. Immune responses to AAV of variable magnitudes were observed in all patients. • 99-patient phase 3 trial launched.	Immunohistochemistry data showed 69% of dystrophin-positive fibers in the high dose group.
AAVrh74.MHCK. Microdystrophin [also known as SRP-9001] (Nationwide Children's/ Sarepta Therapeutics) NCT03375164 NCT03769116	• Phase 1/2 open-label study enrolled 4 DMD subjects with no placebo group dosed with $2x10^{14}$ vg/kg. • Reported no serious adverse events in the study to date. • Whilst three patients had elevated liver enzyme gamma-glutamyl transpeptidase, steroid treatment resolved this. • Patients are being recruited for placebo-controlled phase 2 trial.	An average of 3.3 copies of the therapeutic gene were present per nucleus and western blot data showed mean microdystrophin expression of 95.8% versus normal after adjusting for fat and fibrotic tissue. Immunohistochemistry data showed 81.2% of dystrophin-positive fibers. Improvements in North Star Ambulatory Assessment (NSAA) score seen in all 4 patients (mean of 5.5) (Mendell et al, 2020). No functional improvement seen from NSAA in Phase 2 trial (Mullard, 2021).

[4] Table created using data from PPMD 2019 Conference presentations by Genevieve Laforet (Solid Biosciences), Michael Binks (Pfizer) and Doug Ingram (Sarepta).

The idea of microdystrophin gene transfer therapy is to reduce the size of the *DMD* gene as much as possible so that the miniaturised gene can be accommodated in AAVs; at the same time maintaining crucial domains of the protein that provide functional benefits in patients. This resulted in generation of multiple microdystrophin constructs, some of which have provided more clinical benefit than the others (discussed above). It is however important to note that these microdystrophins are unlikely to provide the full protections that are provided by the full-length, wild-type dystrophin. A workshop report published by leading DMD clinicians in the UK (Heslop et al, 2021) also argues that referring the phenotype of DMD patients following treatment as 'turning Duchenne into Becker' is also incorrect scientifically as BMD patients are able to produce semi-functional dystrophin protein without any intervention and new nuclei of BMD patients are able to produce such semi-functional dystrophin protein. On the other hand, in DMD patients treated with AAVs carrying microdystrophin gene, only the transduced nuclei will express the semi-functional truncate dystrophin protein and the cycles of muscle degeneration and regeneration will 'dilute' the vector genome because the vector genome is nonintegrating. As such, whether to acknowledge the benefits provided by microdystrophin as 'cure for DMD' remains a controversial topic.

1.3 Adeno-associated virus (AAV) as a gene delivery vector

1.3.1 AAV journey from bench to bedside

Originally discovered by accident in the preparation of simian adenovirus (Atchison *et al*., 1965), AAV was soon found to be present in human tissues (Blacklow, Hoggan & Rowe, 1967). The nursery population (infants six months to three years of age) at Junior Village, Washington D.C. that experienced frequent infection with various adenovirus serotypes provided the opportunity to isolate and characterise AAV strains of human origin (Blacklow, Hoggan & Rowe, 1967). The journey of understanding the basic biology of AAV was driven purely by scientific curiosity, at a time when the potential of this virus as a gene therapy vector was unknown (Wang, Tai and Gao, 2019). The following quote from Professor Kenneth Berns in 2013 epitomises early studies in the field which were considered somewhat not worth pursuing, later turned out to be fundamental in moving the field of gene therapy forward.

".....skeptics wondered why I was wasting my time working with it and suggested that AAV really stood for "almost a virus." Of course, time has shown that the joke was on the critics; today, AAV is one of, if not the most widely used vector for gene therapy. Success in using the virus in this way has required a detailed understanding of the molecular mechanisms underlying the biology of the virus. This is a classic example of the value of basic research leading to applicability in the real world."

In 1984, nineteen years after first discovery, AAV was vectorised for the purpose of gene transfer (Hermonat and Muzyczka, 1984). Eleven years following this, the viral vector was first used in a cystic fibrosis human patient in 1995 (Flotte et al, 1996). Fast forwarding the timeline, the EMA approved the first AAV-based gene therapy drug Glybera for the treatment of lipoprotein lipase deficiency in 2012 (Ylä-Herttuala, 2012), followed by the approval of Luxturna by the FDA in 2017 for the treatment of inherited retinal disease (Utz et al, 2018)

and another FDA approval of Zolgensma in 2019 for the treatment of spinal muscular atrophy (Hoy, 2019).

1.3.2 Genetics, biology and structure of AAV

AAV is a small (~26 nm in diameter), non-enveloped virus with linear, single stranded DNA genome (Mingozzi and High, 2017). The approximately 4.7 kb long genome of wild-type AAV consists of the *rep* and *cap* genes flanked by two inverted terminal repeats (ITRs) and is packaged within a non-enveloped capsid (Figure 1.16) (Kotterman and Schaffer, 2014).

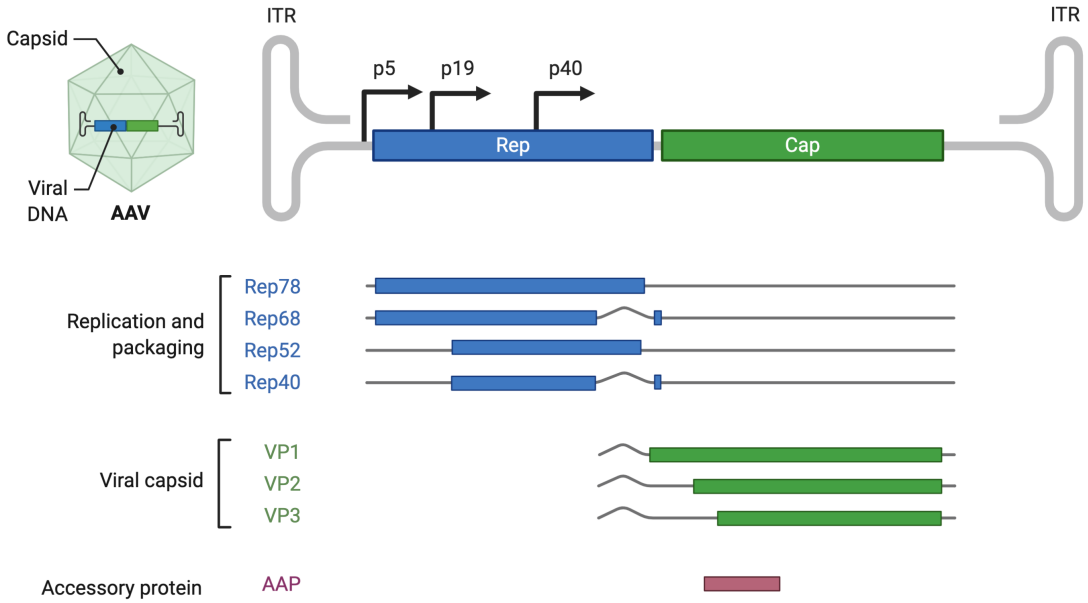

Figure 1.16 **AAV genome**. The rep gene, controlled by three promoters; p5, p19 and p40 codes for four non-structural proteins essential for the viral genome replication; rep78, rep68, rep52 and rep40. The cap gene codes for three structural proteins; VP1, VP2 and VP3 that form the viral capsid components. Assembly of the capsid is also dependent on the presence of assembly-activating protein (AAP) which is coded by an alternative open reading frame on the cap gene (Kotterman and Schaffer, 2014).

Using two promoters, p5 and p19, and alternative splicing, the *rep* ORF encodes four *rep* proteins. Rep68 and Rep78 are required for AAV replication and demonstrate DNA binding, endonuclease and helicase activities (Pasquale and Stacey, 1998). Whilst the Rep 52 and Rep 40 do not bind DNA directly, the two proteins that correspond to the C-terminal regions of Rep 78 and Rep 68 respectively seem to be essential in the accumulation and encapsidation of single-stranded genomes (Pasquale and Stacey, 1998). The *cap* ORF encodes VP1, VP2 and VP3 under the control of the p40 promoter. VP1, VP2 and VP3 proteins coded by the *cap* ORF are produced at a stoichiometric ratio of 1:1:10, where 60 capsid protein subunits assemble into an AAV capsid in a T=1 icosahedral symmetry (Sonntag, Schmidt and Kleinschmidt, 2010). An alternative ORF of the *cap* encodes for the assembly-activating protein (AAP) and this gene product of AAV is required for assembling the capsid (Kotterman and Schaffer, 2014).

AAV is a member of the Dependoparvovirus family and requires helper viruses such as adenovirus or herpes simplex virus to successfully infect and replicate in the host cell (Wu, Asokan and Samulski, 2006). The human parvovirus is endemic in a large percentage of the world population but is non-pathogenic and has never been known to cause any human disease (Smith, 2008). In the absence of a helper virus, latent infection is established where the AAV genome is either integrated into the host genome in a site-specific manner, or by existing in episomal forms (Samulski et al. 2015) (Figure 1.17). This main specific site of AAV integration is unique to chromosome 19 in the human genome (Kotin et al, 1990) and is called AAVS1, where the genome integration is mediated by specific DNA sequence on chromosome 19 (Giraud, Winocour and Berns, 1994). Expression of at least one of the initiator proteins, Rep68 or Rep78 is required to mediate the site-specific integration of AAV into chromosome 19 (Pasquale and Stacey, 1998; Smith, 2008). In the absence of AAV Rep proteins, AAV is not targeted to AAVS1 (Smith, 2008), and so the AAV-derived vectors used for gene transfer generally do not integrate, but remain episomal in the host cell nuclei.

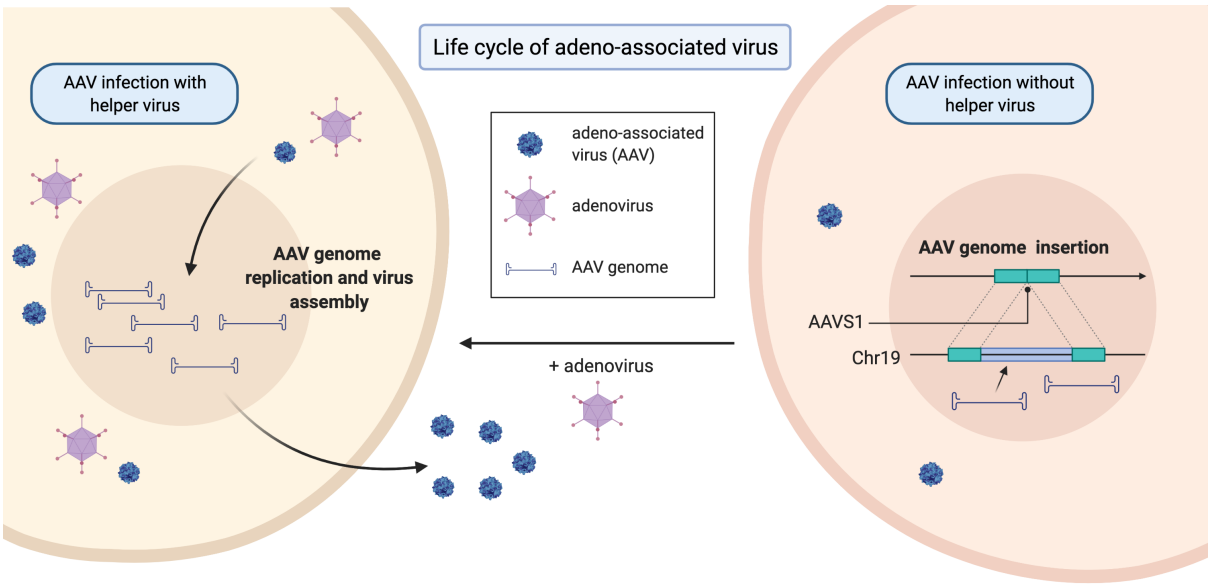

Figure 1.17 **AAV life cycle**. Being a member of the Dependoparvovirus, AAV requires helper viruses such as Adenovirus to facilitate infection and replication (Wu, Asokan and Samulski, 2006). In the absence of helper viruses, AAV integrates its genome into a specific integration site in human chromosome 19 at a locus designated AAVS1; where the latent AAV genome remain quiescent until a favourable replication condition arises which is usually the encounter of helper viruses Samulski et al. 2015.

1.3.3 Diversity and tropism of AAVs and derived rAAV vectors

The diversity and occurrence of multiple AAV serotypes in human and non-human primate tissues were first elucidated by studies performed by (Gao et al, 2004) (Figure 1.18). Wu, Asokan and Samulski, 2006, defined a new serotype as *"a newly isolated virus that does not efficiently cross-react with neutralizing sera specific for all other existing and characterized serotypes"*. Epidemiological studies show that 40-80% of the human population have circulating antibodies against one or other AAVs indicating previous exposure to the virus and seroepidemiological studies have shown that some AAV serotypes such as AAV1, AAV2, AAV3, AAV5, AAV6, AAV7, AAV8 and AAV9 are endemic to humans (Wang, Tai and Gao, 2019). Patients who receive AAV based gene therapy products are often screened and excluded if they test positive for the circulating antibody against the AAV serotype that the particular therapeutics is based on, and as such, this prevalence of the non-pathogenic virus in the human population could be a limitation in determining the subset of patients that could receive AAV gene therapy treatments. Therefore, the discovery of new serotypes of AAV is not limited to natural discovery, and scientists have produced many other AAV capsids (serotypes) that were engineered for specific properties (Table 1.6).

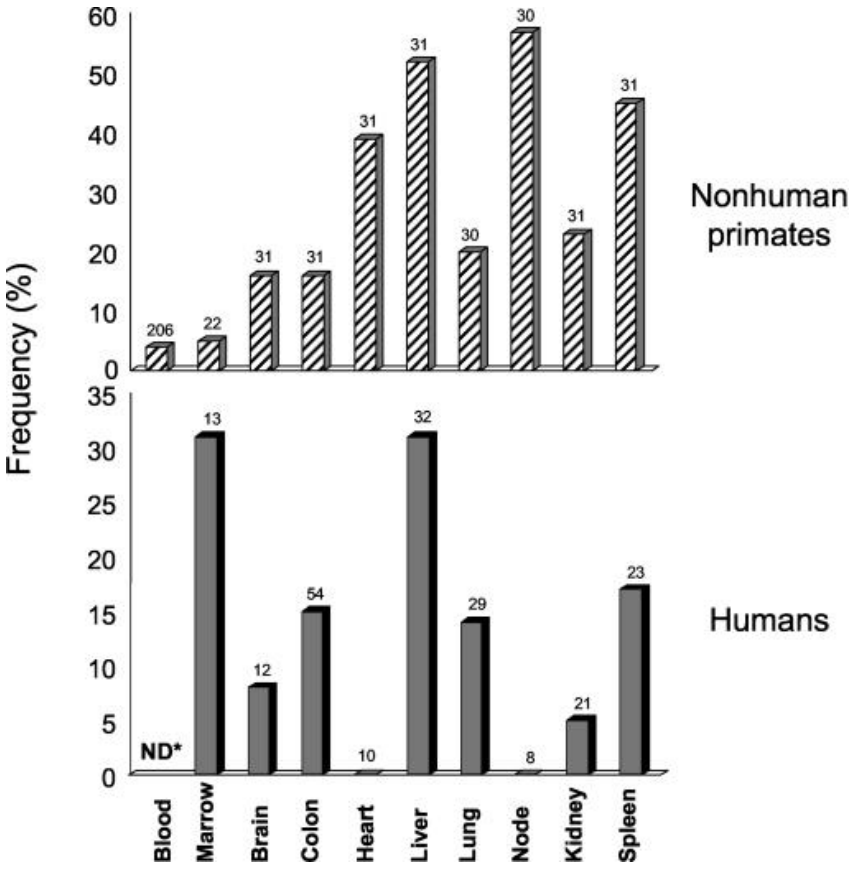

Figure 1.18 **Distribution of AAV genome in human and non-human primate tissues**. The number at the top of each bar represents the total number of samples examined for the particular tissue. AAV is present in high frequencies in liver and spleen in both human and non-human primates, and also are found in abundance in marrow of humans and lymph nodes of non-human primates (Gao et al., 2004). Figure adapted from Gao et al., 2004. Such prevalence of the virus in human and non-human primate tissues led to multiple AAV serotypes being discovered and characterised. Some of the serotypes that were isolated from specific tissues also show high level of tissue specificity for the tissues they were isolated from.

To enter the host cell, most viruses bind to a generalized receptor via the viral attachment protein and this mediates the interaction with a co-receptor that is more cell specific (Kalia and Jameel, 2011). As shown in Table 1.5, proteoglycan conjugates are used as primary receptor by AAVs to facilitate attachment to the cell membrane (Nonnenmacher and Weber, 2012).

Table 1.5 Glycan receptor and co-receptors for AAV serotypes 1-9.

Virus	Glycan receptor	Co-receptor
AAV1	N-linked sialic acid	Unknown
AAV2	HSPG	FGFR, HGFR, LamR, CD9 tetraspanin
AAV3	HSPG	FGFR, HGFR, LamR
AAV4	O-linked sialic acid	Unknown
AAV5	N-linked sialic acid	PDGFR
AAV6	N-linked sialic acid, HSPG	EGFR
AAV7	Unknown	Unknown
AAV8	Unknown	LamR
AAV9	N-linked galactose	LamR

Abbreviations: EGFR, epidermal growth factor receptor; FGFR1, fibroblast growth factor receptor 1; HGFR, hepatocyte growth factor receptor; HSPG, heparan sulfate proteoglycan; LamR, laminin receptor; PDGFR, platelet-derived growth factor receptor. Table adapted from Nonnenmacher and Weber, 2012.

Variations between studies pose difficulties in establishing AAV serotype tissue tropism (Wu, Asokan and Samulski, 2006). The tropism of the viral capsids are largely due to presence of respective viral receptors on target cells, which varies largely between species (Keeler and Flotte, 2019). The difference in receptor expression between species causes variations in potency of different AAV capsid (which is sometimes overlooked). With this consideration in mind, different capsid serotypes have been selected or proposed for experiments or clinical trials targeting different tissues based on *in vivo* efficacy (Keeler and Flotte, 2019).

Table 1.6 Overview of tissue and species tropism of rAAV gene therapy vector serotypes currently utilized in pre-clinical and clinical applications.

Organ	Mouse	Other large animal	Nonhuman primate	Human
Central nervous system	AAV9, AAVrh10, AAVrh8, AAV2, AAV5, ANC80L65, AAV-PHP.B	AAV9, AAVrh10, AAVrh8, AAV5	AAV9, AAVrh10, AAVrh8, AAV5	AAV2, AAV9, AAVrh10, AAVrh8
Liver	AAV8, AAV9	AAV8, AAV5	AAV8, AAV9, AAV3B	AAV2, AAV5, AAV8, AAV9, AAV3B
Lung	AAV5, AAV6, AAV8, AAV1, AAV6.2, AAV6.2FF, AAVrh10, AAV2-ESGHGYF	AAV5, AAV2/HBoV1	AAV1, AAV5, AAVrh10	AAV2
Muscle	AAV1, AAV8, AAVrh74, AAV9, AAV-B1	AAV1, AAV8, AAVrh74, AAV9	AAV1, AAV8, AAVrh74, AAV9	AAV1, AAVrh74, AAV8, AAV9, AAV2.5
Retina	AAV2, AAV5, AAV7, AAV8, AAV9, ANC80L65	AAV2, AAV5	AAV2, AAV5, AAV9, ANC80L65	AAV2, AAV4, AAV5

Table adapted from Keeler and Flotte, 2019.

Despite the potential of AAV in gene therapy, the different serotypes of AAV show varied transduction efficiencies in vivo (Zincarelli *et al.*, 2008). As such, in the case of DMD for instance, the AAV serotype with the best muscle tropism remain elusive. From the point the AAV attaches itself to the host cell membrane till crossing the nuclear membrane (Figure 1.19), several complex steps are involved and it has been shown that transduction efficiency is highly dependent on the post-attachment steps involving endosomal escape or nuclear import (Nonnenmacher and Weber, 2012).

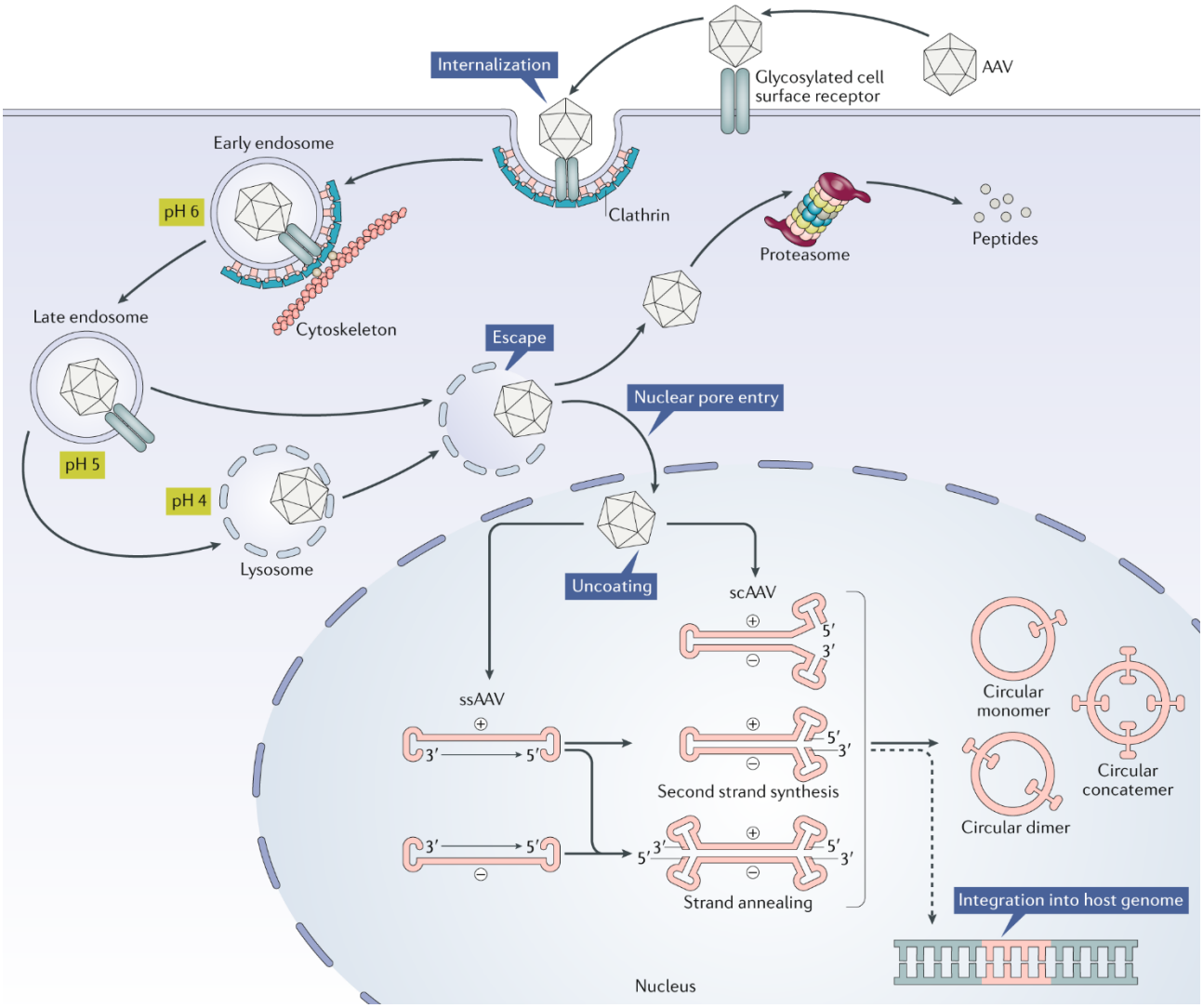

Figure 1.19 **Proposed model of transport of AAV in the cell**. AAV binds to the receptor or co-receptor complex which in turn mediates endocytosis via clathrin-mediated pathway. The virus particles are transported via early endosomes and then, late endosomes. As the pH of the compartment in which AAVs reside continue to drop (possibly due to accumulation of H^+ in the endosomes), AAV capsid undergoes modification where a specific domain: phospholipase A2 (PLA2) domain are exposed causing release of AAV into the cytoplasmic space, and subsequently transported into the nucleus via the nuclear pore complex (Nonnenmacher and Weber, 2012). In the nucleus, the capsid accumulate in the nucleolus first before moving to the nucleoplasm where uncoating and release of viral genome takes place (Nonnenmacher and Weber, 2012). The AAVs that failed to enter the nucleus are degraded by proteasomes in the cytoplasm. Two types of AAV vector genomes are currently used in AAV gene therapy: single-stranded AAV (ssAAV) and self-complementary AAV (scAAV). ssAAV genomes

are packaged into AAV either as sense (plus-stranded) or anti-sense (minus-stranded) genomes. Therefore, the ssAAV genome require a second strand synthesis when they reach the nucleus as the single-stranded genome is transcriptionally inert. The host cell DNA polymerase can synthesise the second strand or two single stranded genomes of plus- and minus-strand can anneal. scAAVs are transcriptionally active as the genome are already double-stranded by design, and as such can undergo transcription immediately. AAVs do not usually integrate into the host genome, however the possibility of such event should not be completely ruled out. So far, no such integration have been reported in humans. rAAV genome however, remain as episomes in the nucleus and this is possible as the inverted terminal repeats (ITRs) present in the rAAV genome can drive inter-molecular or intra-molecular recombination to form circularized episomal genomes: either as circular monomer, dimer or concatemer (Wang, Tai and Gao, 2019). Figure adapted from Wang, Tai and Gao, 2019.

1.3.4 Replication-defective recombinant AAV as a gene transfer vector

A breakthrough in the AAV gene therapy field came when (Samulski, Chang & Shenk, 1989) described a method for the production of recombinant AAV (rAAV) using two plasmid system, where the final stock contained no wild type AAV (wtAAV). In this system, the *rep* and *cap* genes of the wtAAV genome are replaced with a so-called gene-of-interest (GOI) to produce rAAV (Kotterman and Schaffer, 2014). The AAV ITRs are retained and are required *in cis* for replication and packaging of rAAV (Flotte, 2004a): as such, the ITRs tend to be the only sequences of wtAAV origin that are incorporated into rAAV (Wang, Tai and Gao, 2019). The *rep, cap* and helper virus genes are provided *in trans* (Flotte, 2004a). rAAV are able to transduce target cell populations which express appropriate receptors (Table 1.5), but due to the absence of *Rep* gene products, rAAVs do not undergo site-specific integration in the human chromosome (Flotte, 2004b). The rAAV genomes in transduced cells and tissues remain in episomal form and have been shown to form circular monomeric, dimeric and concatemeric structure.

A very robust and popular method of rAAV production is via plasmid transfection of adherent human embryonic kidney 293 (HEK293) cells, where the transgene in between ITRs are delivered in *cis* and the *rep*, *cap* and helper genes are delivered in *trans* (Wang, Tai and Gao, 2019). A modified version of this method is suspension culture of HEK293 that allows rapid production of rAAV and scaling-up the yield which are essential in clinical applications (Grieger, Soltys and Samulski, 2016). Following production, rAAVs are purified via either column chromatography or gradient centrifugation; and it is worth mentioning that the purity differs based on the method used which can impact the outcome of preclinical and clinical studies (Colella, Ronzitti & Mingozzi, 2017).

1.4 Safety and effectiveness of rAAV-mediated gene therapy.

rAAV-mediated gene therapy substances like vectors and modified cells are classified as advanced therapy medicinal products (ATMPs). Regulatory bodies such as the Medicines and Healthcare products Regulatory Agency (MHRA) and European Medicines Agency (EMA) define ATMPs as "medicines for human use that are based on genes, tissues or cells". Whilst translating ATMPs from bench to bedside has been possible and successful in many settings (Ylä-Herttuala, 2012; Utz et al, 2018; Hoy, 2019), many issues of safety and efficacy still remain to be tackled that mainly revolve around the areas of (1) immunogenicity, (2) potency and efficacy, (3) genotoxicity, and (4) persistence (Colella, Ronzitti & Mingozzi, 2017).

(1) Vector immunogenicity: Neutralizing anti-capsid antibodies limit the number of virus that eventually are available for transduction. Cells that have been transduced by AAV present the AAV capsid antigens loaded on major histocompatibility complex class I molecule (MHC-I) complexes; and these cells elicit cytotoxic CD8+ T cell responses.

(2) Genotoxicity: Whilst being very rare, there is also a concern that integration of the AAV vector DNA in the genome may have genotoxic effects.

(3) Persistence: Since AAV vector genomes mainly exist in episomal forms in the nucleus of the transduced cells, therapeutic efficacy can be lost in highly proliferating cells.

(4) Potency and efficacy: Therapeutic dose and therapeutic efficacy of the treatment depends on the efficiency of AAV vectors at infecting and transducing target cells.

1.4.1 Immunogenicity

Whilst mouse models have been extremely useful in proof-of-principle studies, some of them, in particular in-bred mouse strains fail to capture the magnitude of potential immune responses caused by AAV delivery, and often times have minimised safety concerns. In fact, low immunogenicity is often cited as an advantage of rAAVs but this is simplistic and misleading: innate and adaptive immune responses to wtAAVs and rAAVs, both humeral and cell-mediated, are well documented (Ronzitti, Gross and Mingozzi, 2020; Verdera, Kuranda and Mingozzi, 2020). AAV seropositivity associated with neutralising antibodies (NAbs) is highly prevalent in human populations (~80%) due to natural exposure to the virus (Xie *et al.*, 2002; Arruda and Xiao, 2007).The first barrier posed by the immune system against rAAV capsids similar to wtAAV is thus pre-existing neutralising antibodies (NAbs) which will reduce or eliminate the dose-effectiveness of gene delivery by rAAV.

Vector immunogenicity could however also arise from cells that have been successfully transduced by rAAV, where the rAAV capsid or indeed transgene antigens are displayed on the MHC-I complex, eliciting cytotoxic $CD8^+$ T cell response (Colella, Ronzitti & Mingozzi, 2017). In this case elimination of transduced cells and tissue damage may occur. Experiments involving mouse models have generally not documented such cytotoxic effects, but in larger animal models such as dogs and NHPs however, AAV capsid and transgene product do often elicit significant cytotoxic T cell responses (Wang *et al.*, 2011). Thus, outbred larger animal models are important and more sensitive models to evaluate potential adverse adaptive immune responses against rAAV gene therapies.

Systemic AAV gene delivery of high doses of ~10^{13} to 10^{14} vector genomes/kg have also been shown to elicit the activation of the innate immune response in large animal models. In dystrophin-deficient neonatal dog model, two puppies treated at 4-days-old in an AAV microdystrophin gene therapy study had to be euthanised at 16 weeks of age due to toxicity related to innate immune

responses; showing early inflammatory response following vector delivery (Kornegay et al, 2010). Another alert came from studies in juvenile non-human primates (NHPs) and piglets, where all three piglets in one study, and one NHP in the second were euthanised due to observed toxicity: the remaining two NHPs in the latter demonstrated elevated level of transaminase (liver enzyme) and thrombocytopenia (platelet deficiency in blood) (Hinderer et al, 2018). It is also important to note that none of these studies have clearly demonstrated strong evidence supporting a cellular immune response (that involves cytotoxic T-lymphocytes); pointing to activation of innate immune response as the cause for the toxicities observed (Duan, 2018).

The exact factors that modulate the degree of immunogenicity of AAV vectors are still unclear, but the likelihood of AAV causing an immune response is high and should not be underestimated (Mingozzi and High, 2013). If AAV vector delivery elicits cytotoxic T lymphocyte (CTL)-mediated immune responses (Figure 1.20), this would cause short-lived transgene expression (Prea *et al.*, 2015). This CTL-mediated immune response following AAV transduction leading to clearance of transduced cells would pose a problem in the clinical setting as efficient gene therapy requires stable, long-term expression of the therapeutic gene (Wang, Tai and Gao, 2019; Mingozzi and High, 2013). AAVs can be targeted to the muscles by direct delivery (intramuscular injection) or transcriptionally targeted following systemic delivery (where the AAVs can end up in many other tissues such as liver but the transgene product may be highly localised to muscle due to use of tissue restrictive promoters). In the case of AAVs targeted to the muscles where regulatory T (T_{reg}) cells play a role in suppressing the effect of CTLs, the effects of CTL-mediated immune response may not be as detrimental as in other tissue sites (Mueller et al, 2013). Mueller et al, 2013, reported persistent, long-term transgene expression for up to 12 months in humans and as such, immunomodulation of T cell populations may not be needed for transcriptionally-targeted AAV gene delivery to skeletal muscle. In addition, healthy skeletal muscle cells have low expression of MHC I and this could also contribute to the reduced T-lymphocyte mediated immune response (Mingozzi and High, 2013). In

another clinical case, muscle biopsy samples from a patient with severe haemophilia B, that was injected with human factor IX-encoding AAV tested positive for factor IX, 10 years post-treatment, indicating long-term expression of the transgene in the skeletal muscle (Buchlis *et al.*, 2012).

Following AAV administration, an innate immune system response can also be provoked via the toll-like receptor 9 (TLR9)-MyD88 pathway (Rogers et al, 2011). The hyper-activation of the TLR9-MyD88 pathway in response to high rAAV dosage could also result in a so-called cytokine storm that induces the production of type I interferons and can be a dangerous clinical situation (Uematsu and Akira, 2007). TLR9 is a pathogen recognition receptor (PRR) that binds to unmethylated CpG islands that are often found in abundance in codon-optimised AAV vector genomes (Wright, 2020). Codon-optimisation is the process of optimising the mRNA sequence for enhanced translation (discussed in detail in Section 1.4.4). TLR-9 binds to double-stranded DNA and as such, there is a possibility that single-stranded AAV genomes may not provoke a strong, deleterious TLR-9 induced immune response. Self-complimentary genomes (Figure 1.19) that are double stranded are shown to cause a stronger TLR9-dependent immune response in a dose-dependent manner (Martino et al, 2011). Such dose dependent innate immune responses are pro-inflammatory and can thus contribute to the initiation and strength of subsequent adaptive immune responses against the viral capsid but not necessarily against the transgene (Martino et al, 2011). Active design of rAAV vector genome sequences to minimise or eliminate CpG islands (Faust et al, 2013) and/or induced CpG methylation via novel vector production and processing strategies could alleviate innate immune responses against AAV (Wright, 2020).

The barrier posed by NAbs can potentially be overcome by some of the strategies currently being developed such as plasmapheresis, capsid engineering and using empty capsids as decoys (Wang, Tai and Gao, 2019). Nevertheless, excluding seropositive patients from the trials is the only current strategy to avoid issues related to NAbs (Duan, 2018). In the case of DMD (and in many other diseases

treated by AAV gene therapy such as inherited blindness and haemophilia), glucocorticosteroids (GCs) that are widely used anyway as standard of care in DMD (Matthews et al, 2016) also help in managing some of the immune system complications through the immunomodulatory activities of these drugs (Rosenberg et al, 2015).

1.4.2 Genotoxicity

Genotoxicity arises when genetic information within a cell is damaged causing mutations that are potentially cancer-causing. In gene therapy clinical trials, insertional oncogenesis (leukaemia in the main) caused by chromosomal insertion of retroviral and lentiviral vector genomes has been a major issue, with several important examples studied in detail. By and large insertional oncogenesis arises by effects of strong vector promoter-enhancer sequences integrated in the vicinity of oncogenes, and where target cell populations are undergoing intense chronic proliferation (eg the haematopoietic stem cell pool). Despite the predominantly episomal nature of rAAV-derived genomes in target cells, there remains a possibility of limited chromosomal integration of AAV genome sequences into the genome of transduced host tissue and hence of insertional mutagenesis and genotoxicity leading to unwanted secondary disease such as cancer. Concerns regarding genotoxicity emerged as there seemed to be a dose-dependent correlation between AAV gene delivery and hepatocellular carcinoma (HCC) in particular mouse disease models, indicating that increasing the AAV dosage could increase genotoxicity (Chandler *et al.,* 2015). Theoretically, both the wtAAV and rAAV containing transgene could integrate part of their genome into the host genomic DNA, triggering the formation of HCC by activating the expression of proto-oncogenes (Russell & Grompe, 2015). This genotoxicity seems more prominent in rodent models and such risk was not very much evident in larger animal models such as dogs and nonhuman primates (Colella, Ronzitti & Mingozzi, 2017). Patients in human clinical trials for haemophilia B that have received AAV gene therapy for >9 years post gene transfer have not developed any tumors so far (Nathwani et al, 2014). Studies

investigating integration events that originated from rAAV genome have also reported no genotoxicity of systemically administered rAAV in non-human primates and humans (Gil-Farina et al, 2016). Although no genotoxic safety concern has been raised so far in humans, this is a risk that should be overseen and extended periods of follow-up in gene therapy trials and in authorised ATMPs is still warranted (Colella, Ronzitti & Mingozzi, 2017).

1.4.3 Persistence

In the majority of cases, stable, long-term transgene expression is a desirable outcome in achieving therapeutic efficacy following AAV gene therapy. This is particularly important in chronic diseases such as DMD that requires continuous expression of the corrective transgene product (modified dystrophin in the case of DMD). Loss of transgene expression over time may arise from immune elimination of transduced cells, from loss of episomal transgene during cell division, or transcriptional silencing. Varied capsids and tropism, vector genome sequence modifications and immunosuppression or immunomodulation may help reduce or prevent loss of transgene expression in the course of gene therapies due to deleterious immune responses (Keeler and Flotte, 2019). The loss of episomal AAV transgenes during cell division may not be important in post-mitotic and slowly replicating adult tissues. In the liver, with a cellular turnover half-life of ~8 weeks, AAV-delivered transgene persistence is observed for years (Nathwani et al, 2014). This may require invocation of hypothetical transgene replication or integration to be explained. However, in practice, in translating observations from studies in animal models to humans, it is essential to note the difference in turnover rates of different tissues in different species. In DMD, considering the need for body-wide skeletal muscle gene delivery, growth of muscle tissues over development, and normal or pathological muscle degeneration-regeneration cycles, it is very likely that repeat administration will be needed.

1.4.4 Potency and efficacy

For AAV gene therapy to be efficacious and therapeutic in nature, persistent, long-term transgene expression is necessary. As discussed above in Section 1.4.1, high vector doses in AAV gene therapy can potentially elicit undesirable immune responses, however, such high doses may also be necessary and effective in rescuing the disease phenotype (Kornegay et al, 2010). AAV gene therapy in a canine model of X-linked myotubular myopathy (XLMTM) showed great improvements in muscle strength and survival of the dogs in a dose-dependent manner, where the highest survival was observed in the group receiving the highest dose of rAAV expressing the therapeutic gene myotubularin (MTM1) (Mack *et al*., 2017). However, as discussed in Section 1.4.1, high capsid dose could also trigger unwanted immune response. Therefore, a balance needs to be achieved between the vector (capsid) dose and therapeutic efficacy for a good clinical outcome (Figure 1.20) (Mingozzi and High, 2013). Recent human clinical trial of XLMTM utilising AAV8 reported three deaths in the high dose group powerfully reinforcing the crucial need for carefully managing vector dose for safety and therapeutic efficacy (Keown, 2020). It is also a reminder that both in positive and sadly negative senses the most valuable data in the field of gene therapy are indeed derived from human studies, as pre-clinical studies pose some limitations in capturing the full effects, both wanted and unwanted, of a treatment.

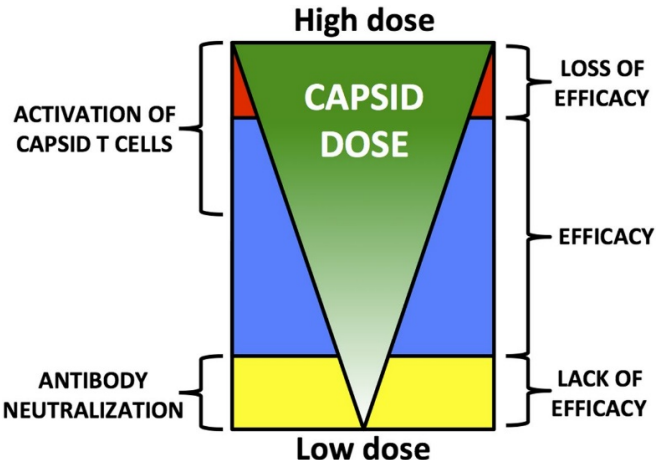

Figure 1.20 **Model of therapeutic efficacy based on capsid dose following systemic AAV vector delivery**. At a lower dose of AAV, NAb activity diminishes the efficacy of treatment. On the other hand, a very high vector dose may trigger the activation of T cells against the viral capsid. There is still a small overlap between the activation of T cells and treatment efficacy, but above a certain critical threshold, the immune response elicited by the T cells results in significant loss of efficacy. It is therefore essential to remain within the narrow range in the middle when choosing a capsid dose for maximum efficacy (Mingozzi and High, 2013). Figure adapted from Mingozzi and High, 2013.

In the context of DMD gene therapy, intramuscular and systemic administration of codon-optimized microdystrophin cDNA gene constructs was shown to potentially increase transgene expression compared to non-codon optimised or wild type forms in mdx mice (Foster *et al*, 2008). The genetic code consists of 64 nucleotide triplets (codons) and code for specific amino acids. The twenty amino acids are specified by 61 triplets and 3 codons serve as stop codons. Only methionine and tryptophan are coded by single codons and the rest of the 18 amino acids are coded by 2, 3, 4 or 6 codons. The degeneracy of the genetic code results in bias in codon usage where some codons are preferred over the other to code for the same amino acid and this frequency of codon usage is thought to affect protein expression. The codon usage differs between species and as such, codon optimisation takes into account this codon usage bias to elevate protein expression by improving the efficiency of translation.

In the process of codon-optimization, the GC content was significantly increased from 45–46% to over 60% (Foster *et al*, 2008). This increase in GC content is essential to promote the stability of mRNA as the A+U-rich cis-acting sequences activate rapid mRNA decay (Murray and Schoenberg, 2017). However, as reviewed in Section 1.4.1, the CpG sequences that are often found in abundance in codon optimised vector genomes could provoke a deleterious immune response via the TLR9-MyD88 pathway (Rogers et al, 2011). The 'p' in 'CpG' refers to the phosphate group linking the two bases. As such, this process of optimising the mRNA sequence for enhanced translation should be proceeded with caution, ensuring no CpG islands are introduced in the process which could trigger an immune response.

In terms of rAAV capsid choice, AAV8 and AAV9 serotypes have shown better muscle tissue transduction over the other known AAV serotypes, and hence are widely used in development of gene therapy for muscle diseases (Mack *et al.*, 2017; Le Guiner *et al.*, 2017; Solid Biosciences [NCT03368742], 2017; Pfizer [NCT03362502], 2018). AAVrh74 is a serotype isolated from nonhuman primate that exhibits affinity for skeletal muscles and as such has been utilised in human gene therapy for DMD; with the hope that there will be reduced likelihood of patients exhibiting pre-existing immunity to the vector (Mendell et al, 2020). Care should also be taken as some AAV serotypes that efficiently transduce tissues in a specific transgenic mouse may not show similar transduction profile in another mouse strain, non-human primates or humans potentially due to molecular differences between the strains/ species (Hordeaux et al, 2018) (refer to Table 1.6). Many groups are also working to generate myotropic and/ or liver detargeted AAVs which may exhibit important improvements for clinical applications in muscle diseases (Weinmann et al, 2020).

In the case of muscle gene transfer, previously, the most commonly utilized route to administer AAV vectors is via direct intramuscular (IM) injection (Wang *et al.*,

2011). Multiple studies however have shown that large doses of vectors injected at one site such as the muscle can potentially trigger immune response against the transgene (Boisgerault and Mingozzi, 2015). The route of delivery is changing over the years as human clinical trials are currently being planned and conducted using systemic intravascular (IV) administration to deliver the gene therapy products (Le Guiner *et* al., 2017; Kornegay *et al*., 2010; Chamberlain and Chamberlain, 2017). IV route of vector delivery enables body wide transduction that is essential in muscle gene therapy, however, a large vector dose delivered systemically would expose the vectors to NAbs in the circulation and as such could then trigger immune response towards the viral capsid (Boisgerault and Mingozzi, 2015). Careful planning of the vector dose is therefore essential (discussed above) (Figure 1.20).

In addition, the use of a strong muscle-restrictive promoters such as the Spc5.12 and MCK, have also been proposed to target expression of the microdystrophin transgene in muscle and heart tissues (Li *et al*., 1999; Foster *et al*, 2008; Le Guiner *et al*., 2017). The Spc5.12 is an artificial hybrid promoter generated from random assembly of several myogenic regulatory elements including E-box, MEF-2, TEF-1 and SRE sites in synthetic promoter recombinant libraries (Li *et al*., 1999). This particular element had strong transcriptional activity in vitro and in vivo often exceeding the potencies of natural myogenic and viral gene promoters (Li *et al*., 1999). Other muscle-specific promoters that have been utilised in DMD gene therapy include CK7 promoter [Sarepta Therapeutics clinical trial] that also exhibits enhanced cardiac expression (Mendell et al, 2020) and CK8 promoter [Solid Biosciences clinical trial] (Hakim et al, 2017). These muscle creatine kinase (MCK) derived promoters have been developed from the work of Hauschka and colleagues over many years (Hauser et al, 2000).

Polyadenylation (polyA) signals also play a critical role in transgene expression, particularly in nuclear export, translation and mRNA stability. The SV40 late polyA from Simian virus 40 is one of the strongest polyA signals relative to all other commonly used polyA signals in gene expression constructs (Powell,

Rivera-Soto and Gray, 2015). The SV40 late polyA signal contains a short upstream element sequence (UES); sequences between 13 and 51 nucleotides upstream of the AAUAAA that increases efficiency of transgene expression (Schek, Cooke and Alwine, 1992). The UES also has the capability of increasing transgene expression efficiencies of weak polyA signals when used in tandem (Choi et al, 2014). Nevertheless, the SV40 late polyA signal remains one of the strongest known polyAs with an advantage of being slightly shorter (135 bps) compared to the next best polyA in terms of relative strength that is bovine growth hormone poly A which is 250 bps in length (Powell, Rivera-Soto and Gray, 2015). The sizes of the individual gene expression elements are important in the context of AAV gene therapy as wild-type AAV has a packaging capacity of 4.7 kb and keeping the ITR to ITR length close to 4.7 kb would be ideal to ensure genome integrity during packaging into AAV. As such, a shorter polyA has an added advantage in this case, especially when a large transgene is involved.

1.5 Enhancing transgene potency using a regulatory element

1.5.1 Enhancing transgene expression from rAAV vectors using engineered intron

AAV-mediated gene therapy efficacy requires appropriate levels and duration of transgene expression. Whilst appropriate therapeutic levels of transgene expression and gene therapy efficacy may be achieved via dose-ranging studies and dose escalation (Mack *et al*., 2017), it is also generally accepted that increased vector dosage enhances the risks of adverse clinical events or undesirable immune responses leading to loss of transduced cells, loss of transgene expression and reduced gene therapy efficacy (Mingozzi and High, 2013). From a practical level, very high AAV vector dose levels if required may lead to operational and cost-effectiveness challenges for the manufacture of clinical grade vector both pre- and post- regulatory approval. One potential route to reduce or minimise the vector dose required for gene therapy to be effective may be to alter transgene sequence or configuration to enhance transcription, translation or RNA stability, or indeed to reduce immunogenicity (Colella, Ronzitti and Mingozzi, 2017). It must be also born in mind, however, that overexpression of any particular transgene product could in itself lead to unwanted cytotoxic effects, perhaps a proteinopathy for example (Hetz, 2012). This possibility may be especially the case with mononucleated cells (for example in lung, liver, CNS), but also remains a potential issue in multinuclear cells like skeletal myofibres, as in the situation of DMD gene therapy (Discussed in Section 4.1).

Turning to DMD, for a gene therapy treatment to be wholly effective in the widest sense, delivery of active microdystrophin transgene systemically to skeletal muscles throughout the body and to the heart is desirable. Indeed, expression of relevant isoforms in appropriate CNS and smooth muscle cells would also be desirable if it could be achieved as patients suffer from severe gastrointestinal issues as they transition into adulthood and a proportion of patients experience cognitive deficits and mental health issues (Birnkrant et al, 2018). Efficient widespread systemic transduction of skeletal muscle by AAV

vectors appears to require high doses of vector delivered via the blood stream. For example, in pre-clinical and clinical AAV gene therapy studies targeting skeletal muscle diseases, vector doses in the range of $5x10^{13}$ to $5x10^{14}$ vg/kg have been generally required for effectiveness (Mack *et al.*, 2017; Le Guiner *et al.*, 2017; Mendell et al, 2020) which implies up to $5x10^{16}$ vg in total delivered per patient. Using current manufacturing systems for AAV such as the widely-used triple-transfection of HEK293 cells, $5x10^{16}$ vg could require the entire output from a single 4000L bioreactor. For example, assuming a patient population of ~500,000 per year with a requirement of ~10^{15} vg per patient, the projected viral vector requirement is ~$5x10^{20}$ vg. The ability to produce such vector quantities at commercial scale is one of the biggest hurdles in human gene therapy (Masri, Cheeseman and Ansorge, 2019).

It is thus attractive to hypothesise that increasing transgene strength and increased transgene product expression per copy of vector genome may allow enhanced therapeutic effectiveness at lower doses. Such a situation has the added theoretical benefits of a reduced risk of adverse events and immunogenicity, and reduced manufacturing challenges. In the context of AAV expression cassettes, in addition to modulating promoter and polyadenylation strength, the presence of an intron between the promoter and transgene generally increases transgene expression compared to no-intron controls at varying levels: 2-fold increase using SV40 intron (Ostedgaard et al, 2005), 11-fold increase using MVM intron (Wu et al, 2008) and up to 100-fold increase using R6K-RNA-OUT (RRO) intron (Lu et al, 2017). This elevation of transgene expression may however not be observed when the intron is placed elsewhere in an AAV expression cassette, such as in between the transgene and the polyA (Choi et al, 2014) suggesting the importance of positioning of intron in an AAV expression cassette. Therefore, when placed between the promoter and the transgene, an intron could be a very valuable regulatory element to include in an AAV expression cassette to enhance transgene expression and vector potency and efficacy.

The addition of the engineered intron RRO, just downstream of the promoter in a non-coding first exon, in AAV expression cassette has been shown to boost the transgene expression by 100- to 1000-fold (Lu *et al.*, 2017) (Figure 1.21). Using in vivo systemic delivery of AAV vectors in mice and measuring the transgene expression (human factor 9 (hFIX) and human alpha-1 antitrypsin (hAAT)) from mice serum samples, these authors showed firstly that a 1.3 kb engineered intron called *optimised intron with pUC origin and RNA-OUT* (OIPR) increased the transgene expression levels in treated animals by 100- to 1000-fold: OIPR was placed in the AAV expression cassette between the promoter and transgene. The authors also tested other engineered introns of different lengths and discovered that the engineered introns always resulted in enhancement of transgene expression level compared to the control without an intron (Discussed in detail in Section 3.1).

Figure 1.21 **Addition of engineered intron into rAAV cassette enhances transgene expression.** A standard rAAV expression cassette is shown on the left, consisting of two inverted terminal repeats (ITRs), a promoter to initiate transcription, a coding region for the gene of interest and a polyadenylation signal (pA) to terminate transcription. The engineered intron is inserted between the promoter and transgene in the rAAV expression cassette (Lu et al., 2017). Figure modified from Lu et al., 2017.

The aim of the research has been to evaluate whether the RRO intron may be functional and produce enhanced levels of expression in the context of an AAV vector expressing microdystrophin in a manner transcriptionally-targeted to dystrophin-deficient skeletal muscle and heart tissues. We decided to test this engineered intron RRO in this study, which is a more potent intron in enhancing transgene expression compared to other available strong introns such as the minute virus of mice (MVM) intron (Powell, Rivera-Soto and Gray, 2015). The MVM intron has one of the highest 'relative strength' of intron compared to other

known introns and has been tested in AAV gene expression cassette of human factor IX (hFIX); however addition of the intron into the AAV gene expression cassette only exhibited an 11-fold increase in hFIX transgene expression compared to the cassette with no intron (Wu et al, 2008). The engineered intron RRO has the potential of elevating transgene liver expression by 100- to 1000-fold when added into the AAV gene expression cassette (Lu et al, 2017). Given the relative strength of this intron compared to other known introns and also considering this intron has been tested in an AAV expression cassette, we decided to test the RRO intron in our AAV-microdystrophin expression cassettes.

1.5.2 Statement of aims

The main aim of this project is to enhance microdystrophin-1 (MD1) (ΔR4-R23/ΔCT) expression from rAAV2/9 vector using an engineered intron: R6K-RNA-OUT (RRO) (Figure 1.22). The features of RRO are discussed in detail in Section 3.1.

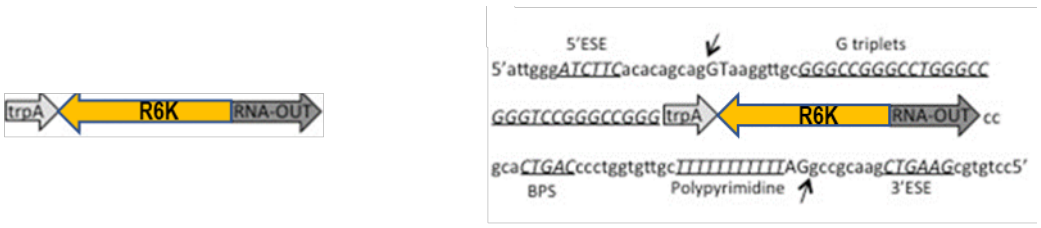

(A) 456 bp R6K-RNA-OUT (B) 585 bp R6K-RNA-OUT

Figure 1.22 **R6K-RNA-OUT intron**. (A) The 456 bp R6K-RNA-OUT miniorigin consists of trpA prokaryotic terminator, replication deficient R6K bacterial origin and RNA-OUT antisense RNA (Lu et al., 2017). The trpA terminator is added to protect the replication origin from insert initiated transcription (Nature Technology, 2013). (B) The engineered R6K-RNA-OUT intron is 585 bp in length. The full sequence of the intron consists of 5'-exon splicing enhancer (5' ESE), G triplets, R6K-RNA-OUT miniorigin described in (A), branch point sequence (BPS), 11 nucleotide polypyrimidine track, and 3′-exon splicing enhancer (3' ESE). The two arrows point to the location of splicing (Lu, Zhang & Kay, 2013; Lu et al., 2017). Image modified from Lu et al., 2017.

R6K-RNA-OUT consists of a replication deficient R6K origin and a non-coding RNA, RNA-OUT which is also an antibiotic-free selection marker (Williams, 2014) (Figure 1.23), although this feature is not utilised in this project for the purpose of bacteria selection (Lu *et al.*, 2017).

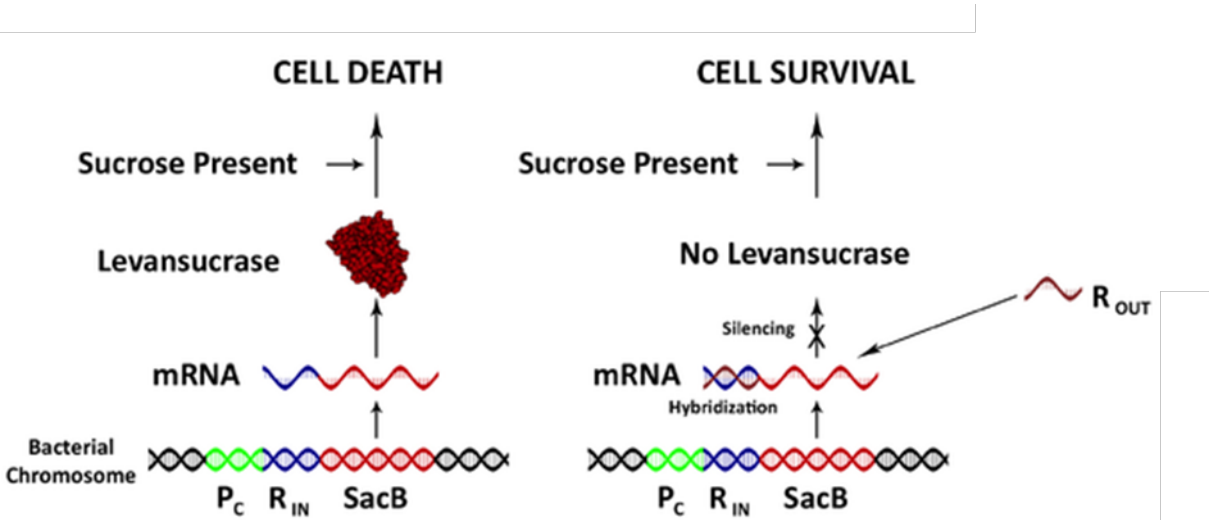

Figure 1.23 **RNA-OUT mechanism**. Levansucrase (SacB) is a conditional-lethal gene on bacterial chromosome. RNA-OUT is an antisense RNA to RNA-IN which is expressed in the mRNA. In the presence of RNA-OUT, silencing occurs and no protein product is formed. In the presence of sucrose in the media, the host bacteria with levansucrase die. This property of allowing plasmid selection in sucrose is exploited to develop an antibiotic-free selection system which is safer and more potent (Luke et al, 2009; Williams, 2014). Figure modified from Williams, 2014.

It is hypothesised that the addition of R6K-RNA-OUT intron into the rAAV-MD1 gene expression construct will enhance the expression of MD1 by several folds. This would be useful in increasing the potency of the treatment and at the same time, possibly reducing the vector dosage in treatment.

- The starting point of this research was characterisation of the codon optimised MD1 plasmids and ensuring that the plasmids were intact.

- Chapter 3 discusses the construction of AAV-microdystrophin expressing cassettes with engineered intron R6K-RNA-OUT. The constructs were then tested in an *in vitro* model to evaluate protein production level.

- Chapter 4 explores the activity of the microdystrophin constructs in an *in vivo* muscle model via plasmid electrotransfer to evaluate transgene expression level and functionality of the constructs. Muscle electrophysiology assays were also performed. We produced and quantified rAAV2/9 vectors containing mouse codon optimised mMD1 and 585 mMD1 (mMD1 construct containing the RRO intron). In this way any confounding effects on AAV production efficiency, titre and infectivity are a minimised.

- Chapter 5 describes work done using rAAV vectors. This chapter includes testing of rAAV2/9-microdystrophin vectors in *mdx* mice via intramuscular injection to evaluate AAV vector quality and transgene expression *in vivo* and functional outcomes.

- Following our findings in Chapter 5, we performed studies to further miniaturise the MD1 expression cassette to accommodate the intact vector genome into rAAV2/9. The constructs were then tested *in vitro* to evaluate transgene expression.

- Chapter 6 discusses the implications of the work performed for this thesis and offers future directions and suggestions of *in vivo* experiments using the newly generated miniaturised AAV2/9-microdystrophin constructs in *mdx* mice.

Chapter 2 Materials and methods

2.1 Molecular biology

Materials

- Restriction enzymes and respective buffers (New England Biolabs)
- 50x TAE: 242 g Tris Base, 57.1 ml Glacial Acetic Acid, 100 ml of 0.5 M EDTA, pH 8.0 at a total volume of 1 L with ddH2O.
- UltraPure Agarose (Invitrogen)
- 1000x SYBR Safe DNA gel stain (Invitrogen).
- 5x Loading buffer (Bioline).
- DNA molecular weight marker Hyperladder I (Bioline)
- QiaQuick gel extraction kit (QIAGEN)
- QiaQuick PCR Purification Kit (QIAGEN)
- T4 DNA ligase (Promega)
- Antarctic Phosphatase (New England Biolabs)

2.1.1 R6K-RNA-OUT synthesis

The 456bp R6K-RNA-OUT construct (Lu *et al.*, 2017) was synthesised by GeneArt (Thermo Fisher Scientific). *ECo*RI sites at both ends of the construct were included in the synthesis for subsequent cloning work. The synthesised construct was verified by Sanger sequencing both by the manufacturer and the author. Samples were sent for sequencing using the Mix2Seq Kit (Eurofins Genomics, Germany). 15 µl of DNA template (100 ng of DNA in total) and 2 µl of 10 mM primer were added in each barcoded tube. R6K-RNA-OUT was sequenced using the following primers (Lu *et al.*, 2017):

R6KRNAOUT (Forward)
5'- CCCGCCTAATGAGCGGGCTTTTTTTTGGCTTG -3'

R6KRNAOUT (Reverse)
5'-CTAATGATTTTTATCAAAATCATTAAGTTAAGGTAGATAC -3'

The 585bp R6K-RNA-OUT intron (Lu *et al.*, 2017) was synthesised by GenScript. *ECo*RI sites at both ends of the construct were included in the synthesis for subsequent cloning work. The synthesised construct was verified by Sanger sequencing both by the manufacturer and the author (as described above).

2.1.2 Cloning of R6K-RNA-OUT in mouse and human codon optimized rAAV-Spc5.12-MD1 vector plasmids

The two R6K-RNA-OUT (456bp and 585bp) constructs were cloned into mouse and human codon optimized rAAV-Spc5.12-MD1 vector plasmids (plasmid maps shown in Figures 3.9 and 3.10 respectively) at the *ECo*RI site between the promoter and transgene. The rAAV-Spc5.12-MD1 vector plasmids and R6K-RNA-OUT inserts were digested using *ECo*RI (New England Biolabs) at 37ºC according to the manufacturer's protocol prior to the vector and insert ligation reaction. The digested rAAV-Spc5.12-MD1 vector plasmids were treated with Antarctic Phosphatase (New England Biolabs) to prevent self-ligation of the vector. The insert and vector were ligated using T4 DNA ligase (Promega) according to the manufacturer's protocol and the reaction was incubated overnight at 4ºC. 456bp R6K-RNA-OUT cloning into the MD1 vector plasmids were performed at Royal Holloway. 585bp R6K-RNA-OUT cloning into the MD1 vector plasmids were performed by GenScript.

The following plasmid constructs were generated:

- Human codon optimized
  p-rAAV-Spc5.12-456R6KRNAOUT-hMD1-SV40 (also called 456hMD1)
  p-rAAV-Spc5.12-585R6KRNAOUT-hMD1-SV40 (also called 585hMD1)

- Mouse codon optimized
  p-rAAV-Spc5.12-456R6KRNAOUT-mMD1-SV40 (also called 456mMD1)
  p-rAAV-Spc5.12-585R6KRNAOUT-mMD1-SV40 (also called 585mMD1)

2.1.3 Minimisation of p-mMD1

The work to minimise the AAV expression cassettes was initiated both at Royal Holloway and University of Nantes. The attempt of minimising the mMD1 construct was successfully done by our collaborators in University of Nantes, France: Dr Audrey Bourdon and Dr Caroline Le Guiner. The minimisation of mMD1 was performed by a series of fragment synthesis and cloning workflows to remove linker sequences found in between the components of the gene expression cassette (Figure 2.1). In addition, the 125 bp SV40 polyA signal was also replaced by a shorter, highly efficient synthetic polyA signal called pCl NeO-pA which is 49 bp in length (Levitt et al, 1989; Himeda, Chen & Hauschka, 2011; Hakim et al, 2017). These strategies brought the mMD1 cassette length down to 4.2 kb which is called mini MD1.

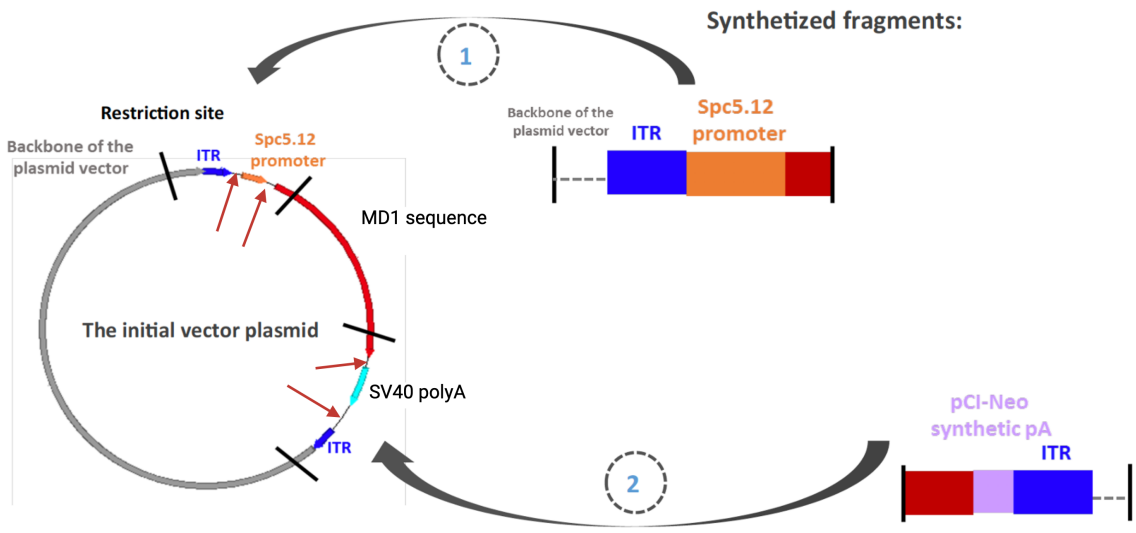

Figure 2.1 **Minimisation strategy of p-mMD1 and p-585mMD1 to produce p-mini MD1 and p-mini 585MD1 respectively.** The original vector plasmid sequences contain 'linker sequences' (shown by red arrows) that originated from previous cloning reactions to assemble the gene expression cassette. To remove the linker sequences, DNA fragments covering the gene expression casettes were synthesised (1 and 2), eliminating the linker sequences in the synthesis. The synthesised fragments were then used to replace the existing sequence using restriction site cloning, where a segment of the gene expression cassette with the linker sequence is removed by restriction digest; after which the fragment without linker sequence is inserted into the vector to replace the removed sequence. In addition, the 125 bp SV40 polyA was also replaced with a shorter synthetic 49bp polyA (Levitt et al, 1989; Himeda, Chen & Hauschka, 2011; Hakim et al, 2017). This work was performed in University of Nantes, France.

2.1.4 Cloning of R6K-RNA-OUT intron into minimised p-mMD1 vector plasmid

The next step of generating minimized 585mMD1 was done here in our lab at Royal Holloway, and this involved a fragment synthesis which included 585 bp R6K-RNA-OUT to be cloned into mini MD1 (Figure 2.2). The fragment synthesis was essential as many single cutter restriction enzyme sites were lost in the minimisation process.

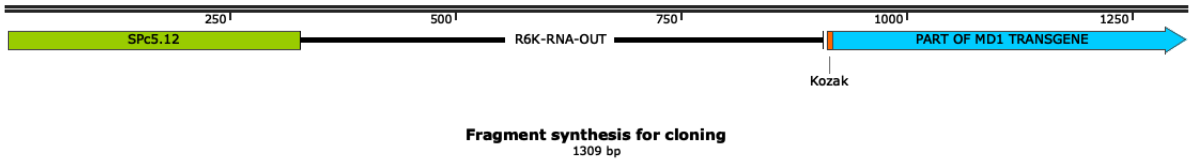

CGTACGGCCGTCCGCCCTCGGCACCATCCTCACGACACCCAAATATGGCGACGGGTGAGGAATGGTGGGGAGTTATT
TTTAGAGCGGTGAGGAAGGTGGGCAGGCAGCAGGTGTTGGCGCTCTAAAAATAACTCCCGGGAGTTATTTTTAGAGC
GGAGGAATGGTGGACACCCAAATATGGCGACGGTTCCTCACCCGTCGCCATATTTGGGTGTCCGCCCTCGGCCGGGG
CCGCATTCCTGGGGGCCGGGCGGTGCTCCCGCCCGCCTCGATAAAAGGCTCCGGGGCCGGCGGCGGCCCACGAGCT
ACCCGGAGGAGCGGGAGGCGGAATTCATTGGGATCTTCACACAGCAGGTAAGGTTGCGGGCCGGGCCTGGGCCGGG
TCCGGGCCGGGCCCGCCTAATGAGCGGGCTTTTTTTTGGCTTGTTGTCCACAACCGTTAAACCTTAAAAGCTTTAAAA
GCCTTATATATTCTTTTTTTTCTTATAAAACTTAAAACCTTAGAGGCTATTTAAGTTGCTGATTTATATTAATTTTATTG
TTCAAACATGAGAGCTTAGTACGTGAAACATGAGAGCTTAGTACGTTAGCCATGAGAGCTTAGTACGTTAGCCATGAG
GGTTTAGTTCGTTAAACATGAGAGCTTAGTACGTTAAACATGAGAGCTTAGTACGTACTATCAACAGGTTGAACTGCT
GATCCACGTTGTGGTAGAATTGGTAAAGAGAGTCGTGTAAAATATCGAGTTCGCACATCTTGTTGTCTGATTATTGAT
TTTTGGCGAAACCATTTGATCATATGACAAGATGTGTATCTACCTTAACTTAATGATTTTGATAAAAATCATTAGCCGC
ACTGACCCCTGGTGTTGCTTTTTTTTTTTTAGGCCGCAAGCTGAAGCGTGTCCGAATTCGCCACCATGCTGTGGTGGGA
GGAAGTGGAGGACTGCTACGAGAGAGAGGACGTGCAGAAGAAAACCTTCACCAAGTGGATCAACGCCCAGTTCAGC
AAGTTCGGCAAGCAGCACATCGACAACCTGTTCAGCGACCTGCAGGACGGCAAGAGACTGCTGGATCTGCTGGAGGG
ACTGACCGGCCAGAAGCTGCCCAAGGAGAAGGGCAGCACCAGAGTGCACGCCCTGAACAACGTGAACAAGGCCCTG
AGAGTGCTGCAGAAGAACAACGTGGACCTGGTGAATATCGGCAGCACCGACATCGTGGACGGCAACCACAAGCTGAC
CCTGGGCCTGATCTGGAACATCATCCTGCACTGGCAGGTGAAGAACGTGATGAAAACCATCATGGCCGGCC

Figure 2.2 **Schematic of the synthesised fragment for subsequent cloning into mini MD1 vector plasmid**. The linker sequences (Figure 2.1) were not included in the synthesis bringing the ends of the promoter, transgene and R6K-RNA-OUT intron together. The sequence of the synthesised fragment is also shown. BsiWI and FseI restriction sites utilised for cloning the fragment into the minimised vector plasmid are underlined.

The cloning of 585 bp R6K-RNA-OUT intron into mini MD1 plasmid (Figure 2.3) was done by GenScript using BsiWI and FseI restriction sites, following synthesis of the fragment covering regions of the promoter, transgene and the entire R6K-RNA-OUT in the middle. These strategies brought the 585mMD1 cassette length down to 4.8 kb which is called mini 585MD1.

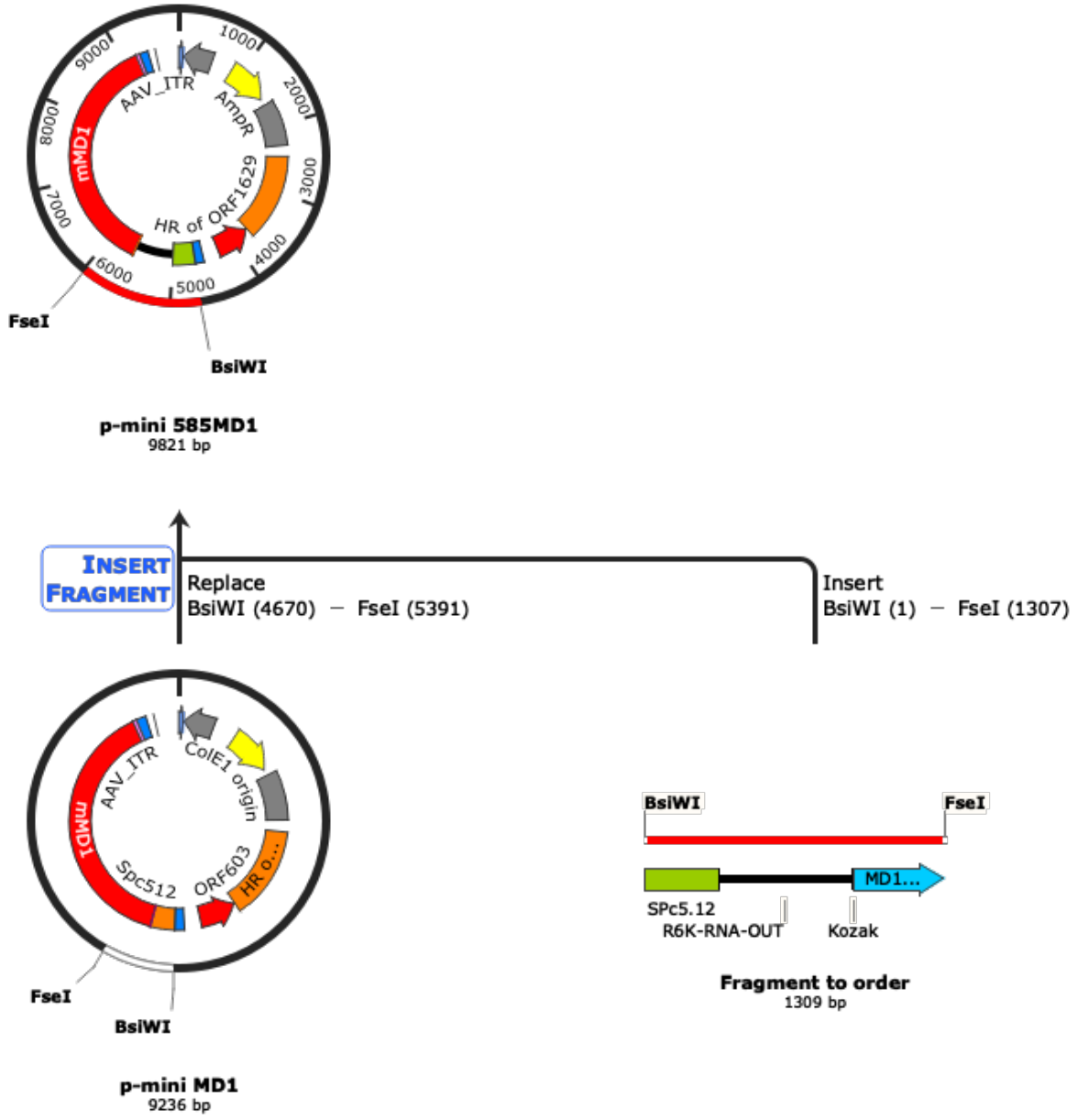

Figure 2.3 **Cloning of R6K-RNA-OUT intron into p-mini MD1.** Fragment synthesis with BsiWI and FseI restriction sites enabled cloning of R6K-RNA-OUT intron into p-mini MD1 generating p-mini 585MD1 where the ITR-ITR length is within the packaging capacity of wild-type AAV (4.7kb).

2.2 Microbiology

Materials

- Ampicillin (Sigma)

  Stock solution was prepared at 50 mg/ml concentration and filtered through 0.22 µm filter (Falcon) and stored at -20°C.

- Kanamycin (Sigma): prepared as 200x stock in ddH2O

  Stock solution was prepared at 20 mg/ml concentration and filtered through 0.22 µm filter (Falcon) and stored at -20°C.

- LB agar (Fisher Scientific)

  LB agar was dissolved in ddH_2O and autoclaved. The agar solution was allowed to cool to 60°C before the appropriate antibiotic was added and poured into petri dishes.

- Glycerol (Sigma)
- LB media (Sigma).

  LB broth powder was dissolved in ddH_2O and autoclaved. The solution was allowed to cool to room temperature and stored at 4°C for long term storage.

- LB SOC

  Prepared by adding 100 µl of 1 M $MgSO_4$ and 20 µl 1 M glucose (0.22µm filtered) to 10 ml LB medium.

- TOP 10 *E.coli* competent cells (Invitrogen | Life Technologies)

2.2.1 Transformation of TOP10 chemically competent *E. coli*

The cloning reactions (described in Section 2.1) was added to TOP10 *E. coli* (Catalog number C404010) and the transformation reaction was carried out according to the manufacturer's protocol (Invitrogen | Life Technologies). Two volumes:50 µl and 100 µl from each transformation were spread on pre-warmed LB agar plates with 50 µg/ml ampicillin. This was to ensure that at least one plate will have well-spaced colonies. The plates were incubated at 32ºC overnight for 14-16 hours.

2.2.2 Miniprep/ starter cultures and glycerol stocks

Each colony from the agar plates was added to 5 ml LB media with 5 µl ampicillin and was incubated at 32ºC overnight for 14-16 hours, with shaking at 200 rpm. Glycerol stocks were made by adding 0.7 ml of miniprep culture to 0.3 ml of 80% glycerol and were stored at -80 ºC.

2.2.3 Maxiprep cultures

500 µl from overnight miniprep culture was added to 500 ml LB media with 500 µl ampicillin and incubated at 32ºC overnight for 14-16 hours, with shaking at 200 rpm.

2.2.4 Gigaprep cultures

2000 µl from overnight miniprep culture was added to 2000 ml LB media with 2000 µl ampicillin and incubated at 32ºC overnight for 14-16 hours, with shaking at 200 rpm.

2.3 DNA and RNA assays

2.3.1 Plasmid DNA purification

Materials:

- EndoFree Plasmid Mini Kit (QIAGEN)
- EndoFree Plasmid Maxi Kit (QIAGEN)
- EndoFree Plasmid Giga Kit (QIAGEN)
- Isopropanol (VWR)
- Absolute ethanol (VWR)
- ND-1000 NanoDrop spectrophotometer (Thermo Fisher)
- Microcentrifuge (Thermo Fisher)
- Superspeed centrifuge (Thermo Fisher)

All plasmid DNA samples were purified using EndoFree Plasmid Kit (QIAGEN) according to the manufacturer's protocol. Purified plasmid concentrations were measured using ND-1000 spectrophotometer (NanoDrop Technologies).

2.3.2 RNA extraction and reverse transcription (RT)

Materials:

- QIAshredder kit (QIAGEN)
- RNeasy Mini Kit (QIAGEN)
- RNeasy Fibrous Tissue Mini Kit (QIAGEN)
- RNase-free DNase-I (QIAGEN)
- Absolute ethanol (VWR)
- ND-1000 NanoDrop spectrophotometer (Thermo Fisher).
- TissueLysser (QIAGEN)
- Stainless steel 5mm beads (QIAGEN)
- Random primers (Promega)
- Oligo (dt) (Thermo Fisher Scientific)
- GoScript reverse transcriptase (Promega)

Total RNA was extracted from cells using RNeasy Mini Kit and QIAshredder (QIAGEN) according to the manufacturer's protocol. Total RNA from muscle tissues (cryosections) were extracted using RNeasy Fibrous Tissue Mini Kit (QIAGEN) according to the manufacturer's protocol. RNAse-free DNAse I (QIAGEN) treatment was included in both the total RNA extraction protocol.

500 ng of the total RNA were reverse transcribed using 0.5 µg random primers (Promega), 0.5 µg Oligo (dT) (Thermo Fisher Scientific) and GoScript reverse transcriptase (Promega) according to the manufacturer's protocol. Following addition of random primers and Oligo (dT) to 500 ng of total RNA in a total volume of 10 µl, the reaction mixture is incubated at 70^{o}C for 5 minutes followed by 4^{o}C for 5 minutes. The following mastermix was then added to the reaction tube.

Components	Volume/ µl
Goscript 5X buffer	4
25 mM $MgCl_2$	2
10 mM dNTP	1
Enzyme 160u/ul	1
Water	2

The reverse transcription cycling program is outlined below:

Step 1 (Annealing): 25°C for 5 minutes

Step 2 (Extension): 42°C for 60 minutes

Step 3 (Inactivation of reverse transcriptase): 70°C for 15 minutes

Step 4 (Storage): 4°C

2.3.3 Polymerase chain reaction (PCR)

Materials

- GoTaq Polymerase (Promega)
- Thermocycler (VWR)
- Primers (IDT)
- dNTP mix 100mM (Bioline)
- iProof High-Fidelity PCR kit (BIO-RAD)
- Nuclease free water (ThermoFisher)

To check for the presence of R6K-RNA-OUT insert after cloning, PCR was performed using the following primer set:
R6KRNAOUT (Forward)
5'- CCCGCCTAATGAGCGGGCTTTTTTTTGGCTTG -3'
R6KRNAOUT (Reverse)
5'-CTAATGATTTTTATCAAAATCATTAAGTTAAGGTAGATAC -3'
The annealing temperature for the PCR was calculated using Tm Calculator (Thermo Fisher Scientific). The PCR was carried out with a high fidelity polymerase, iProof High-Fidelity PCR kit (BIO-RAD) according to the manufacturer's protocol. 200 ng of DNA templates were used, with annealing temperature of 60.0 ºC and extension time of 17s.

For mRNA analysis to check for levels of transcription *in vitro*, PCR was performed using the following primer sets: MD1_mRNA (Forward) 5'-GCACGCCCTGAACAAC-3' and MD1_mRNA (Reverse) 5'-GCTGTTCCAGTCGAACAG-3'. 4 µl of cDNA template was used in each reaction. The annealing temperature for the PCR was calculated using Tm Calculator (Thermo Fisher Scientific). The PCR was carried out with GoTaq polymerase (Promega) according to the manufacturer's protocol outlined below:

Component	Volume (µl)
Template cDNA	4
Primer Forward	0.3
Primer Reverse	0.3
GoTaq 5X buffer	5
25 mM MgCl2	1.5
10 mM dNTP	0.5
GoTaq polymerase 5u/ul	0.25
Water	13.15
Total final volume	25

Annealing temperature of 50.0 ºC and extension time of 30s was used.

To check for splicing activity, PCR was performed as described above using R6KRNAOUT (Forward) 5'- CCCGCCTAATGAGCGGGCTTTTTTTTGGCTTG -3' and R6KRNAOUT (Reverse) 5'-CTAATGATTTTTATCAAAATCATTAAGTTAAGGTAGATAC -3'. Annealing temperature of 60.0 ºC and extension time of 17s was used.

For normalisation of the mRNA concentration, the following housekeeping primers sets targeting human b-actin was used: b-actin (Forward) 5'-AGCGAGCATCCCCCAAAGTT-3' and b-actin (Reverse) 5'-GGGCACGAAGGCTCATCATT-3'. Annealing temperature of 55.0 ºC and extension time of 30s was used.

2.3.4 Gel electrophoresis

Samples were loaded onto 1% agarose gel (BIOLINE) with 5X loading dye (BIOLINE) and the gel was ran in 1X TAE buffer until optimal migration was achieved. The gel was visualised using E-Box Gel Documentation Imaging (VILBER) under UV light.

2.3.5 Restriction digest

All restriction digest reactions were performed using restriction enzymes from New England Biolabs in their respective optimal buffers and optimal temperatures according to manufacturer's protocol. 2000 ng of DNA were used in all reactions.

2.3.6 Gel extraction

The correctly sized PCR product bands were excised and purified using QIAquick Gel Extraction Kit (QIAGEN). All purified DNA concentrations were measured using ND-1000 spectrophotometer (NanoDrop Technologies).

2.4 Mammalian cell culture

Materials

- Sterile Phosphate buffered saline (PBS)

  1 PBS Tablet (Gibco) dissolved in 500ml of ddH_2O followed by autoclaving.
- Trypan blue (Gibco)
- 0.5% trypsin (Sigma) in PBS
- T175cm^2 and T75 cm^2 Tissue Culture Flasks (Corning)
- Tissue culture grade DMSO (Sigma)
- Sterile stripettes 1ml, 5ml, 10ml and 25ml (Starlabs)
- 15ml and 25ml Falcon Tubes (Corning)
- Screw top cryovials (Corning)

2.4.1 Human Embryonic Kidney 293T (HEK293T)

HEK293T cells bought from ATCC were grown in Dulbecco's Modified Eagle's Medium (DMEM) with 4.5 g/l glucose and glutamax (Gibco), supplemented with 10% heat inactivated Foetal Calf Serum (PAA / Gibco) and 1% penicillin-streptomycin (Sigma) in a 5% CO_2 incubator at 37ºC. $1x10^6$ cells were grown in T175 flasks until 80% confluent.

2.4.2 H2kb.mdx transgenic mice myoblast

H2kb.mdx cells are derived from transgenic mice (H-2Kb-tsA58 X *mdx/mdx* F1 male mice) yielding dystrophin-deficient myoblasts (Morgan *et al.*, 1994). This cell line was kindly provided by Dr Mike Antoniou (King's College London). H2kb.mdx were grown in Dulbecco's Modified Eagle's Medium (DMEM) with 4.5 g/l glucose and glutamax (Gibco) supplemented with 20% Heat Inactivated Foetal Calf Serum (PAA / Gibco), 0.5% Chick Embryo Extract (Sera Laboratories International), 0.2% Gamma Interferon (Peprotech) and 1% penicillin-streptomycin (Sigma). The cells were incubated in a 10% CO_2 incubator at 33ºC to prevent differentiation. $3x10^5$ cells were grown in T175 flasks until 70% confluent.

2.4.3 C2C12 mouse myoblast cell line

C2C12 mouse myoblast cell line (91031101; Sigma-Aldrich) were grown in Dulbecco's Modified Eagle's Medium (DMEM) with 4.5 g/l glucose and Glutamax (Gibco) supplemented with 20% Heat Inactivated Foetal Calf Serum (PAA / Gibco) and 1% penicillin-streptomycin (Sigma). The cells were incubated in a 5% CO_2 incubator at 37ºC.

2.5 Transient transfection

- Viafect Transient Transfection Reagent (Promega)
- Serum Free Dulbecco's Modified Eagle's Medium (DMEM) (Gibco)
- Tissue culture grade 6-well plates (ThermoFisher)

2.5.1 Human Embryonic Kidney 293T (HEK293T)

HEK293T were seeded at a density of $5x10^5$ cells/well in 6-well plates where 70-80% confluency is attained after 24 hours. Viafect Transient Transfection Reagent (Promega) was used with a transfection reagent volume (µl) to DNA mass (µg) ratio of 5:1. Plasmids for transfection were diluted in serum free DMEM (Gibco) and total volume of 200 µl transfection mixture was added per well. Plates were kept in a 5% CO_2 incubator at 37ºC. The cells were harvested and total proteins were extracted in 100µl PAPBNI RIPA Buffer (NaCl 0.15M, HEPES 0.05M, NP-40 1%, Sodium Deoxycholate 0.5%, SDS 0.10%, EDTA 0.01M, Protease Inhibitor tablet 1 in 50ml (Roche)) after 72 hours.

2.5.2 H2kb.mdx transgenic mice myoblast

H2kb.mdx were seeded at a density of $1.25x10^5$ cells/well in extracellular matrix coated 6-well plates where 70-80% confluency is attained after 24 hours. Viafect Transient Transfection Reagent (Promega) was used with a transfection reagent volume (µl) to DNA mass (µg) ratio of 3:1. Plasmids for transfection were diluted in serum free DMEM (Gibco) and total volume of 200 µl transfection mixture was added per well. Plates were kept in a 10% CO_2 incubator at 33ºC. The cells were harvested and total proteins were extracted in 100µl PAPBNI RIPA Buffer (NaCl

0.15M, HEPES 0.05M, NP-40 1%, Sodium Deoxycholate 0.5%, SDS 0.10%, EDTA 0.01M, Protease Inhibitor tablet 1 in 50ml (Roche) after 72 hours.

2.5.3 C2C12 mouse myoblast cell line

C2C12 were seeded at a density of $5x10^4$ cells/well in 6-well plates where 70-80% confluency is attained after 48 hours. When the cells were around 70-80% confluency, to allow differentiation, the cells were exposed to a specific differentiation media: Dulbecco's Modified Eagle's Medium (DMEM) with 4.5 g/l glucose and Glutamax (Gibco) supplemented with 2% horse serum (Euroclone) and 1% penicillin-streptomycin (Sigma). The cells were incubated in a 5% CO_2 incubator at 37ºC (Loperfido et al, 2016). Viafect Transient Transfection Reagent (Promega) was used with a transfection reagent volume (µl) to DNA mass (µg) ratio of 4:1. Plasmids for transfection were diluted in serum free DMEM (Gibco) and total volume of 200 µl transfection mixture was added per well. Plates were kept in a 5% CO_2 incubator at 37ºC. The cells were harvested and total proteins were extracted in 100µl PAPBNI RIPA Buffer (NaCl 0.15M, HEPES 0.05M, NP-40 1%, Sodium Deoxycholate 0.5%, SDS 0.10%, EDTA 0.01M, Protease Inhibitor tablet 1 in 50ml (Roche)) after 72 hours.

2.6 Total protein assays

2.6.1 Total protein extraction and quantification from cell and tissue samples

Materials

- Sterile PBS

  1 PBS Tablet (Gibco) dissolved in 500ml of ddH_2O followed by autoclaving.
- PAPBNI RIPA Buffer

  NaCl 0.15M, HEPES 0.05M, NP-40.1%, Sodium Deoxycholate (SOC) 0.5%, SDS 0.10%, EDTA 0.01M, Protease Inhibitor tablet 1 in 50ml (Roche).
- Cells Scrapers (Invitrogen)
- Eppendorf tubes (Starlabs)
- Benchtop Microcentrifuge (Fisher Scientific)
- DC Assay protein kit: Reagent A, S and B (BioRad).
- 2µg bovine serum albumin (BSA) standard (Invitrogen)
- 96 Well plate (Corning)
- 96 Well plate reader (Genbank)
- 5mm steel bead (QIAGEN)
- TissueLyser (QIAGEN)

For total protein extraction from cells cultured in 6-well plates, the media was removed and the cells were washed with 500 µl pre-chilled PBS. Following removal of PBS after the washing step, 100 µl PABPN1 RIPA buffer was added. The cells were then scraped down to the bottom of the well and incubated at 4°C for 5 minutes. The samples were then transferred to pre-chilled Eppendorf tubes and vortexed for 15 minutes. The total protein lysates were then centrifuged at 13,000 rpm for 15 minutes at 4°C. The supernatant was then transferred to a fresh pre-chilled 0.5ml screw cap tube and stored at -20°C.

For total protein extraction from cryosectioned TA muscle tissue, 100 µl PABPN1 RIPA buffer was added to the Eppendorf tubes containing the samples. The samples were vortexed for 15 minutes. The homogenised TA was then

centrifuged at 13,000 rpm for 15 minutes at 4°C. The supernatant was then transferred to a fresh pre-chilled 0.5ml screw cap tube and stored at -20°C.

Protein concentrations from the extracted total proteins were quantified using *DC*™ (detergent compatible) protein assay (BIO-RAD) measured at 750 nm (BioTek).

2.6.2 Western blot analysis

Materials

- NuPage 10X Reducing Agent (ThermoFisher)
- NuPage 4x Loading Dye Sample buffer (ThermoFisher)
- NuPage 3-8% Tris Acetate precast gradient gels (ThermoFisher)
- NuPage Antioxidant (ThermoFisher)
- Prestained HiMark Ladder (Life technologies)
- NuPage 3-8% Tris Acetate Running Buffer (ThermoFisher)
- NuPage 20X Transfer Buffer (ThermoFisher)
- Absolute Methanol (VWR)
- I-Cell Blot Tank (Thermo Fisher)
- 0.45 µM Nitrocellulose membrane (GE Healthcare)
- Ponceau Stain (ThermoFisher)
- Filter paper
- Milk powder (MARVEL)
- Tween 20 (Sigma)
- Phosphate Buffered Saline (PBS)
- Odyssey CLx Imager (LI-COR Bioscience)

50 µg of protein extracts from HEK293T and C2C12 cells; and 35 µg of protein extracts from H2kb.mdx were loaded on NuPAGE Novex 3–8% Tris Acetate gel (Thermo Fisher Scientific). For total protein extracted from muscle tissue sample cryosections, 10 µg of sample were loaded on NuPAGE Novex 3–8% Tris Acetate gel. Electrophoresis gels were run for 1 hour 15 minutes at 150V. The subsequent transfer of resolved protein bands over to nitrocellulose membrane

was carried out at 30V for 2 hours. The nitrocellulose membrane was then blocked in 5% skim milk in PBS, 0.1% Tween-20 for 1 hour at room temperature. Following blocking, the membrane was cut using the protein ladder as guide to separate the antibody incubations to detect microdystrophin and the protein sample loading control, alpha-tubulin. For microdystrophin detection, the membrane was incubated with MANEX 1011C (1:100 dilution; provided by Dr Glenn Morris), an anti-dystrophin mouse monoclonal antibody specific for exons 10 and 11 of the dystrophin protein (Glenn Morris; Le Guiner et al., 2017) and with a secondary goat anti-mouse IgG antibody (1: 10000 dilution; LICOR 926-32210). For protein sample loading control, the lower molecular weight portion of the membrane was incubated with anti-alpha tubulin antibody raised in rabbit (1:2500 dilution; ABCAM 4074) and with a secondary donkey anti-rabbit antibody (1: 10000 dilution; LICOR 926-68073). Immunoblots were visualized by Odyssey CLx Imaging System (LI-COR) using fluorescence detection. Direct detection was possible as the secondary antibodies used were labelled with near-infrared fluorescent dyes. The secondary antibody used for detection of microdystrophin fluoresces at 800 nm channel (green signals on immunoblots) and for the protein loading control, the secondary antibody used for detection fluoresces at 700 nm channel (red signals on immunoblots).

The fluorescence intensity of the bands (both microdystrophin and alpha-tubulin) were quantified using Image Studios software (LI-COR) and the background (noise values) were subtracted to obtain the intensity values. The ratio of MD1 fluorescence intensity value: α-tubulin fluorescence intensity value is a readout of relative abundance of MD1 protein following the treatment.

2.7 Adeno-associated virus (AAV) production, purification and quantification

Materials:

- DMEM/10%: 500 ml DMEM, 50 ml heat inactivated FCS, 1% Pen/Strep, 1% L-Glutamine

- Polyethylenimine (MW ~25,000, Polysciences Inc #23966): dissolved in water heated to 50°C at 1 mg/ml (pH 7.0). Filtered, aliquoted and stored long term at -20°C or 4 °C for 6 months.

- DMEM/2%: 500 ml DMEM, 10 ml heat inactivated FCS, 1% Pen/Strep, 1% L-Glutamine

- 40% Polyethylene glycol (PEG) 8000:- 40% [w/v] PEG 8000 with 2.5 M NaCl in water. (For 500 ml – 200 g PEG 8000, 73.05 g NaCl). Autoclaved for 15 minutes and allowed to cool and store at room temperature. 50 ml of 40%PEG was added for every 200 ml supernatant.

- Lysis buffer (500ml): 4.38 g NaCl (0.15M), 25 ml 1M Tris HCl pH8.5 (50mM), 1 ml 1M $MgCl_2$ (2 mM). Buffer was made up to 500 ml with ddH_2O and autoclaved.

- 5x PBS-MK (500 ml): 2.5 ml 1M $MgCl_2$ (5mM) and 6.25 ml 1M KCl (12.5mM) were added to autoclaved 1x PBS (final solution volume of 500 ml).

- 1x PBS-MK with non-ionic surfactant (2L): 400 ml 5x PBS-MK added to 1600 ml sterile water. 200µl of 10% Pluronic F-68 (Gibco 24040-032) added to 1x PBS-MK, filtered and stored at room temperature.

- Iodixanol (Optiprep Density Gradient Medium [60% (w/v) solution of iodixanol in water] Sigma D1556).
- Phenol Red solution (0.5% in PBS; Sigma P-0290)

- Iodixanol Fractions. For 50 ml of each concentrations:

	Iodixanol	**5M NaCl**	**5x PBS-MK**	**H_2O**	**Phenol Red**
15%	12.5 ml	10 ml	10 ml	17.5 ml	-
25%	20.8 ml	-	10 ml	19.2 ml	100µl
40%	33.3 ml	-	10 ml	6.7 ml	-
60%	50 ml	-	-	-	100µl

- Pierce Universal Nuclease for cell lysis (Thermo Fisher 88701)

For each virus, HEK293T cells were cultured in roller bottles (Corning; Catalogue number 430849) in Dulbecco modified Eagle medium, supplemented with 10% (v/v) fetal bovine serum (Invitrogen) and incubated at 37°C, 5% CO_2. Recombinant pseudotyped AAV2/9 vector stocks were generated by double transfection of HEK293T cells, where AAV2 *rep* and AAV9 *cap* genes were provided in *trans* together with the helper functions from Adenovirus via the pDP9rs plasmid (Figure 2.4).

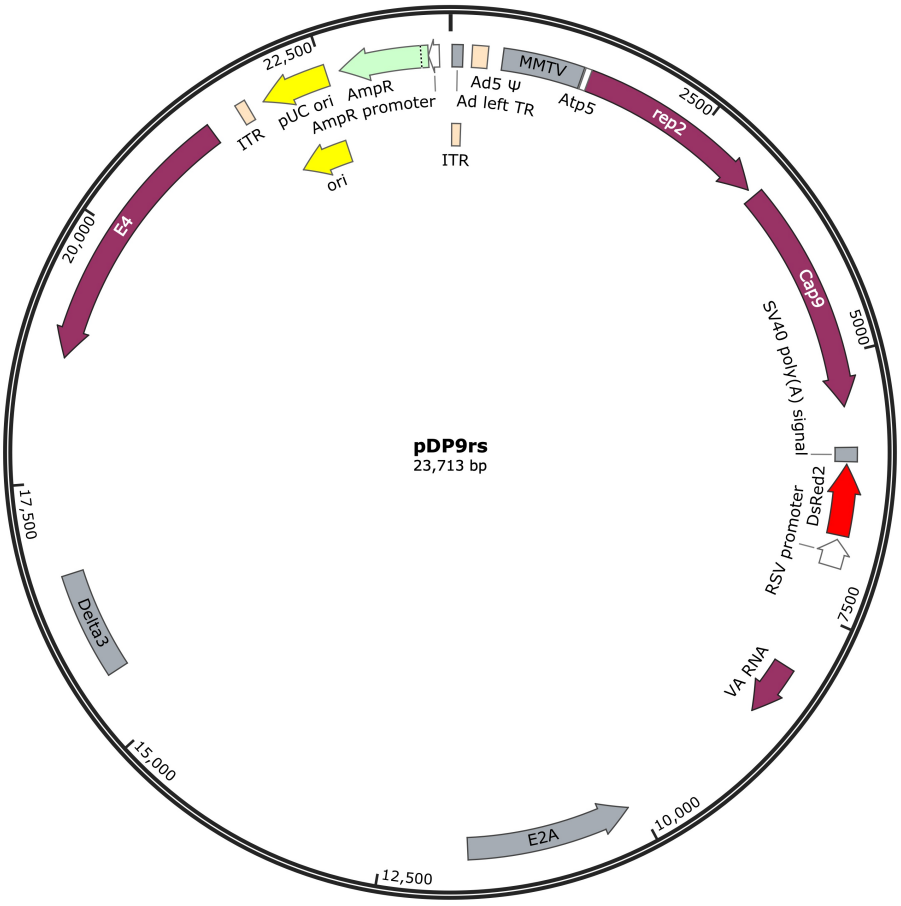

Figure 2.4 **Helper plasmid pDP9rs**. The pDP9r plasmid is provides the AAV2 *rep* and AAV9 *cap* genes in *trans* together with the helper functions from Adenovirus in the production of rAAV9 carrying the microdystrophin-1 (MD1) therapeutic cassette.

After 72 hours, the cells were lysed and rAAV vectors were purified using iodixanol step gradients centrifugation (Figure 2.5).

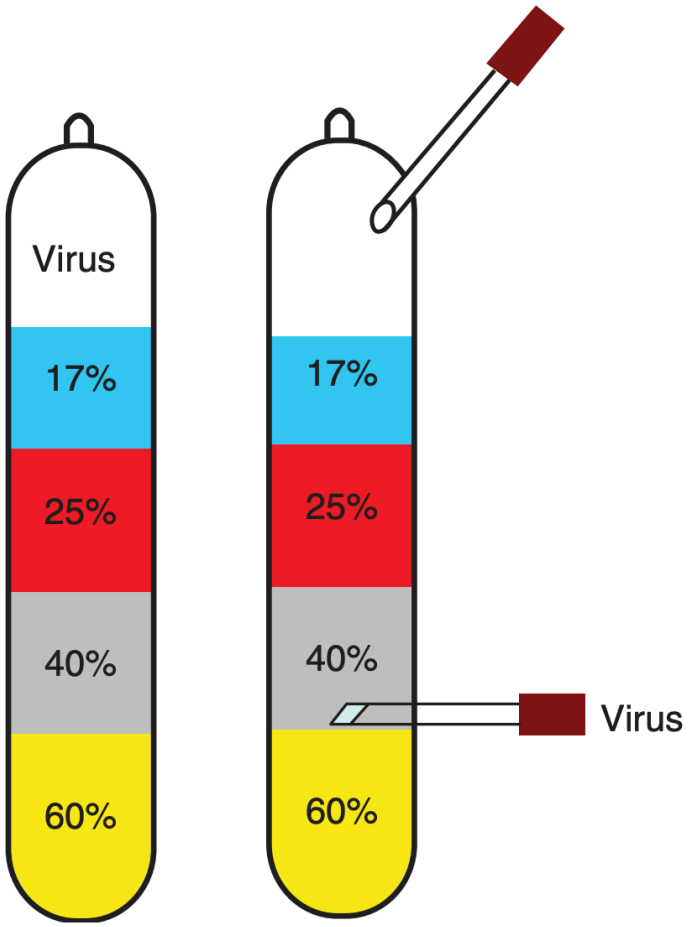

Figure 2.5 **Iodixanol gradients before (left) and after (right) ultracentrifugation for purification of rAAV**. Iodixanol solution of different concentrations are layered as shown in the figure to create a gradient. The crude lysate from HEK293T cells that contain the virus is added on the topmost layer of 15-17% iodixanol. Genome containing virions are found in the 40%-60% interface and a needle is inserted at the interface to extract the virus. The needle at the top is to allow airflow to enable extraction (Grieger, Samulski and Choi, 2006). Contaminants with lower densities, including empty capsids are collected in the 25% step and 25%-40% interface (Zolotukhin et al, 1999). Image from Grieger, Samulski and Choi, 2006.

Desalting and concentration of the virus was carried out using Amicon Ultra-15 100 000K (PL100) (Millipore) centrifugal filter device for concentrating samples. The filter was pre-rinsed with 5ml of 1x PBS-MK and centrifuged for 15 minutes at 4000 x g. 5ml of 1x PBS-MK was added to AAV fraction and the total volume was added to the filter device; and centrifuged at 4000 x g for 15-20 minutes or until the volume has been reduced to ~ 2ml. 15ml of 1 x PBS-MK was added to the filter and the spin was repeated. This step was repeated twice (two further 15ml of 1 x PBS-MK added to filter followed by centrifugation). During the final spin, the volume retained in the filter was reduced to ~ 250 µl. The retentant (concentrated, desalted AAV) was removed from the filter, aliquoted in 50 µl volumes and stored at -80°C.

For viral DNA extraction, 10 µl of the virus stock was diluted in 75 µl PCR buffer (50 mM KCl, 10 mM Tris-HCl pH 8.0, 5 mM $MgCl_2$, 0.01% gelatin). The mixture was incubated with 5 µl of DNaseI at 37°C for 1 hour. DNaseI was inactivated at 70°C for 10 minutes. 10 µl (10 µg) of proteinase K was added and incubated for 1 hour at 50°C. Proteinase K was inactivated at 95°C for 20 min. The virus DNA was stored at –20°C.

Quantitative polymerase chain reaction (qPCR) was performed to quantify the final yield of viruses using the following primers (amplicon size of 151 bp):

AAV qPCR PolyA F2 5'- GAGTTTGGACAAACCACAAC -3'
AAV qPCR PolyA R 5'- CCCCCTGAACCTGAAACATAAAATG-3'

The qPCR was carried out using BioLine SensiMix SYBR No-ROX kit (Meridian Bioscience; QT650-02) following the manufacturer's protocol outlined below:

Component	**Volume**
Nuclease free water H_20	4.2 µl
qPCR MasterMix 2 x	10 µl
Forward Primer (10 µM)	0.4 µl
Reverse Primer (10 µM)	0.4 µl
Template DNA (viral DNA extract)	5 µl

The cycling program is as below:
Polymerase activation: 95°C for 10 minutes;
followed by 40 cycles of:
95°C for 15 seconds
60°C for 15 seconds
72°C for 15 seconds

2.8 Infectious centre assay

Briefly, HeRC32 cells were seeded in 48-well plates (7.0E+4 cells/well). The cells were infected the next day with 10-fold dilutions of the rAAV vector preparations in duplicates, in the presence of wild-type Adenovirus type-5 (Ad5) at a multiplicity of 500 infectious units per cell. Cells were harvested 26 hours post-infection and filtered through Zeta-Probe nylon membranes (Bio-Rad) using a vacuum device. Membrane filters were hybridized overnight at 65°C with vector-specific probes generated with the PCR Fluorescein Labelling Mix (Roche). Detection was performed using the CDP-Star ready-to-use labelling kit (Roche). Titers were determined by counting dots (that correspond to AAV infected cells) on membranes autoradiography, which was done blind by two independent scientists. This protocol was initially described in (Salvetti et al, 1998). This work was done in University of Nantes, France.

2.9 *In vivo* gene delivery

2.9.1 Animal husbandry

C57BL/10ScSn-Dmdmdx (*mdx*) mice were bred in house and maintained in minimal disease facilities (Royal Holloway, University of London) with food and water *ad libitum*. *In vivo* experimentation was conducted under statutory Home Office recommendation, regulatory, ethical and licensing procedures, and under the Animals (Scientific Procedures) Act 1986.

2.9.2 Plasmid DNA electrotransfer

Plasmid DNA electrotransfer was performed in young male mdx mice (~10 weeks old) using p-mMD1 and p-585 mMD1. The treatment drug in this study was plasmid DNA diluted in saline solution (sterile 0.9% sodium chloride solution) to required concentration of 0.5 µg/ µl in a total volume of 50 µl per TA injection.

- Treatment **p-mMD1** consists of plasmid DNA expressing a mouse codon optimised microdystrophin cDNA controlled by a muscle-specific promoter Spc5.12 and SV40 polyA signal.
- Treatment **p-585mMD1** consists of plasmid DNA expressing a mouse codon optimised microdystrophin cDNA controlled by a muscle-specific promoter Spc5.12, SV40 polyA signal and an engineered intron 585 R6K-RNA-OUT positioned in between the promoter and the transgene cDNA.

Mice were anesthetized with 2%–4% isoflurane vaporised in 100% O_2 and then reduced to 1.5%-3% as required. To prepare the mice for injection, the skin covering tibialis anterior (TA) muscle was shaved. For electrotransfer of plasmid DNA, the TA muscles were injected with 10 U of bovine hyaluronidase (25 µl at 0.4 U/µl; Sigma). After 2 hours, the mice were anesthetized again as described above and the TA muscle was injected intramuscularly with 0.5 µg/µl of plasmid DNA diluted in sterile saline solution (0.9% sodium chloride solution). The total volume injected per muscle was 50 µl. Control muscle was injected with 50 µl of saline solution. Electrode gel (MediSupplies) was placed on the electrode plates to increase the contact area with the skin of mouse. Electrical field was then

applied to the injected TA muscle using external electrodes at 175 V/cm in 20-msec square wave pulses at 1 Hz using a BTX ECM 830 electroporator (BTX, Tweezertrodes, Kramel Biotech).

2.9.3 Intramuscular AAV delivery

AAV administration was performed in 8-week old male *mdx* mice. The mice were anesthetized with 2%–4% isoflurane vaporised in 100% O_2 and then reduced to 1.5%-3% as required. To prepare the mice for injection, the skin covering tibialis anterior (TA) muscle was shaved. Mice were injected intramuscularly with 50 µl of AAV9/mMD1 or AAV9/585mMD1 diluted in sterile saline solution. Control muscle was injected with 50 µl of saline solution only. Two doses: high (5×10^{11} vp/muscle) and low (5×10^{10} vp/muscle) were tested, and the dosages were determined based on previously published work by (Koo et al, 2011). The number of TA muscles treated was ten in all five treatment groups.

The treatments in this study was rAAV2/9 diluted in saline solution (sterile 0.9% sodium chloride solution) to required concentration as described below in a total volume of 50 µl per TA injection.

- Treatment **saline control** consists of 50 µl of sterile saline solution delivered intramuscularly to the TA muscle.

- Treatment **AAV9/mMD1 low dose** consists of AAV2/9 expressing a mouse codon optimised microdystrophin cDNA controlled by a muscle-specific promoter Spc5.12 and SV40 polyA signal delivered intramuscularly at a dose of 5×10^{10} vp/ TA muscle.

- Treatment **AAV9/585mMD1 low dose** consists of AAV2/9 expressing a mouse codon optimised microdystrophin cDNA controlled by a muscle-specific promoter Spc5.12, SV40 polyA signal and an engineered intron 585 R6K-RNA-OUT positioned in between the promoter and the transgene cDNA, delivered intramuscularly at a dose of 5×10^{10} vp/ TA muscle.

- Treatment **AAV9/mMD1 high dose** consists of AAV2/9 expressing a mouse codon optimised microdystrophin cDNA controlled by a muscle-specific promoter Spc5.12 and SV40 polyA signal delivered intramuscularly at a dose of 5 x 10^{11} vp/ TA muscle.

- Treatment **AAV9/585mMD1 high dose** consists of AAV2/9 expressing a mouse codon optimised microdystrophin cDNA controlled by a muscle-specific promoter Spc5.12, SV40 polyA signal and an engineered intron 585 R6K-RNA-OUT positioned in between the promoter and the transgene cDNA, delivered intramuscularly at a dose of 5 x 10^{11} vp/ TA muscle.

2.9.4 Muscle electrophysiology

Muscle *in situ* electrophysiology was performed by measuring the *in situ* isometric muscle contraction in response to nerve stimulation as described in (Koo *et al*, 2011) under the section "Measurement of the *in-situ* lengthening contraction". Surgical work was performed by Dr Ngoc Lu-Nguyen and measurements were performed by Dr Alberto Malerba. Briefly, mice were anesthetized intraperitoneally using 60mg/kg pentobarbital. As described in (Koo et al, 2011), pins and clamps were used to fix the knee and foot, and the distal tendon of the muscle was attached to a lever arm of a servomotor system using a silk ligature. The sciatic nerve was proximally crushed and stimulated distally using a bipolar silver electrode using supramaximal square wave pulses of 0.1 msec duration. During isometric contractions following electrical stimulation (at different frequencies up to 180 Hz, train of stimulation of 500 msec), absolute maximal isometric tetanic force was measured. The sciatic nerve was stimulated for 700 msec at a frequency of 150 Hz for the muscle to attain maximum isometric force and the initial length of the TA muscle L_0 was recorded. In the first 500 msec, a maximal isometric contraction of the TA muscle was initiated, followed by muscle lengthening (1.1 mm, 10% L_0) at a velocity of 5.5 mm/sec (about 0.5 L_0/ sec) in the last 200 msec. Maximal isometric force was measured following each eccentric contraction and the force measured was expressed as a percentage of the initial maximal isometric force. Eleven isometric lengthening contractions of the TA muscles were performed, each contraction separated by a 60-sec rest period.

2.9.5 Muscle harvest and processing

TA muscles samples were harvested tendon-to-tendon and snap-frozen in isopentane cooled in liquid nitrogen and stored at −80 °C. The TA muscle is collected tendon to tendon, with the overlaying fascia removed as described in (Terry and Wells, 2016). Once the first TA tendon was cut, the TA was carefully detached leaving behind the extensor digitorum longus (EDL) muscle. The TA was mounted upright on a cork disc as shown in Figure 4.4. The TA muscle was sectioned throughout, collecting intermediate sections into 1.5 ml microcentrifuge tubes and picking up one section per level onto microscope slide. The intermediate sections in the tubes were used for assays such as total protein extraction for Western blot.

2.9.6 Immunohistochemistry and histology

For all histological analysis, 10-µm cryosections of muscles were collected on glass slides and air-dried before stored long-term at −80 °C. Before staining, the sections were fixed in cold acetone at −20°C. To reduce background effects, the Mouse on Mouse (M.O.M) kit (Vector Labs) was used to stain muscle sections for immunohistochemistry. Microdystrophin was immunostained using MANEX 1011C (1:100, provided by Dr Glenn Morris), an anti-dystrophin antibody specific for exons 10 and 11 of the dystrophin protein (Le Guiner et al., 2017). The signal was visualized using Alexafluor 568–conjugated anti-mouse IgG (1:200, Invitrogen). Laminin was immunostained using rat anti-laminin monoclonal antibody (1:1000, L0663 Sigma Aldrich). For laminin signal visualisation, anti-rat biotinylated antibody followed by Alexafluor 568–conjugated streptavidin was used. The nuclei were stained with 0.1 µg/ml DAPI and the slides were mounted using mounting medium (Vector Labs). All samples were handled in a blinded manner. Microscope images were acquired using Nikon Eclipse NiE at x20 magnification and analysed using Muscle J plugin in Image J (FIJI).

2.9.7 Percentage microdystrophin-positive fibers calculation

Immunostained laminin facilitated the manual counting of total muscle fibers. TA cross-section immunostained for dystrophin were used to count microdystrophin-positive fibers manually. Percentage microdystrophin-positive fibers were calculated by expressing microdystrophin-positive fibers versus total fibers as a percentage. Approximately 700–1,200 total fibers were counted per muscle (which corresponds to 2-3 fields of views of microscope images taken at x20 objective magnification).

2.9.8 Haematoxylin and eosin staining

Tissue sections were fixed in ice-cold acetone for 5 minutes. Conventional haematoxylin and eosin staining was carried out for morphological assessment according to the TREAT-NMD SOP MDC1A_M.1.2.004. All samples were handled in a blinded manner. Microscope images were acquired using Nikon Eclipse NiE at x20 magnification.

2.9.9 Percentage centronucleated fibers (CNFs) calculation

Immunostained laminin facilitated the counting of total muscle fibers and defining the region of interest for counting of centrally located nuclei. DAPI staining shows the distribution of nuclei. MuscleJ software was used to automate the counting of centronuclei within the fibers. Percentage centronucleated fibers (CNFs) were calculated by expressing CNFs versus total fibers as a percentage. Approximately 700–1,200 total fibers were counted per muscle (which corresponds to 2-3 fields of views of microscope images taken at x20 objective magnification).

2.10 Statistical analysis

All statistical analyses were performed using Prism 8. Where one-way ANOVA was performed, this was followed by Tukey's *post hoc* test. Where two-way ANOVA was performed, this was followed by Bonferroni's *post hoc* test. All data represent mean ± standard error of the mean (SEM). *P ≤ 0.05, **P ≤ 0.01, ***P ≤ 0.001, ****P ≤ 0.0001.

2.11 Bioinformatics analysis

The EMBOSS Cpgplot bioinformatics tool (Madeira et al, 2019) was used to predict the presence of CpG islands along the codon optimised MD1 sequences and the RRO intron sequence. The Cpgplot tool scans the nucleotide sequences over a 200 bp window, moving the window one nucleotide at a time along the sequence, recalculating the ratio of observed to expected number of CG dinucleotides patterns until the end of the specified sequence. The observed number of CpG is the number of times a 'C' is found followed immediately by a 'G'. The expected number of CpG is calculated based on the frequency of C's and G's in that window and is calculated using the formula: [Expected = (number of C's * number of G's) / window length]. A CpG island is defined as a region that satisfies the following parameters: (i) window of more than 200 bases scanned, (ii) calculated (%G + %C) content is over 50% and (iii) calculated Observed/Expected ratio is over 0.6.

2.12 Graphics and illustrations

Where a figure is adapted or modified from another publication, this is clearly stated in the legend linked to the figure. All other figures that were not adapted or modified were created by the author using BioRender illustration software.

Chapter 3 Evaluating expression levels from microdystrophin gene constructs harbouring R6K-RNA-OUT (RRO) sequence elements

3.1 Introduction

The RRO intron (Figure 3.1) used in this thesis (also known as 585 RRO indicating the size of the construct in base pairs) is a synthetic engineered intron as previously described (Lu et al, 2017). Using in vivo systemic delivery of AAV vectors in mice and measuring the transgene expression (human factor 9 (hFIX) and human alpha-1 antitrypsin (hAAT)) from mice serum samples, these authors showed firstly that a 1.3 kb engineered intron called *optimised intron with pUC origin and RNA-OUT* (OIPR) increased the transgene expression levels in treated animals by 100- to 1000-fold: OIPR was placed in the AAV expression cassette between the promoter and transgene. The OIPR intron contains an optimised pUC replication origin and this is the only distinguishing factor of this intron compared to the RRO intron (used in this thesis) which contains a shorter R6K replication origin. The R6K intron at 585bp is ~700 bp shorter than OIPR. Replacing the pUC origin with R6K origin did not diminish the potential of the intron construct to enhance expression and both the engineered introns has comparable levels of transgene expression in treated animals (Lu et al, 2017). No data was presented on expression in other tissues such as skeletal muscle. Based on these studies we therefore wished to test the hypothesis that adding RRO intron in the microdystrophin expressing AAV cassette can enhance transgene expression level in skeletal muscle when the genetic cargo is delivered intramuscularly or systemically using AAV vectors. In particular, we wished to evaluate the RRO intron in AAV-microdystrophin1 (MD1) cassettes using both human and mouse codon optimised MD1 sequences.

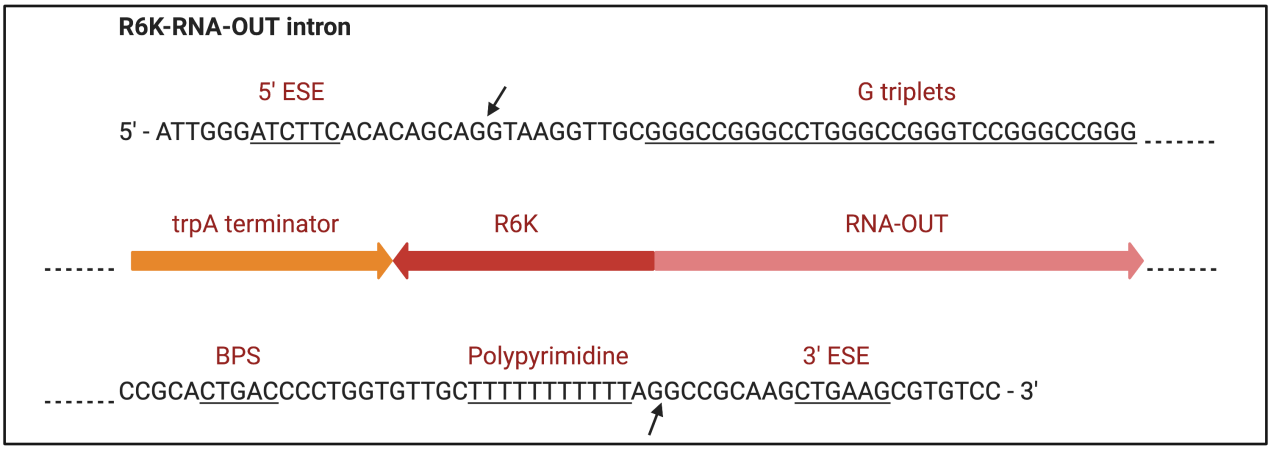

Figure 3.1 **Components of RRO intron**. The 585 bp RRO intron is made up of R6K replication origin, the prokaryotic RNA-OUT (described in Chapter 1) and flanked by other components to ensure efficient splicing: synthesised strong exonic splicing enhancers (ESEs), G triplets, branch point sequence (BPS) and polypyrimidine tract. The 5' and 3' ESEs are binding sites for SR proteins (serine and arginine rich proteins) that aid accurate splicing. The G triplets are commonly found in human 5' splice sites and help in defining the exon-intron borders to ensure overall splicing efficiency. An additional 'protective' feature: trpA terminator was added to prevent prokaryotic transcription initiated by the R6K origin; as such the trpA terminator ensures the R6K to be replication-deficient. The BPS contains an adenine that initiates the first nucleophilic attack in the splicing reaction; the sequence of BPS always contain an adenine and otherwise is not conserved. 4 to 24 nucleotides downstream of BPS, the polypyrimidine tract promotes the assembly of spliceosomes; diminishing this sequence prevents the lariat formation in splicing (Nature Technology, 2013). The two arrows indicate splicing locations (Lu et al, 2017).

The studies of (Lu et al, 2017) have indicated that both the origin of replication (R6K) and RNA-OUT sequences within the intron are essential to maintain enhanced expression associated with the functionality of the intron; where removing either one of the component sequences diminishes the capability of the intron in terms of transgene elevation. However, the origin of replication can be replaced with other known bacterial origins; in the case of using the intron in AAV gene expression constructs, this choice is mainly based on the size of the origins as AAV has a packaging capacity limitation (~4.7 kb). The parental R6K origin has 3 replication origins, α, γ and ß (Rakowski and Filutowicz, 2013); only the γ origin is present in the R6K origin utilised in the intron. Whilst the γ origin itself is a minimal replicon enough to function without the α and ß origins, the activation of this γ origin requires its cognate π protein, encoded by the *pir* gene (Inuzuka and Helinski, 1978) that is absent in the RRO intron as such making it replication deficient.

The Dickson lab have shown that administration of codon optimized microdystrophin significantly increase the transgene expression (Foster *et al*, 2008). The miniaturised gene construct of dystrophin utilised in this project is ΔR4-R23/ΔCT (Figure 3.2). Two versions of microdystrophin-1 (MD1) coding plasmids within AAV expression cassettes were utilised in this study: mouse- and human-codon optimised plasmids (referred to as mMD1 and hMD1 plasmids respectively). These pAAV plasmids consist of synthetic promoter Spc5.12 (Li *et al*., 1999), an optimum Kozak sequence, codon-optimised (mRNA sequence optimised) MD1 transgene coding sequence, SV40 polyadenylation signal and two flanking inverted terminal repeats (ITRs) derived from AAV serotype 2 (disclosure of sequences can be found in Supplementary Data in Section 3.6 Appendix of this chapter). Studies by (Rasowo et al, 2014) have shown that the Spc5.12 promoter induces strong, muscle-specific transgene expression when delivered using AAV9. Kozak sequence is a nucleic acid motif that functions as translation initiation site in most eukaryotes (a feature specific to eukaryotic mRNA). The SV40 polyadenylation signal contains additional sequences upstream and downstream of the consensus sequence AAUAAA that results in

more efficient termination of transcription (Schek, Cooke and Alwine, 1992). The short upstream element sequence (UES); sequences between 13 and 51 nucleotides upstream of the AAUAAA of SV40 late polyA is known to be the essential component in increasing efficiency of transgene expression (Schek, Cooke and Alwine, 1992).

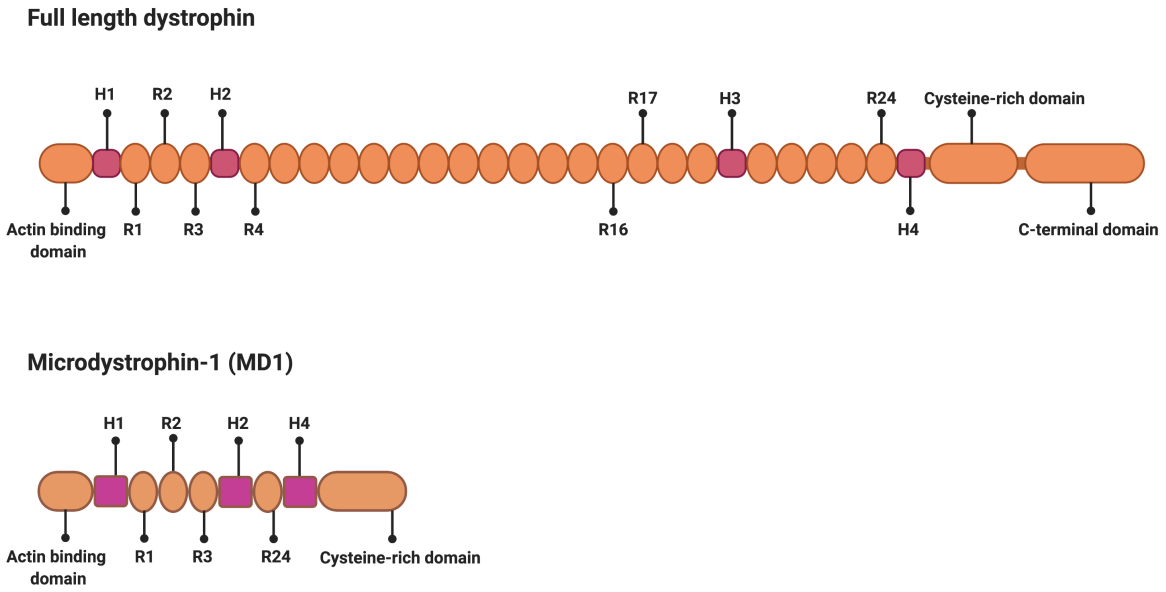

Figure 3.2: **Schematic representation of microdystrophin-1 (MD1) used in this study**. The full-length dystrophin protein consists of an actin binding domain (also the N-terminal domain), four hinges (H1-H4), 24 spectrin repeats called rods (labelled with Rs), a cysteine rich domain and a C-terminal domain. The miniaturised dystrophin protein called microdystrophin; in this instance microdystrophin-1 consists of actin binding domain, hinges 1, 2 and 4, rods 1, 2, 3 and 24, and the cysteine-rich domain (Foster et al, 2008, Le Guiner et al, 2017).

The MD1 coding sequence was inserted into plasmid vectors carrying AAV gene expression cassettes (Figure 3.3).

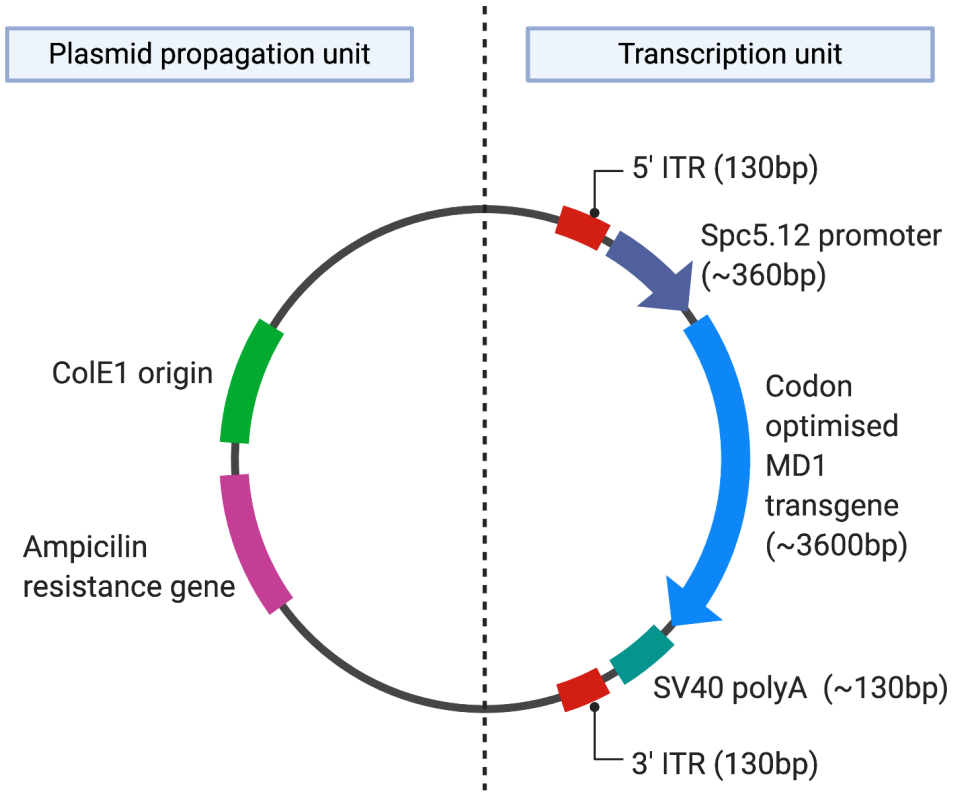

Figure 3.3 **Plasmid vector carrying AAV-MD1 gene expression cassette**. Plasmid vectors for AAV-MD1 consist of two parts: plasmid propagation unit and transcription unit. The plasmid replication is essential for the survival of the transformed bacteria during the selection process. The ampicillin resistance gene codes for the enzyme ß-lactamase that is secreted into the periplasmic space (space between the inner and outer membrane of the bacteria); where the enzyme breaks down ampicillin molecules by hydrolysing the b-lactam rings turning ampicillin into inactive metabolites. The ColE1 is an origin of replication essential for the replication of the plasmid. The transcription unit contains the AAV expression cassette that contains the promoter, transgene and polyA flanked by two ITRs. The sizes of the elements are shown in brackets. The ITR to ITR length of the MD1 expression cassette is ~4.6 kb (which includes all the spacer/ linker sequences in between each individual elements).

In this chapter, the RRO intron was synthesised and the sequence elements were characterised. Microdystrophin transgene coding AAV gene expression cassettes were also characterised and produced, following which the plasmids were verified of their sequence integrity. The RRO intron was cloned into the AAV-microdystrophin cassettes in between the promoter and the transgene. The newly generated plasmid constructs were then tested in cell culture model to evaluate transgene expression levels.

3.2 Results

3.2.1 Synthesis of RRO-intron

The R6K-RNA-OUT intron (RRO intron or 585 RRO) was synthesised by GenScript. The sequence is outlined in Section 3.5 Appendix. EcoRI restriction sites were added at both ends of the synthesised fragment to enable subsequent cloning work described in Section 3.2.3. We also generated 456 bp RRO consisting of only trpA terminator, R6K origin and RNA-OUT; lacking all the other components essential for splicing. This 456 bp RRO will act as a control to test the effect of splicing on the transgene elevation. As the 456 bp RRO will not be spliced out from the transcript, it remains as a 5' untranslated region (UTR). The 456 bp RRO was synthesised by GeneArt (Thermofisher Scientific). The sequence of 456 bp RRO is given in Section 3.5 Appendix on this chapter.

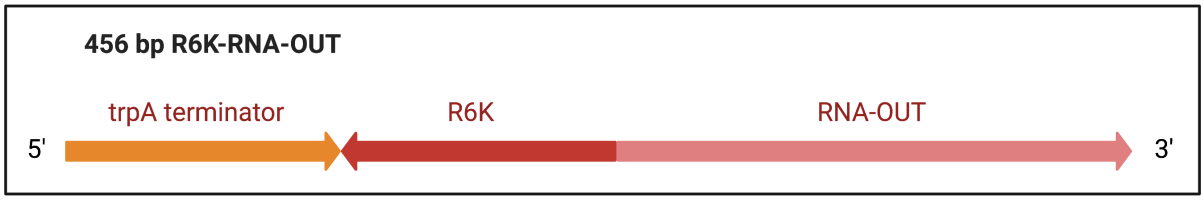

Figure 3.4 **Components of 456 bp R6K-RNA-OUT (456 RRO)**. The 456 bp RRO consists of R6K replication origin, the prokaryotic RNA-OUT (described in Chapter 1) and trpA terminator; but lacks all the other components essential for splicing (Figure 3.1). An additional 'protective' feature: trpA terminator was added to prevent prokaryotic transcription initiated by the R6K origin; as such the trpA terminator ensures the R6K to be replication-deficient (Lu et al, 2017).

3.2.2 Codon optimisation did not introduce CpG islands to the transgene sequence

The Dickson lab have shown that codon optimisation of the MD1 cDNA sequence results in significant increase in mRNA level and increase in number of dystrophin-positive fibers after intramuscular plasmid gene transfer and systemic rAAV gene transfer in DMD mice model: the dystrophin-deficient *mdx* mice (Foster *et al*, 2008). As discussed in Chapter 1, unmethylated CpG islands that are often found in abundance in codon-optimised AAV vector genomes (Wright, 2020) could potentially provoke an innate immune system response via the toll-like receptor 9 (TLR9)-MyD88 pathway (Rogers et al, 2011). As such, it is optimal to reduce such occurrence of CpG islands in the process of codon optimisation.

The EMBOSS Cpgplot bioinformatics tool (Madeira et al, 2019) was used to predict the presence of CpG islands along the codon optimised MD1 sequences and the RRO intron sequence. The Cpgplot tool scans the nucleotide sequences over a 200 bp window, moving the window one nucleotide at a time along the sequence, recalculating the ratio of observed to expected number of CG dinucleotides patterns until the end of the specified sequence. The observed number of CpG is the number of times a 'C' is found followed immediately by a 'G'. The expected number of CpG is calculated based on the frequency of C's and G's in that window and is calculated using the formula: [Expected = (number of C's * number of G's) / window length]. A CpG island is defined as a region that satisfies the following parameters: (i) window of more than 200 bases scanned, (ii) calculated (%G + %C) content is over 50% and (iii) calculated Observed/Expected ratio is over 0.6. No putative CpG islands were predicted in both the mouse- and human-codon optimised microdystrophin protein sequences (Figures 3.6 and 3.7). The RRO sequence was also checked for the presence of potential CpG islands and none was predicted by the EMBOSS Cpgplot tool (Figure 3.8).

Wild-type dystrophin

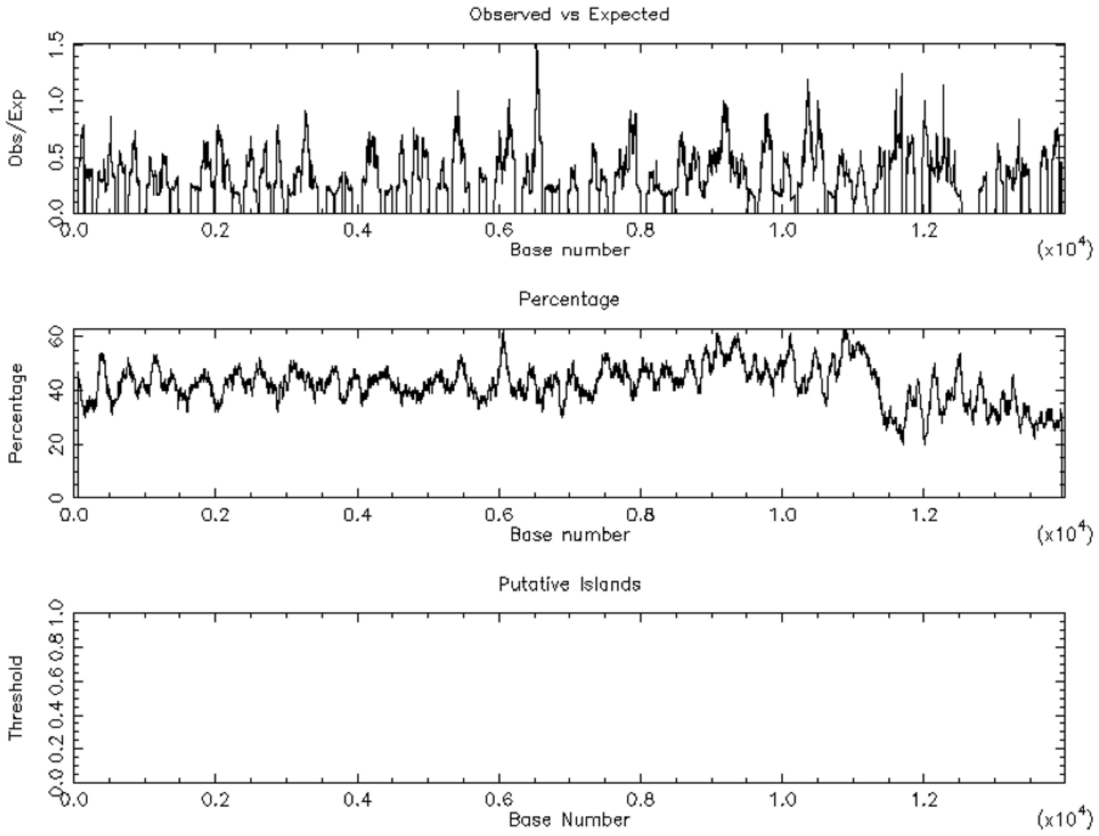

Figure 3.5 **Bioinformatic prediction of CpG islands in wild-type human dystrophin gene.** The wild-type human dystrophin gene sequence [>NM_004006.3 Homo sapiens dystrophin (DMD), transcript variant Dp427m, mRNA] does not contain any CpG islands as predicted by the The EMBOSS Cpgplot bioinformatics tool (Madeira et al, 2019). To satisfy as a CpG island, the window of more than 200 bases scanned must contain a calculated (%G + %C) content of over 50% and calculated Observed/Expected ratio of over 0.6. The Cpgplot tool scans the nucleotide sequences over a 200 bp window, moving the window one nucleotide at a time along the sequence, recalculating the ratio of observed to expected number of CG dinucleotides patterns until the end of the specified sequence. (Top) Observed/ Expected ratio of CpG over the window of 200 bases scanned. (Middle) Percentage %G + %C calculated over the window of 200 bases scanned. (Bottom) Predicted CpG islands over the window of 200 bases scanned.

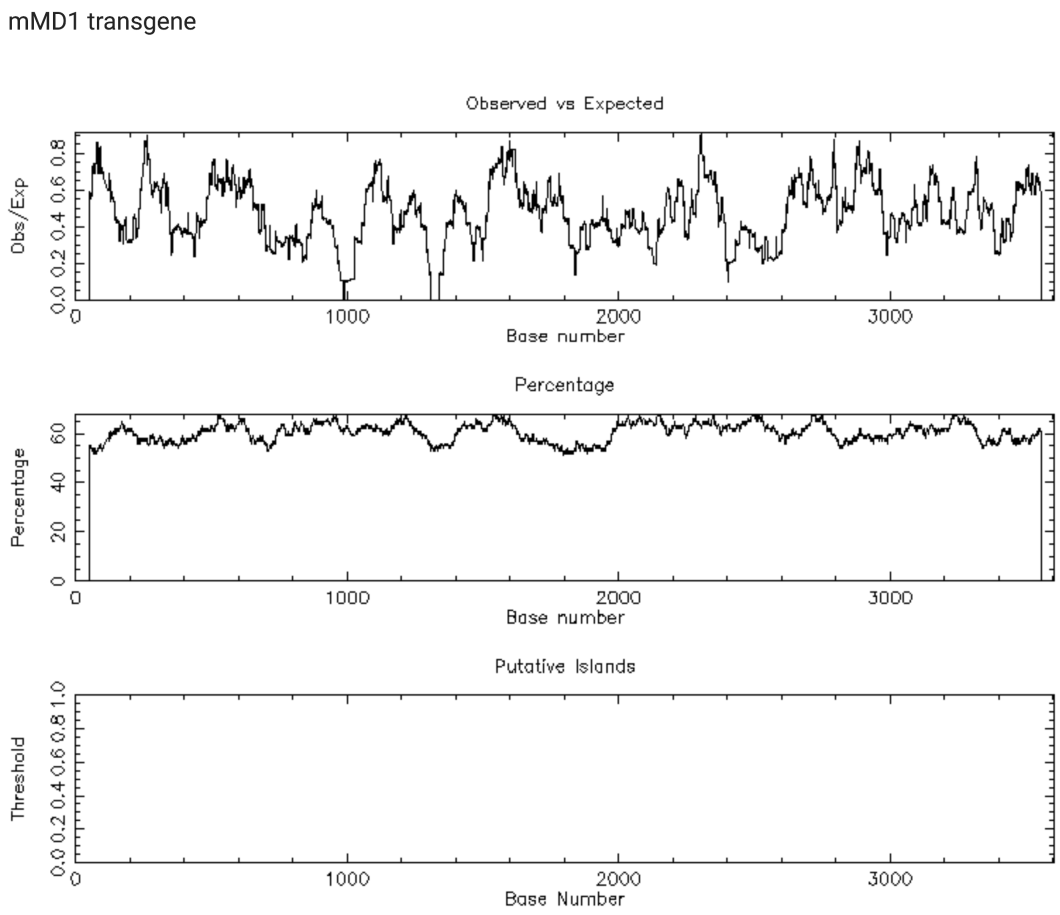

Figure 3.6 **Bioinformatic prediction of CpG islands in mouse codon-optimised mMD1 gene sequences.** The mMD1 gene sequence (sequence in Section 3.5.2) does not contain any CpG islands as predicted by the The EMBOSS Cpgplot bioinformatics tool (Madeira et al, 2019). To satisfy as a CpG island, the window of more than 200 bases scanned must contain a calculated (%G + %C) content of over 50% and calculated Observed/Expected ratio of over 0.6. The Cpgplot tool scans the nucleotide sequences over a 200 bp window, moving the window one nucleotide at a time along the sequence, recalculating the ratio of observed to expected number of CG dinucleotides patterns until the end of the specified sequence. (Top) Observed/ Expected ratio of CpG over the window of 200 bases scanned. (Middle) Percentage %G + %C calculated over the window of 200 bases scanned. (Bottom) Predicted CpG islands over the window of 200 bases scanned.

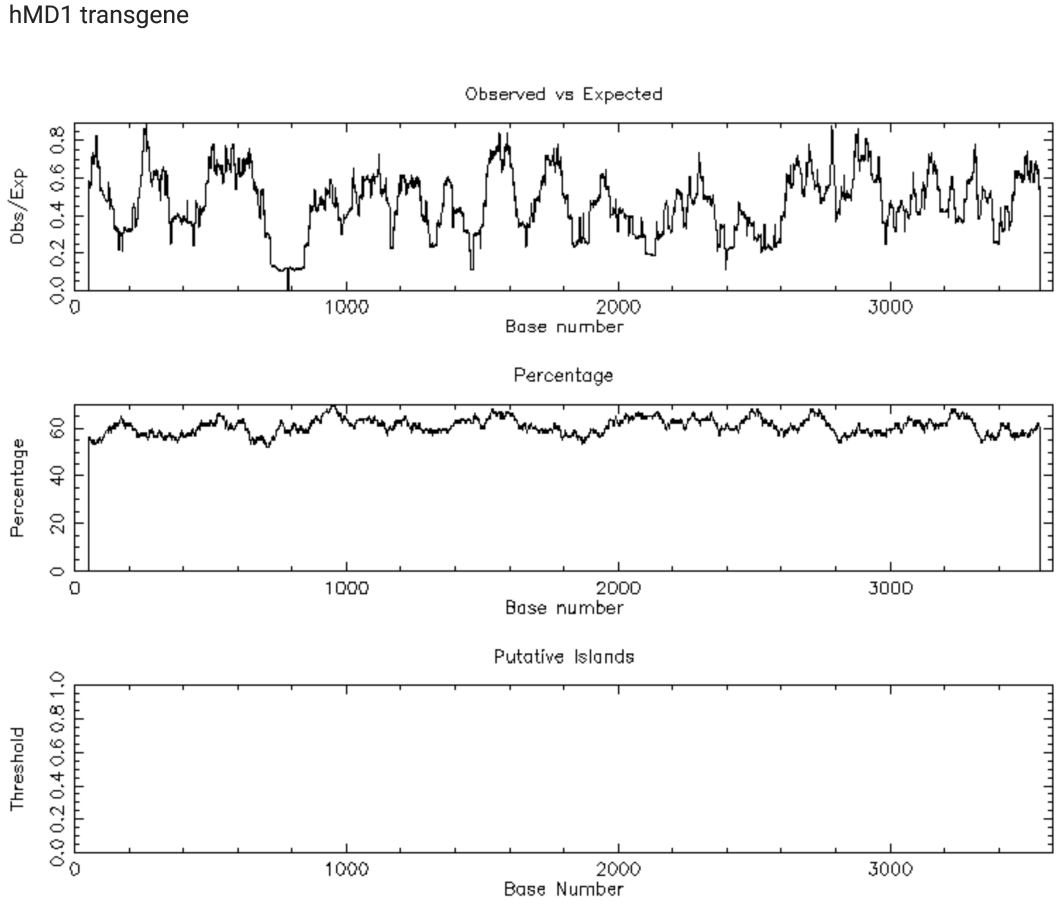

Figure 3.7 **Bioinformatic prediction of CpG islands in human codon-optimised mMD1 gene sequences.** The hMD1 gene sequence (sequence in Section 3.5.3) does not contain any CpG islands as predicted by the The EMBOSS Cpgplot bioinformatics tool (Madeira et al, 2019). To satisfy as a CpG island, the window of more than 200 bases scanned must contain a calculated (%G + %C) content of over 50% and calculated Observed/Expected ratio of over 0.6. The Cpgplot tool scans the nucleotide sequences over a 200 bp window, moving the window one nucleotide at a time along the sequence, recalculating the ratio of observed to expected number of CG dinucleotides patterns until the end of the specified sequence. (Top) Observed/ Expected ratio of CpG over the window of 200 bases scanned. (Middle) Percentage %G + %C calculated over the window of 200 bases scanned. (Bottom) Predicted CpG islands over the window of 200 bases scanned.

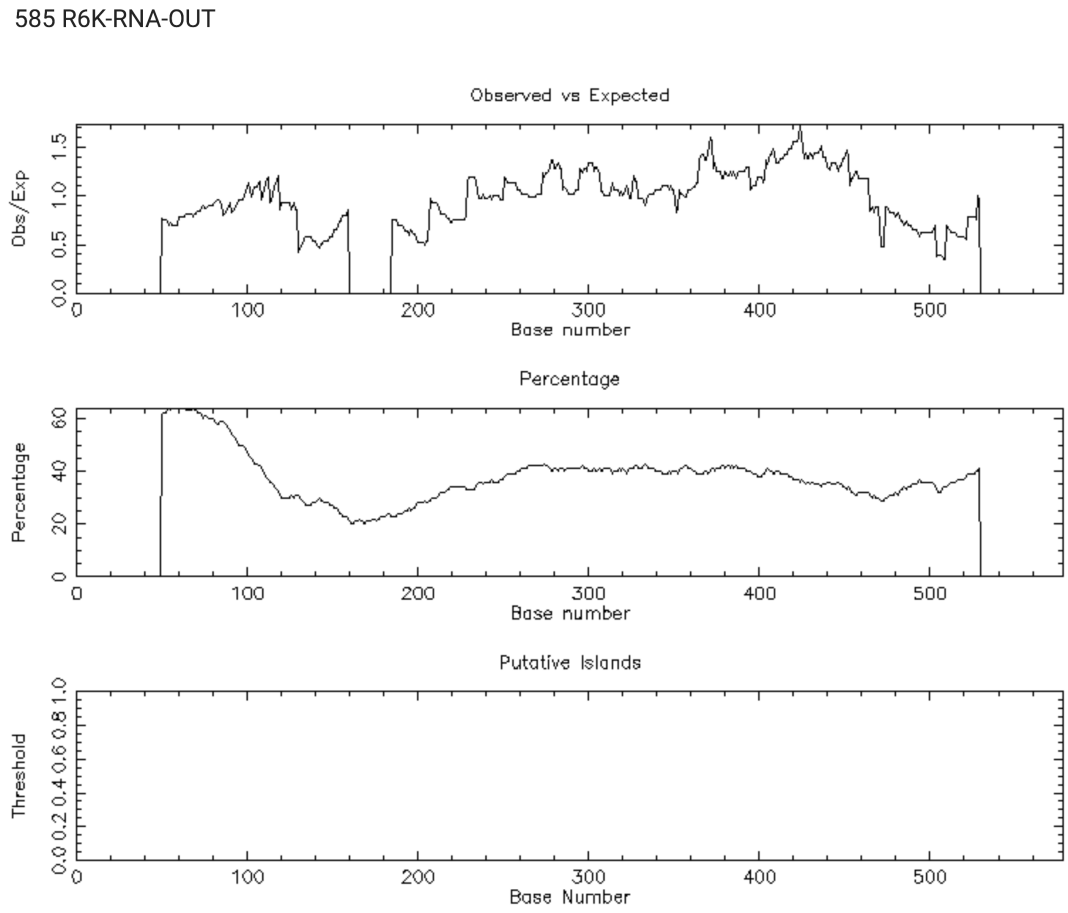

Figure 3.8 **Bioinformatic prediction of CpG islands in 585 RRO intron sequence.** The 585 RRO sequence (sequence in Section 3.5.7) does not contain any CpG islands as predicted by the The EMBOSS Cpgplot bioinformatics tool (Madeira et al, 2019). To satisfy as a CpG island, the window of more than 200 bases scanned must contain a calculated (%G + %C) content of over 50% and calculated Observed/Expected ratio of over 0.6. The Cpgplot tool scans the nucleotide sequences over a 200 bp window, moving the window one nucleotide at a time along the sequence, recalculating the ratio of observed to expected number of CG dinucleotides patterns until the end of the specified sequence. (Top) Observed/ Expected ratio of CpG over the window of 200 bases scanned. (Middle) Percentage %G + %C calculated over the window of 200 bases scanned. (Bottom) Predicted CpG islands over the window of 200 bases scanned.

3.2.3 Characterisation of initial plasmids used in cloning: Restriction digest using multiple restriction enzymes shows integrity of purified rAAV-Spc5.12-MD1 plasmids

Due to their secondary structure and repetitive nature, the inverted terminal repeat (ITR) regions in AAV plasmids are particularly unstable during processes such as plasmid propagation and subcloning and are prone to deletions. To reduce such events, recombination deficient bacterial strains are necessary for such workflow and TOP10 cells (Wilmott et al, 2019) were used in this study. An optimized protocol is used in plasmid propagation where the AAV plasmids are produced in bacterial host cells growing at 32ºC instead of 37ºC; with a culture time between 14 and 16 hours (Wilmott et al, 2019). Nevertheless, after every cycle of bacterial growth and plasmid preparation, a quality control step is necessary. Direct sequencing would be ideal, but routine Sanger sequencing is inadequate due to the high GC content and the secondary structure of the ITRs restricting the movement of DNA polymerase along the sequence. Alternatively, detailed restriction enzyme site evaluations targeting specific regions around the ITRs are often use routinely to confirm the integrity of these regions in the plasmids (Figure 3.5). Restriction digest profiles of the MD1 plasmids revealed that the AAV gene expression cassettes within the plasmids appeared to be intact without any deletions detectable by these methods.

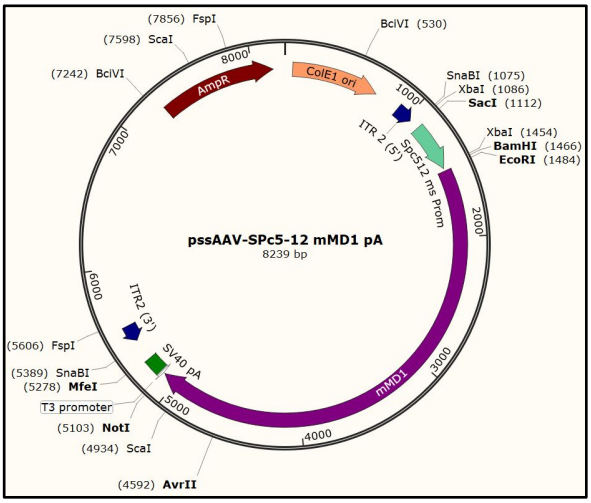

Restriction enzymes	Expected fragments
AvrII	8239
SnaBI	3925, 4314
BamHI-HF + BciVI	936, 1527, 5776
MfeI-HF + FspI	328, 2250, 5661
SacI-HF	8239
NotI-HF	8239
EcoRI-HF	8239
ScaI-HF	2664, 5575
XbaI	368, 7871

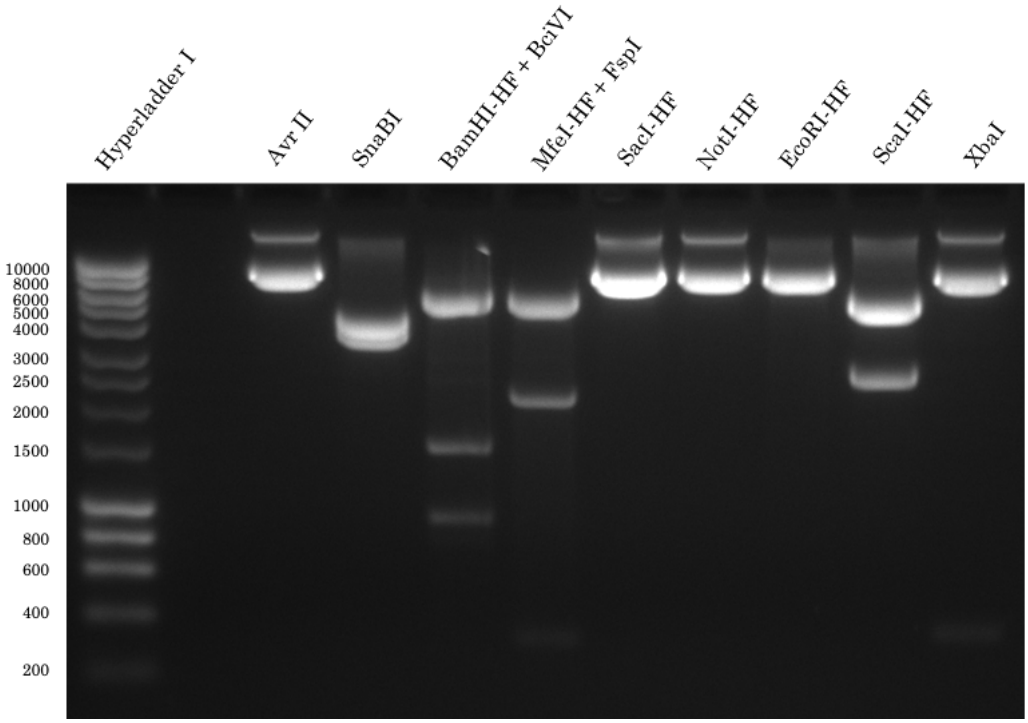

Figure 3.9 **Restriction enzyme digest profile of mouse-codon optimized pAAV-Spc5.12-MD1.** Plasmid map with restriction sites mapped in are shown on the top left (image generated using SnapGene). Numbers in round brackets next to restriction enzymes indicate positions of the cutting sites of the respective enzymes. Agarose gel image show the presence of all the expected bands confirming the integrity of the constructs. The expected fragment sizes in base pairs (bps) are shown on the respective tables (top right). All restriction enzyme digests were performed using the recommended buffers supplied by New England Biolabs with the restriction enzymes, at respective optimal temperatures provided by the manufacturer. HF: high-fidelity.

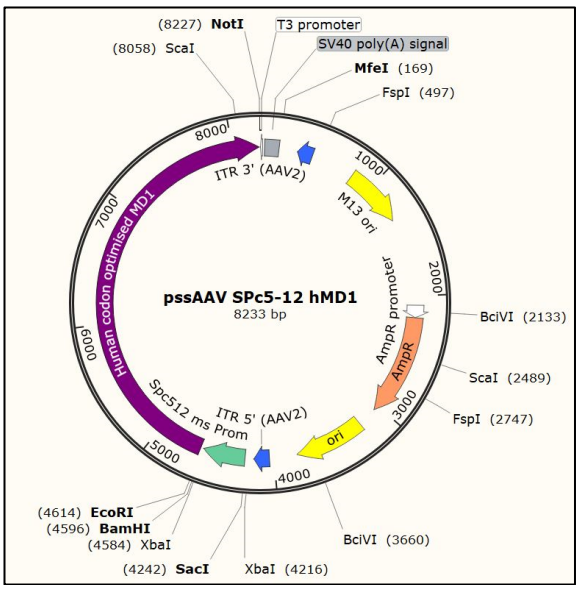

Restriction enzymes	Expected fragments
BamHI-HF + BciVI	936, 1527, 5770
MfeI-HF + FspI	328, 2250, 5655
SacI-HF	8233
NotI-HF	8233
EcoRI-HF	8233
ScaI-HF	2664, 5569
XbaI	368, 7865

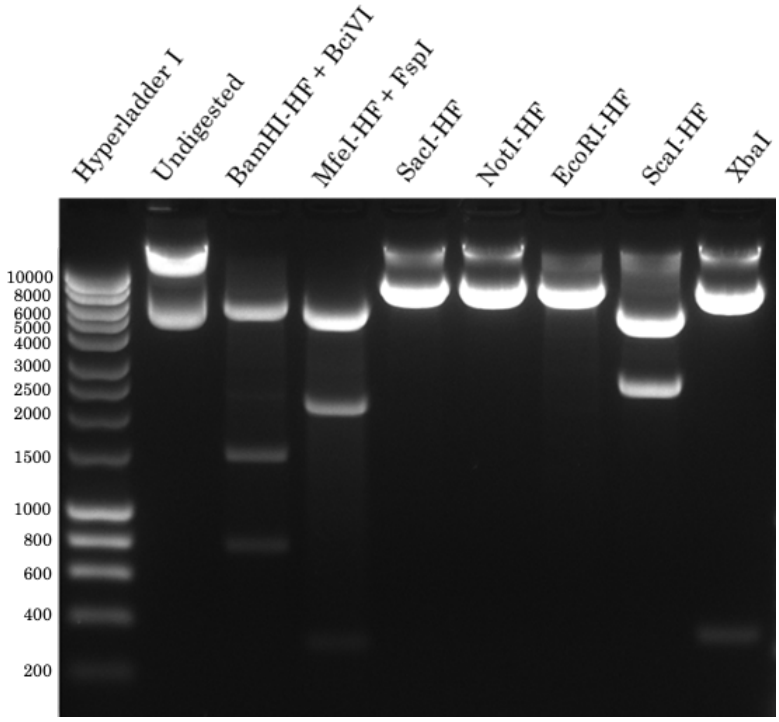

Figure 3.10 **Restriction enzyme digest profile of human-codon optimized pAAV-Spc5.12-MD1.** Plasmid map with restriction sites mapped in are shown on the top left (image generated using SnapGene). Numbers in round brackets next to restriction enzymes indicate positions of the cutting sites of the respective enzymes. Agarose gel image show the presence of all the expected bands confirming the integrity of the constructs. The expected fragment sizes in base pairs (bps) are shown on the respective tables (top right). All restriction enzyme digests were performed using the recommended buffers supplied by New England Biolabs with the restriction enzymes, at respective optimal temperatures provided by the manufacturer. HF: high-fidelity.

3.2.4 Plasmid cloning of RRO elements into the AAV expression cassettes harbouring codon-optimized MD1 genes.

We wished to clone both the 585bp (intronic) and 456bp (non-intronic) RRO elements into the MD1 AAV plasmid vectors. Cloning of the 456 bp RRO into human (h) and mouse (m) codon optimized MD1 expression cassettes were done in-house using the EcoRI site between the promoter and the transgene in the existing codon optimised pAAV-Spc5.12-MD1 plasmids (see Figures 3.9 and 3.10) and the cloning workflow shown in Figures 3.11 and 3.12). The success of the cloning workflow was verified using (i) PCR using primers that amplify the 456 bp RRO region and (ii) sequencing of the 456 bp RRO region which include both the insert-vector junctions.

The cloning of 585 bp RRO intron into the MD1 AAV plasmid vectors were done by GenScript, following synthesis of the intron. The same approach was used by GenScript, where the EcoRI site between the promoter and the transgene in the existing codon optimised pAAV-Spc5.12-MD1 plasmids were used to insert the 585 bp RRO intron into the vector plasmids.

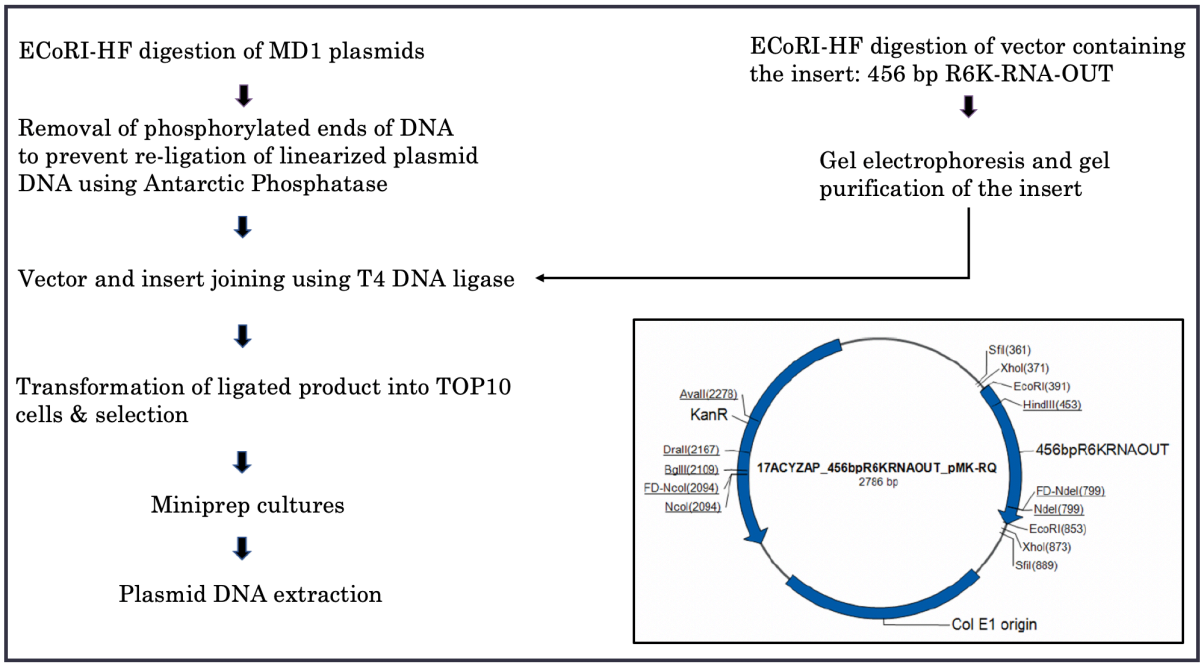

Figure 3.11 **Cloning of the 456 RRO element into MD1 plasmids**. Following synthesis of 456 bp RRO by GeneArt (ThermoFisher), the fragment was cloned into a kanamycin-resistant vector plasmid by the manufacturer (shown in the smaller box) via two ECoRI sites, which were added at the ends of the 456 RRO fragment during synthesis. The presence of an ECoRI site in both the mMD1 and hMD1 plasmids in between the Spc5.12 promoter and MD1 transgene enabled restriction digest cloning of 456 RRO into the plasmids. Antartic phosphatase non-specifically catalyzes the dephosphorylation of 5´ and 3´ ends of DNA; and as such, the linearised vector plasmids were treated with Antartic phosphatase to remove phosphorylated ends to prevent religation of the linearized plasmid DNA. In a mixture of the plasmid vector and RRO insert, DNA ligase catalyzes the formation of phosphodiester bond between juxtaposed 5' phosphate and 3' hydroxyl termini. The workflow from transformation onwards are described in detail in Figure 3.12.

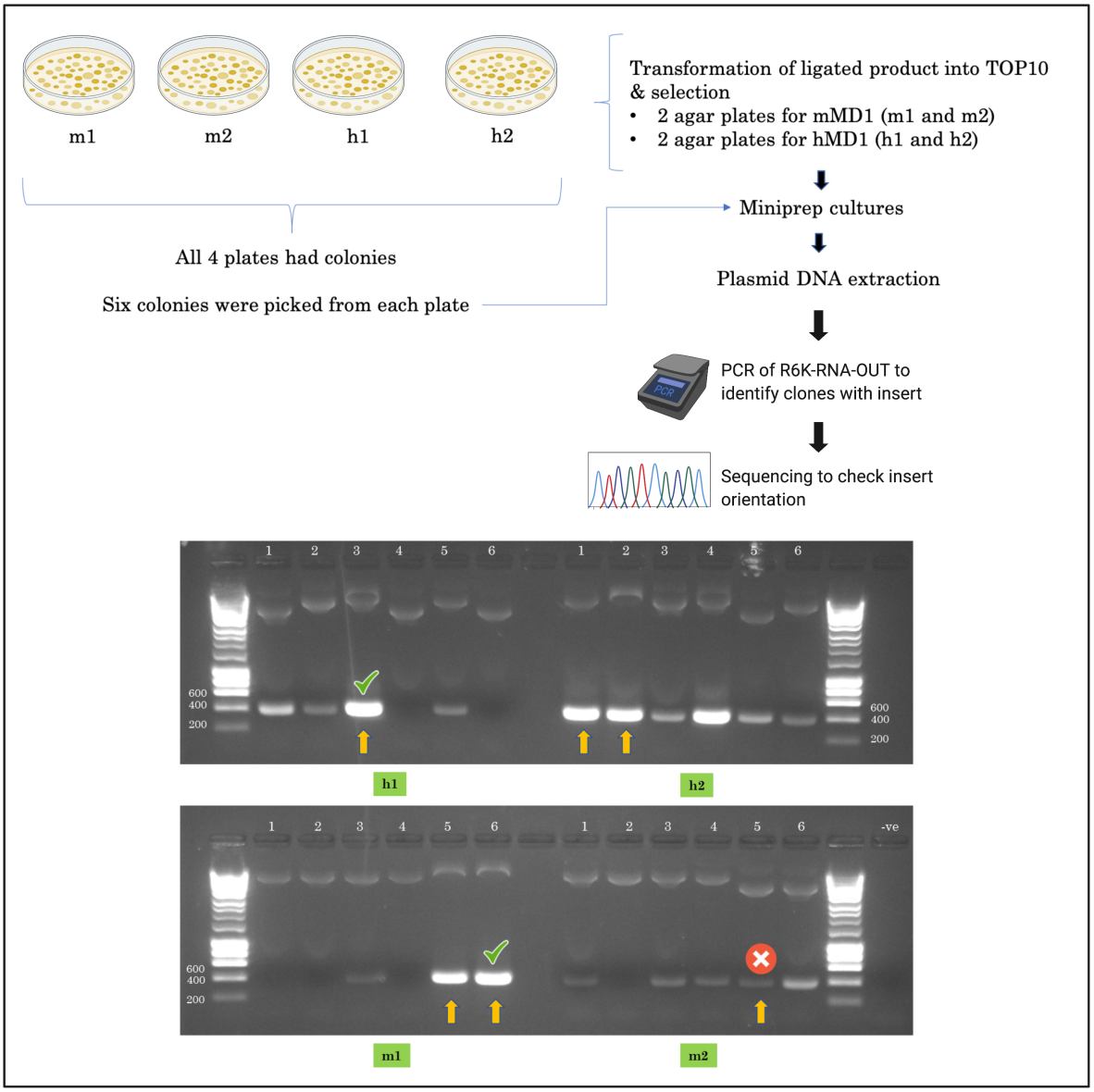

Figure 3.12 **PCR screening to identify plasmids harbouring the 465bp RRO in the correct orientation**. The ligated products were transformed and selected in TOP10 cells. Two agar plates were set up for mMD1 (m1 and m2) and hMD1 (h1 and h2). All plates had colonies. Six colonies from each plate were miniprepped and plasmids were purified. To check whether the cloning reaction using ECoRI worked, PCR reaction targeting the RRO region was set up. Six samples were negative for the presence of RRO: h1-4, h1-6, m1-1, m1-2, m1-4, m2-2. This was probably due to vector re-ligation without the insert during the cloning reaction. For the positive samples, there is a 50% chance of incorrect orientation of insert. To identify which sample had the 456 RRO insert in the correct orientation, three randomly selected positive samples from mMD1 & hMD1 were sent for sequencing. Yellow arrows indicate samples that were gel-purified and sent for sequencing. Green ticks indicate positive samples with correct

orientation. Red cross indicate failed sequencing. Bands with yellow arrows but without ticks are samples with reversed insert. Gel electrophoresis was performed on a 1% agarose gel at 80 V for 1 hour.

Following successful cloning, four new plasmids (noted as 'p') were generated in addition to pAAV-Spc5.12-mMD1 (also called p-mMD1) and pAAV-Spc5.12-hMD1 (also called p-hMD1) (Figure 3.13):

pAAV-Spc5.12-456R6KRNAOUT-mMD1	(also called p-456mMD1)
pAAV-Spc5.12-585R6KRNAOUT-mMD1	(also called p-585mMD1)
pAAV-Spc5.12-456R6KRNAOUT-hMD1	(also called p-456hMD1)
pAAV-Spc5.12-585R6KRNAOUT-hMD1	(also called p-585hMD1)

In p-585mMD1 and p-585hMD1, the RRO is expressed as 5' untranslated region (UTR) harbouring an intron with all the signals necessary for splicing, whereas in p-456mMD1 and p-456hMD1, the RRO element is expressed as a 5' untranslated region with no canonical splicing signals.

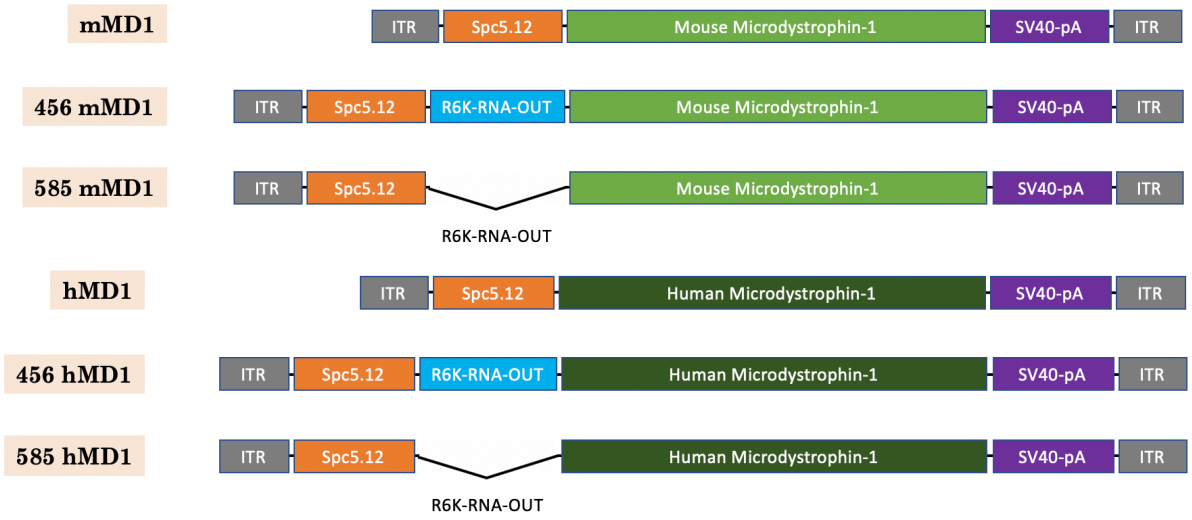

Figure 3.13 **Transcription units generated following cloning of the 585bp and 465bp RRO elements into mMD1 and hMD1 AAV plasmids**. Cloning of 456 bp RRO into p-mMD1 and p-hMD1 generated p-456mMD1 and p-456hMD1 respectively. 456 bp RRO exists as 5' untranslated region in the construct. Cloning of 585 bp intronic version of RRO into p-mMD1 and p-hMD1 generated p-585mMD1 and p-585hMD1 respectively.

Multiple restriction enzyme digests around the ITRs of the newly generated plasmids were performed to check the integrity of the 456mMD1 and 585mMD1 constructs, and the AAV ITRs (Figure 3.14). Restriction profiles of these plasmids revealed that the AAV gene expression cassettes within the plasmids were as predicted without any obvious unwanted deletions including in the ITRs.

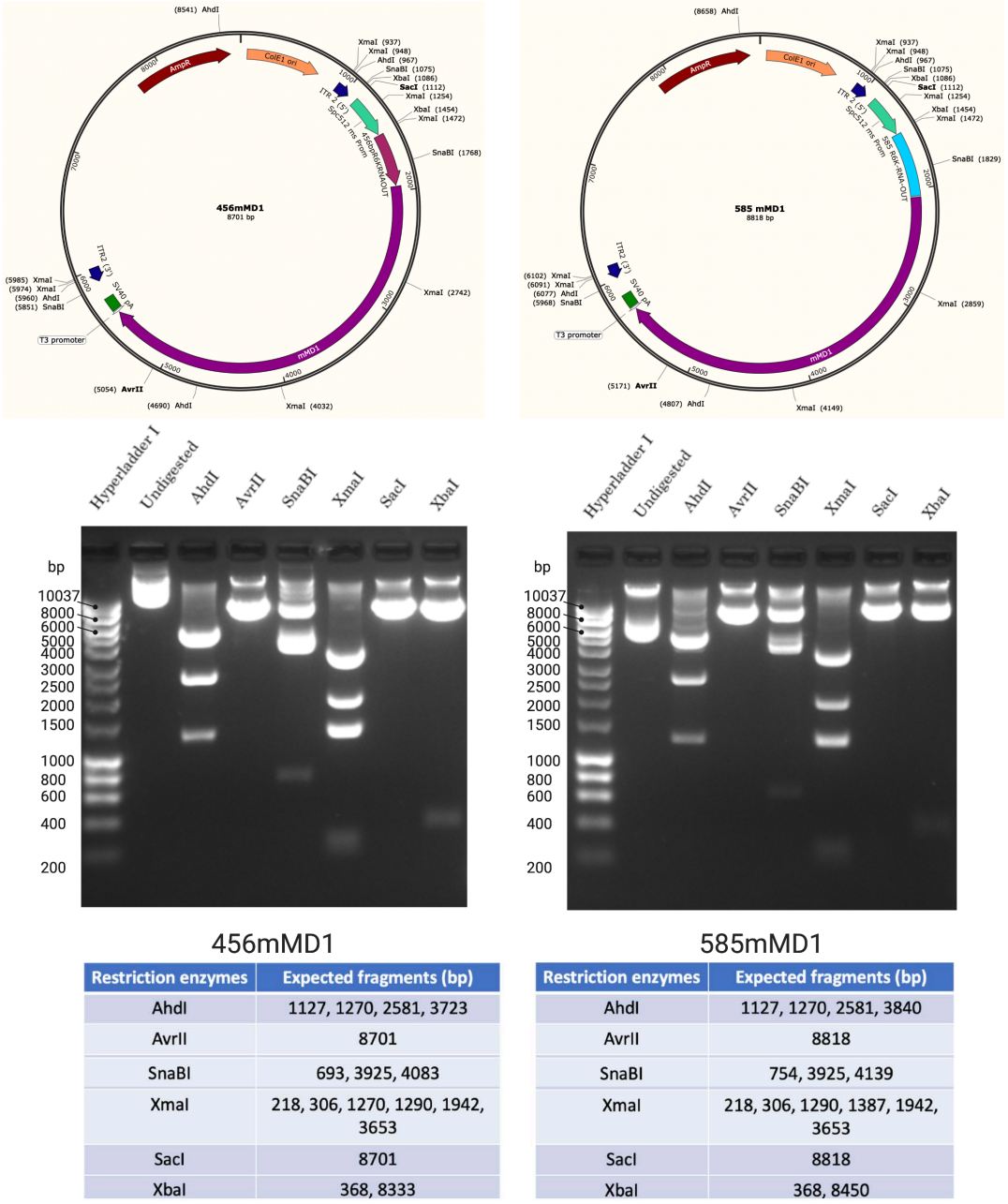

456mMD1

Restriction enzymes	Expected fragments (bp)
AhdI	1127, 1270, 2581, 3723
AvrII	8701
SnaBI	693, 3925, 4083
XmaI	218, 306, 1270, 1290, 1942, 3653
SacI	8701
XbaI	368, 8333

585mMD1

Restriction enzymes	Expected fragments (bp)
AhdI	1127, 1270, 2581, 3840
AvrII	8818
SnaBI	754, 3925, 4139
XmaI	218, 306, 1290, 1387, 1942, 3653
SacI	8818
XbaI	368, 8450

Figure 3.14 **Restriction enzyme digest profile of mouse-codon optimized p-456mMD1 and p-585mMD1.** Plasmid maps with restriction sites mapped in are shown at the top (image generated using SnapGene). Numbers in round brackets next to restriction enzymes indicate positions of the cutting sites of the respective enzymes. Agarose gel image (middle) show the presence of all the expected bands confirming the integrity of the constructs. The expected fragment sizes in base pairs (bps) are shown on the respective tables (bottom). All restriction enzyme digests were performed using the recommended buffers supplied by New England Biolabs with the restriction enzymes, at respective optimal temperatures provided by the manufacturer.

The cloning workflow to generate 585hMD1 was performed commercially by the gene synthesis company GenScript. They synthesised the RRO intron fragment and cloned it into the p-hMD1 vector we supplied. Restriction enzyme digest fragment analyses demonstrated the integrity of the vector plasmid p-hMD1 and the ITRs (Figure 3.10). However, for transparency we would report that GenScript also suggested that a small deletion of unknown size and nature may have been present in the 5' ITR of the original hMD1 vector plasmid. This prediction was based on observing regions of sequencing outputs which were smoothly readable or unreadable, but not on direct nucleotide sequence data per se. During standard Sanger sequencing the whole ITR sequence will not normally yield readable outputs due to highly stable secondary structure. However, the company surmised that occasional small smoothly-readable outputs of ITR sequence may indicate a relaxation of secondary structure caused by a deletion(s). The predicted region where the possible unknown deletion may exist, postulated by the GenScript analysis is indicated in Figure 3.15.

Deletions and rearrangements of ITR sequences is a well-recognised phenomenon is the field of AAV vector production and can affect encapsidation efficiency and vector yields (Wilmott et al, 2019). It is worth noting here that the studies performed in this thesis of transcriptional and translational activity using the hMD1 construct sets (hMD1, 456hMD1 and 585hMD1) were entirely plasmid-based, and as such these studies would be unlikely to be affected by any putative ITR variation, if it exists. The hMD1 plasmid constructs were not vectorised or evaluated in infectious AAV format, but if they were in the future, we would recommend that specialised ITR-compatible sequencing be performed and cloning work carried out if necessary to repair the defective 5' ITR.

Figure 3.15 **Conventional Sanger sequencing suggests that a small deletion may potentially exist in the 5'-ITR of hMD1 plasmid.** Sanger sequencing output around 5'-ITR region of hMD1 plasmid is shown. Normally only a few bases (10-12) can be read on the extremes of the ITRs, due to complex secondary structure. However, as can be seen some additional sequence is clearly readable between nucleotide position ~4120 nt

and ~4170 nt. The commercial company GenScript suggested that this may be due to a more relaxed secondary structure arising potentially from a small deletion in the ITR between ~4040 nt and ~4120 nt of the sequence shown.

3.2.5 Testing of microdystrophin constructs in an *in vitro* model to evaluate transgene expression level and splicing activity.

To evaluate relative levels of protein expression from the microdystrophin constructs, transient transfection experiments using mouse- and human- codon optimized MD1 plasmids (m/hMD1, 456m/hMD1 and 585m/hMD1) were carried out in HEK293T (Figure 3.16). The HEK293T cells were transfected with the maximum optimised plasmid dose of 4 μg for 9.4 cm^2 growth area (well size of a 6-well plate) (Moore, 2018). At 48 hours following transfection, the cells were harvested and total RNA was extracted and reverse-transcribed into cDNA for further analysis. A constant amount of 500 ng of total RNA was used for reverse transcription of each sample and 100 ng of the cDNA generated was used as template for PCR reactions. The PCR protocol was optimised to ensure the reactions were in the exponential phase where the substrate components and DNA polymerase are not rate limiting (Section 3.6 Supplementary data). The abundance of each PCR product was calculated via densitometry and MD1 was normalised to ß-actin loading control; where the ratio of MD1: ß-actin abundance is a readout of transcription level. At the transcription level, no difference was observed between the mouse and human codon optimised MD1, 456MD1 and 585MD1 (Figure 3.16), indicating that the RNA production was unaffected by the presence of RRO as a 5'UTR or in the intronic form.

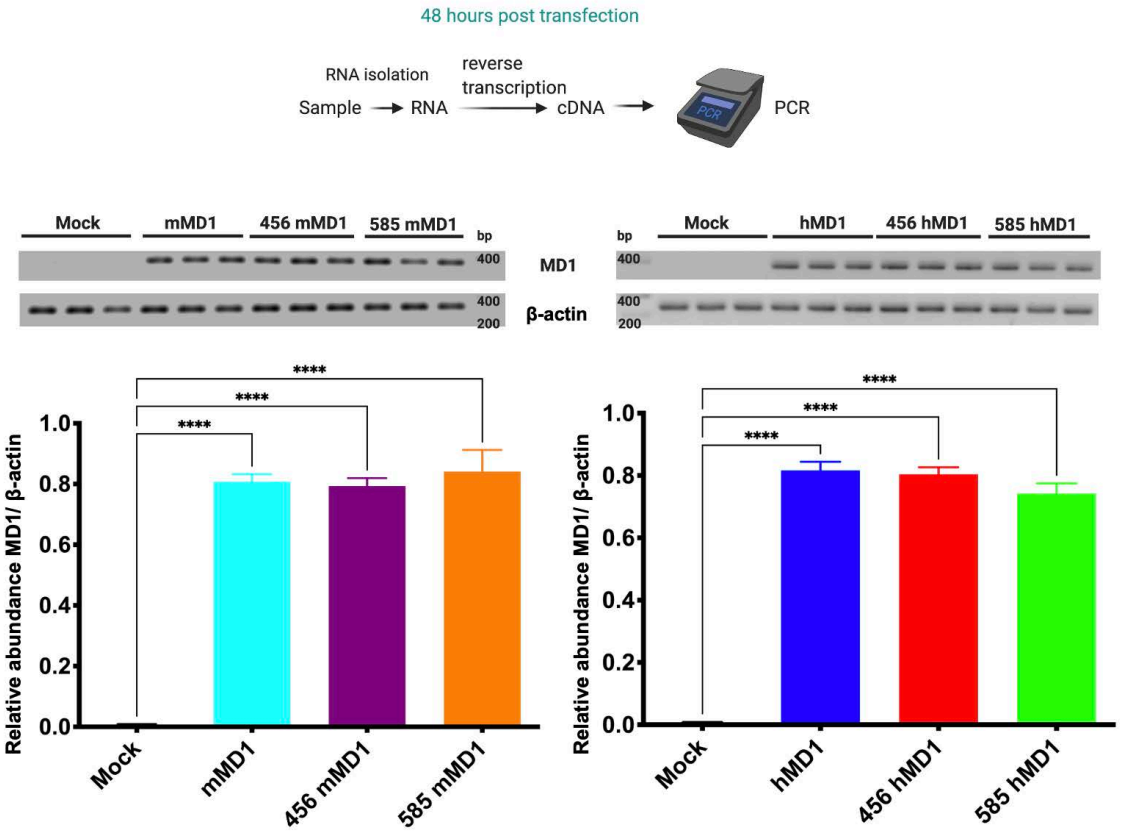

Figure 3.16 **Total RNA analysis following transient transfection of HEK293T with the codon optimised MD1 plasmid constructs**. Top: Transient transfection workflow to evaluate transgene expression capabilities of the plasmid constructs. Six plasmids were tested (p-mMD1, p-hMD1, p-456mMD1, p-456hMD1, p-585mMD1 and p-585hMD1). HEK293T cells were transfected with plasmid dose of 4 µg for 9.4 cm^2 growth area (well size of a 6-well plate). At 48 hours following transfection, the cells were harvested and total RNA was extracted and reverse-transcribed into cDNA for further analysis. A constant amount of 500 ng of total RNA was used for reverse transcription of each sample and 100 ng of the cDNA generated was used as template for PCR reactions. The abundance of each PCR product was calculated via densitometry and MD1 was normalised to ß-actin loading control; where the ratio of MD1: ß-actin abundance is a readout of transcription level. cDNA: complementary DNA; PCR: polymerase chain reaction. Statistical analysis by one-way ANOVA. All data represent mean ± SEM. N=3 for each treatment. ****$P \leq 0.0001$.

We also tested the splicing activity of the constructs by performing a total RNA analysis targeting the RRO region. The presence of RRO sequences in the mRNA indicates that splicing has not taken place. The data (Figure 3.17) showed that splicing indeed happened in the codon-optimised 585 MD1 constructs as the RRO is present as an intron. In the 456 MD1 constructs, the RRO sequence was retained as the splicing signals were not present in the constructs.

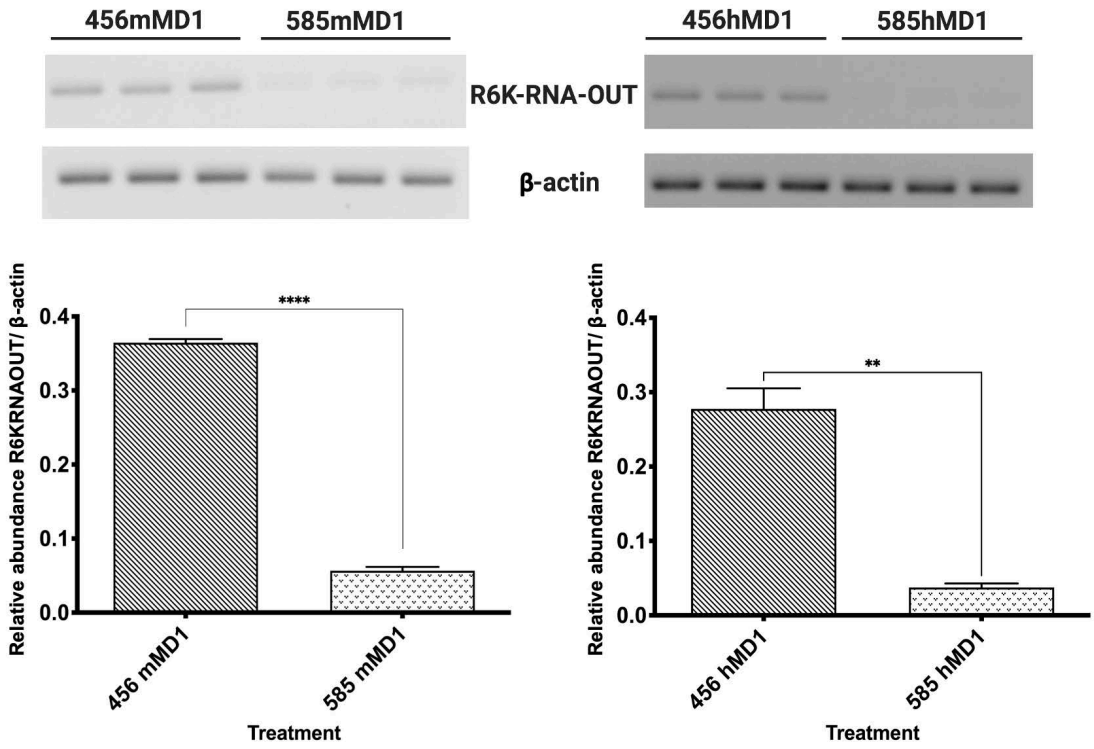

Figure 3.17 **Total RNA analysis evaluating splicing of RRO following transient transfection of HEK293T with codon optimised MD1 constructs**. Four plasmids were tested (p-mMD1, p-hMD1, p-585mMD1 and p-585hMD1). HEK293T cells were transfected with plasmid dose of 4 μg for 9.4 cm^2 growth area (well size of a 6-well plate). At 48 hours following transfection, the cells were harvested and total RNA was extracted and reverse-transcribed into cDNA for further analysis. A constant amount of 500 ng of total RNA was used for reverse transcription of each sample and 100 ng of the cDNA generated was used as template for PCR reactions. The abundance of each PCR product was calculated via densitometry and RRO was normalised to ß-actin loading control; where the ratio of RRO: ß-actin abundance is a readout of splicing of RRO. Statistical analysis by one-way ANOVA. All data represent mean ± SEM. N=3 for each treatment. ****$P \leq 0.0001$.

For evaluation of the activity of the various MD1 gene expression cassettes at the level of protein production, HEK293T cells were again transfected and harvested after 72 hours for total protein extraction, quantification and Western blotting immunological analyses. Protein concentrations from the extracted total proteins were quantified using DC™ (detergent compatible) protein colorimetric assay measured at 750 nm. 50 µg of protein extracts from HEK293T were loaded on NuPAGE Novex 3–8% Tris Acetate gel. Following blocking, the membrane was cut using the protein ladder as guide to separate the antibody incubations to detect microdystrophin and the protein sample loading control, alpha-tubulin. The membrane was incubated with MANEX 1011C (1:100 dilution), an anti-dystrophin antibody specific for exons 10 and 11 of the dystrophin protein (Glenn Morris; Le Guiner et al., 2017) and with a secondary goat anti-mouse antibody (1: 10000 dilution). For protein sample loading control, the membrane was incubated with anti-alpha tubulin antibody raised in rabbit (1:2500 dilution) and with a secondary donkey anti-rabbit antibody (1: 10000 dilution). Complete details of the workflow including suppliers and manufacturers of the materials can be found in Chapter 2: Materials and Methods. Immunoblots were visualized by Odyssey CLx Imaging System (LI-COR) using fluorescence detection. Direct detection was possible as the secondary antibodies used were labelled with near-infrared fluorescent dyes. The secondary antibody used for detection of microdystrophin fluoresces at 800 nm channel (green signals on immunoblots) and for the protein loading control, the secondary antibody used for detection fluoresces at 700 nm channel (red signals on immunoblots).

As shown in Fig 3.18, an increase in level of MD1 transgene product expression was seen with constructs containing the 585 RRO intron in both the mouse- and human-codon optimised constructs when compared to unmodified or the 465-containing constructs.

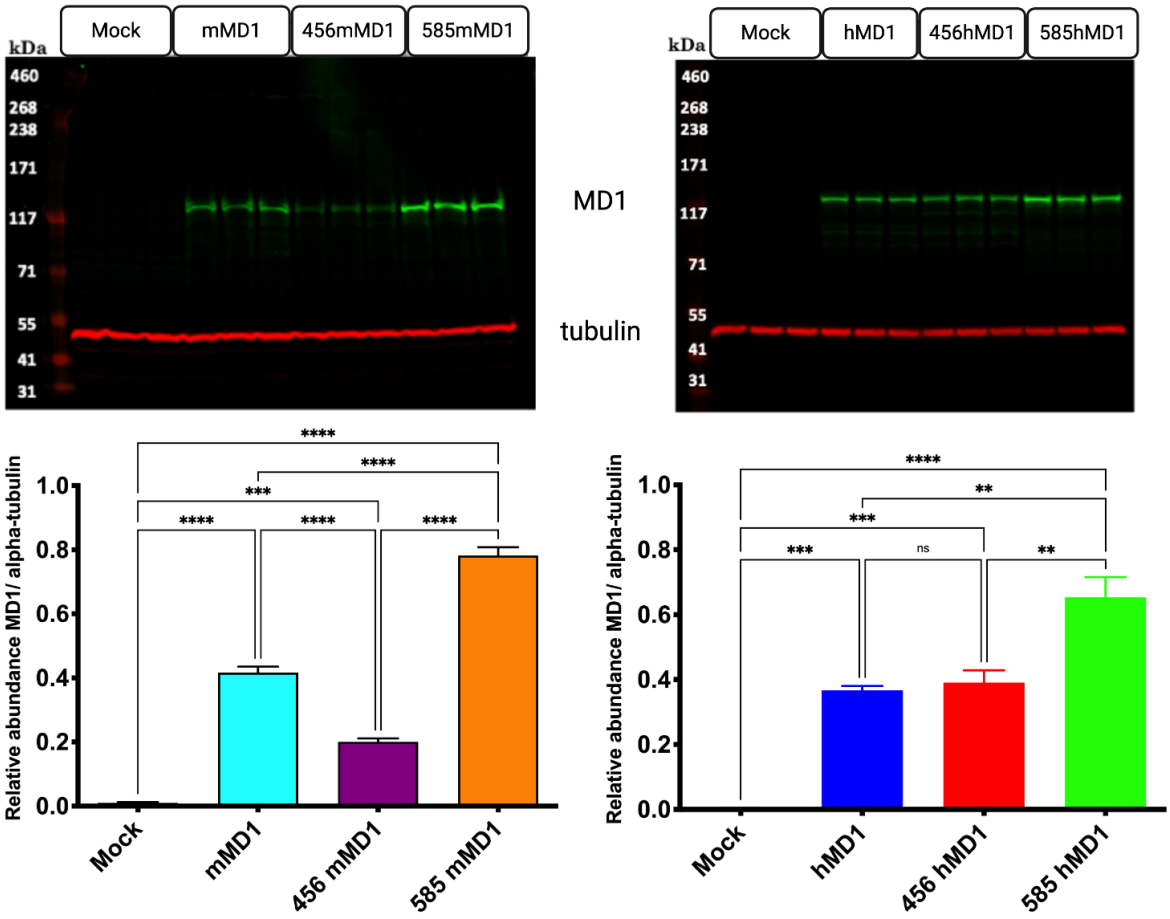

Figure 3.18 **Western blot analysis following transient transfection of HEK293T with codon optimised MD1 constructs**. Six plasmids were tested (p-mMD1, p-hMD1, p-456mMD1, p-456hMD1, p-585mMD1 and p-585hMD1). HEK293T cells were transfected with plasmid dose of 4 µg for 9.4 cm^2 growth area (well size of a 6-well plate). 72-hours post transfection, total protein were extracted from the cultures and an SDS-PAGE Western blot assay was performed. The immunoblot membrane was hybridized with MANEX 1011C, a mouse anti-dystrophin antibody specific for exons 10 and 11 of the dystrophin protein and with a secondary goat anti-mouse antibody labelled with near-infrared fluorescent dyes that fluoresces at 800 nm channel (green signals on immunoblots) visualized by near infra-red imaging on an Odyssey CLx Imaging System (LI-COR). For protein sample loading control, the same membrane was hybridized with rabbit anti-alpha tubulin antibody and secondary donkey anti-rabbit antibody labelled with labelled with near-infrared fluorescent dyes that fluoresces at 700 nm channel (red signals on immunoblots) visualized by near infra-red imaging on an Odyssey CLx Imaging System (LI-COR). The fluorescence intensity of the bands (both microdystrophin and alpha-tubulin) were quantified using Image Studios software (LI-

COR) and the background (noise values) were subtracted to obtain the intensity values. The ratio of MD1 fluorescence intensity value: α-tubulin fluorescence intensity value is a readout of relative abundance of MD1 protein following the treatment. All data represent mean ± SEM. N=3 for each treatment. Statistical analysis was by one-way ANOVA. **P ≤ 0.01, ***P ≤ 0.001, ****P ≤ 0.0001.

The microdystrophin protein expression was not elevated following addition of the 456 RRO as a 5'-UTR in 456mMD1 compared to the unmodified gene construct in the mMD1; and indeed the expression could be diminished. Nevertheless, the level of expression of transgene protein suggested that splicing could be part of the mechanism in which an elevated transgene expression strength is achieved. Transfection carried out in HEK293T using hMD1 plasmid samples showed that there was no difference in transgene expression strength between hMD1 and 456hMD1 transfected samples. This indicates that the MD1 construct with 456bp RRO does not result in elevated transgene expression compared to the MD1 construct without RRO as 5'UTR.

The strength of transgene expression in samples transfected with 456(m/h)MD1 is lower than the samples transfected with 585(m/h)MD1. This may be due to the presence of AUG sequences in the RRO, where occurrence of multiple AUG sequences in 5'UTR causes an inhibitory effect on protein expression (Al-Ali & Gonzalez-Sarmiento, 2016). The 456 bp RRO is present as a UTR in the 5' region (and is retained in the mRNA) while the 585 bp RRO is present in an intronic form (where the RRO is spliced out). It is worth mentioning that the RRO contains 10 AUG sequences and Lu *et al.*, 2017 have shown that the inhibitory effect on gene expression is not seen in intronic AUG sequences. We decided not to test 456 MD1 further.

The 4 μg plasmid DNA transfection (for 9.4 cm^2 growth area (well size of a 6-well plate)) experiment results showed that there was an increase in microdystrophin expression following the addition of the 585 bp intron which is approximately two fold. 4 μg was the maximum tolerable dosage optimised for HEK293T cells for 9.4 cm^2 growth area (Moore, 2018). At this maximal plasmid DNA dosage, the difference in transgene expression levels between MD1 and 585 MD1 plasmid sets may not be very pronounced (due to possible issues such as toxicity). As such, a dose response of 1 μg, 2 μg and 4 μg transfections were carried out in HEK293T in 9.4 cm^2 growth area (Figure 3.19). 2 μg plasmid DNA transfection (for 9.4 cm^2 growth area (well size of a 6-well plate)) experiment results showed that there was an increase in microdystrophin expression following the addition of the 585 bp intron which is approximately four-fold.

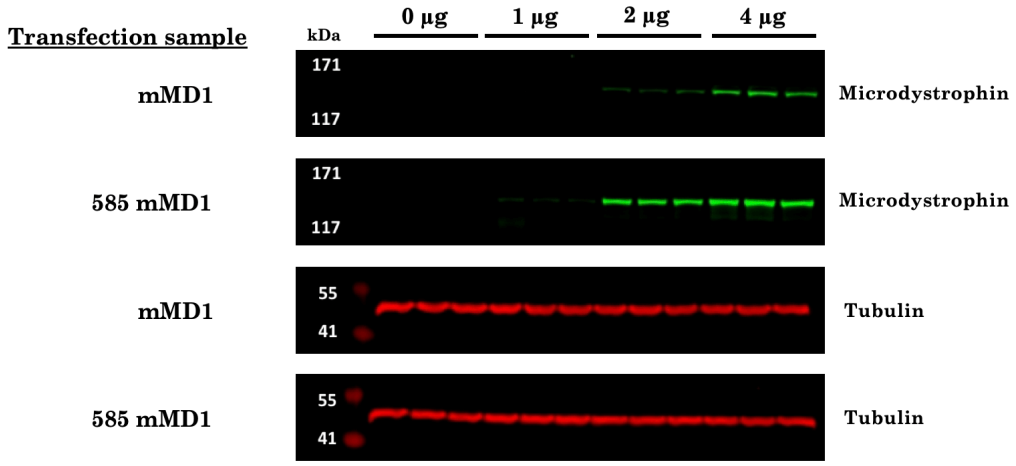
Transfection sample
kDa
0 µg
1 µg
2 µg
4 µg
mMD1
171
117
Microdystrophin
585 mMD1
171
117
Microdystrophin
mMD1
55
41
Tubulin
585 mMD1
55
41
Tubulin

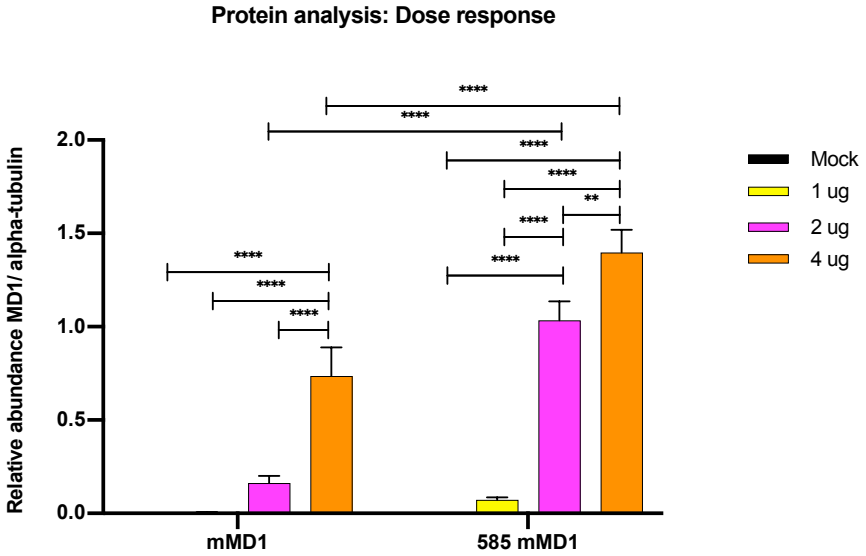
Protein analysis: Dose response
Relative abundance MD1/ alpha-tubulin
2.0
1.5
1.0
0.5
0.0
mMD1
585 mMD1
Mock
1 ug
2 ug
4 ug

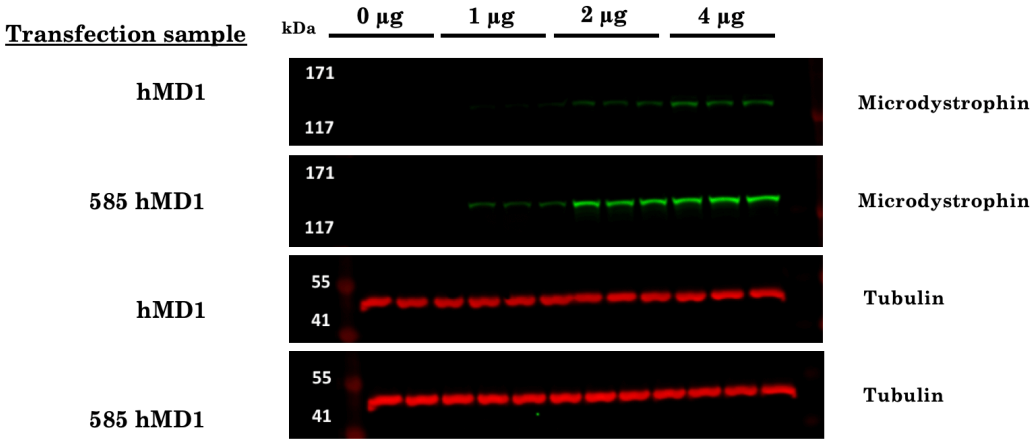
Transfection sample
kDa
0 µg
1 µg
2 µg
4 µg
hMD1
171
117
Microdystrophin
585 hMD1
171
117
Microdystrophin
hMD1
55
41
Tubulin
585 hMD1
55
41
Tubulin

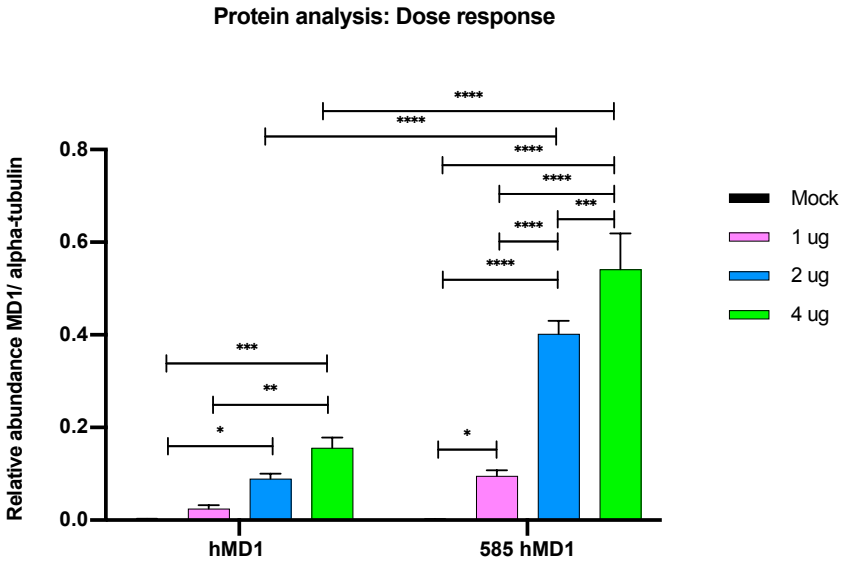
Protein analysis: Dose response
Relative abundance MD1/ alpha-tubulin
0.8
0.6
0.4
0.2
0.0
hMD1
585 hMD1
Mock
1 ug
2 ug
4 ug

Figure 3.19 **Western blot analysis following transient transfection of HEK293T with codon optimised MD1 constructs**. Four plasmids were tested (p-mMD1, p-hMD1, p-585mMD1 and p-585hMD1). HEK293T cells were transfected with a plasmid dose ranging from 1-4 μg for 9.4 cm^2 growth area (well size of a 6-well plate). 72-hours post transfection, total protein were extracted from the cultures and an SDS-PAGE Western blot assay was performed. The immunoblot membrane was hybridized with MANEX 1011C, a mouse anti-dystrophin antibody specific for exons 10 and 11 of the dystrophin protein and with a secondary goat anti-mouse antibody labelled with near-infrared fluorescent dyes that fluoresces at 800 nm channel (green signals on immunoblots) visualized by near infra-red imaging on an Odyssey CLx Imaging System (LI-COR). For protein sample loading control, the same membrane was hybridized with rabbit anti-alpha tubulin antibody and secondary donkey anti-rabbit antibody labelled with labelled with near-infrared fluorescent dyes that fluoresces at 700 nm channel (red signals on immunoblots) visualized by near infra-red imaging on an Odyssey CLx Imaging System (LI-COR). The fluorescence intensity of the bands (both microdystrophin and alpha-tubulin) were quantified using Image Studios software (LI-COR) and the background (noise values) were subtracted to obtain the intensity values. The ratio of MD1 fluorescence intensity value: α-tubulin fluorescence intensity value is a readout of relative abundance of MD1 protein following the treatment. All data represent mean ± SEM. N=3 for each treatment. Statistical analysis was by one-way ANOVA. *$P \leq 0.05$, **$P \leq 0.01$, ***$P \leq 0.001$, ****$P \leq 0.0001$.

3.3 Discussion

High doses AAV-mediated gene delivery to the skeletal musculature and heart has been demonstrated to be safe and effective experimentally in small and large animal models (Mack *et al.*, 2017; Le Guiner *et al.*, 2017; Sarcar et al, 2019). This is also the case in a limited number of human clinical trials (Pfizer [NCT03362502], 2018; Mendell *et al.*, 2017; Mendell et al, 2020). Increasing the vector dose is one possible route to enhance vector to tissue delivery and biodistribution, and in consequence transgene product levels. However, this approach brings with it both safety risks and manufacturing challenges. In human clinical studies, the effect of a higher vector dose has not always been positive as seen in the clinical trial of X-linked myotubular myopathy utilising AAV8 that reported three deaths in the high dose group (Keown, 2020). This is also a reminder that the most valuable data in the field of gene therapy are indeed derived from human studies, as pre-clinical studies pose some limitations in capturing the full effects of a treatment (immune responses seen in the human clinical trials are often not seen in animal models, especially in small animal models). The risk of a higher vector dose is mainly due to the increase in risk of triggering the immune system (reviewed in Chapter 1, Section 1.4). As such, in the skeletal muscle setting, there is a need to develop AAV gene expression cassettes with a higher transgene potency; which would result in a higher level of transgene expression and the need for a lower vector dose. A lower vector dose would not only address the issues around immunogenicity, but also ease the burden around the vector manufacturing bottleneck.

The addition of an engineered intron just downstream of the promoter in a non-coding first exon, in AAV expression cassette has been shown to boost the transgene expression by 100- to 1000-fold (Lu *et al.*, 2017). As this system has not been tested in a muscle setting where AAV gene expression cassettes are targeted to the muscle (skeletal and cardiac), we decided to test this. We included an engineered intron RRO into the AAV-MD1 expressing cassettes as a gene regulatory element in an attempt to increase the transgene expression level. This synthetic intron system was specifically chosen for two reasons: (i) an

upregulation of up to 100-fold in transgene expression in liver was observed following addition of this intron in an AAV gene expression cassette (Lu et al, 2017) and (ii) the size of the intron (~0.6 kb) made it feasible to be added to the AAV-MD1 expression cassette where the ITR-ITR length is already ~4.6kb. AAV has a natural packaging capacity of ~4.7 kb. This size potentially poses a major limitation especially in carrying a large gene such as the *DMD* gene, which eventually had to be miniaturised to be packaged into the viral vector. However, the packaging capacity of rAAVs seem to differ from serotype to serotype (Wu et al, 2010) and oversized genomes larger than 5.2 kb are preferentially targeted by the proteosomes for degradation, indicating tolerability of packaging up to 5.2 kb of genome in rAAV (Grieger and Samulski, 2005). We decided to proceed with the constructs as the largest constructs generated were the codon optimised 585 MD1s which are ~5.2 kb in length, ITR to ITR, which is just at the maximum upper packaging threshold of AAV (Orefice, 2020). In addition, studies by (Kross et al, 2020) demonstrated packaging of up to 6 kb of genome into AAV serotype 8, although data on stability and infectivity of the viral particles were not reported.

The RRO element consists of a replication-deficient bacterial origin R6K and a non-coding RNA sequence RNA-OUT. RRO will be cleaved out during pre-mRNA processing (splicing) as it is present as an intron in the therapeutic AAV expression cassette. As such, these additional bacterial sequences inserted as an intron into the AAV expression cassette will be removed and degraded during splicing, reducing the potential for any unwanted or unexpected safety-related consequences. Also being replication incompetent, the R6K origin should not initiate vector replication in the event of an inadvertent transfer of plasmid or AAV sequences to endogenous bacterial populations; and there is no risk of cryptic bacterial peptide production as RNA-OUT is a non-protein coding sequence (Lu et al, 2017).

The ITR-ITR structure of the AAV genome is at risk of instability during plasmid propagation in *E. coli* due to complex secondary structure and the palindromic sequences contained. Good practice in AAV plasmid cloning and propagation

protocols can be valuable in maintaining the ITR integrity such as: (i) selection of smaller colonies of bacteria from agar plates as loss of ITRs confers growth advantage to the host bacteria, (ii) minimisation of bacterial culture times to 14-16 hours and (iii) growing bacterial culture at a reduced temperature lower than 37°C (ideally 32°C) (Wilmott et al, 2019). It is thus also necessary to directly check for the integrity of the AAV ITR sequences following plasmid propagation. A classic way of performing this task is to digest the plasmids with multiple restriction enzymes and analyse the restriction profile to ensure the expected bands are present at the appropriate sizes. Direct sequencing is an alternative, but due to the high GC content (70%) and stable secondary structures, standard Sanger sequencing of ITRs is generally unreliable and indeed unproductive. Stable and complex ITR secondary structures have been shown to cause stalling of the DNA polymerase during the sequencing reaction (Wilmott et al, 2019).

The initial source plasmids used in this study (p-mMD1 and p-hMD1) were digested using multiple restriction enzymes to ensure the ITR integrity and all the appropriately sized bands were observed confirming the overall plasmid integrity. Following restriction site cloning, four new microdystrophin constructs were generated; two of each mouse- and human-codon optimised versions: 456mMD1, 585mMD1, 456hMD1 and 585hMD1. The 456mMD1 and 585mMD1 were also digested using multiple restriction enzymes to ensure the ITR integrity and all the appropriately sized bands were observed confirming the overall plasmid integrity. Whilst useful, some small deletions in the ITR region may not be captured by restriction enzyme digest profiles and this may be the case for the hMD1 plasmid used in this study. In our restriction profile of the hMD1, we did not detect any deletions in the plasmid as suggested by the bands observed following the digests. However, a quality control Sanger sequencing assay performed by GenScript suggested a small deletion in the 5' ITR of the hMD1 plasmid; which if true would be carried over to the 456hMD1 and 585hMD1. This prediction was based on the 'run' of the sequencing reaction indicated on the chromatogram, where if the ITR region was intact, the ITR portion will be skipped in the sequencing reaction. The presence of peaks on the 5' ITR region

(~80 base pairs) suggest a partial deletion in the ITR region that might have relaxed the ITR for sequencing to proceed. This however, is not conclusive and there is also a possibility of sequencing artefact that might have given rise to this observation.

The studies performed using the hMD1 plasmid sets (hMD1, 456hMD1 and 585hMD1) were *in vitro* studies to test the transcription and translation activities, where the ITRs have limited function in these assays and do not affect the results of this study. Loss of ITR regions affects vector genome encapsidation during AAV vector production; however, the hMD1 derived plasmid constructs were not vectorised in this thesis. In the future, if these constructs were to be vectorised, some cloning work may be necessary to replace the potentially defective 5' ITR.

Codon optimisation resulted in 63% of codons being modified in the microdystrophin ΔR4-R23/ΔCT, inevitably increasing the GC content to over 60% (Foster et al, 2008). The current vector production strategies do not increase methylation of CpG and unmethylated CpG sequences can act as pathogen associated molecular patterns (PAMPs) triggering the innate immune system (Rogers et al, 2011) in a dose dependent manner (Martino et al, 2011). Fortunately, no unwanted CpG islands were found in the constructs including the GC rich RRO. As for the human codon optimised constructs, it is important to note that whilst this optimisation is performed for use in humans (in future clinical studies), codon usage and transfer RNA frequencies are similar across vertebrates (Foster et al, 2008). Therefore, these constructs can be tested in small animal models of DMD in preclinical studies.

The RRO sequence is shown to enhance transgene expression when present as an intron between the promoter and the transgene in the gene expression cassette (Lu *et al.*, 2017). The presence of introns in gene expression cassettes and the process of removing introns called splicing, are thought to affect gene expression at the following levels: transcription, polyadenylation, mRNA export,

translational efficiency, and the rate of mRNA decay (Nott, Meislin and Moore, 2003). The 456 MD1 and 585 MD1 differ from each other by the presence of splicing signals, where splicing signals are included in the 585 MD1 constructs. As such, the RRO is present as intron in 585 MD1 and as 5' UTR in 456 MD1. This 456 MD1 control enabled us to show that splicing of RRO was a necessary for the elevation of transgene expression to be achieved.

The plasmid constructs were tested *in vitro* in HEK293T cell line. This cell line is capable of expressing transgenes controlled by various promoters including the Spc5.12. The promiscuity of the cell line in expressing genes controlled by various promoters and the high transfection efficiency makes HEK293T a very attractive candidate for this set of experiments.

Following 4 μg of plasmid DNA transfection of HEK293T (for 9.4 cm^2 growth area), total RNA analysis showed that there was no effect of adding RRO at the transcription level. Total RNA analysis also revealed that splicing occurred in the 585 MD1 constructs and the RRO as 5' UTR was retained in the mRNA of 456 MD1 constructs. These findings are also consistent with previous studies that revealed that nucleocytoplasmic distribution of mRNA and mRNA stability are unaffected by the presence of introns (Nott, Meislin and Moore, 2003). We used the human codon optimised hMD1 and 585hMD1 plasmids and performed a DNA dose response study via HEK293T transfection, followed by RT-PCR analysis from total RNA to confirm that the PCR reaction is in the exponential phase (Supplementary figure 3.1). The dose dependent effect seen confirmed that the PCR reaction is indeed in the exponential phase; where the PCR reaction components are not limiting and the DNA polymerase have not reached exhaustion.

At the translation level, both the mouse- and human-codon optimised 585 MD1 plasmids enhanced transgene expression level by two folds compared to the respective MD1 plasmids (4 μg plasmid dose for 9.4 cm^2 growth area). These observations indicate that splicing is a mechanism that is essential in enhancing

transgene expression at the translational level, but the exact details of the mechanism are not very well understood. Previous studies have also shown that intron splicing has an effect on increasing translational yields compared to intronless transcripts (Nott, Meislin and Moore, 2003; Powell and Rivera-Soto, 2015). No enhancement was seen with the 456 MD1 plasmids; in fact, the mMD1 construct performed better than the 456 mMD1. Studies have shown that the occurrence of multiple AUG sequences in 5'UTR causes an inhibitory effect on protein expression (Al-Ali & Gonzalez-Sarmiento, 2016). RRO contains 10 AUG sequences (Lu *et al.*, 2017) and these sequences are present in the mRNA of 456 MD1 in the cytoplasm, potentially inhibiting protein expression. This would also mean that expressing the RRO as 5' UTR has no benefit in this case, and as such, the 456 MD1 constructs were not utilised in further experiments. The inhibitory effect on gene expression is not seen in intronic AUG sequences, as these sequences are spliced out before the mRNA exits the nucleus into the cytoplasm (Lu *et al.*, 2017).

Another possible explanation for the enhancement of transgene expression at the translation level following splicing is the presence of exon junction complexes (EJCs). EJCs are protein complexes exclusively found on spliced mRNAs as they bind to the regions of mRNA where two exons are joined together in the splicing process at a conserved position, 20–24 nt upstream of exon–exon junctions (Le Hir et al, 2000). EJCs remain bound to the mRNA during mRNA export and the EJCs are displaced by moving ribosomes during translation (Alberts et al, 2008). During translation, an mRNA is often bound by multiple ribosomes at any point, giving rise to the 'beads on a thread' appearance under electron microscope (such multiple ribosome-mRNA complex is called polysome); and it has been shown that spliced mRNAs are more efficiently incorporated into polysomes compared to the non-spliced identical mRNA (Nott et al, 2003). As such, per mRNA molecule, the spliced transcripts produce more molecules of protein compared to the identical transcripts not made by splicing (Nott, Le Hir, and Moore, 2004).

In the *in vitro* experiments discussed above, 4 μg of plasmid DNA was used per transfection (for 9.4 cm^2 growth area). The optimal amount of DNA used in transfection is largely dependent on the cell line used and previous work by (Moore, 2018) have shown that HEK293T cells can be transfected with up to 4 μg of plasmid DNA without apparent toxicity. As we started off with the maximum amount of DNA for transfection (for 9.4 cm^2 growth area), we had a concern of not capturing the full effect of the treatments (due to possible toxicity masking the effect at the maximal DNA dose). To rule out such concern, we performed a dose response study. A dose dependent enhancement of transgene expression was observed in all the plasmid constructs, and the 585 MD1 constructs always performed better than the MD1 constructs. At 2 μg plasmid transfection (for 9.4 cm^2 growth area), both the mouse- and human-codon optimised 585 MD1 plasmids enhanced transgene expression level (protein production) by four folds compared to the respective MD1 plasmids.

Whilst there is a theoretical possibility of transfection efficiency of the plasmids affecting the final results of fold-difference observed in transgene expression, it is very highly unlikely due to the following reasons: (i) Plasmid DNA for transfection studies were always prepared using EndoFree Plasmid kits (QIAGEN) for purification of endotoxin-free advanced transfection-grade plasmids. The EndoFree Plasmid QIAGEN kit workflow contains an endotoxin removal steps that results in virtually no exdotoxin present in the final formulation (<0.1 endotoxin unit (EU)/μg plasmid DNA). All plasticware utilised in the workflow were also certified to be endotoxin-free. The plasmid DNA was also purified and eluted in sterile water; and ensured they were free of protein, RNA and chemical contamination by ensuring the A260/A280 ratio remain in the range of 1.7–1.9. 260 nm and 280 nm are the absorbance wavelengths used to assess the purity of nucleic acids, where the maximum absorbance is observed at 260 nm for nucleic acids. The ratio of absorbance at 260 nm to the absorbance at 280 nm indicates purity in both DNA and RNA extractions. All the plasmid DNA used in this study had A260/A280 ratio within the 'contamination-free' range

around 1.8 which is generally accepted as pure DNA (which is also outlined in the manufacturer's instructions of Viafect transfection reagent).

(ii) Plasmid size is another factor that can affect transfection efficiency; however, in a study by (McLenachan, Sarsero and Ioannou, 2007), 16% reduction of transfection efficiency was observed as the plasmid size was increased from 4.7 kb to 21 kb; and a 7.5% reduction of transfection efficiency was observed as the plasmid size was increased from 21 kb to 200 kb. Given the difference between the smallest plasmid (MD1) and the largest plasmid (585 MD1) is only ~0.6 kb, it is highly unlikely that the 6.6% difference in the plasmid sizes between the largest and smallest plasmids may have caused differences in plasmid transfection efficiencies. In addition, similar fold-level differences in transgene expression between the MD1 and 585 MD1 constructs were observed in both the mouse and human codon optimised plasmid sets.

This chapter provided the proof-of-principle in an *in vitro* setting that the addition of RRO intron in the MD1 constructs can enhance transgene expression (protein production) by several folds (four folds increase in this *in vitro* study). As such, we decided to proceed with testing the constructs in a more relevant, muscle tissue model as described in Chapter 4.

3.4 Supplementary data

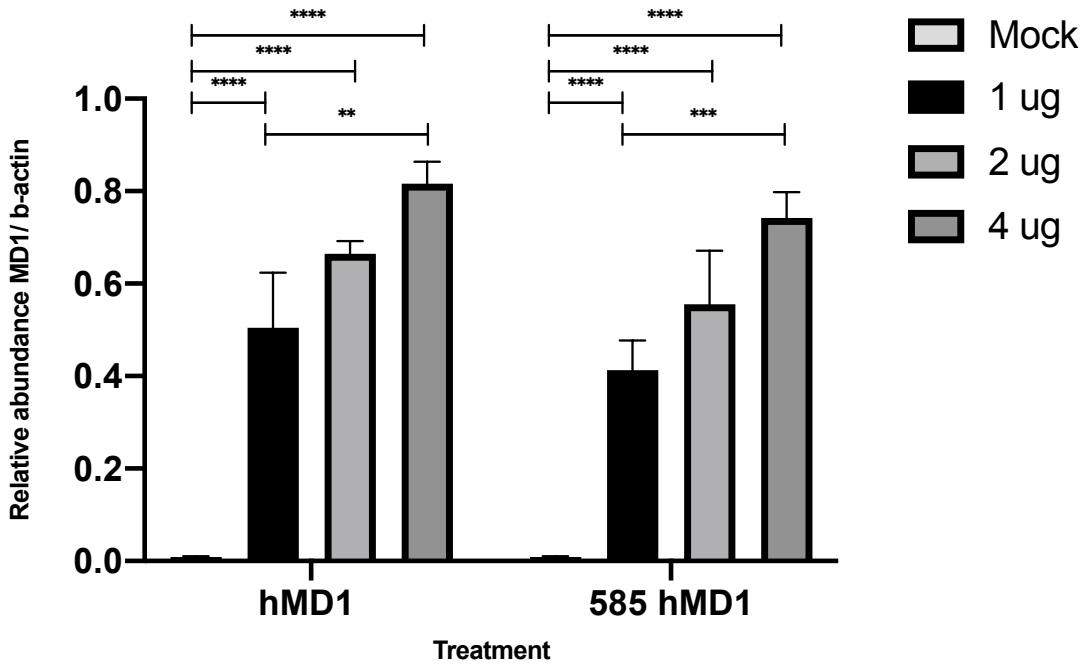

Supplementary figure 3.1 **Total RNA analysis following transient transfection of HEK293T with the human codon optimised hMD1 and 585hMD1 constructs**. Two plasmids were tested (hMD1 and 585hMD1) at 1, 2 and 4 µg DNA dose via transfection of HEK293T cells using Viafect transfection reagent (Promega). Samples for total RNA analysis were collected 48 hours post transfection. The cells were harvested and total RNA was extracted and reverse-transcribed into cDNA for further analysis. A constant amount of 500 ng of total RNA was used for reverse transcription of each sample and 100 ng of the cDNA generated was used as template for PCR reactions. The abundance of each PCR product was calculated via densitometry and MD1 was normalised to ß-actin loading control; where the ratio of MD1: ß-actin abundance is a readout of transcription level. Statistical analysis by one-way ANOVA. All data represent mean ± SEM. N=3 for each treatment. A dose dependent effect was seen with the increasing doses of each treatment confirming that the PCR reaction is in the exponential phase. No difference was observed between the treatments at respective doses, showing no effect of RRO intron at the transcription level. **P ≤ 0.01, ***P ≤ 0.001, ****P ≤ 0.0001.

3.5 Appendix for Chapter 3

3.5.1 Sequence of Spc5.12 promoter

cggccgtccgccctcggcaccatcctcacgacacccaaatatggcgacgggtgaggaatggtggggagttatttttagagcggtgaggaaggtgggcaggc
agcaggtgttggcgctctaaaaaataactcccgggagttatttttagagcggaggaatggtggacacccaaatatggcgacggttcctcacccgtcgccatatt
tgggtgtccgccctcggccggggccgcattcctgggggccgggcggtgctcccgcccgcctcgataaaaggctccgggggccggcggcggcccacgagctaccc
ggaggagcgggaggcg

3.5.2 Sequence of mMD1

Kozak sequence is underlined

gccaccatgctgtggtgggaggaagtggaggactgctacgagagagaggacgtgcagaagaaaaccttcaccaagtggatcaacgcccagttcagcaagt
tcggcaagcagcacatcgacaacctgttcagcgacctgcaggacggcaagagactgctggatctgctggagggactgaccggccagaagctgcccaagga
gaagggcagcaccagagtgcacgccctgaacaacgtgaacaaggccctgagagtgctgcagaagaacaacgtggacctggtgaatatcggcagcaccga
catcgtggacggcaaccacaagctgaccctgggcctgatctggaacatcatcctgcactggcaggtgaagaacgtgatgaaaaccatcatggccggcctgca
gcagaccaacagcgagaagatcctgctgagctgggtgaggcagagcaccagaaactacccccaggtgaacgtgatcaacttcaccagcagctggagcgac
ggcctggccctgaacgccctgatccacagccacagacccgacctgttcgactggaacagcgtggtgtcccagcacagcgccacccagagactggagcacgcct
tcaacatcgccaagtgccagctgggcatcgagaagctgctggaccccgaggacgtggccaccacctaccccgacaagaaaagcatcctcatgtatatcacct
ctctgtttcaggtgctgccccagcaggtgtccatcgaggccatccaggaagtggaaatgctgccccggaccagcagcaaagtgacccgggaggagcacttcc
agctgcaccaccagatgcactatagccagcagatcaccgtgtccctggcccagggctacgagcagaccagcagctcccccaagcccagattcaagagctacg
ccttcacccaggccgcctacgtggccacaagcgatagcacccagagcccctaccccagccagcacctggaggcccctagagacaagagcctggacagcagcc
tgatggagacagaagtgaacctggacagctaccagaccgccctggaggaagtgctgtcttggctgctgtccgccgaggacaccctgagagcccagggcgag
atcagcaacgacgtggaagaagtgaaggagcagttccacgcccacgagggcttcatgatggacctgacctcccatcagggcctggtgggcaacgtgctgca
gctgggcagccagctcgtgggaaagggcaagctgagcgaggacgaggaggccgaagtgcaggaacagatgaacctgctgaacagcagatgggagtgcct
gagagtggccagcatggagaagcagagcaagctgcacaaagtgctgatggatctgcagaaccagaagctgaaggaactggacgactggctgaccaagac
cgaggagcggaccaagaagatggaggaggagcccttcggccccgacctggaggacctgaagtgccaggtgcagcagcataaggtcctgcaggaggacct
ggaacaggagcaggtgcgcgtgaacagcctgacccacatggtggtcgtggtggacgagagcagcggcgaccacgccacagccgccctggaagagcagctg
aaagtgctgggcgacagatgggccaatatctgccggtggaccgaggatagatggatcgtgctgcaggacatcctgctgaagtggcagcacttcaccgagga
gcagtgcctgtttagcacctggctgagcgagaaagaggacgccatgaagaacatccagaccagcggcttcaaggaccagaacgagatgatgagcagcctg
cacaagatcagcaccctgaagatcgacctggagaagaaaaagcccacaatggagaagctgtccagcctgaaccaggacctgctgagcgccctgaagaaca
agagcgtgacccagaaaatggagatctggatggagaatttcgcacagaggtgggacaacctgacccagaagctggagaagagcagcgcccagatcagcc
aggccgtgaccaccacccagcccagcctgacacagaccaccgtgatggagaccgtgaccatggtgaccacccgggagcagatcatggtgaagcacgcccag
gaggagctgccccctcccccccctcagaagaagcggcagatcacagtggatgccctggagagactgcaggagctgcaggaagccgccgacgagctggatct
gaagctgagacaggccgaagtgatcaagggcagctggcagcctgtgggcgatctgctgatcgacagcctgcaggaccacctggagaaagtgaaggccctg
cggggcgagatcgcccccctgaaggagaacgtgaaccgcgtgaacgacctggcccatcagctgaccaccctgggcattcagctgagcccctacaacctgagc
accctggaggatctgaacacccggtggagactgctgcaggtggccgtggaggatagagtgaggcagctgcacgaggcccacagagacttcggccctgcctc
ccagcacttcctgagcaccagcgtgcagggcccctgggagagagccatcagccccaacaaagtgccctactacatcaaccacgagacccagaccacctgctg
ggaccaccctaagatgaccgagctgtaccagagcctggccgacctgaacaatgtgcggttcagcgcctacagaaccgccatgaagctgcggagactgcaga
aggccctgtgcctggacctgctgtccctgagcgccgcctgcgacgccctggaccagcacaacctgaagcagaacgaccagcccatggatatcctgcagatcat
caactgcctgaccaccatctacgatcggctggagcaggagcacaacaacctggtgaacgtgcccctgtgcgtggacatgtgcctgaattggctgctgaacgtg
tacgacaccggcaggaccggcagaatcagagtgctgtccttcaagaccggcatcatcagcctgtgcaaggcccacctggaggataagtaccgctacctgttc
aagcaggtggccagcagcaccggcttctgcgatcagaggagactgggcctgctgctgcacgatagcatccagatccctaggcagctgggcgaagtggccag
ctttggcggcagcaacatcgagccctctgtgaggagctgcttccagttcgccaacaacaagcccgagatcgaggccgccctgttcctggattggatgaggctg
gagccccagagcatggtgtggctgcctgtgctgcacagagtggccgccgccgagaccgccaagcaccaggccaagtgcaacatctgcaaggagtgccccatc
atcggcttccggtacaggagcctgaagcacttcaactacgacatctgccagagctgctttttcagcggcagagtggccaagggccacaagatgcactacccca
tggtggagtactgcacccccaccacctccggcgaggatgtgagagacttcgccaaagtgctgaagaataagttccggaccaagcggtactttgccaagcacc
ccaggatgggctacctgcccgtgcagaccgtgctggagggcgacaacatggagaccgacaccatgtgatgatga

3.5.3 Sequence of hMD1

Kozak sequence is underlined

gccaccatgctgtggtgggaggaagtggaggactgctacgagagaggaggacgtgcagaagaaaaccttcaccaagtgggtgaacgcccagttcagcaagt
tcggcaagcagcacatcgagaacctgttcagcgacctgcaggatggcaggagactgctggatctgctggagggactgaccggccagaagctgcccaagga
gaagggcagcaccagagtgcacgccctgaacaacgtgaacaaggccctgagagtgctgcagaacaacaacgtggacctggtgaatatcggcagcaccgac
atcgtggacggcaaccacaagctgaccctgggcctgatctggaacatcatcctgcactggcaggtgaagaacgtgatgaagaacatcatggccggcctgca
gcagaccaacagcgagaagatcctgctgagctgggtgaggcagagcaccagaaactacccccaggtgaacgtgatcaacttcaccacctcctggagcgacg
gcctggccctgaacgccctgatccacagccacagacccgacctgttcgactggaacagcgtggtgtgtcagcagagcgccacccagagactggagcacgcctt
caacatcgccagataccagctgggcatcgagaagctgctggaccccgaggacgtggacaccacctaccccgacaagaaaagcatcctgatgtatattacctc
tctgtttcaggtgctgccccagcaggtgtccatcgaggccatccaggaagtggaaatgctgcccaggccccccaaagtgaccaaggaggagcacttccagct
gcaccaccagatgcactatagccagcagatcaccgtgtccctggcccagggctatgagagaaccagcagccccaagcccagattcaagagctacgcctacac
ccaggccgcctacgtgaccacctccgacccccaccagaagccccttccccagccagcacctggaggcccccgaggacaagagcttcggcagcagcctgatgga
gagcgaagtgaacctggacagataccagaccgccctggaggaagtgctgtcttggctgctgtccgccgaggacaccctgcaggcccagggcgagatcagca
acgacgtggaagtggtgaaggaccagttccacacccacgagggctacatgatggatctgaccgcccaccagggcagagtgggcaatatcctgcagctgggc
agcaagctgatcggcaccggcaagctgagcgaggacgaggagaccgaagtgcaggagcagatgaacctgctgaacagcagatgggagtgcctgagagt
ggccagcatggagaagcagagcaacctgcaccgcgtgctgatggacctgcagaaccagaagctgaaggagctgaacgactggctgaccaagaccgagga
gcggaccagaaagatggaggaggagcccctgggccccgacctggaggacctgaagagacaggtgcagcagcacaaagtgctgcaggaggacctggaac
aggagcaggtgcgcgtgaacagcctgacccacatggtggtcgtggtggacgagagcagcggcgaccacgccacagccgccctggaagagcagctgaaagt
gctgggcgacagatgggccaacatctgccggtggaccgaggacagatgggtgctgctgcaggacatcctgctgaagtggcagagactgacagaggagcag
tgcctgtttagcgcctggctgagcgagaaggaggacgccgtgaacaagatccacaccaccggcttcaaggaccagaacgagatgctgagcagcctgcagaa
gctggccgtgctgaaggccgatctggagaagaaaaagcagagcatgggcaagctgtactccctgaagcaggacctgctgtccaccctgaagaacaagagc
gtgacccagaaaaccgaggcctggctggacaatttcgcccggtgctgggacaatctggtgcagaaactggagaagagcaccgcccagatcagccaggccgt
gaccaccacccagcccagcctgacacagaccaccgtgatggagaccgtgaccacagtgaccaccagggagcagatcctggtgaagcacgcccaggaggag
ctgccccctccccccctcagaagaagcggcagatcacagtggacaccctggagagactgcaggagctgcaggaagccaccgacgagctggacctgaagct
gagacaggccgaagtgatcaagggcagctggcagcctgtgggcgatctgctgatcgacagcctgcaggaccacctggagaaagtgaaggccctgcggggc
gagatcgcccccctgaaggagaatgtgagccacgtgaacgacctggccagacagctgaccaccctgggcatccagctgagcccctacaatctgagcaccctg
gaagatctgaacacccggtggaaactgctgcaggtggccgtggaggatagagtgaggcagctgcacgaggcccacagagacttcggccctgcctcccagca
cttcctgagcaccagcgtgcagggcccctgggagagagccatctcccccaacaaagtgccctactacatcaaccacgagacccagaccacctgctgggaccac
cctaagatgaccgagctgtaccagagcctggccgacctgaacaatgtgcggttcagcgcctacagaaccgccatgaagctgcggagactgcagaaggccct
gtgcctggacctgctgagcctgagcgccgcctgcgacgccctggaccagcacaacctgaagcagaacgaccagcccatggacattctgcagatcatcaactgc
ctgaccaccatctacgatcggctggagcaggagcacaacaacctggtgaacgtgcccctgtgcgtggacatgtgcctgaattggctgctgaacgtgtacgac
accggcaggaccggcagaatcagagtgctgtccttcaagaccggcatcatcagcctgtgcaaggcccacctggaggataagtaccgctacctgttcaagcag
gtggccagcagcaccggcttctgcgatcagaggagactgggcctgctgctgcacgatagcatccagatccctaggcagctgggcgaagtggccagctttggc
ggcagcaacatcgagccctctgtgaggagctgcttccagttcgccaacaacaagcccgagatcgaggccgccctgttcctggattggatgaggctggagcccc
agagcatggtgtggctgcctgtgctgcacagagtggccgccgccgagaccgccaagcaccaggccaagtgcaacatctgcaaggagtgccccatcatcggct
tccggtacaggagcctgaagcacttcaactacgacatctgccagagctgctttttcagcggcagagtggccaagggccacaagatgcactaccccatggtgg
agtactgcacccccaccacctccggcgaggatgtgagagacttcgccaaagtgctgaagaataagttccggaccaagcggtactttgccaagcaccccagga
tgggctacctgcccgtgcagaccgtgctggagggcgacaacatggagaccgacaccatgtgatgatga

3.5.4 Sequence of SV40 polyadenylation signal

taagatacattgatgagtttggacaaaccacaactagaatgcagtgaaaaaaatgctttatttgtgaaatttgtgatgctattgctttatttgtaaccattata
agctgcaataaacaagtt

3.5.5 Sequence of 5' AAV2 ITR

ctgcgcgctcgctcgctcactgaggccgcccgggcaaagcccgggcgtcgggcgacctttggtcgcccggcctcagtgagcgagcgagcgcgcagagaggga
gtggccaactccatcactaggggttcct

3.5.6 Sequence of 3' AAV2 ITR

aggaacccctagtgatggagttggccactccctctctgcgcgctcgctcgctcactgaggccgggcgaccaaaggtcgcccgacgcccgggctttgcccgggcg
gcctcagtgagcgagcgagcgcgcag

3.5.7 Sequence of 585 RRO

AATTCATTGGGATCTTCACACAGCAGGTAAGGTTGCGGGCCGGGCCTGGGCCGGGTCCGGGCCGGGCC
CGCCTAATGAGCGGGCTTTTTTTTGGCTTGTTGTCCACAACCGTTAAACCTTAAAAGCTTTAAAAGCCTT
ATATATTCTTTTTTTTCTTATAAAACTTAAAACCTTAGAGGCTATTTAAGTTGCTGATTTATATTAATTTT
ATTGTTCAAACATGAGAGCTTAGTACGTGAAACATGAGAGCTTAGTACGTTAGCCATGAGAGCTTAGTA
CGTTAGCCATGAGGGTTTAGTTCGTTAAACATGAGAGCTTAGTACGTTAAACATGAGAGCTTAGTACGT
ACTATCAACAGGTTGAACTGCTGATCCACGTTGTGGTAGAATTGGTAAAGAGAGTCGTGTAAAATATCG
AGTTCGCACATCTTGTTGTCTGATTATTGATTTTTGGCGAAACCATTTGATCATATGACAAGATGTGTAT
CTACCTTAACTTAATGATTTTGATAAAAATCATTAGCCGCACTGACCCCTGGTGTTGCTTTTTTTTTTTA
GGCCGCAAGCTGAAGCGTGTCCG

3.5.8 Sequence of 456 RRO

GAATTCCCCGCCTAATGAGCGGGCTTTTTTTTGGCTTGTTGTCCACAACCGTTAAACCTTAAAAGCTTTA
AAAGCCTTATATATTCTTTTTTTTCTTATAAAACTTAAAACCTTAGAGGCTATTTAAGTTGCTGATTTATA
TTAATTTTATTGTTCAAACATGAGAGCTTAGTACGTGAAACATGAGAGCTTAGTACGTTAGCCATGAGA
GCTTAGTACGTTAGCCATGAGGGTTTAGTTCGTTAAACATGAGAGCTTAGTACGTTAAACATGAGAGCT
TAGTACGTACTATCAACAGGTTGAACTGCTGATCCACGTTGTGGTAGAATTGGTAAAGAGAGTCGTGTA
AAATATCGAGTTCGCACATCTTGTTGTCTGATTATTGATTTTTGGCGAAACCATTTGATCATATGACAAG
ATGTGTATCTACCTTAACTTAATGATTTTGATAAAAATCATTAGGAATTC

Chapter 4 Evaluating the functionality of the new microdystrophin expression plasmid constructs in a muscle tissue model

4.1 Introduction

Skeletal muscle cells (myofibres) are multinucleated and are involved in muscle contraction. Myofibres can contain hundreds of nuclei distributed over large distances within a shared cytoplasm (Taylor-Weiner et al, 2020). Such distribution of nuclei can result in variations in gene expression within a common cytoplasm (Newlands et al, 1998). This raises questions of how regulation of gene expression is achieved within myofibers. The "myonuclear domain hypothesis" states that each nucleus within a muscle cell supports a certain volume of the cell; as such, for the maintenance of nuclear-to-cytoplasmic ratio, new nuclei are added or lost following hypertrophy and atrophy respectively (Schwartz et al, 2019). This concept originated from Strassburger's proposal of "Wirkungssphäre" or "sphere of influence" saying an individual nucleus can only support a certain volume of cytoplasm (Strassburger, 1893). Within the domains, gene expression patterns also vary. For instance, transcriptional programs such as postsynaptic machinery are reserved to specialised domains within the cell while others such as contractile proteins do not show spatial confinement (Taylor-Weiner et al, 2020). Since gene expression patterns within myonuclear domains vary, where some proteins do and some do not show spatial confinement, this could be an advantage or a disadvantage in gene replacement therapies.

In DMD for example, restoration of functional dystrophin protein above a certain level in the skeletal muscle can be expected to alleviate the disease phenotype (Godfrey et al, 2015). One strategy of achieving this is by gene replacement therapy using vectors such as plasmids or viruses. Since each myofiber is multinucleated, transfer of the therapeutic nucleic acid to a proportion of nuclei within each myofiber might be enough to protect the muscle fibres against contraction-induced damage. In addition, for dystrophin gene transfer therapy to be effective, the therapeutic level of protein production is necessary along the

fibre length. In this thesis, a regulatory element (an engineered intron named R6K-RNA-OUT) was used in an attempt to enhance protein production. This intron had previously been shown to enhance transgene expression by several orders of magnitude in mouse liver (Lu et al, 2017). In that respect, it is worth noting that a very high level of transgene expression may be not always be advantageous. It may be detrimental in some cases especially if the protein product is not secreted out of the cells and result in a proteinopathy (Hetz, 2012). However, such effects of protein misfolding and aggregation due to high level of transgene expression may be more prominent in mononucleated cells. In multinucleated skeletal muscle cells where the volume of a cell can be 100 000 times greater than an average mononucleated cell (Bruusgaard et al, 2003), higher levels of ectopic induced transgene expression may be tolerated.

The mouse codon-optimised constructs generated in Chapter 3 (p-mMD1 and p-585mMD1) were further tested in two relevant muscle models in this chapter: C2C12 mouse myoblast cell line (*in vitro*) and the *mdx* mice muscle (*in vivo*). The dystrophin-deficient *mdx* mice model is the most commonly utilised animal model in DMD research (McGreevy *et al*., 2015). Large animal models such as dogs are becoming increasingly popular in the field (Echigoya et al., 2017; Le Guiner et al., 2017) as they exhibit a more severe phenotype compared to the *mdx* mouse, thus better representing human DMD (McGreevy et al., 2015). In addition, the dog model also displays immune sensitivity similar to humans and thus is able to predict potential immune response following gene delivery using AAV (Chamberlain and Chamberlain, 2017). However, larger animal models are more difficult to be generated and housed.

In muscle gene therapy, direct injection of plasmid DNA into skeletal muscle is one of the simplest ways of gene transfer *in vivo* (McMahon et al, 2001). This proof-of-principle was first established by (Wolff et al, 1990) and early studies have shown low transfection efficiencies in skeletal muscle (approximately 1% of muscle fibres) (Acsadi et al, 1991). Modifications to the experimental protocol for direct plasmid injection into skeletal muscle involving differing solute use, injection techniques, animal age and plasmid construct design have resulted in modest improvements in transfection efficiency, nevertheless none of these improvements can be considered dramatic when compared to the advance that was achieved applying electrotransfer techniques to increase gene transfer in skeletal muscle (McMahon et al, 2001).

Electrotransfer involves injecting plasmid DNA into the target tissue and applying a short, intense electric field pulses to the tissue to induce transient permeabilization and allow plasmid DNA to penetrate through the plasma membrane and migrate to the nucleus (Sokołowska and Błachnio-Zabielska, 2019) (Figure 24). As plasmid production is relatively easier compared to viral vector production, electrotransfer provides an attractively simple way of assessing gene expression constructs.

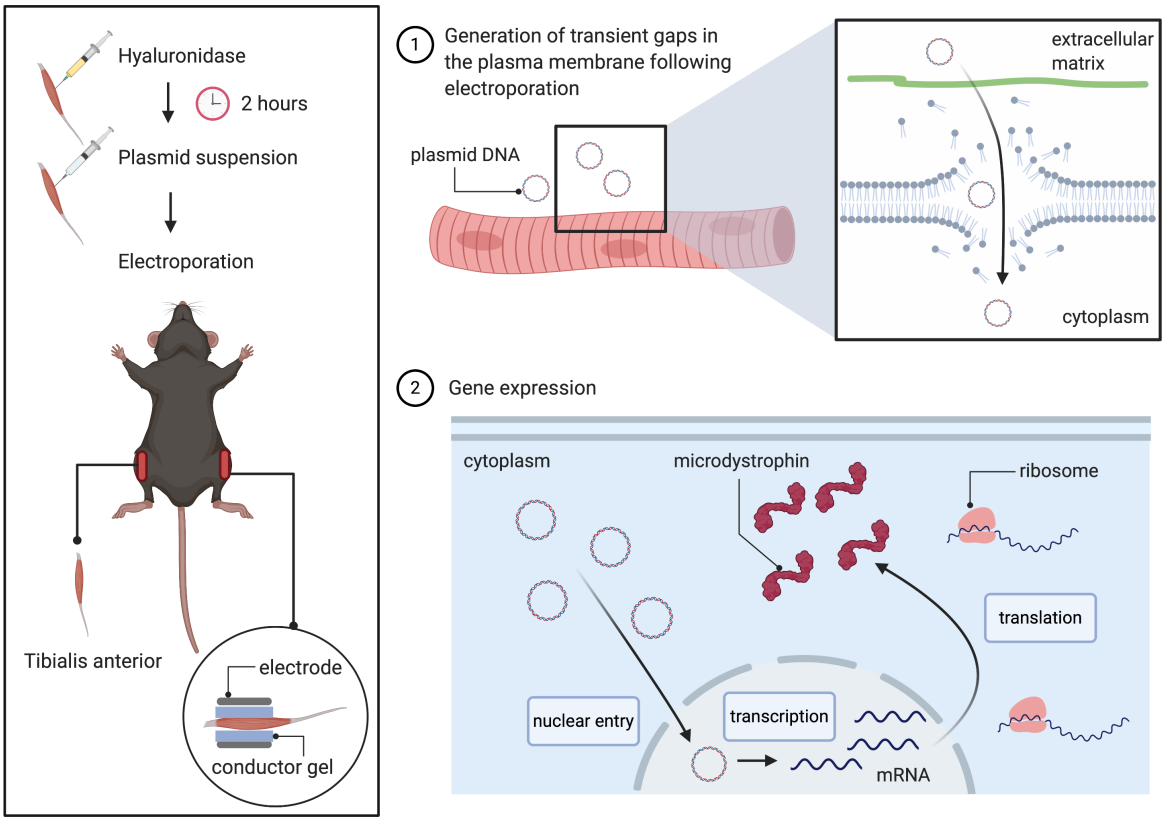

Figure 4.1 **Electrotransfer of plasmid DNA in tibialis anterior (TA) muscle of mdx mice**. Pre-treatment of the muscle with hyaluronidase (enzyme that breaks down components of the extracellular matrix) before electrotransfer has been shown to increase the efficiency of the plasmid delivery (McMahon et al, 2001). The application of a short, intense electric field to the muscle following plasmid delivery will generate transient gaps in the plasma membrane that allow entry of the plasmid, which will then move to the nucleus for gene expression (Sokołowska and Błachnio-Zabielska, 2019).

In order to test the functionality of the newly generated p-585 mMD1 construct *in vivo* and comparatively evaluate the protein production levels from p-mMD1 and p-585 mMD1, the *tibialis anterior* (TA) muscle of *mdx* mice (Figure 4.2) was selected as a dystrophin-deficient muscle model. Plasmid constructs were delivered via electrotransfer, microdystrophin production levels evaluated by Western blot assay and microdystrophin localisation to the sarcolemma by immunohistochemistry assay.

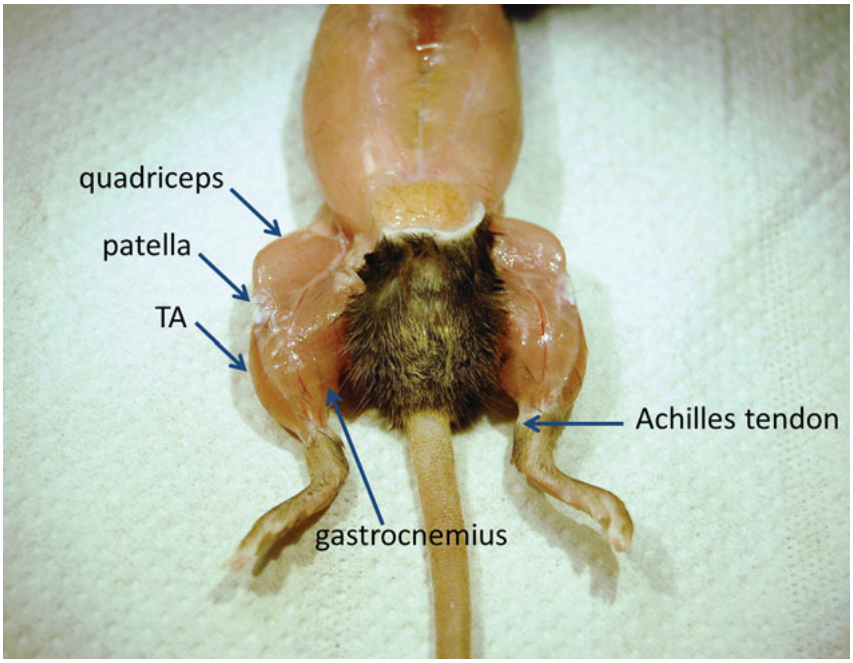

Figure 4.2 **Mouse muscle anatomy**. Key muscles in mouse hindlimb with skin removed to show the position of the TA. The TA muscle was targeted in this study, in both legs. Figure from (Terry and Wells, 2016).

4.2 Results

4.2.1 Testing of microdystrophin constructs in an *in vitro* muscle model to evaluate transgene expression level

As described in Chapter 3, following transfection studies performed in HEK293T cell line, a four-fold elevation in microdystrophin protein production was seen using the 585MD1 constructs compared to the MD1 treatment. HEK293T cells are a useful initial model since they can be transfected with plasmid DNA with very high efficiency and are capable of expressing transgenes that are considered specific to other tissue types (personal communication with Prof George Dickson, 4 Dec 2018). A muscle cell model however would be more relevant to test the relative and absolute protein production capability of the microdystrophin expressing constructs since they are designed with the skeletal muscle- and heart-specific artificial promoter Spc5.12. The C2C12 cell line which is an immortalised mouse myoblast cell line was chosen, and to evaluate relative levels of the protein expression from the microdystrophin expressing plasmid constructs, transient transfection experiments using mouse-codon optimized MD1 plasmids (p-mMD1 and p-585mMD1) were carried out (Figure 4.3). The main outcome of this study was microdystrophin protein level evaluated by Western blot. A dose-response plasmid DNA transfection study was performed. The cells were seeded and grown in 6-well plates (9.4 cm^2 growth area) and were transfected with plasmid DNA before they differentiated into myotubes. Differentiation of C2C12 myoblasts into myotubes occur as the cells become very confluent within the growth area over time, eventually fusing together. Plasmid DNA transfection was performed 48 hours following seeding of cells (5 x 10^4 cells seeded in 9.4 cm^2 growth area) and at this stage, the cells remain as myoblasts at 70-80% confluency. The transfected C2C12 cultures were then allowed to differentiate into myotubes (differentiation protocol outlined in Chapter 2 Materials and Methods), and 72 hours following transfection, total protein was extracted from the cultures. Extracted total protein was quantified using DC™ (detergent compatible) protein colorimetric assay measured at 750 nm and processed for SDS-PAGE. 50 μg of total protein extracts from C2C12 were loaded

on NuPAGE Novex 3–8% Tris Acetate gels. Following blocking, the membrane was cut using the protein ladder as guide to separate the antibody incubations to detect microdystrophin and the protein sample loading control, alpha-tubulin. The membrane was incubated with MANEX 1011C (1:100 dilution), an anti-dystrophin antibody specific for exons 10 and 11 of the dystrophin protein (Glenn Morris; Le Guiner et al., 2017) and with a secondary goat anti-mouse antibody (1: 10000 dilution). For protein sample loading control, the membrane was incubated with anti-alpha tubulin antibody raised in rabbit (1:2500 dilution) and with a secondary donkey anti-rabbit antibody (1: 10000 dilution). Complete details of the workflow including suppliers and manufacturers of the materials can be found in Chapter 2: Materials and Methods. Immunoblots were visualized by Odyssey CLx Imaging System (LI-COR) using fluorescence detection. Direct detection was possible as the secondary antibodies used were labelled with near-infrared fluorescent dyes. The secondary antibody used for detection of microdystrophin fluoresces at 800 nm channel (green signals on immunoblots) and for the protein loading control, the secondary antibody used for detection fluoresces at 700 nm channel (red signals on immunoblots).

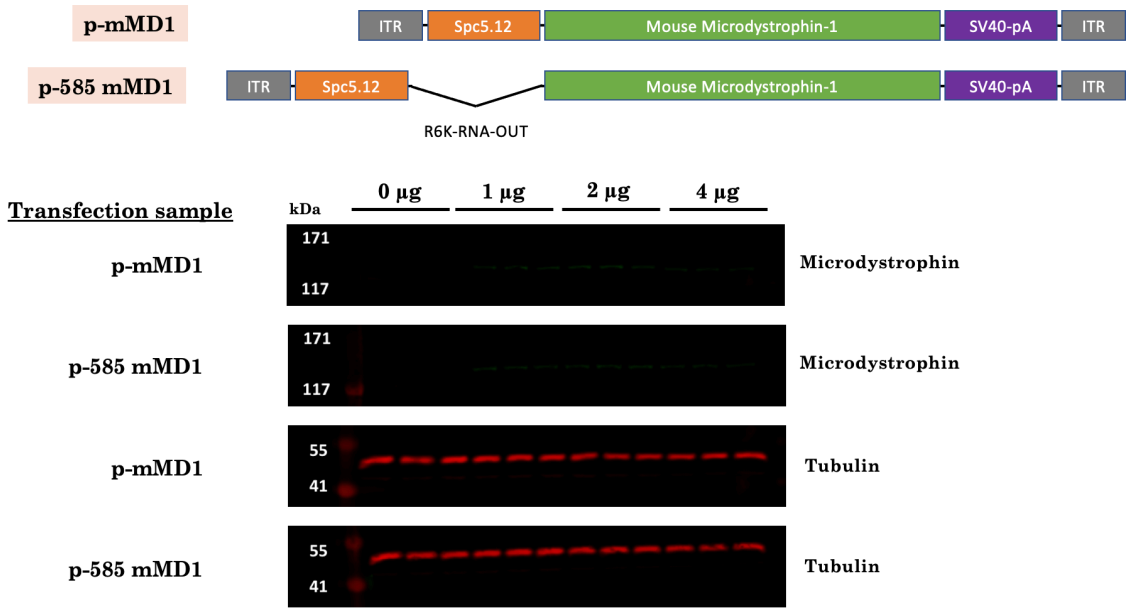

Figure 4.3 **Western blot analysis following transient transfection of C2C12 cells with p-mMD1 and p-585 mMD1**. Transcription units of plasmids p-mMD1 and p-585 mMD1 are shown at the top. The undifferentiated C2C12 cells were transfected with either p-mMD1 or p-585 mMD1 at a plasmid dose ranging from 1-4 µg for 9.4 cm^2 growth area (well size of a 6-well plate). 72-hours post transfection and following differentiation into myotubes, total protein were extracted from the cultures and an SDS-PAGE Western blot assay was performed. The immunoblot membrane was hybridized with MANEX 1011C, a mouse anti-dystrophin antibody specific for exons 10 and 11 of the dystrophin protein and with a secondary goat anti-mouse antibody labelled with near-infrared fluorescent dyes that fluoresces at 800 nm channel (green signals on immunoblots) visualized by near infra-red imaging on an Odyssey CLx Imaging System (LI-COR). For protein sample loading control, the same membrane was hybridized with rabbit anti-alpha tubulin antibody and secondary donkey anti-rabbit antibody labelled with labelled with near-infrared fluorescent dyes that fluoresces at 700 nm channel (red signals on immunoblots) visualized by near infra-red imaging on an Odyssey CLx Imaging System (LI-COR). Very thin and faint bands for microdystrophin can be seen in all the treated samples of all plasmid doses; quantification was not attempted in this instance. (N, number of samples per treatment at each dosage=3).

All the doses of plasmid (1, 2 and 4 μg) of both plasmids (p-mMD1 and p-585 mMD1) resulted in faint bands observed for the microdystrophin protein most likely due to a low level of plasmid transfer into the nucleus. The experiment was repeated, and similar data was obtained (representative data is shown in Figure 4.3). Myoblasts and myotubes are known to be difficult to transfect (Jackson et al, 2013). In this instance, following the attempts described above, we decided not to proceed further with this model as we had a better muscle tissue model: the *mdx* mice and a technique to quickly evaluate gene expression using plasmid constructs called electrotransfer (discussed in next section).

4.2.2 Electro-transfer of p-mMD1 and p-585mMD1 plasmids in muscle tissue of *mdx* mice model to evaluate transgene expression level *in vivo*

The main aim of this study was to evaluate the plasmid AAV gene expression constructs in a muscle model. The *in vitro* studies in C2C12 proved uninformative since detectable MD expression levels were very low most likely due to transfection efficiency limitations (data described Section 4.2.1). In a transfection study, flaws in the plasmid construct such as mutations during plasmid propagation resulting in missing components such as the open reading frame or part of the promoter, could pose limitations to the study. However, in the transfection study described in Section 4.2.1, this limitation is highly unlikely. The plasmid constructs underwent quality control steps such as restriction enzyme digest profiling (data described in Chapter 3) and also were utilised in experiments described in Chapter 3 where protein production was observed following Western blot assays.

In vivo skeletal muscle plasmid electrotransfer technique (described in Section 4.1) was selected then to enable the newly generated 585mMD1 construct to be potentially evaluated *in vivo* in the *mdx* mouse model: this *in vivo* myofibre expression model may be considered a more physiologically relevant compared to the muscle cell culture. Muscle electrotransfer has limitations in terms of overall efficiency and variability of the technique to deliver nucleic acids into myofibres. However, applying the electrotransfer approach was considered as a potentially useful proof-of-concept study to test the functionality of the newly generated 585mMD1, and especially to check the correct protein production *in vivo* by Western blot and immunohistochemistry.

Plasmid DNA electrotransfer was performed in young male *mdx* mice (~10 weeks old) using p-mMD1 and p-585 mMD1. Despite being dystrophin-negative, in young *mdx* mice, the phenotype observed is relatively mild. The severity of the disease indicated by loss of muscle weight, fat accumulation, fibrosis and severe muscle weakness is not observed until the *mdx* mice is almost 2 years old (Yucel et al, 2018). At around 3-4 weeks of age, necrosis and regeneration in the tibialis

anterior (TA) muscles peak, after which they plateau (Dangain and Vrbova, 1984). As the muscle histopathology in the young *mdx* mice is relatively mild, such as no extensive fibrosis (which could affect transfection), mice of 10 weeks of age were selected for the study. At 10 weeks, the cycles of necrosis and regeneration in the tibialis anterior (TA) muscles would have plateaued; nevertheless, the regenerative mechanism could potentially affect transfection efficiency as some of the plasmids that have reached the nuclei may be lost in the turnover process; which could also pose a limitation to this study.

Briefly, the mice were anesthetized with 2%–4% isoflurane vaporised in 100% O_2 and then reduced to 1.5%-3% as required. To prepare the mice for injection, the skin covering tibialis anterior (TA) muscle was shaved. For electrotransfer of plasmid DNA, the TA muscles were injected with 10 U of bovine hyaluronidase (25 µl at 0.4 U/µl were injected). The hyaluronidase breaks down components of the extracellular matrix which increases the distribution of the injected plasmid through the muscle tissue and the efficiency of plasmid uptake. After 2 hours, the mice were anesthetized again as described above and the TA muscle was injected intramuscularly with 25 µg of plasmid DNA delivered in a total volume of 50 µl per TA muscle. Control muscle was injected with 50 µl of saline solution. Electrode gel (MediSupplies) was placed on the electrode plates to increase the contact area with the skin of mouse. Electrical field was then applied to the injected TA muscle using external electrodes at 175 V/cm in 20-msec square wave pulses at 1 Hz using a BTX ECM 830 electroporator, to transiently disrupt the plasma membrane to enable plasmid uptake.

The treatment drug in this study was plasmid DNA diluted in saline solution (sterile 0.9% sodium chloride solution) to required concentration of 0.5 µg/ µl in a total volume of 50 µl per TA injection.

- Treatment **p-mMD1** consists of plasmid DNA expressing a mouse codon optimised microdystrophin cDNA (sequence in Section 3.6.2) controlled by a muscle-specific promoter Spc5.12 and SV40 polyA signal.
- Treatment **p-585mMD1** consists of plasmid DNA expressing a mouse codon optimised microdystrophin cDNA (sequence in Section 3.6.2) controlled by a muscle-specific promoter Spc5.12, SV40 polyA signal and an engineered intron 585 R6K-RNA-OUT (sequence in Section 3.6.7) positioned in between the promoter and the transgene cDNA.

A study by Akerstrom et al (2015) has shown that plasmid transfection efficiency in TA muscle in an electrotransfer experiment is not dependent on plasmid dose or plasmid dilution volume. The 25 µg of plasmid DNA dosage used in this study was selected based on a previous study by Koo et al (2011) where this dosage was tested in the TA of *mdx* mice in an electrotransfer study.

All outcome analyses were performed two weeks following treatment. The number of TA muscle treated was six in all three groups: saline, p-mMD1 and p-585mMD1. Two weeks following treatment, muscle tissues were harvested and processed for Western blot and immunohistochemistry (IHC). Tissue collection for total protein sample extraction is described in Figure 4.4. TA muscles samples were harvested tendon-to-tendon and snap-frozen in isopentane cooled in liquid nitrogen and stored at −80 °C. Cryo-sections were then collected either for IHC, or for protein extraction and processing for SDS-PAGE immunoblotting.

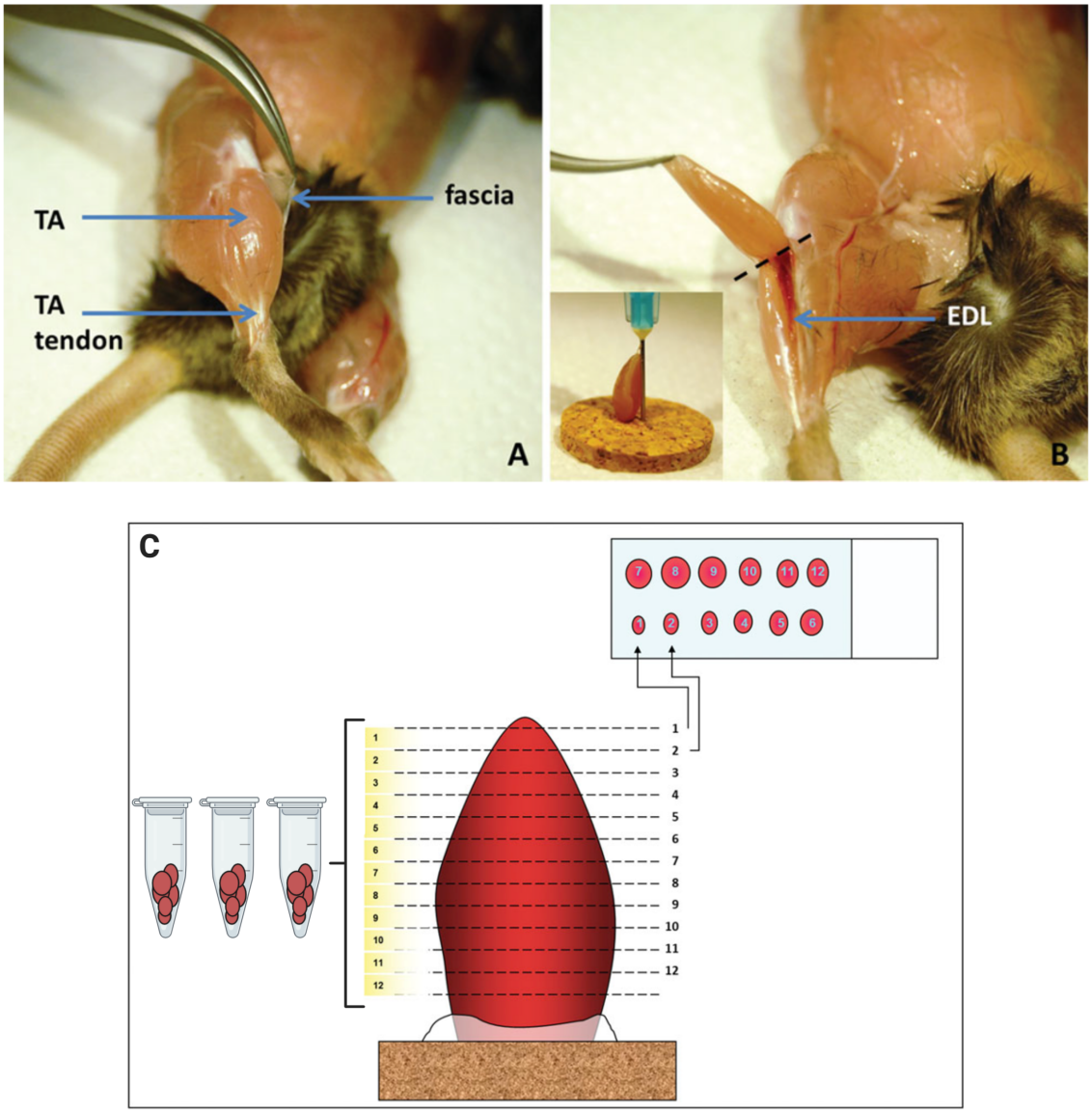

Figure 4.4 **Tissue collection (TA muscle) and processing following treatment**. (A) The TA muscle is collected tendon to tendon, with the overlaying fascia removed. (B) Once the first TA tendon was cut, the TA was carefully detached leaving behind the extensor digitorum longus (EDL) muscle. The next tendon to be cut is shown by dashed line. The TA is mounted upright on a cork disc as shown in the insert. (C) The TA muscle was sectioned throughout; collecting intermediate sections into 1.5 ml microcentrifuge tubes and picking up one section per level onto microscope slide. The intermediate sections in the tubes were used for assays such as total protein extraction for Western blot (Terry and Wells, 2016). Figure adapted and modified from (Terry and Wells, 2016).

Western blot analysis was performed as a readout for level of microdystrophin expression in treated TA muscle samples. Extracted total protein was quantified using DC™ (detergent compatible) protein colorimetric assay measured at 750 nm and processed for SDS-PAGE. 10 μg of total protein extracts from TA cryosections were loaded on NuPAGE Novex 3–8% Tris Acetate gels. Electrophoresis gels were run for 1 hour 15 minutes at 150V. The subsequent transfer of resolved protein bands over to nitrocellulose membrane was carried out at 30V for 2 hours. The nitrocellulose membrane was then blocked in 5% skim milk in PBS, 0.1% Tween-20 for 1 hour at room temperature. Following blocking, the membrane was cut using the protein ladder as guide to separate the antibody incubations to detect microdystrophin and the protein sample loading control, alpha-tubulin. The membrane was hybridized with MANEX 1011C (1:100 dilution), an anti-dystrophin antibody specific for exons 10 and 11 of the dystrophin protein (Glenn Morris; Le Guiner et al., 2017) and with a secondary goat anti-mouse antibody (1: 10000 dilution). For protein sample loading control, the membrane was hybridized with anti-alpha tubulin antibody raised in rabbit (1:2500 dilution) and with a secondary donkey anti-rabbit antibody (1: 10000 dilution). Complete details of the workflow including suppliers and manufacturers of the materials can be found in Chapter 2: Materials and Methods. Immunoblots were visualized by Odyssey CLx Imaging System (LI-COR) using fluorescence detection. Direct detection was possible as the secondary antibodies used were labelled with near-infrared fluorescent dyes. The secondary antibody used for detection of microdystrophin fluoresces at 800 nm channel (green signals on immunoblots) and for the protein loading control, the secondary antibody used for detection fluoresces at 700 nm channel (red signals on immunoblots).

As shown in Fig 4.5, in the case of TAs transfected with the p-mMD1 and p-585mMD1, detectable levels of microdystrophin production were found by Western immunoblotting. This observation confirmed at the simplest level that the newly generated plasmid construct p-585mMD1 was functional *in vivo* producing the protein of interest. Given the relatively low efficiency method of gene transfer utilising plasmid vectors (Acsadi et al, 1991) which results in relatively low levels of transgene expression, the observations made here for both the plasmid treatments p-mMD1 and p-585mMD1 were encouraging.

(A)

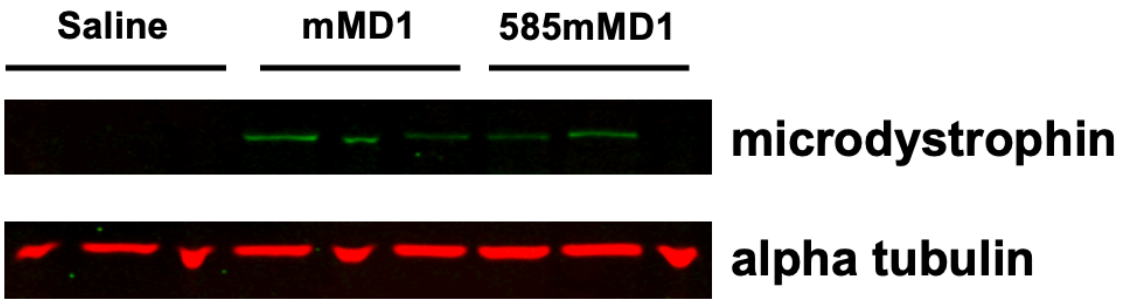

(B)

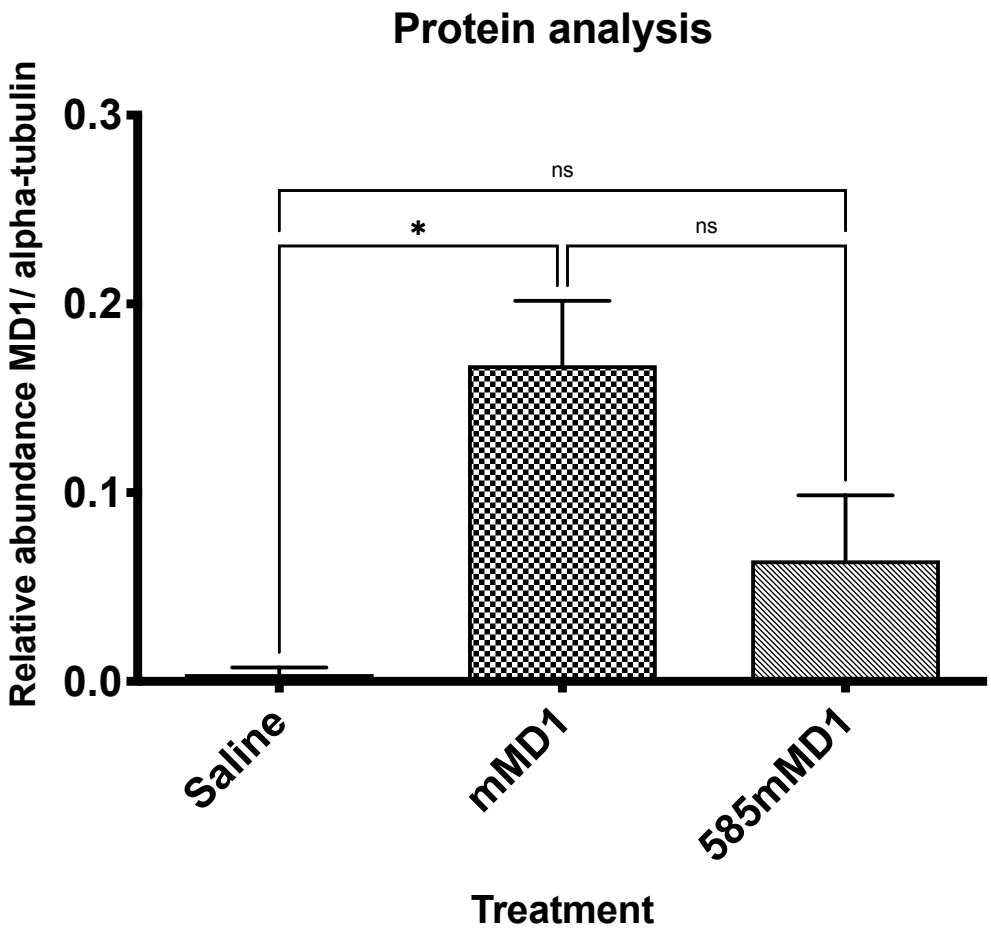

Figure 4.5 **Western blot analysis of expression of microdystrophin in *mdx* TA muscle following *in vivo* plasmid electrotransfer.**

[Continued on next page]

[From previous page]

The TA muscles of *mdx* mice were subjected to plasmid electrotransfer transfection with either p-mMD1 or p-585 mMD1 at a plasmid dose of 25 μg, or saline control. At 2 weeks post treatment, tissues were harvested, cryosections extracted for total protein and SDS-PAGE Western blot assay performed. The immunoblot membrane was hybridized with MANEX 1011C, a mouse anti-dystrophin antibody specific for exons 10 and 11 of the dystrophin protein and with a secondary goat anti-mouse antibody labelled with near-infrared fluorescent dyes that fluoresces at 800 nm channel (green signals on immunoblots) visualized by near infra-red imaging on an Odyssey CLx Imaging System (LI-COR). For protein sample loading control, the same membrane was hybridized with rabbit anti-alpha tubulin antibody and secondary donkey anti-rabbit antibody labelled with labelled with near-infrared fluorescent dyes that fluoresces at 700 nm channel (red signals on immunoblots) visualized by near infra-red imaging on an Odyssey CLx Imaging System (LI-COR). The fluorescence intensity of the bands (both microdystrophin and alpha-tubulin) were quantified using Image Studios software (LI-COR) and the background (noise values) were subtracted to obtain the intensity values. The ratio of MD1 fluorescence intensity value: α-tubulin fluorescence intensity value is a readout of relative abundance of MD1 protein following the treatment. All data represent mean ± SEM. (N, number of TA muscle sample=3). Statistical analysis was by one-way ANOVA. * = $P \leq 0.05$.

Native dystrophin is a structural protein of the sub-sarcolemmal cytoskeleton and for the expressed microdystrophins to serve a functional purpose, it is essential they localise correctly to the sarcolemma This correct localisation of microdystrophin protein to the sarcolemma is also an indication of correct protein production and protein folding. Sarcolemmal localisation of MD1 following plasmid electrotransfer in mdx TA muscle was assessed by immunohistochemistry workflow (Figures 4.6-4.8).

For all histological analysis, 10-µm cryosections of muscles were collected on glass slides (Figure 4.4), air-dried and stored at −80 °C. Before staining, the sections were fixed in acetone at −20°C. To reduce background effects, the Mouse on Mouse (M.O.M) kit (Vector Labs) was used to stain muscle sections for immunohistochemistry. The presence of microdystrophin was examined by immunostaining with MANEX 1011C, an anti-dystrophin antibody specific for exons 10 and 11 of the dystrophin protein (Glenn Morris; Le Guiner et al., 2017). The signal was visualized using Alexafluor 568–conjugated anti-mouse IgG (Invitrogen). Laminin was immunostained using rat anti-laminin monoclonal antibody (Sigma Aldrich). For laminin signal visualisation, anti-rat biotinylated antibody followed by Alexafluor 568–conjugated streptavidin was used. Laminin staining facilitates the determination of individual muscle fibers. The nuclei were stained with 0.1 µg/ml DAPI and the slides were mounted using mounting medium (Vector Labs). All samples were handled in a blinded manner. Microscope images were acquired using Nikon Eclipse NiE confocal microscope, where complete TA section images were acquired for analysis. Complete details of the workflow including antibody dilutions, suppliers and manufacturers of the materials can be found in Chapter 2: Materials and Methods.

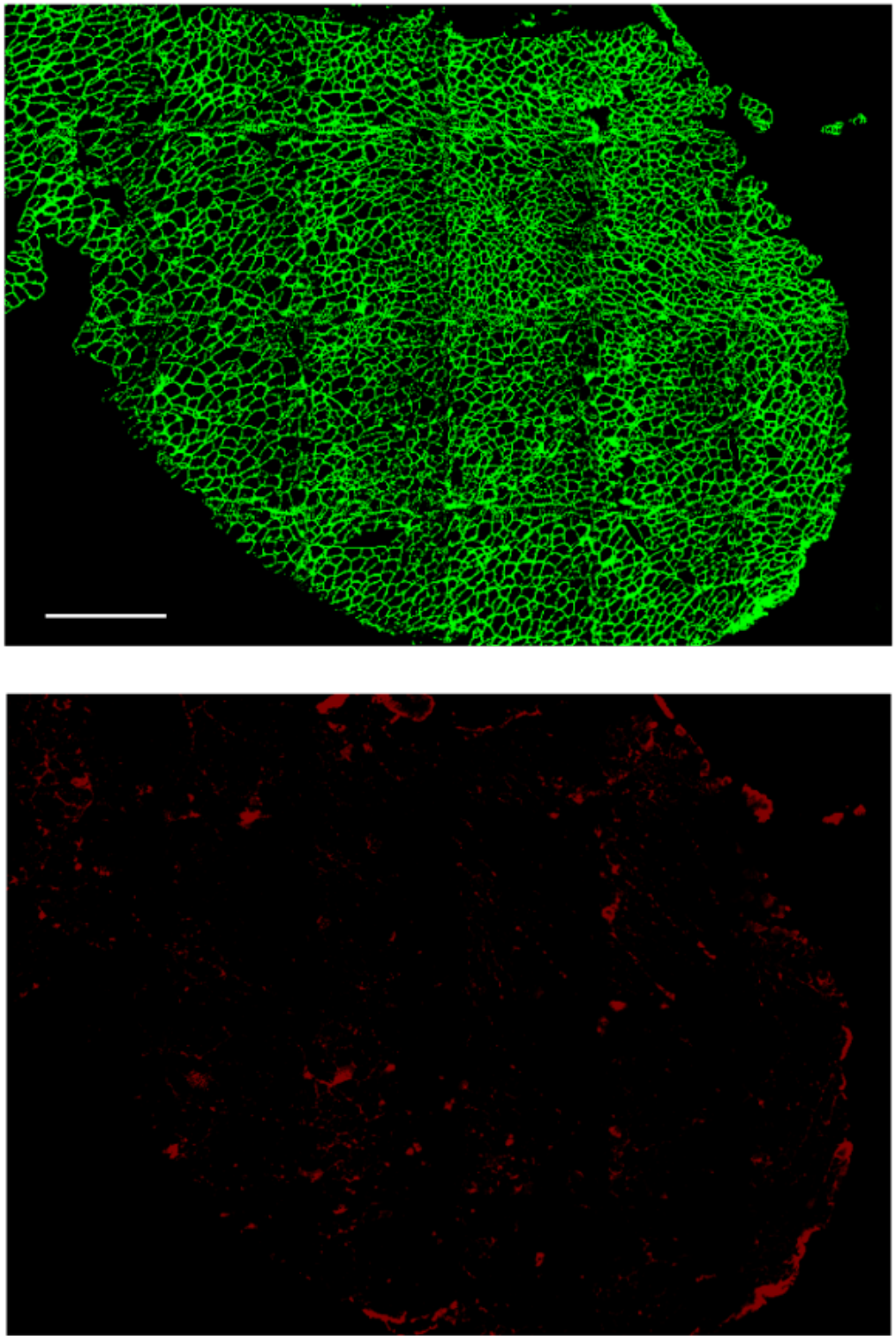

Figure 4.6 **Immunohistochemistry analysis of expression of microdystrophin in *mdx* TA muscle following *in vivo* plasmid electrotransfer (representative image of a saline treated TA).**

[Continued on next page]

[From previous page]

The TA muscles of mdx mice were subjected to plasmid electrotransfer transfection with either p-mMD1 or p-585 mMD1 at a plasmid dose of 25 μg, or saline control. The TA muscle in this figure was treated with saline. 2 weeks post treatment, 10 μm cryosections of the TA muscles were obtained. The sections were fixed in acetone at −20°C and to reduce background effects, the Mouse on Mouse (M.O.M) kit (Vector Labs) was used to stain muscle sections. The presence of microdystrophin was examined by immunostaining with MANEX 1011C, an anti-dystrophin antibody specific for exons 10 and 11 of the dystrophin protein (Glenn Morris; Le Guiner et al., 2017). The signal was visualized using Alexafluor 568–conjugated anti-mouse IgG (Invitrogen). Laminin was immunostained using rat anti-laminin monoclonal antibody (Sigma Aldrich). For laminin signal visualisation, anti-rat biotinylated antibody followed by Alexafluor 568–conjugated streptavidin was used. The slides were mounted using mounting medium (Vector Labs). All samples were handled in a blinded manner. Microscope images were acquired using Nikon Eclipse NiE confocal microscope, where complete TA section images were acquired for analysis. Top: TA cross-section showing immunostained laminin facilitating the visualisation of all individual muscle fibers. Bottom: TA cross-section showing dystrophin immunostaining (nominally of revertant fibres). Red channel: microdystrophin, green channel: laminin. Scale bar: 500 μm.

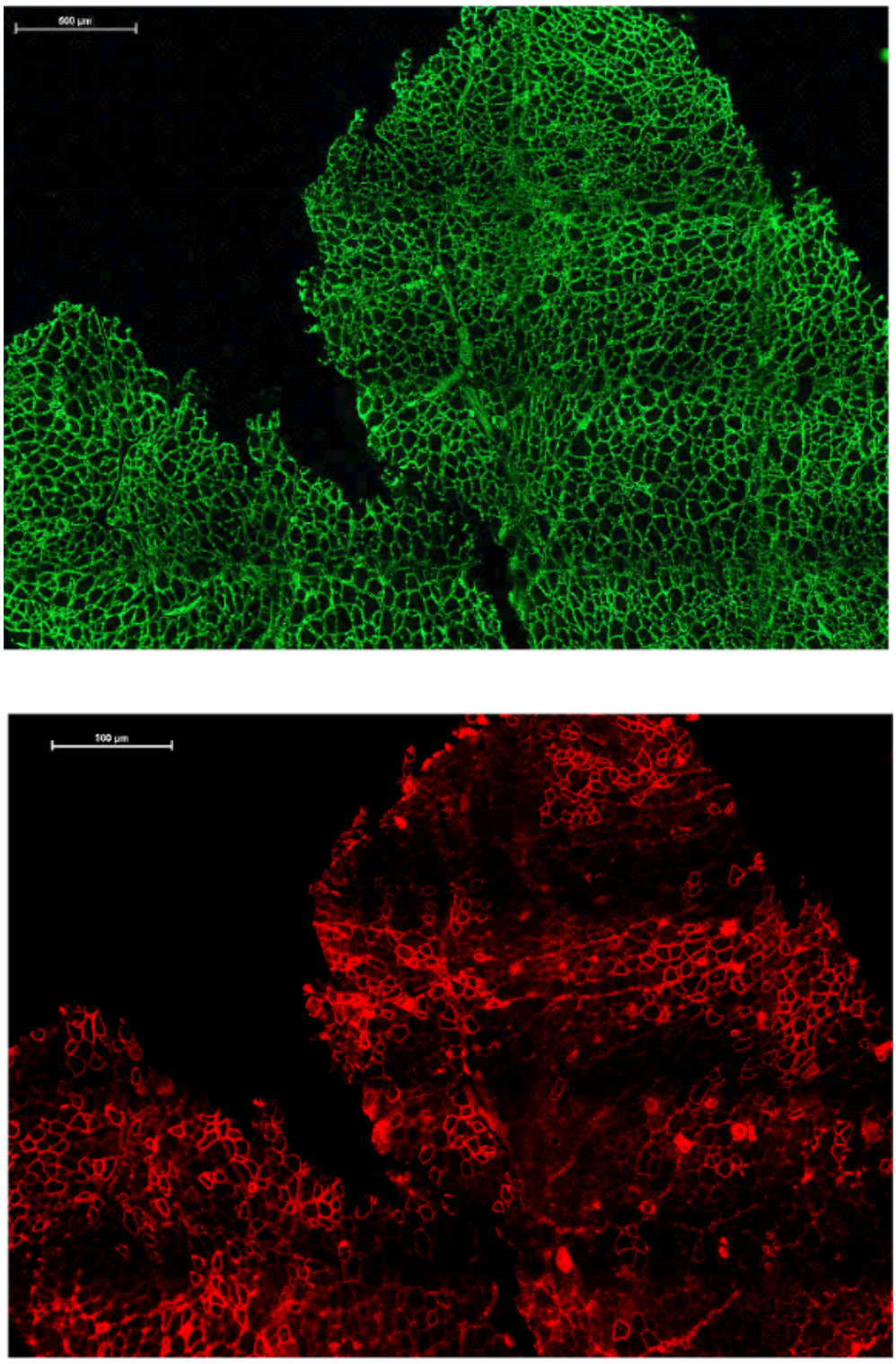

Figure 4.7 **Immunohistochemistry analysis of expression of microdystrophin in *mdx* TA muscle following *in vivo* plasmid electrotransfer (representative image of a p-mMD1 treated TA).**

[Continued on next page]

[From previous page]

The TA muscles of mdx mice were subjected to plasmid electrotransfer transfection with either p-mMD1 or p-585 mMD1 at a plasmid dose of 25 μg, or saline control. The TA muscle in this figure was treated with p-mMD1 at a plasmid dose of 25 μg. 2 weeks post treatment, 10 μm cryosections of the TA muscles were obtained. The sections were fixed in acetone at −20°C and to reduce background effects, the Mouse on Mouse (M.O.M) kit (Vector Labs) was used to stain muscle sections. The presence of microdystrophin was examined by immunostaining with MANEX 1011C, an anti-dystrophin antibody specific for exons 10 and 11 of the dystrophin protein (Glenn Morris; Le Guiner et al., 2017). The signal was visualized using Alexafluor 568–conjugated anti-mouse IgG (Invitrogen). Laminin was immunostained using rat anti-laminin monoclonal antibody (Sigma Aldrich). For laminin signal visualisation, anti-rat biotinylated antibody followed by Alexafluor 568–conjugated streptavidin was used. The slides were mounted using mounting medium (Vector Labs). All samples were handled in a blinded manner. Microscope images were acquired using Nikon Eclipse NiE confocal microscope, where complete TA section images were acquired for analysis. Top: TA cross-section showing immunostained laminin facilitating the visualisation of all individual muscle fibers. Bottom: TA cross-section immunostained for dystrophin showing the distribution of the microdystrophin-positive fibers. Red channel: microdystrophin, green channel: laminin. Scale bar: 500 μm.

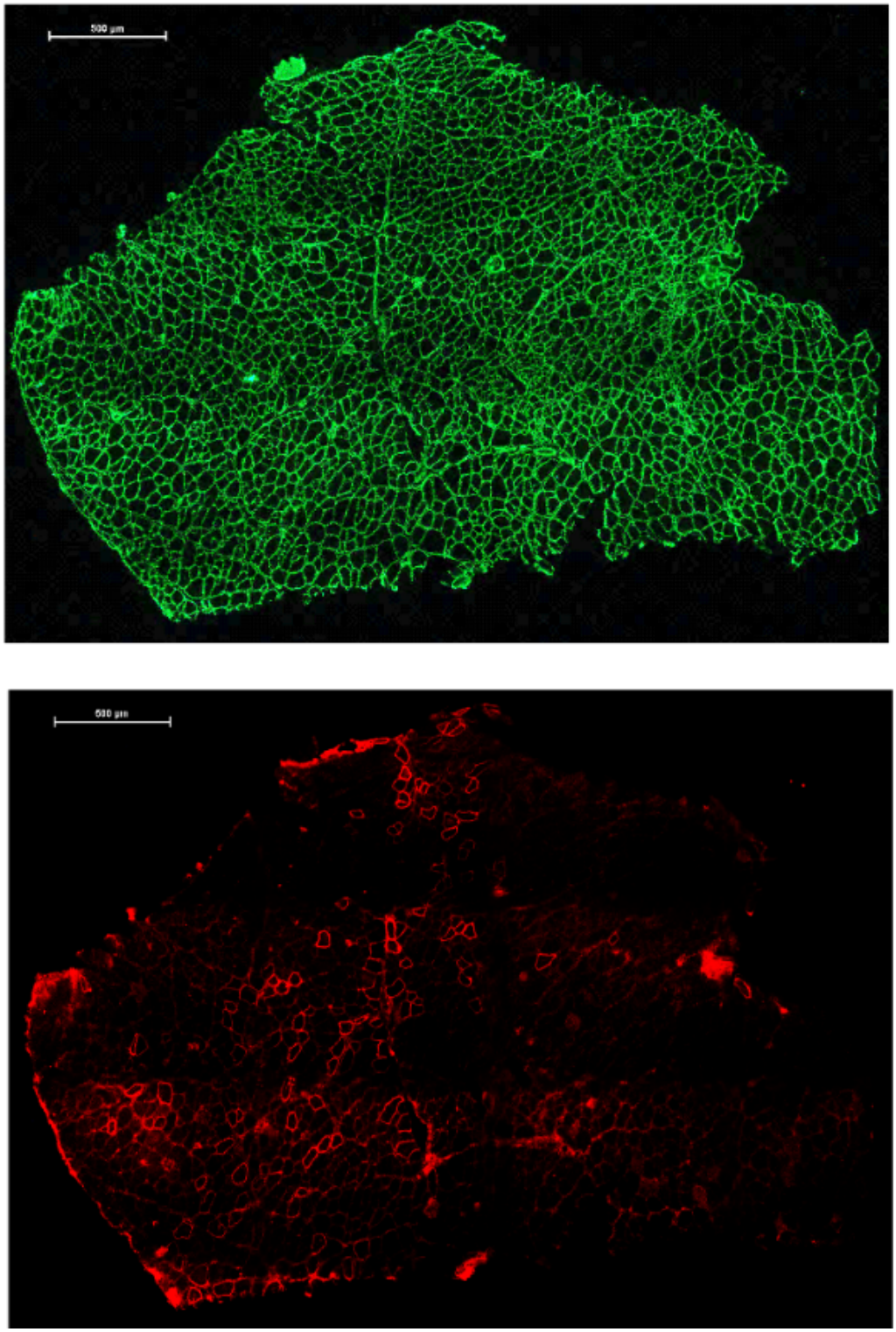

Figure 4.8 **Immunohistochemistry analysis of expression of microdystrophin in *mdx* TA muscle following *in vivo* plasmid electrotransfer (representative image of a p-585 mMD1 treated TA).**

[Continued on next page]

[From previous page]

The TA muscles of mdx mice were subjected to plasmid electrotransfer transfection with either p-mMD1 or p-585 mMD1 at a plasmid dose of 25 μg, or saline control. The TA muscle in this figure was treated with p-585 mMD1 at a plasmid dose of 25 μg. 2 weeks post treatment, 10 μm cryosections of the TA muscles were obtained. The sections were fixed in acetone at −20°C and to reduce background effects, the Mouse on Mouse (M.O.M) kit (Vector Labs) was used to stain muscle sections. The presence of microdystrophin was examined by immunostaining with MANEX 1011C, an anti-dystrophin antibody specific for exons 10 and 11 of the dystrophin protein (Glenn Morris; Le Guiner et al., 2017). The signal was visualized using Alexafluor 568–conjugated anti-mouse IgG (Invitrogen). Laminin was immunostained using rat anti-laminin monoclonal antibody (Sigma Aldrich). For laminin signal visualisation, anti-rat biotinylated antibody followed by Alexafluor 568–conjugated streptavidin was used. The slides were mounted using mounting medium (Vector Labs). All samples were handled in a blinded manner. Microscope images were acquired using Nikon Eclipse NiE confocal microscope, where complete TA section images were acquired for analysis. Top: TA cross-section showing immunostained laminin facilitating the visualisation of all individual muscle fibers. Bottom: TA cross-section immunostained for dystrophin showing the distribution of the microdystrophin-positive fibers. Red channel: microdystrophin, green channel: laminin. Scale bar: 500 μm.

Microdystrophin expression can be seen in both the p-mMD1 and p-585mMD1 treated samples and correct sarcolemma localisation of the protein was also seen (Figures 4.7 and 4.8). Again, as observed in the Western blot workflow (Figure 4.5), this observation in the IHC workflow confirmed at the simplest level that the newly generated plasmid construct p-585mMD1 was functional *in vivo* producing the protein of interest. The microdystrophin positive fibres were widely distributed in the TA treated with p-mMD1. This was not seen in the p-585mMD1 treated samples and the distribution of the microdystrophin positive fibres seems slightly limited (less widespread) compared to p-mMD1 treated TAs. Calculation of percentage of microdystrophin positive fibres was attempted (Figure 4.9). This calculation was performed by counting the number of microdystrophin positive fibers versus total fibres on whole TA sections, expressed as a percentage.

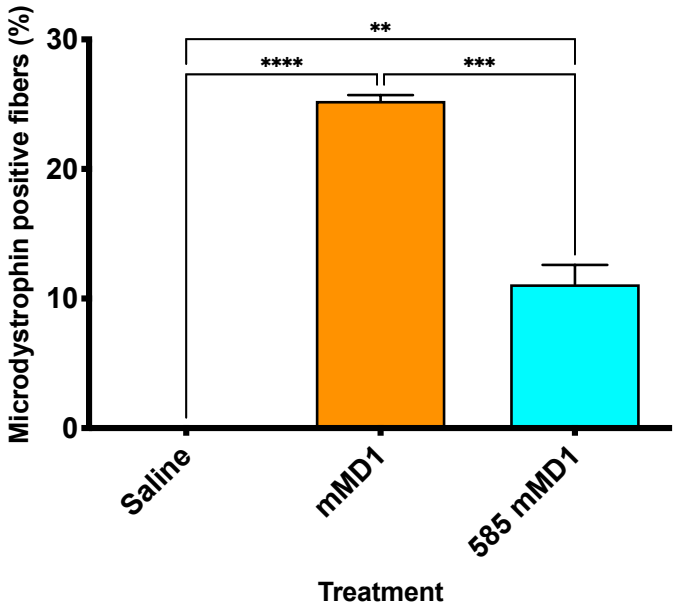

Figure 4.9 **Percentage microdystrophin positive fibers analysis in *mdx* TA muscle following *in vivo* plasmid electrotransfer.** The TA muscles of mdx mice were subjected to plasmid electrotransfer transfection with either p-mMD1 or p-585 mMD1 at a plasmid dose of 25 µg, or saline control. 2 weeks post treatment, 10 µm cryosections of the TA muscles were obtained. The sections were fixed in acetone at −20°C and to reduce background effects, the Mouse on Mouse (M.O.M) kit (Vector Labs) was used to stain muscle sections. The presence of microdystrophin was examined by immunostaining with MANEX 1011C, an anti-dystrophin antibody specific for exons 10 and 11 of the dystrophin protein (Glenn Morris; Le Guiner et al., 2017). The signal was visualized using Alexafluor 568–conjugated anti-mouse IgG (Invitrogen). Laminin was immunostained using rat anti-laminin monoclonal antibody (Sigma Aldrich). For laminin signal visualisation, anti-rat biotinylated antibody followed by Alexafluor 568–conjugated streptavidin was used. The slides were mounted using mounting medium (Vector Labs). All samples were handled in a blinded manner. Microscope images were acquired using Nikon Eclipse NiE confocal microscope, where complete TA section images were acquired for analysis. Immunostained laminin facilitated the manual counting of total muscle fibers. TA cross-section immunostained for dystrophin were used to count microdystrophin-positive fibers manually. Percentage microdystrophin-positive fibers were calculated by expressing microdystrophin-positive fibers versus total fibers as a percentage. All data represent mean ± SEM (N, number of TAs analysed per treatment group=6). Statistical analyses by one-way ANOVA: **P ≤ 0.01, ***P ≤ 0.001, ****P ≤ 0.0001.

In this study, ~25% and ~10% microdystrophin positive fibers were observed following treatments of p-mMD1 and p-585mMD1 respectively. To evaluate whether the treatments provided any functional benefits, we performed physiological assessments of muscle function.

Isolated muscle function that includes isometric and eccentric contractions are routine protocols of physiological assessments of muscle function in preclinical studies (Moorwood et al, 2013). Isometric force is an assessment of muscle strength and eccentric contractions is an assessment of sarcolemma stability. In DMD, both the muscle strength and sarcolemma stability are compromised, so the isometric force and eccentric contractions readouts following treatments with therapeutic constructs can provide useful information about efficacy of the treatment.

In *mdx* mice, during isometric force assessment, the absolute force can be higher compared to wild-type mice due to compensatory hypertrophy and as such, the isometric tetanic force generated is normalised by the cross-sectional area to calculate specific force (Chan, Head and Morley, 2007). When the cross-sectional area is accounted for, the weakness in dystrophic muscle will become apparent. This however is also dependent on the age of *mdx* mice as the mouse model itself shows very mild disease phenotype especially in young mice (McGreevy et al., 2015). The eccentric contraction data shows progressive loss of force generating capacity of the muscle and this loss is more obvious in *mdx* mice as the lack of dystrophin and the associated proteins increases membrane fragility (Moorwood et al, 2013). In this study, electrophysiology experiment was performed two weeks following treatment to evaluate muscle function (Figures 4.10 and 4.11).

Muscle electrophysiology evaluation was performed with Dr Alberto Malerba and Dr Ngoc Lu Nguyen at Royal Holloway, University of London. Briefly, mice were anesthetized intraperitoneally using 60mg/kg pentobarbital. As described in (Koo et al, 2011), pins and clamps were used to fix the knee and foot, and the distal tendon of the muscle was attached to a lever arm of a servomotor system using a silk ligature. The sciatic nerve was proximally crushed and stimulated distally using a bipolar silver electrode using supramaximal square wave pulses of 0.1 msec duration. During isometric contractions following electrical stimulation (at different frequencies up to 180 Hz, train of stimulation of 500 msec), absolute maximal isometric tetanic force was measured. The sciatic nerve was stimulated for 700 msec at a frequency of 150 Hz for the muscle to attain maximum isometric force and the initial length of the TA muscle L_0 was recorded. In the first 500 msec, a maximal isometric contraction of the TA muscle was initiated, followed by muscle lengthening (1.1 mm, 10% L_0) at a velocity of 5.5 mm/sec (about 0.5 L_0/ sec) in the last 200 msec. Maximal isometric force was measured following each eccentric contraction and the force measured was expressed as a percentage of the initial maximal isometric force. Eleven isometric lengthening contractions of the TA muscles were performed, each contraction separated by a 60-sec rest period.

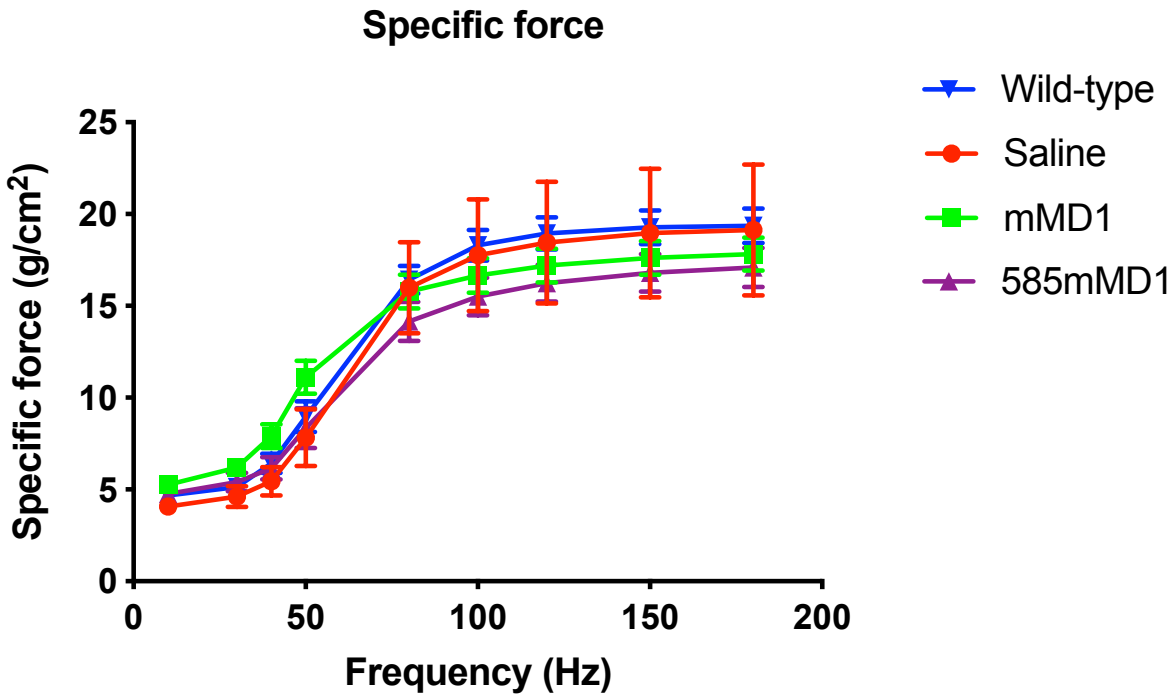

Figure 4.10 **Electrophysiological evaluation of specific force generation in untreated C57/BL10 wild-type and *mdx* TA muscles following *in vivo* plasmid electrotransfer.** The TA muscles of *mdx* mice were subjected to plasmid electrotransfer transfection with either p-mMD1 or p-585 mMD1 at a plasmid dose of 25 µg, or saline control. 2 weeks post treatment, muscle electrophysiology assays were performed. Briefly, mice were anesthetized intraperitoneally using 60mg/kg pentobarbital. As described in (Koo et al, 2011), pins and clamps were used to fix the knee and foot, and the distal tendon of the muscle was attached to a lever arm of a servomotor system using a silk ligature. The sciatic nerve was proximally crushed and stimulated distally using a bipolar silver electrode using supramaximal square wave pulses of 0.1 msec duration. During isometric contractions following electrical stimulation (at different frequencies up to 180 Hz, train of stimulation of 500 msec), absolute maximal isometric tetanic force was measured. Specific force is an indication of muscle strength. Specific force is calculated by dividing the isometric tetanic force generated, by the cross-sectional area of the TA muscle. Cross-sectional area was calculated by dividing the TA muscle's mass by the product of its initial length L_0 and the density of mammalian muscle (1.06 mg/mm^3) (Chan, Head and Morley, 2007). Specific force shows no

significant difference between the saline and the treated groups (p-mMD1 and p-585 mMD1). Natural history data for the age and sex-matched wild-type mice is included in the graphs (in blue) to show that the specific force in young 10-week old mdx mice is similar to that of untreated wild-type. Note that the untreated wild-type mice also did not experience further muscle damage caused by the electroporation technique itself. Compensatory hypertrophy of the muscle and very mild disease phenotype in young mdx mice explains the greater specific force matching untreated wild-type. Statistical analyses by two-way ANOVA with Bonferroni post hoc test: no significant differences were found between the treatments. n=10 for wild type, n=3 for saline, n=6 for both plasmid treatments (p-mMD1 and p-585 mMD1).

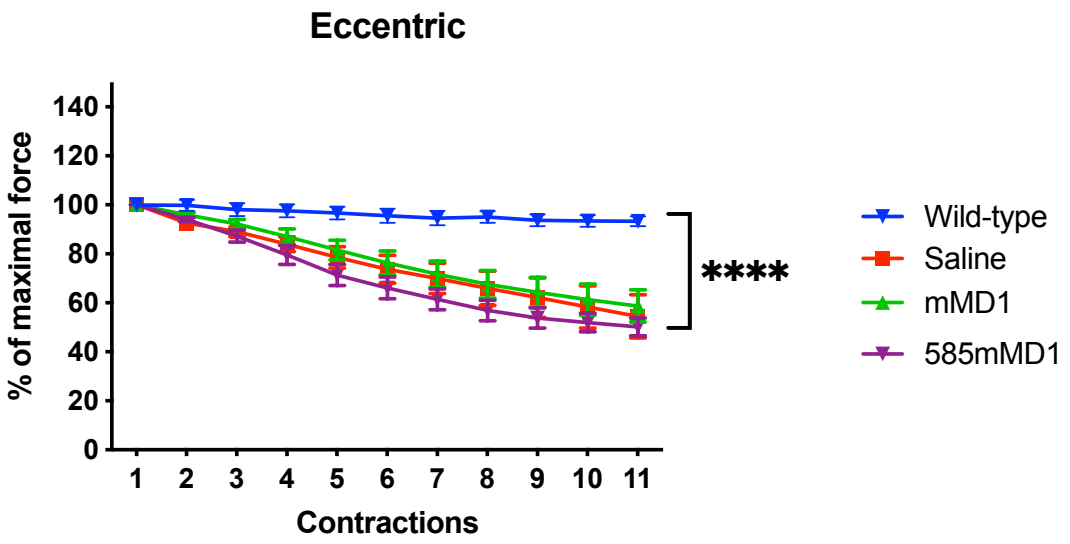

Figure 4.11 **Electrophysiological evaluation of loss of force following repetitive eccentric contractions in untreated C57/BL10 wild-type and *mdx* TA muscles following *in vivo* plasmid electrotransfer.** The TA muscles of mdx mice were subjected to plasmid electrotransfer transfection with either p-mMD1 or p-585 mMD1 at a plasmid dose of 25 µg, or saline control. 2 weeks post treatment, muscle electrophysiology assays were performed. Following evaluation of specific force generation in the TA muscle as discussed in Figure 4.10, the sciatic nerve was stimulated for 700 msec at frequency of 150 Hz for the muscle to attain maximum isometric force and the initial length of the TA muscle L_0 was recorded. In the first 500 msec, a maximal isometric contraction of the TA muscle was initiated, followed by muscle lengthening (1.1 mm, 10% L_0) at a velocity of 5.5 mm/sec (about 0.5 L_0/ sec) in the last 200 msec. Maximal isometric force was measured following each eccentric contraction and the force measured was expressed as a percentage of the initial maximal isometric force. Eleven isometric lengthening contractions of the TA muscles were performed, each contraction separated by a 60-sec rest period. Eccentric contraction evaluation is an assessment of sarcolemma stability. The loss of force of *mdx* mice was significantly greater than the wild-type mice as the lack of dystrophin destabilises the membrane and increases membrane fragility (Moorwood et al, 2013). No difference was observed between the saline, p-mMD1 and p-585 mMD1 treated samples. Two-way ANOVA with Bonferroni post hoc test. All data represent mean ± SEM. ****P ≤ 0.0001. n=10 for wild type, n=3 for saline, n=6 for both plasmid treatments (p-mMD1 and p-585 mMD1).

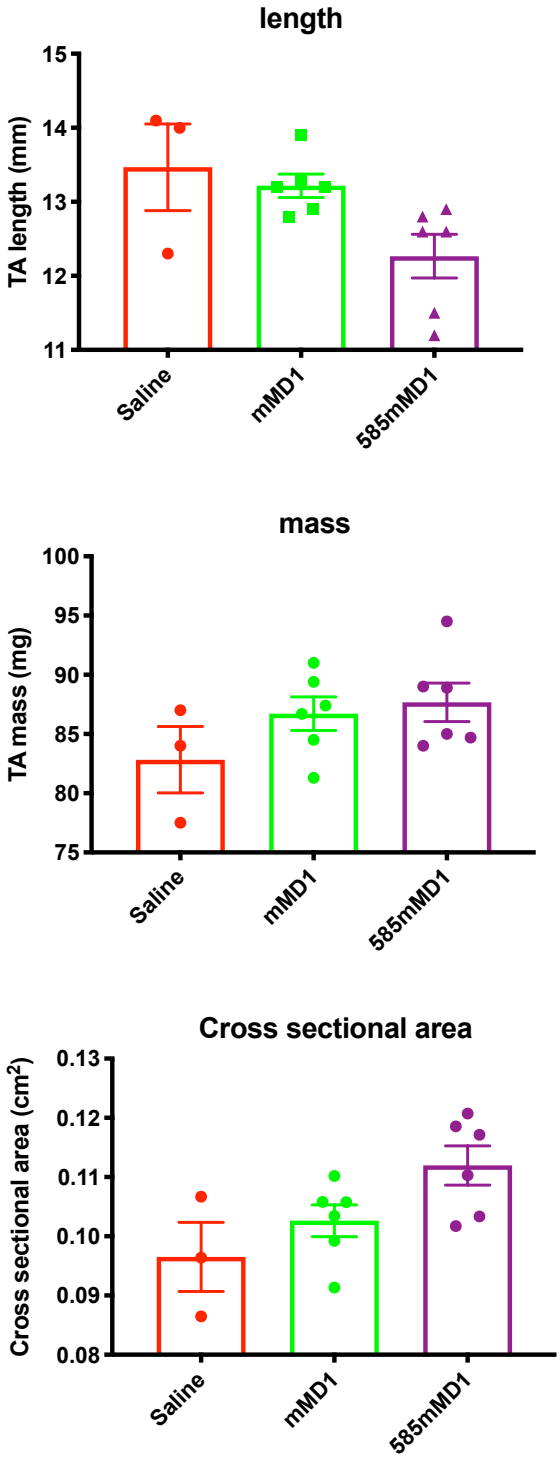

Figure 4.12 **Evaluation of TA length, mass and cross sectional-area (CSA) of *mdx* TA muscles following *in vivo* plasmid electrotransfer.** The TA muscles of mdx mice were subjected to plasmid electrotransfer transfection with either p-mMD1 or p-585 mMD1 at a plasmid dose of 25 µg, or saline control. 2 weeks post treatment, the TA muscle length, mass and CSA were measured to evaluate changes to the muscle

following treatment. Cross-sectional area was calculated by dividing the TA muscle's mass by the product of its initial length L_0 and the density of mammalian muscle (1.06 mg/mm^3) (Chan, Head and Morley, 2007). Statistical analyses by one-way ANOVA: no significant differences were found between the treatments for all three parameters. n=3 for saline, n=6 for both plasmid treatments (p-mMD1 and p-585 mMD1).

The isometric force and eccentric contractions analyses showed no difference in the treated groups versus saline treatment. This is partly due to the electrotransfer technique itself that damages the muscle during treatment; and the muscle electrophysiology assay being performed 2 weeks later, where the treated muscle would still be undergoing recovery following the injury (discussed in Section 4.3 Discussion). A better gene delivery system is by using viral vectors such as AAV. However, AAV vector production is both time consuming and costly; as such, plasmid electrotransfer treatment was attempted to establish proof-of-principle before moving into vector production. The Western blot and IHC results from the electrotransfer experiment provided the proof-of-principle that the plasmid constructs are functional *in vivo*, capable of expressing the transgene of interest: microdystrophin. Microdystrophin was also localised to the sarcolemma in both plasmid (p-mMD1 and p-585 mMD1) treated muscle samples. As such, following the electrotransfer study, the mMD1 and 585 mMD1 constructs were vectorised in rAAV2/9: recombinant AAV serotype 9 where the *rep* gene sequence is derived from AAV2 and *cap* gene sequence is derived from AAV9.

4.3 Discussion

Manipulation of skeletal muscle cells *in vitro* using techniques such as plasmid transfection is known to be difficult, especially when myoblasts (undifferentiated muscle cell lines), myotubes or myosatellites (primary muscle stem cells) are involved (Jackson et al, 2013). We attempted to transfect C2C12 mouse myoblast cell line with the mouse codon-optimised p-mMD1 and p-585 mMD1 plasmids; however, transfection was possibly limited, as outlined by the Western blot data. Following the *in vitro* experiments described in Chapter 3 and Section 4.2, an *in vivo* experiment: plasmid DNA electrotransfer was carried out with the main aim of testing whether the constructs express the protein of interest: microdystrophin *in vivo*. The electro-transfer experiment is a quick way of assessing whether the newly generated plasmid constructs are functional in an *in vivo* setting. The efficiency of this method is very low, where previous studies have reported approximately 1-5% of myofibers expressing dystrophin in *mdx* mice treated with plasmids (Zhang et al, 2004). The procedure itself is invasive and the expression of transgene is very localised at the injection site, making it an unattractive method of therapeutic gene delivery in the clinical setting (Robinson-Hamm and Gersbach, 2016). Despite the limitations, nevertheless, the plasmid delivery via this method is capable of expressing the protein of interest, and as such, this experiment would verify if the constructs we generated can be expressed *in vivo*, especially the newly generated p-585 mMD1.

In both p-mMD1 and p-585mMD1 treated samples, microdystrophin expression was observed as shown by the Western blot and IHC data (approximately 25% and 10% of dystrophin positive fibers respectively). This provides proof-of-principle that the microdystrophin constructs were able to express *in vivo*. Immunohistochemistry analysis also revealed that the microdystrophin protein was correctly localised at the sarcolemma, which is important to stabilise the dystrophin-associated protein complex (DAPC), which then protects the muscle against contraction-induced damage. The p-585 mMD1 treatment did not seem to elevate transgene expression, and both the plasmid treatments did not show any functional rescue of the disease phenotype as shown by the electrophysiology

experiment data. However, these were not a concern at this stage for the following reasons:

The plasmid DNA delivered has several barriers before reaching the nucleus including extracellular matrix, plasma membrane, cytoplasm and nuclear membrane. As such, the efficiency of this DNA delivery method is lower and the extensive connective tissue network in dystrophic muscle tissue also limits the plasmid delivery to the myofibers (Jiao et al, 1992).

The presence of bacterial DNA in the plasmid expression cassette has been shown to play a role in transcriptional silencing of the transgene (Riu *et al*, 2005). It is hypothesised that this may be due to the extensive methylation of the bacterial DNA by DNA methylases, leading to chromatin remodelling of the bacterial sequence to adopt a heterochromatin structure, subsequently silencing the transgene as well (Riu *et al*, 2005). The p-585 mMD1 plasmid is slightly bigger than the p-mMD1 plasmid and the additional sequence carried by p-585 mMD1 is derived from bacteria, potentially leading to higher level of transgene silencing compared to the smaller p-mMD1. The slightly bigger size of the p-585 mMD1 plasmid (~585bp difference) compared to the p-mMD1 also opens up a possibility of the p-585 mMD1 plasmid migrating towards the nucleus at a lower efficiency compared to p-mMD1. Studies have shown that electrotransfer of smaller plasmids are more efficient than larger plasmids (Bloquel et al, 2004).

Before reaching the nucleus, the plasmid DNA migrates through the cytoplasm and the cytoplasmic nucleases can degrade DNA found here. Whilst both plasmid DNAs are prone to the degradation, the 585 mMD1 plasmid could be at a higher risk due to the presence of additional bacterial derived sequences in the R6K-RNA-OUT (Lu *et al*., 2017). In another scenario where if the gene expression cassettes were delivered using a viral vector for instance, the DNA would be delivered straight to the nucleus by the vector and as such, the DNA is not exposed to nucleases in the cytoplasm.

Significant muscle damage occurs as electrotransfer is performed and this damage itself is enough to cause a significant loss of transfected muscle fibres (McMahon et al, 2001). A cascade of degeneration, regeneration, inflammation, oxidative stress and progressive damage is triggered in the dystrophic muscle of *mdx* mice as seen in human DMD following muscle injury (Burns et al, 2018). The physical damage caused by electrotransfer could also activate the innate immune system by acting as a damage-associated molecular pattern (DAMP) (Mann et al, 2012). As such, the physiological traits exhibited by the *mdx* mice two weeks following the electrotransfer protocol may not necessarily capture the effects of restoring dystrophin deficiency; but reflect the underlying processes at play.

After establishing proof-of-principle *in vivo* where both the p-mMD1 and p-585mMD1 constructs expressed microdystrophin that was correctly localised to the sarcolemma, we decided to vectorise the constructs to perform further *in vivo* studies described in Chapter 5.

Chapter 5 Evaluating AAV/mMD1 and AAV/585mMD1 *in vivo* via intramuscular delivery of the vectors

5.1 Introduction

Overall, lack of dystrophin protein in DMD patients causes muscle weakness and results in DMD patients losing ambulation by the age of 12-14, if no corticosteroid intervention has been present. On the other hand, Becker muscular dystrophy (BMD) patients with mutated *DMD* gene are ambulant beyond their teenage years and in some patients, ambulation was never lost (England et al, 1990). The observations in BMD patients (some of whom carry very large deletions in the DMD gene) (England et al, 1990) resulted in generation of miniaturised versions of dystrophin (so called microdystrophin) to replace the missing gene in DMD patients using adeno-associated virus (AAV) vectors as vehicles that carry the truncated gene. So far, adeno-associated virus (AAV) gene transfer has proven to be the most promising approach that has the potential of treating DMD (Table 1.4). This is a direct approach of replacing the missing dystrophin protein in the muscle and heart tissues of the patients.

The nature of the disease calls for high doses of AAV delivered systemically for body-wide transduction to treat a large amount of muscle, by replacing the missing gene with a truncated but functional copy of the gene. The key challenge in AAV gene therapy, especially for muscle diseases is the delivery of safe yet efficient amount of the virus, where therapeutic efficacy is achieved without provoking the immune system, especially at very high doses. In clinical trials for spinal muscular atrophy (SMA), high AAV9 vector dose of 2×10^{14} vg/kg have been tested without causing any serious adverse effects, leading to the approval of the AAV-based drug Zolgensma by the FDA in May 2019 (Hoy, 2019). On the other hand, in clinical trial of X-linked myotubular myopathy, the high AAV8 vector dose of 3×10^{14} vg/kg (highest dose tested so far for any AAV-based gene therapy to date) resulted in the death of three patients, caused by progressive liver dysfunction followed by sepsis or gastrointestinal bleeding (Agarwal, 2020; Taylor, 2020). These observations suggest that a high dose AAV treatment

delivered systemically in a muscle disease setting (such as the AAV treatment for X-linked myotubular myopathy) can trigger unwanted immune responses. At the same time, these observations also raise a fundamental question: is AAV immunogenicity serotype dependent?

As discussed in the Introduction and previous chapters, one way to reduce dosage of AAV in treatment is to increase the potency of the gene expression cassette by the addition of regulatory elements (Powell et al, 2015). An efficient gene expression cassette capable of producing high amount of transgene product can potentially reduce the dose of vector needed to reach therapeutic efficacy. High transgene expression is especially important in diseases like DMD, where high systemic delivery of a structural protein to widespread muscle tissues is needed to achieve therapeutic efficacy. In this chapter, an engineered intron, R6K-RNA-OUT which has demonstrated log-fold increases in transgene expression in liver, is incorporated into the AAV-microdystrophin gene expression cassette and tested in the *mdx* mice model via intramuscular injection. AAV vector quality, and transgene expression and functional outcome in vivo was evaluated.

Potential limitations to the advantages of high transgene productivity must also be considered. Firstly, an overexpressing cassettes may produce no clinical benefit and/ or risk of potential proteinopathy (Hetz, 2012) or other cellular toxicities due to protein misfolding and aggregation. Such effects may be more pronounced in mono-nucleated target cells, whereas production of high level intracellular protein in multinucleated cells (such as skeletal muscle) may be tolerated due to transgene spreading in the large common cytoplasm of the cells (discussed in Section 4.1 of Chapter 4). The route of delivery via intramuscular injection is commonly used in preclinical studies to test gene therapy for muscle diseases (Zhao et al, 2020), however, this route is also more immunogenic compared to the systemic delivery route (Boisgerault and Mingozzi, 2015). The inflamed muscle environment (often seen in muscular dystrophies) and tissue damage from injection per se further exacerbates the immunogenicity issue

(Boisgerault and Mingozzi, 2015). The *mdx* mice model lacks functional dystrophin protein, however, some features of DMD are poorly replicated in this animal model especially in young *mdx* mice. For example, the progressive loss of muscle strength seen in DMD patients is not seen in the *mdx* mice, and mice remain fully ambulant (Massopust et al, 2020). However, muscle degeneration, myofibre turnover and high serum CK are observed in young *mdx* mice (McGreevy et al, 2015). For comparing transduction efficiency and transgene expression use of young *mdx* mice is generally adopted, rather than housing the mice for >1 year (at which point the muscle fibrosis and wasting phenotype becomes more apparent) (McGreevy et al, 2015). As such, interpretations of the results (especially immunohistopathology and electrophysiology results from young *mdx* mice) should be made with care when comparing the treatment groups.

5.2 Results

5.2.1 AAV production and quantification

The plasmids p-mMD1 and p-585 mMD1 were used to produce rAAV using the HEK293T double transfection method. This cell line derived from human embryonic kidney 293 cells is highly transfectable and is competent for replication of viral vectors such as rAAVs. AAV2 *rep* and AAV9 *cap* genes were provided in *trans* together with the helper functions from adenovirus in the production process via another plasmid pDP9rs (described in Chapter 2). At 72 hour post-transfection, the HEK293T cells were lysed and the rAAV vectors purified using iodixanol step gradients (Figure 5.1). Iodixanol is an isomolar density gradient medium that allows virus purification from a crude lysate from cells. It is also considered inert and non-toxic to mammalian cells, which means the presence of trace amounts of iodixanol in the final formulation will not affect the use of the purified virus in preclinical studies. Full details of the vector production, purification and quantification can be found in Chapter 2: Materials and Methods.

Two rAAVs containing the therapeutic cassettes mMD1 and 585mMD1 were produced using transient transfection of HEK293T cells, as follows:

- rAAV9-Spc5.12-mMD1 (also called AAV9/mMD1)
- rAAV9-Spc5.12-585R6KRNAOUT-mMD1 (also called AAV9/585mMD1)

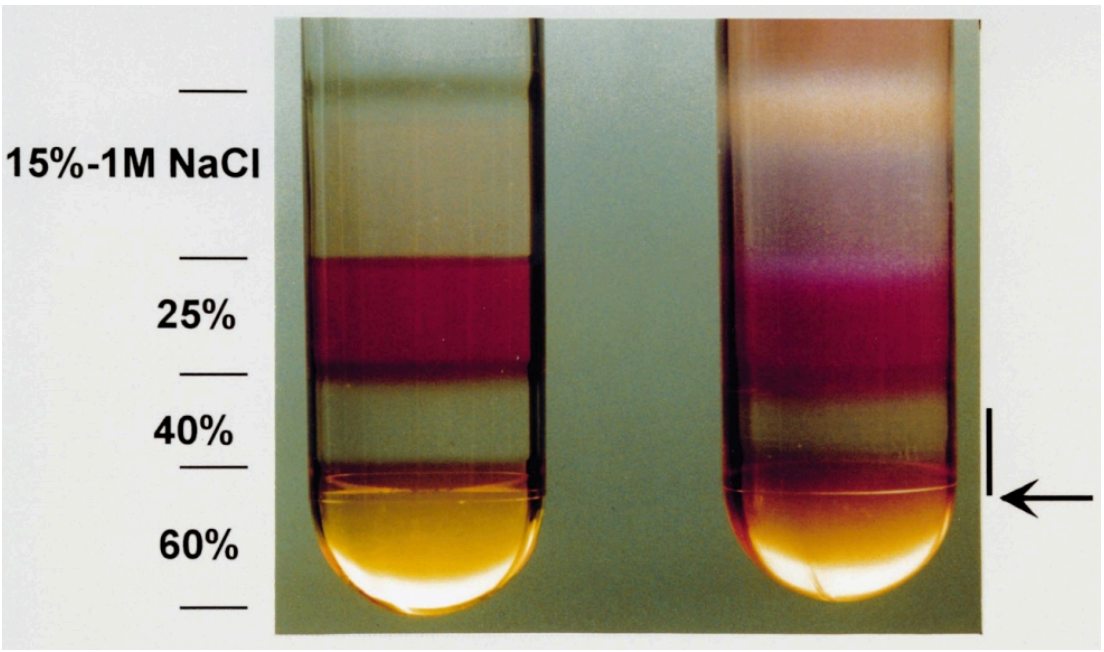

Figure 5.1 **rAAV purification using iodixanol gradient**. Left: Iodixanol gradient before ultracentrifugation. An iodixanol gradient was set-up using 15%, 25%, 40% and 60% iodixanol solutions. 25% and 60% iodixanol contain phenol red to aid visibility when 'layering' the gradient. 1M NaCl in the 15% iodixanol destabilises ionic interactions between macromolecules (multiple proteins from the cell lysate). The crude lysate from HEK293T cells that contain the virus were loaded on the 15%-1M NaCl layer. Right: Iodixanol gradient after ultracentrifugation. Genome containing virions are found in the 40%-60% interface (shown by the line) and a needle is inserted where the arrow is pointing to extract the virus. Contaminants with lower densities, including empty capsids are collected in the 25% step and 25%-40% interface (Zolotukhin et al, 1999). Figure adapted from (Zolotukhin et al, 1999).

Following Iodixanol purification, rAAVs were desalted, concentrated and quantified. Quantitative polymerase chain reaction (qPCR) assay was performed to quantify the final yield of viruses using SYBR Green technology (Figure 5.2). SYBR Green is a non-specific double-stranded DNA binding dye, where there is emission of fluorescence following DNA binding that allows measurement of the amount of amplified PCR products. Primers targeting the SV40 polyA region were used in the qPCR reactions. A titre of 5.61 x 10^{13} vp/ml in approximately 500 µl was obtained for AAV9/mMD1. For AAV9/585mMD1, a titre of 2.87 x 10^{13} vp/ml in approximately 400 µl was obtained.

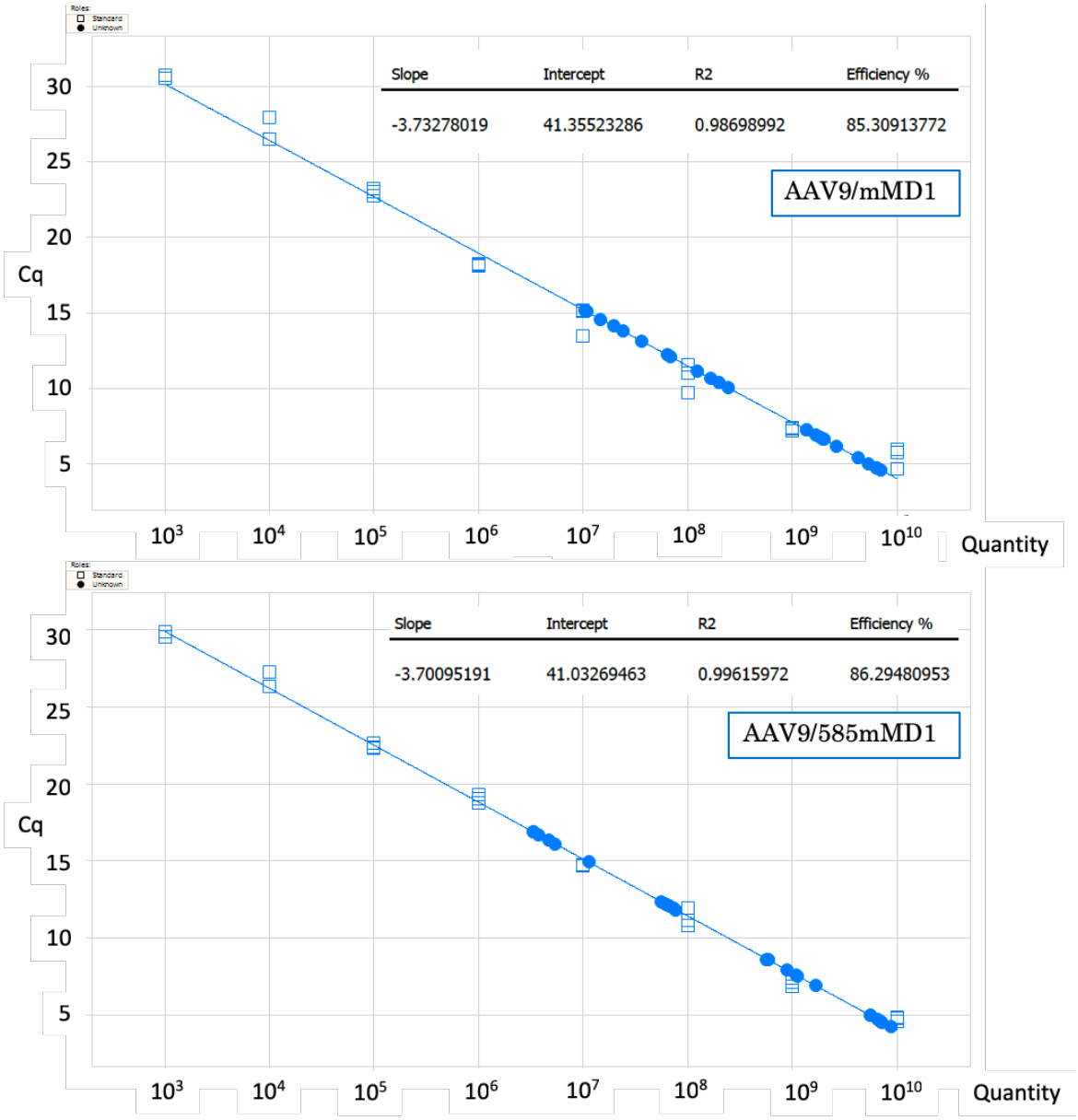

Figure 5.2 **Quantification of rAAV titres using qPCR.**

[Continued on next page]

[From previous page]

Figure 5.2 **Quantification of rAAV titres using qPCR.** Both AAV9/mMD1 and AAV9/585mMD1 were produced using transient transfection of HEK293T cells where the *rep* and *cap* genes, and Adenovirus helper functions were provided in trans. Following purification and concentration of the viruses, the viral titre was determined using qPCR. Plasmids p-mMD1 and p-585 mMD1 were used to prepare respective standards ranging from 10^3 to 10^{10} copies/µl. Squares represent standards plot points. The viral DNA was extracted and serially diluted. Shaded circles represent plot points for the viral cassette ranging from 'undiluted' to 1000-fold dilution. All standards and samples were ran in triplicates to account for technical errors such as pipetting errors. Primers targeting the SV40 poly A region were used in the qPCR reactions. Efficiencies of the qPCR are acceptable at 85% and 86% for AAV9/mMD1 and AAV9/585 mMD1 respectively. R^2 values for both the plots were very close to 1 (≥ 0.96), indicating a good fit of the trend line to the data. The standard curves were of good quality as the differences observed in Cq values were appropriate for the dilutions (~3.3 difference Ct for a 10-fold dilution is usually considered appropriate). Data analysis to determine viral titers was performed using the instrument's software, adjusting the DNA quantity reported to account for dilutions and single-strandedness of the vector genomes.

In the process of characterising rAAV vector stocks, qPCR is a commonly used method to quantify encapsidated vector genome (D'Costa et al, 2016). However, qPCR is a very sensitive assay and as such, significant variabilities in the titre values have been reported in both inter- and intra-laboratory qPCR values (D'Costa et al, 2016). This raises an issue in dosage harmonisation and as such, the titre values for AAV9/mMD1 and AAV9/585mMD1 were confirmed by two additional qPCRs performed in a different laboratory by Dr Le Guiner's team in Nantes, France (Table 5.1). Two sets of qPCR reactions were run for each virus: one using primer sets targeting the SV40 polyA (similar to the qPCR performed by the author) and one using primer sets targeting the ITR (called ITR2 free qPCR as outlined in d'Costa et al, 2016). Briefly, for the ITR2 free qPCR, the plasmids used in preparation of standard curve were linearised just outside the ITR region on each end using PvuII restriction enzyme, facilitating the melting of the ITR sequences during the PCR reaction (d'Costa et al, 2016). Primers targeting the ITR2 sequence were then used in the qPCR reaction to determine viral titers.

Table 5.1 **Quantification of titre values of AAV9/mMD1 and AAV9/585mMD1**

Vector batch	vg/mL titer (SV40 qPCR) DICKSON LAB	vg/mL titer (SV40 qPCR) NANTES	vg/mL titer (ITR2 free qPCR) NANTES
AAV2/9_spc5.12_mMD1_ STANDARD	N/A	9.00E+12	9.00E+12
AAV9/mMD1	5.61E+13	3.20E+13	4.90E+13
AAV9/585mMD1	2.87E+13	2.50E+13	4.80E+13

Consistent titre values were observed for both the AAV9/mMD1 and AAV9/585mMD1 preparations enabling the dosage to be accurately characterised for subsequent *in vivo* work.

5.2.2 Intramuscular injection of AAV vector in *mdx* mice model to evaluate transgene expression level *in vivo* and functional outcomes.

The main aim of this study was to evaluate the microdystrophin transgene expression level and functional outcome following treatment of dystrophin-deficient *mdx* mice with rAAV vectors carrying mMD1 and 585 mMD1. We performed an *in vivo* study where AAV9 vector containing mMD1 and 585mMD1 were injected intramuscularly into the tibialis anterior (TA) muscles in young male *mdx* mice (~10 weeks old). As discussed in Chapter 4, despite being dystrophin-negative, in young *mdx* mice, the phenotype observed is relatively mild. The severity of the disease indicated by loss of muscle weight, fat accumulation, fibrosis and severe muscle weakness is not observed until the *mdx* mice is almost 2 years old (Yucel et al, 2018). At around 3-4 weeks of age, necrosis and regeneration in the tibialis anterior (TA) muscles peak, after which they plateau (Dangain and Vrbova, 1984). The muscle histopathology in the young *mdx* mice is relatively mild, such as no extensive fibrosis. At 10 weeks, the cycles of necrosis and regeneration in the tibialis anterior (TA) muscles would have plateaued. Briefly, the mice were anesthetized with 2%–4% isoflurane vaporised in 100% O_2 and then reduced to 1.5%-3% as required. To prepare the mice for intramuscular (IM) injection, the skin covering tibialis anterior (TA) muscle was shaved. Two doses: high (5×10^{11} vp/muscle) and low (5×10^{10} vp/muscle) were tested, and the dosages were determined based on previously published work by (Koo et al, 2011). The treatments are described on next page.

The treatments in this study were rAAV2/9 diluted in saline solution (sterile 0.9% sodium chloride solution) to required concentration as described below in a total volume of 50 µl per TA injection.

- Treatment **saline control** consists of 50 µl of sterile saline solution delivered intramuscularly to the TA muscle.

- Treatment **AAV9/mMD1 low dose** consists of AAV2/9 expressing a mouse codon optimised microdystrophin cDNA (sequence in Section 3.6.2) controlled by a muscle-specific promoter Spc5.12 and SV40 polyA signal delivered intramuscularly at a dose of 5 x 10^{10} vp/ TA muscle.

- Treatment **AAV9/585mMD1 low dose** consists of AAV2/9 expressing a mouse codon optimised microdystrophin cDNA (sequence in Section 3.6.2) controlled by a muscle-specific promoter Spc5.12, SV40 polyA signal and an engineered intron 585 R6K-RNA-OUT (sequence in Section 3.6.7) positioned in between the promoter and the transgene cDNA, delivered intramuscularly at a dose of 5 x 10^{10} vp/ TA muscle.

- Treatment **AAV9/mMD1 high dose** consists of AAV2/9 expressing a mouse codon optimised microdystrophin cDNA (sequence in Section 3.6.2) controlled by a muscle-specific promoter Spc5.12 and SV40 polyA signal delivered intramuscularly at a dose of 5 x 10^{11} vp/ TA muscle.

- Treatment **AAV9/585mMD1 high dose** consists of AAV2/9 expressing a mouse codon optimised microdystrophin cDNA (sequence in Section 3.6.2) controlled by a muscle-specific promoter Spc5.12, SV40 polyA signal and an engineered intron 585 R6K-RNA-OUT (sequence in Section 3.6.7) positioned in between the promoter and the transgene cDNA, delivered intramuscularly at a dose of 5 x 10^{11} vp/ TA muscle.

All outcome analyses were performed 12 weeks following treatment. The number of TA muscles treated was ten in all five treatment groups. Twelve weeks following treatment, muscle tissues were harvested and processed for Western blot and immunohistochemistry (IHC). Tissue collection for total protein sample extraction is described in Figure 4.4. TA muscles samples were harvested tendon-to-tendon and snap-frozen in isopentane cooled in liquid nitrogen and stored at −80 °C. Cryo-sections were then collected either for IHC, or for protein extraction and processing for SDS-PAGE immunoblotting. Electrophysiology experiments were also performed to analyse functional effects on the muscles prior to the tissue harvest.

Western blot analysis was performed as a readout for level of microdystrophin expression in treated TA muscle samples. Extracted total protein was quantified using the DC™ (detergent compatible) protein colorimetric assay measured at 750 nm and samples then processed for SDS-PAGE. 10 µg of total protein extracts from TA cryosections were loaded on NuPAGE Novex 3–8% Tris Acetate gels. Electrophoresis gels were run for 1 hour 15 minutes at 150V. The subsequent transfer of resolved protein bands over to nitrocellulose membrane was carried out at 30V for 2 hours. The nitrocellulose membrane was then blocked in 5% skim milk in PBS, 0.1% Tween-20 for 1 hour at room temperature. Following blocking, the membrane was cut using the protein ladder as guide to separate the antibody incubations to detect microdystrophin and the protein sample loading control, alpha-tubulin. For microdystrophin detection, the membrane was incubated with MANEX 1011C (1:100 dilution), an anti-dystrophin mouse monoclonal antibody specific for exons 10 and 11 of the dystrophin protein (Glenn Morris; Le Guiner et al., 2017) and with a secondary goat anti-mouse IgG antibody (1: 10000 dilution). For protein sample loading control, the lower molecular weight portion of the membrane was incubated with anti-alpha tubulin antibody raised in rabbit (1:2500 dilution) and with a secondary donkey anti-rabbit Ig antibody (1: 10000 dilution). Complete details of the workflow including suppliers and manufacturers of the materials can be found in Chapter 2: Materials and Methods. Immunoblots were visualized by

Odyssey CLx Imaging System (LI-COR) using fluorescence detection. Direct detection was possible as the secondary antibodies used were labelled with near-infrared fluorescent dyes. The secondary antibody used for detection of microdystrophin fluoresces at 800 nm channel (green signals on immunoblots) and for the protein loading control, the secondary antibody used for detection fluoresces at 700 nm channel (red signals on immunoblots).

Western blot analysis showed that the TA samples treated with higher doses of AAV9/mMD1 and AAV9/585mMD1 both showed elevated levels of microdystrophin production compared to the respective lower doses (approximately 5-fold higher). The lower doses were capable of producing detectable levels of microdystrophin as well. However, the relative abundance of microdystrophin in TAs treated with lower doses of both AAV9/mMD1 and AAV9/585mMD1 could not be shown to be significantly different to background reading in the saline treated controls. The relative abundance of microdystrophin in TAs treated with both doses (lower and higher) of AAV9/585mMD1 were also not significantly different to the respective doses of AAV9/mMD1 treatment.

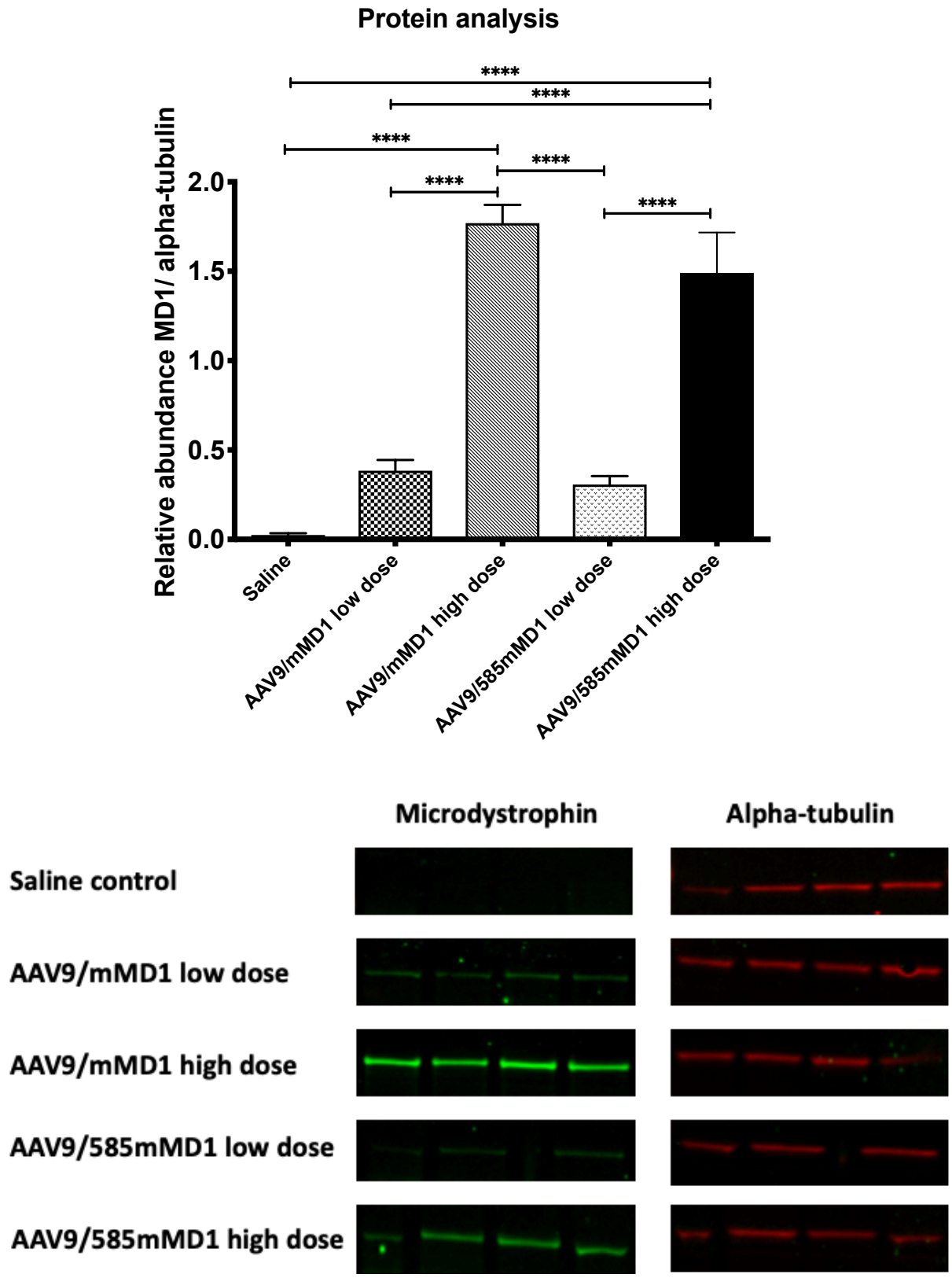

Figure 5.3 **Western blot analysis of expression of microdystrophin in *mdx* TA muscle following IM injection with either saline, AAV9/mMD1 or AAV9/585mMD1 at two doses.** *[Continued on next page]*

[From previous page]

The TA muscles of *mdx* mice were subjected to intramuscular injection of either saline, AAV9/mMD1 or AAV9/585mMD1 at a dosage of either 5 x 10^{11} vp/muscle (high dose) or 5 x 10^{10} vp/muscle (low dose). At 12 weeks post treatment, tissues were harvested, cryosections extracted for total protein and SDS-PAGE Western blot assay performed. The immunoblot membrane was hybridized with MANEX 1011C, a mouse anti-dystrophin antibody specific for exons 10 and 11 of the dystrophin protein and with a secondary goat anti-mouse antibody labelled with near-infrared fluorescent dyes that fluoresces at 800 nm channel (green signals on immunoblots) visualized by near infra-red imaging on an Odyssey CLx Imaging System (LI-COR). For protein sample loading control, the same membrane was hybridized with rabbit anti-alpha tubulin antibody and secondary donkey anti-rabbit antibody labelled with labelled with near-infrared fluorescent dyes that fluoresces at 700 nm channel (red signals on immunoblots) visualized by near infra-red imaging on an Odyssey CLx Imaging System (LI-COR). The fluorescence intensity of the bands (both microdystrophin and alpha-tubulin) were quantified using Image Studios software (LI-COR) and the background (noise values) were subtracted to obtain the intensity values. The ratio of MD1 fluorescence intensity value: α-tubulin fluorescence intensity value is a readout of relative abundance of MD1 protein following the treatment. All data represent mean ± SEM. (N, number of representative TA muscle sample shown=4). Statistical analysis was by one-way ANOVA. ****$P \leq 0.0001$.

Native dystrophin is a structural protein of the sub-sarcolemmal cytoskeleton and for the expressed microdystrophins to serve a functional purpose, it is essential they localise correctly to the sarcolemma This correct localisation of microdystrophin protein to the sarcolemma is also an indication of correct protein production and protein folding. Sarcolemmal localisation of microdystrophin protein following AAV IM injection in *mdx* TA muscle was assessed by immunohistochemistry workflow (Figure 5.4).

For all histological analysis, 10-µm cryosections of muscles were collected on glass slides (Figure 4.4), air-dried and stored at −80 °C. Before staining, the sections were fixed in acetone at −20°C. To reduce background effects, the Mouse on Mouse (M.O.M) kit (Vector Labs) was used to stain muscle sections for immunohistochemistry. The presence of microdystrophin was examined by immunostaining with MANEX 1011C, an anti-dystrophin antibody specific for exons 10 and 11 of the dystrophin protein (Glenn Morris; Le Guiner et al., 2017). The signal was visualized using Alexafluor 568–conjugated anti-mouse IgG (Invitrogen). Laminin was immunostained using rat anti-laminin monoclonal antibody (Sigma Aldrich). For laminin signal visualisation, anti-rat biotinylated antibody followed by Alexafluor 568–conjugated streptavidin was used. Laminin staining facilitates the determination of individual muscle fibers. The nuclei were stained with 0.1 µg/ml DAPI and the slides were mounted using mounting medium (Vector Labs). All samples were handled in a blinded manner. Microscope images were acquired using Nikon Eclipse NiE confocal microscope, where complete TA section images were acquired for analysis. Complete details of the workflow including antibody dilutions, suppliers and manufacturers of the materials can be found in Chapter 2: Materials and Methods.

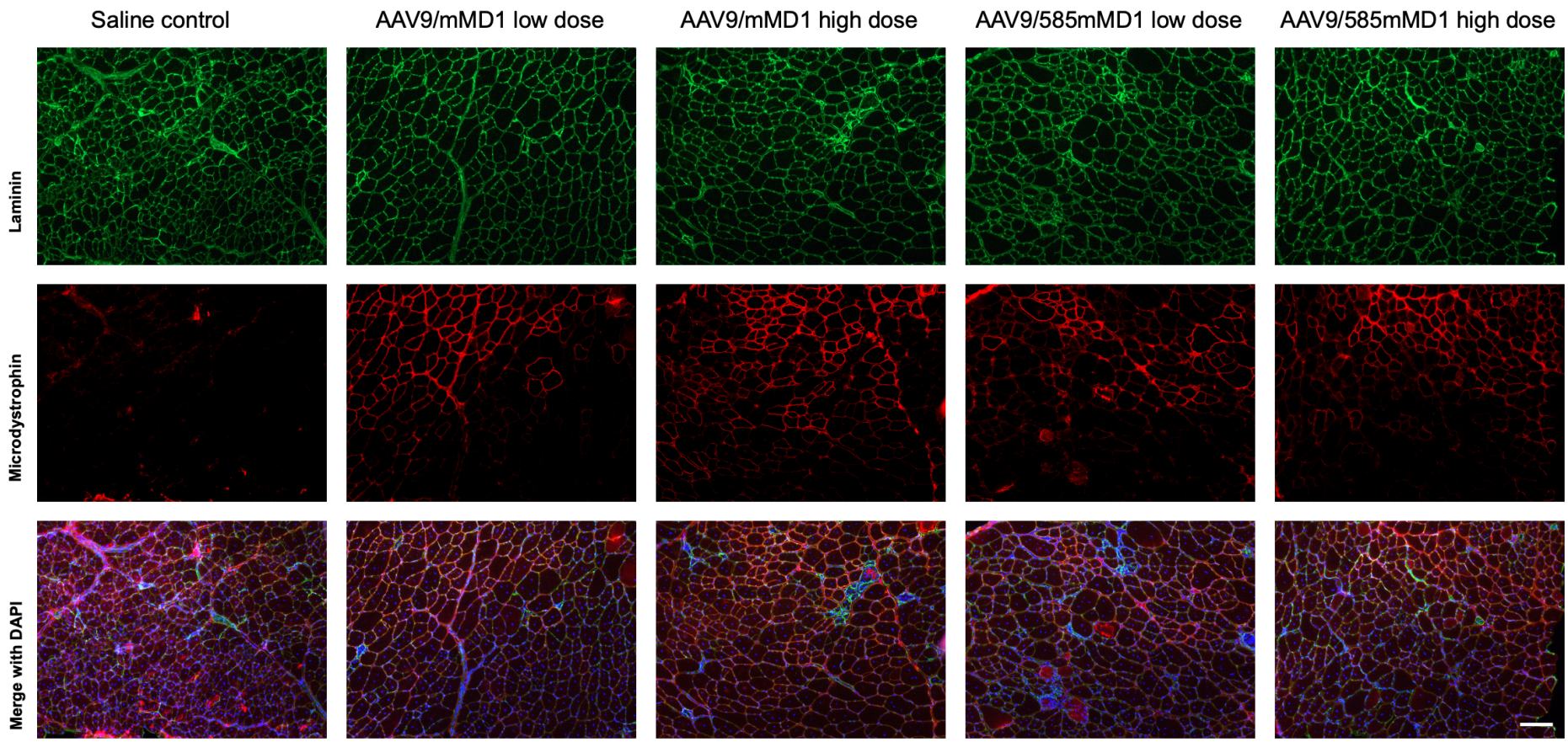

Figure 5.4 **Immunohistochemistry analysis of expression of microdystrophin in *mdx* TA muscle following IM injection with either saline, AAV9/mMD1 or AAV9/585mMD1 at two doses.** *[Continued on next page]*

[From previous page]

The TA muscles of *mdx* mice were subjected to intramuscular injection of either saline, AAV9/mMD1 or AAV9/585mMD1 at a dosage of either 5 x 10^{11} vp/muscle (high dose) or 5 x 10^{10} vp/muscle (low dose). At 12 weeks post treatment, 10 µm cryosections of the TA muscles were obtained. The sections were fixed in acetone at −20°C and to reduce background effects, the Mouse on Mouse (M.O.M) kit (Vector Labs) was used to stain muscle sections. The presence of microdystrophin was examined by immunostaining with MANEX 1011C, an anti-dystrophin antibody specific for exons 10 and 11 of the dystrophin protein (Glenn Morris; Le Guiner et al., 2017). The signal was visualized using Alexafluor 568–conjugated anti-mouse IgG (Invitrogen). Laminin was immunostained using rat anti-laminin monoclonal antibody (Sigma Aldrich). For laminin signal visualisation, anti-rat biotinylated antibody followed by Alexafluor 568–conjugated streptavidin was used. The nuclei were stained with DAPI. The slides were mounted using mounting medium (Vector Labs). All samples were handled in a blinded manner. Microscope images were acquired using Nikon Eclipse NiE confocal microscope, where complete TA section images were acquired for analysis. Top: Representative TA cross-section showing immunostained laminin facilitating the visualisation of all individual muscle fibers. Middle: Representative TA cross-section immunostained for dystrophin showing the distribution of the microdystrophin-positive fibers. Bottom: Representative TA cross-section immunostained for laminin and dystrophin merged together, with DAPI staining showing the distribution of nuclei. Red channel: microdystrophin, green channel: laminin, blue channel: DAPI labelling nuclei. Scale bar: 100 µm.

Microdystrophin-positive fibers were present in all the AAV treated samples: high and low doses of both AAV9/mMD1 and AAV9/585mMD1. Correct sarcolemma localisation of the microdystrophin protein was also seen. Next, calculation of percentage of microdystrophin positive fibres was attempted (Figure 5.5). This calculation was performed by counting the number of microdystrophin positive fibers versus total fibres, expressed as a percentage. Approximately 700–1,200 total fibers were counted per muscle (which corresponds to 2-3 fields of views of microscope images taken at x20 objective magnification).

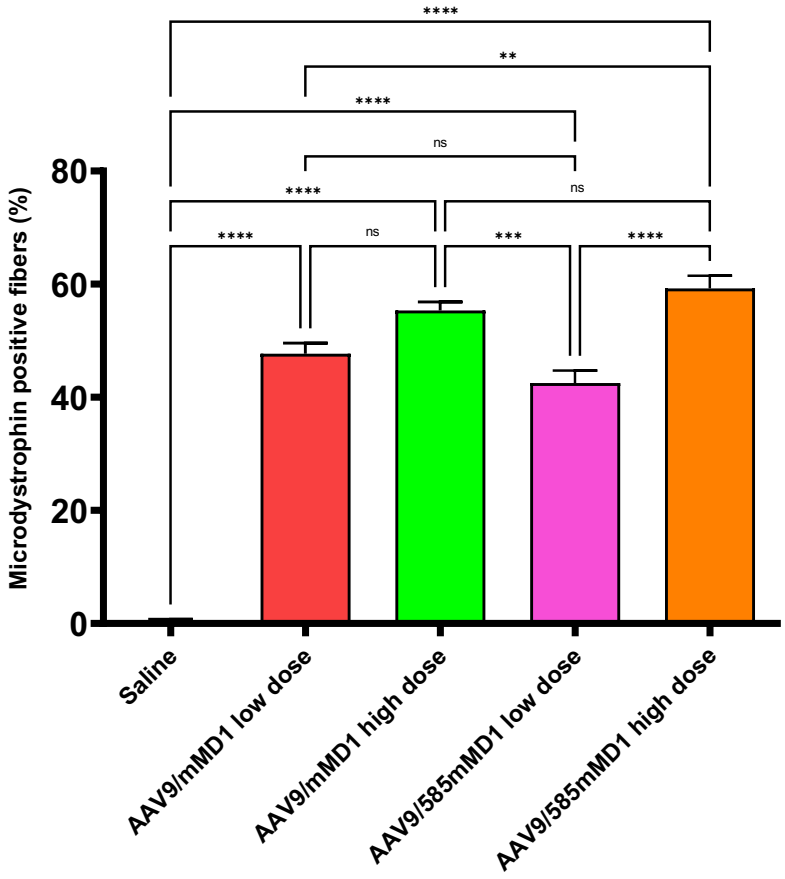

Figure 5.5 **Percentage microdystrophin positive fibers analysis in *mdx* TA muscle following IM injection with either saline, AAV9/mMD1 or AAV9/585mMD1 at two doses.**

[Continued on next page]

[From previous page]

The TA muscles of *mdx* mice were subjected to intramuscular injection of either saline, AAV9/mMD1 or AAV9/585mMD1 at a dosage of either 5 x 10^{11} vp/muscle (high dose) or 5 x 10^{10} vp/muscle (low dose). At 12 weeks post treatment, 10 µm cryosections of the TA muscles were obtained. The sections were fixed in acetone at −20°C and to reduce background effects, the Mouse on Mouse (M.O.M) kit (Vector Labs) was used to stain muscle sections. The presence of microdystrophin was examined by immunostaining with MANEX 1011C, an anti-dystrophin antibody specific for exons 10 and 11 of the dystrophin protein (Glenn Morris; Le Guiner et al., 2017). The signal was visualized using Alexafluor 568–conjugated anti-mouse IgG (Invitrogen). Laminin was immunostained using rat anti-laminin monoclonal antibody (Sigma Aldrich). For laminin signal visualisation, anti-rat biotinylated antibody followed by Alexafluor 568–conjugated streptavidin was used. The slides were mounted using mounting medium (Vector Labs). All samples were handled in a blinded manner. Microscope images were acquired using Nikon Eclipse NiE confocal microscope, where five random representative fields of views were acquired for analysis at total magnification of x200. Immunostained laminin facilitated the manual counting of total muscle fibers. TA cross-section immunostained for dystrophin were used to count microdystrophin-positive fibers manually. Percentage microdystrophin-positive fibers were calculated by expressing microdystrophin-positive fibers versus total fibers as a percentage. Approximately 700–1,200 total fibers were counted per muscle (which corresponds to 2-3 fields of views of microscope images taken at x20 objective magnification). All data represent mean ± SEM (N, number of TAs analysed per treatment group= 6-8). Statistical analyses by one-way ANOVA: **P ≤ 0.01, ***P ≤ 0.001, ****P ≤ 0.0001.

A dose-dependent increase in percentage microdystrophin positive fibers was a general trend observed for both the AAV9/mMD1 and AAV/585mMD1 treated TAs; although no statistical significance was observed for the difference in percentage microdystrophin positive fibers between AAV9/mMD1 low- and high-dose treated samples. Most importantly, no difference in percentage microdystrophin positive fibers was seen between the TAs treated with low dose AAV9/mMD1 and AAV/585mMD1; and between the TAs treated with high dose AAV9/mMD1 and AAV/585mMD1.

To evaluate whether the treatments provided any functional benefits, we performed physiological assessments of muscle function. Muscle electrophysiology evaluation was performed with Dr Alberto Malerba and Dr Ngoc Lu Nguyen at Royal Holloway, University of London. Briefly, mice were anesthetized by intraperitoneal injection of 60mg/kg pentobarbital. As described in (Koo et al, 2011), pins and clamps were used to fix the knee and foot, and the distal tendon of the muscle was attached to a lever arm of a servomotor system using a silk ligature. The sciatic nerve was proximally crushed and stimulated distally using a bipolar silver electrode using supramaximal square wave pulses of 0.1 msec duration. During isometric contractions following electrical stimulation (at different frequencies up to 180 Hz, train of stimulation of 500 msec), absolute maximal isometric tetanic force was measured. The sciatic nerve was stimulated for 700 msec at a frequency of 150 Hz for the muscle to attain maximum isometric force and the initial length of the TA muscle L_0 was recorded. In the first 500 msec, a maximal isometric contraction of the TA muscle was initiated, followed by muscle lengthening (1.1 mm, 10% L_0) at a velocity of 5.5 mm/sec (about 0.5 L_0/ sec) in the last 200 msec. Maximal isometric force was measured following each eccentric contraction and the force measured was expressed as a percentage of the initial maximal isometric force. Eleven isometric lengthening contractions of the TA muscles were performed, each contraction separated by a 60-sec rest period.

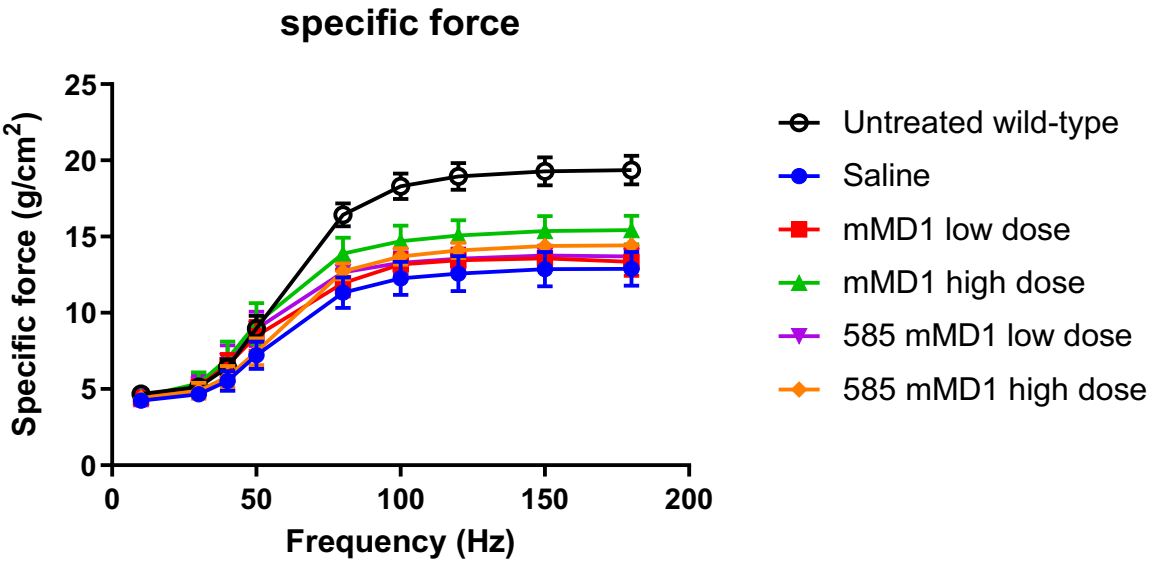

Figure 5.6 **Electrophysiological evaluation of specific force generation in untreated C57/BL10 wild-type and *mdx* TA muscles following IM injection with either saline, AAV9/mMD1 or AAV9/585mMD1 at two doses.** The TA muscles of mdx mice were subjected to intramuscular injection of either saline, AAV9/mMD1 or AAV9/585mMD1 at a dosage of either 5 x 10^{11} vp/muscle (high dose) or 5 x 10^{10} vp/muscle (low dose). At 12 weeks post treatment, muscle electrophysiology assays were performed. Briefly, mice were anesthetized intraperitoneally using 60mg/kg pentobarbital. As described in (Koo et al, 2011), pins and clamps were used to fix the knee and foot, and the distal tendon of the muscle was attached to a lever arm of a servomotor system using a silk ligature. The sciatic nerve was proximally crushed and stimulated distally using a bipolar silver electrode using supramaximal square wave pulses of 0.1 msec duration. During isometric contractions following electrical stimulation (at different frequencies up to 180 Hz, train of stimulation of 500 msec), absolute maximal isometric tetanic force was measured. Specific force is an indication of muscle strength. Specific force is calculated by dividing the isometric tetanic force generated, by the cross-sectional area of the TA muscle. Cross-sectional area was calculated by dividing the TA muscle's mass by the product of its initial length L_0 and the density of mammalian muscle (1.06 mg/mm^3) (Chan, Head and Morley, 2007). Specific force shows no significant difference between the saline and the AAV treated *mdx* mice groups (both doses). Natural history data for the age and sex-matched untreated wild-type C57/BL10 mice is included in the graphs (in black) for comparison.

Statistical significance (****P ≤ 0.0001) was observed between the untreated wild-type C57/BL10 mice and the treated *mdx* mice (all treatments) at frequency of 180 Hz. The AAV treatments did not seem to have an effect on specific force in this experiment. Statistical analyses by two-way ANOVA with Bonferroni post hoc test. All data represent mean ± SEM. n=10 for wild type, n=10 for saline, n=10 for both AAV treatments of both doses.

No significant change in specific force was seen in the AAV treated TA samples (both treatments at both doses). In the previous electrotransfer study (described in Chapter 4), the specific force of the untreated C57 wild-type mice matched the *mdx* mice as the *mdx* mice exhibit myofiber hypertrophy (Masspoust et al, 2020). In this study, however, as the *mdx* mice age, the muscle function become more compromised and such effect can be seen in the difference in specific force between the *mdx* mice and untreated C57/BL10 wild-type mice.

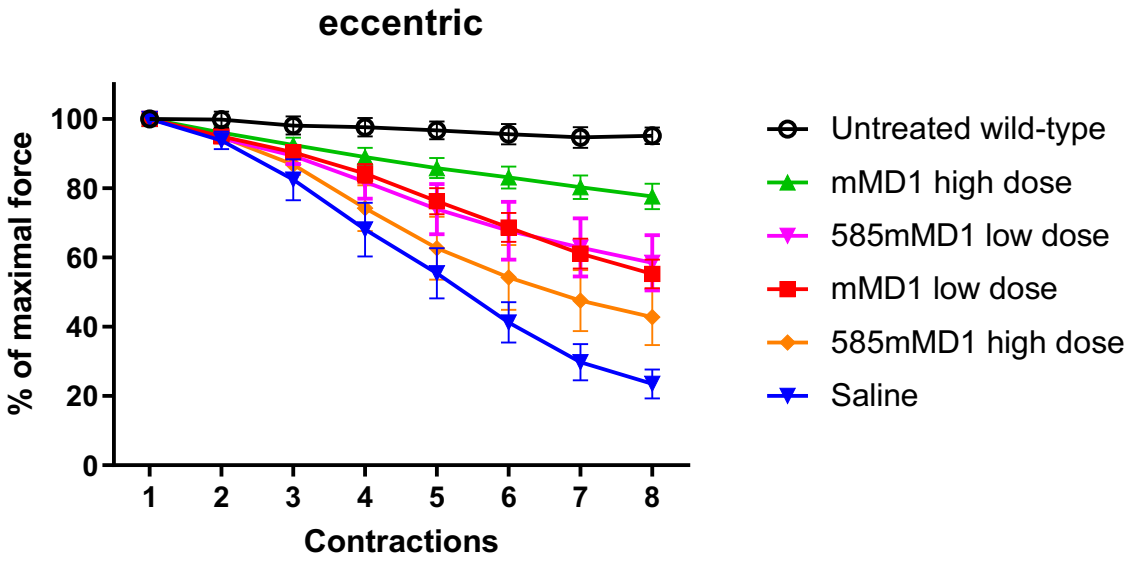

Statistical analyses by two-way ANOVA with Bonferroni post hoc test at eccentric contraction cycle 8

	Saline	AAV9/ mMD1 low dose	AAV9/ mMD1 high dose	AAV9/585 mMD1 low dose	AAV9/585 mMD1 high dose	Untreated C57 wild-type
Saline		**	****	*	n.s.	****
AAV9/mMD1 low dose			**	n.s.	n.s.	****
AAV9/mMD1 high dose				n.s.	*	*
AAV9/585mMD1 low dose					n.s.	*
AAV9/585mMD1 high dose						**
Untreated C57 wild-type						

Figure 5.7 **Electrophysiological evaluation of loss of force following repetitive eccentric contractions in untreated C57/BL10 wild-type and *mdx* TA muscles following IM injection with either saline, AAV9/mMD1 or AAV9/585mMD1 at two doses.**

[Continued next page]

[From previous page]

The TA muscles of mdx mice were subjected to intramuscular injection of either saline, AAV9/mMD1 or AAV9/585mMD1 at a dosage of either 5 x 10^{11} vp/muscle (high dose) or 5 x 10^{10} vp/muscle (low dose). At 12 weeks post treatment, muscle electrophysiology assays were performed. Following evaluation of specific force generation in the TA muscle as discussed in Figure 5.6, the sciatic nerve was stimulated for 700 msec at frequency of 150 Hz for the muscle to attain maximum isometric force and the initial length of the TA muscle L_0 was recorded. In the first 500 msec, a maximal isometric contraction of the TA muscle was initiated, followed by muscle lengthening (1.1 mm, 10% L_0) at a velocity of 5.5 mm/sec (about 0.5 L_0/ sec) in the last 200 msec. Maximal isometric force was measured following each eccentric contraction and the force measured was expressed as a percentage of the initial maximal isometric force. Eleven isometric lengthening contractions of the TA muscles were performed, each contraction separated by a 60-sec rest period. Eccentric contraction evaluation is an assessment of sarcolemma stability. The loss of force of *mdx* mice was significantly greater than the untreated C57/BL10 wild-type mice as the lack of dystrophin destabilises the membrane and increases membrane fragility (Moorwood et al, 2013). A greater loss of force following eccentric contractions was also observed in TAs treated with AAV9/585mMD1 high dose, almost matching saline control. Statistical analyses was performed by two-way ANOVA with Bonferroni post hoc test. All data represent mean ± SEM. n= 8-10 per treatment group. *P ≤ 0.05, **P ≤ 0.01, ***P ≤ 0.001, ****P ≤ 0.0001, n.s.: no significance.

A lower loss of force following eccentric contractions were observed in the AAV9/mMD1 (both doses) and AAV9/585mMD1 low dose treated samples compared to the saline treated TAs. A dose dependent effect was seen in the AAV9/mMD1 treated samples. As microdystrophin is produced, muscle membrane stability is achieved by restoration of the dystrophin-associated protein complex (DAPC). This in turn protects the muscle from contraction-induced damage. As seen in the Western blot analysis in Figure 5.3, the level of microdystrophin produced in the TAs of the low doses treatments of AAV9/mMD1 and AAV9/585mMD1 were similar. As such, similar losses of force following eccentric contractions were observed for the two treatments. AAV9/mMD1 high dose treated samples showed the best muscle protection against loss of force following eccentric contractions compared to all the other treatments. The level of microdystrophin produced in the TAs in the high doses of AAV9/mMD1 and AAV9/585mMD1 were also similar in the Western blot analysis shown in Figure 5.3. However, for AAV9/585mMD1 high dose treated samples, the progressive loss of force generating capacity of the TA almost matched saline samples (no significant difference between the groups).

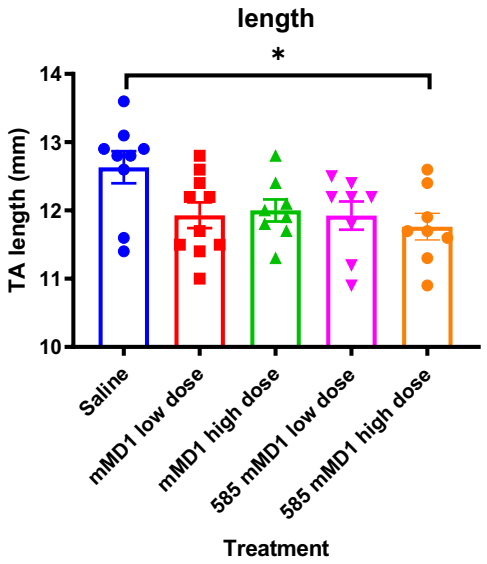
length
*
TA length (mm)
14
13
12
11
10
Saline
mMD1 low dose
mMD1 high dose
585 mMD1 low dose
585 mMD1 high dose
Treatment

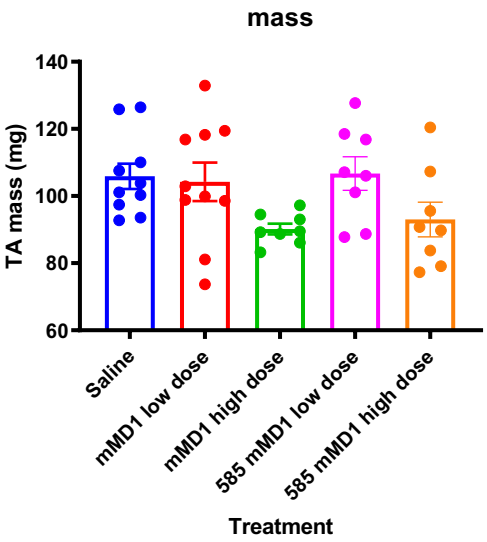
mass
TA mass (mg)
140
120
100
80
60
Saline
mMD1 low dose
mMD1 high dose
585 mMD1 low dose
585 mMD1 high dose
Treatment

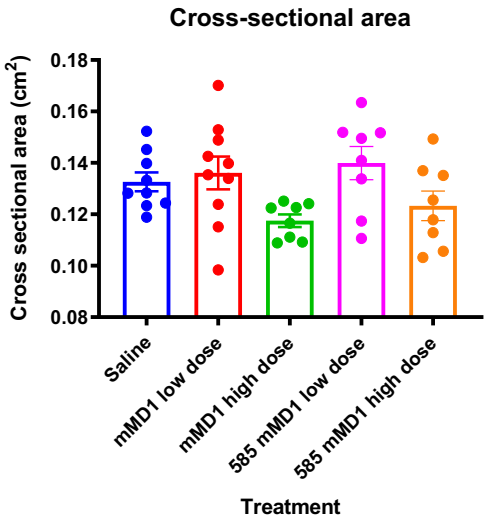
Cross-sectional area
Cross sectional area (cm2)
0.18
0.16
0.14
0.12
0.10
0.08
Saline
mMD1 low dose
mMD1 high dose
585 mMD1 low dose
585 mMD1 high dose
Treatment

Figure 5.8 **Evaluation of TA length, mass and cross sectional-area (CSA) of *mdx* TA muscles following IM injection with either saline, AAV9/mMD1 or AAV9/585mMD1 at two doses.** The TA muscles of mdx mice were subjected to intramuscular injection of either saline, AAV9/mMD1 or AAV9/585mMD1 at a dosage of either 5 x 10^{11} vp/muscle (high dose) or 5 x 10^{10} vp/muscle (low dose). At 12 weeks post treatment, the TA muscle length, mass and CSA were measured to evaluate changes to the muscle following treatment. Cross-sectional area was calculated by dividing the TA muscle's mass by the product of its initial length L_0 and the density of mammalian muscle (1.06 mg/mm^3) (Chan, Head and Morley, 2007). Statistical analyses by one-way ANOVA. All data represent mean ± SEM. n= 8-10 per treatment group. *$P \leq 0.05$.

Following the muscle function analyses, a few histopathology analyses were carried out. Centronucleation and clusters of small fibers are some of the hallmarks of regeneration in muscle (Guiraud and Davies, 2019). In healthy muscle cells, the nuclei are located at the periphery of the cells. For the analysis of centrally nucleated fibers, immunostaining of laminin and DAPI staining of the nuclei were used. Briefly, 10-µm cryosections of muscles were collected on glass slides (Figure 4.4), air-dried and stored at −80 °C. Before staining, the sections were fixed in acetone at −20°C. To reduce background effects, the Mouse on Mouse (M.O.M) kit (Vector Labs) was used to stain muscle sections for immunohistochemistry. Laminin was immunostained using rat anti-laminin monoclonal antibody (Sigma Aldrich). For laminin signal visualisation, anti-rat biotinylated antibody followed by Alexafluor 568–conjugated streptavidin was used. Laminin staining facilitates the determination of individual muscle fibers. The nuclei were stained with 0.1 µg/ml DAPI and the slides were mounted using mounting medium (Vector Labs). All samples were handled in a blinded manner. Microscope images were acquired using Nikon Eclipse NiE confocal microscope, where five random representative fields of views were acquired for analysis at total magnification of x200. Complete details of the workflow including antibody dilutions, suppliers and manufacturers of the materials can be found in Chapter 2: Materials and Methods.

The percentage of centrally nucleated fibers (CNF) was over 50% in all the treated samples (Figure 5.9). A wider range was however observed for AAV9/mMD1 treated samples (Figure 5.9). The distribution of the number of centrally-located nuclei (1 CN, 2 CN and 3+ CN) in the fibers was also pretty similar across all the treatments, indicating similar levels of regeneration activity.

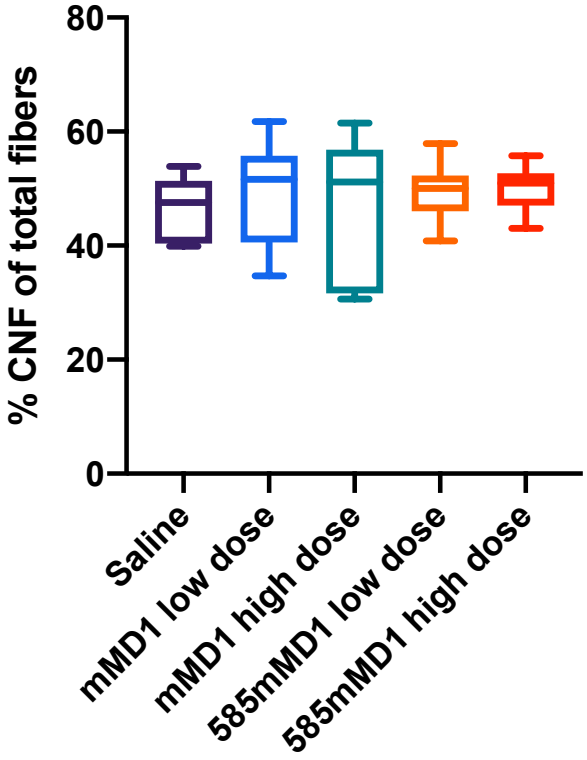
% CNF of total fibers
80
60
40
20
0
Saline
mMD1 low dose
mMD1 high dose
585mMD1 low dose
585mMD1 high dose

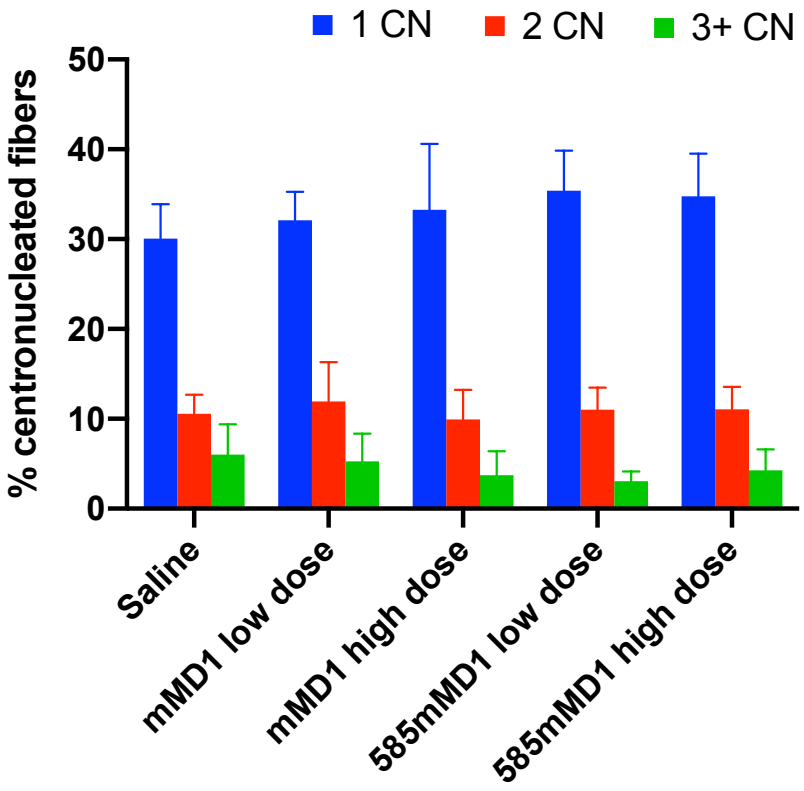
1 CN
2 CN
3+ CN
% centronucleated fibers
50
40
30
20
10
0
Saline
mMD1 low dose
mMD1 high dose
585mMD1 low dose
585mMD1 high dose

Figure 5.9 **Centronucleation (CN) analysis in *mdx* TA muscle following IM injection with either saline, AAV9/mMD1 or AAV9/585mMD1 at two doses.** (Top): Percentage of centrally nucleated fibers versus total number of fibers in the field of view. (Bottom): Distribution of number of centrally located nuclei within the total centrally nucleated fibers. The TA muscles of mdx mice were subjected to intramuscular injection of either saline, AAV9/mMD1 or AAV9/585mMD1 at a dosage of either 5 x 10^{11} vp/muscle (high dose) or 5 x 10^{10} vp/muscle (low dose). At 12 weeks post treatment, 10 µm cryosections of the TA muscles were obtained. The sections were fixed in acetone at −20°C and to reduce background effects, the Mouse on Mouse (M.O.M) kit (Vector Labs) was used to stain muscle sections. Laminin was immunostained using rat anti-laminin monoclonal antibody (Sigma Aldrich). For laminin signal visualisation, anti-rat biotinylated antibody followed by Alexafluor 568–conjugated streptavidin was used. The nuclei were stained with DAPI. The slides were mounted using mounting medium (Vector Labs). All samples were handled in a blinded manner. Microscope images were acquired using Nikon Eclipse NiE confocal microscope, where five random representative fields of views were acquired for analysis at total magnification of x200. Immunostained laminin facilitated the counting of total muscle fibers and defining the region of interest for counting of centrally located nuclei. DAPI staining shows the distribution of nuclei. MuscleJ software was used to automate the counting of centronuclei within the fibers. Percentage centronucleated fibers (CNFs) were calculated by expressing CNFs versus total fibers as a percentage. Approximately 700–1,200 total fibers were counted per muscle (which corresponds to 2-3 fields of views of microscope images taken at x20 objective magnification). All data represent mean ± SEM (N, number of TAs analysed per treatment group=4-6). Statistical analyses by one-way ANOVA.

Haematoxylin and eosin (H&E) staining was performed to study the histopathology of the treated muscle fibers. Signs for degenerating fibers, centro-nucleation, mononucleated inflammatory cells, fibrosis, small rounded fibers indicating cycles of regeneration-degeneration and replacement of muscle by adipose tissue were looked for (according to the TREAT-NMD SOP MDC1A_M.1.2.004) (Figure 5.10). Histological dyes exist as either acid dye [anion (negatively charged) in solution] or basic dye [cation (positively charged) in solution]. H&E is also a charge-based staining, where Hematoxylin is a basic dye that stains basophilic structures that contain nucleic acid such as the ribosomes, nucleus and the cytoplasmatic regions rich in RNA. These structures appear purple-blue. Eosin is an acid dye that stains basic materials in red-pink, such as the cytoplasm, intracellular and extracellular proteins. Structures that are not basophilic or eosinophilic do not stain and remain clear; these include the basal lamina and hydrophobic fat-rich structures (adipocytes, myelin) (TREAT-NMD SOP MDC1A_M.1.2.004).

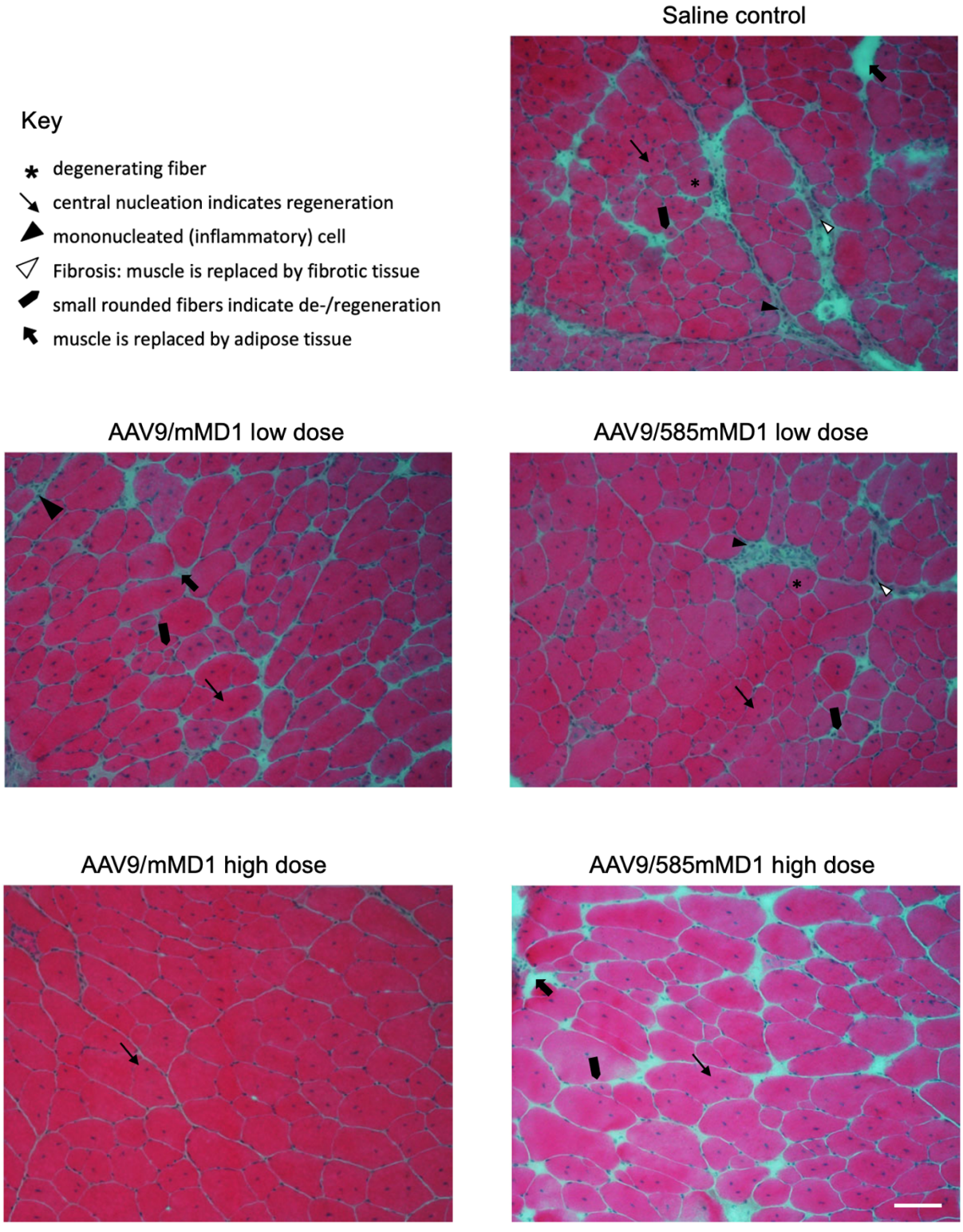

Figure 5.10 **Haematoxylin and eosin (H&E) histopathology evaluation of *mdx* TA muscle following IM injection with either saline, AAV9/mMD1 or AAV9/585mMD1 at two doses.**

[Continued next page]

[From previous page]

The TA muscles of mdx mice were subjected to intramuscular injection of either saline, AAV9/mMD1 or AAV9/585mMD1 at a dosage of either 5 x 10^{11} vp/muscle (high dose) or 5 x 10^{10} vp/muscle (low dose). At 12 weeks post treatment, 10 µm cryosections of the TA muscles were obtained. H&E staining was performed according to the protocol outlined in TREAT-NMD SOP MDC1A_M.1.2.004. All samples were handled in a blinded manner. Microscope images were acquired using Nikon Eclipse NiE confocal microscope, where five random representative fields of views were acquired for analysis at total magnification of x200. N, number of TAs analysed per treatment group=4-6. Scale bar: 100 µm.

Clusters of small fibres were seen in all the treated samples except AAV9/mMD1 high dose treated samples. Centronucleated myofibres were also seen in all the treated samples including AAV9/mMD1 high dose, but it is worth noting that a large proportion of nuclei have moved to the periphery in the AAV9/mMD1 high dose treated samples. The other AAV treated samples also showed movement of nuclei to the periphery. The morphology and structure of the skeletal muscles were well restored in AAV9/mMD1 high dose treatment.

Other hallmarks of dystrophic skeletal muscles such as excessive fibre size variation and large rounded hypertrophic fibres were also seen in all the treated samples except AAV9/mMD1 high dose treated samples. Fibre splitting was more common in AAV9/585mMD1 high dose treated samples. Fibre splitting is a nonpathological component that usually accompany muscle hypertrophy (Murach et al, 2019). The significance of this is not quite well understood but fibre splitting happens following muscle hypertrophy (which is seen on the H&E staining) but may not be pathological (Murach et al, 2019).

5.2.3 AAV9/585mMD1 were less infectious than AAV9/mMD1

The level of microdystrophin expression in TAs treated with 585mMD1 construct carried by AAV9 at both low and high doses remained similar to the level of microdystrophin expression observed in respective doses of AAV9/mMD1 treated samples. To understand this phenomenon better, we decided to study the properties of the viral vector focusing on infectivity of the viral particles.

The packaging capacity of wild-type AAV is approximately 4.7 kb and there have been debates on the maximum threshold of the genetic cargo rAAVs could carry. It has been reported that rAAVs could accommodate genetic cargo up to 5kb (Wu et al., 2010). Even if rAAV is able to package genome beyond this capacity, proteasomes would preferentially degrade the larger genome-containing virions, unless another intervention of proteasome inhibitors is put in place (Grieger and Samulski, 2005). The idea of packaging capacity of AAV also seems to differ from serotype to serotype with a very recent study reporting the ability of AAV8 to package genomes up to 6kb, although the infectivity or stability of the viral particles were not tested (Krooss et al., 2020).

The ITR - ITR length of 585mMD1 gene expression cassette is ~5.2kb, which is above the packaging capacity of wild-type AAV (wt-AAV) by ~500bp. To study the infectivity of the viral vectors carrying microdystrophin therapeutic constructs, infectious centre assay (ICA) was performed by Dr Caroline Le Guiner's team in Nantes, France (Table 5.2). The ICA is widely utilised in quantifying infectious AAV vectors (François et al, 2018). Trans-complementing cells with stably integrated AAV2 *rep* and *cap* genes are infected with adenovirus, therefore allowing incoming rAAV genome to replicate in the nucleus (corresponding to infectious vector particles) (François et al, 2018).

Briefly, HeRC32 cells were seeded in 48-well plates (7.0E+4 cells/well). The cells were infected the next day with 10-fold dilutions of the rAAV vector preparations in duplicates, in the presence of wild-type Adenovirus type-5 (Ad5) at a multiplicity of 500 infectious units per cell. Cells were harvested 26 hours post-infection and filtered through Zeta-Probe nylon membranes (Bio-Rad) using a vacuum device. Membrane filters were hybridized overnight at 65°C with vector-specific probes generated with the PCR Fluorescein Labelling Mix (Roche). Detection was performed using the CDP-Star ready-to-use labelling kit (Roche). Titers were determined by counting dots (that correspond to AAV infected cells) on membranes autoradiography, which was done blind by two independent scientists. This protocol was initially described in (Salvetti et al, 1998). The infectious particles (ip)/mL titer is reported in Table 5.2.

Table 5.2 **Infectious centre assay (ICA) of AAV9/mMD1 and AAV9/585mMD1**

Vector batch	ip/mL titer (ICA)	Ratio vg/ip (with SV40 titer)	Ratio vg/ip (with ITR2 free titer)
AAV2/9_spc5.12_mMD1 NANTES (ID 6828)	3.86E+08	2.33E+04	2.33E+04
AAV2/9_MD1_DICKSON	1.14E+09	2.81E+04	4.30E+04
AAV2/9_585_MD1_DICKSON	8.59E+07	2.91E+05	5.59E+05

The viral titers were obtained by qPCR as described in Section 5.2.1 using two primer sets (SV40 and ITR2 free) that target different regions of the viral genome. The range of infectivity is determined for a given serotype by measuring the viral titer (vg/mL) and the infectious titer (ip/mL) in parallel. In this experiment, the vg/ip ratio was determined using both the titers obtained via SV40 and ITR2 free qPCR for each virus. For AAV serotype 9, the standard reference of vector genome: infectious particle (vg/ip) is between 1 and 5E+04 and this ratio varies between serotypes as it is linked to the efficiencies of the

vectors to infect cells *in vitro* (personal communication with Dr Caroline Le Guiner). This means the infectious titer that can be detected *in vitro* using ICA is usually 1E4 to 5E4 lower than the vg/mL viral titer determined by qPCR. AAV2/9-spc5.12-mMD1 (ID 6828) is an internal control used in University of Nantes to validate the ICA for AAV9. The vg/ip ratio of 2.33E+04 reported for this control means 1 infectious particle was detected amongst 2.33E+04 physical vector genomes. As this ratio is within the 1E+04 and 5E+04 threshold (for AAV9), this vector exhibited a good infectious property. The vg/ip ratio of AAV9/mMD1 generated in the Dickson lab also fall within this range.

For the AAV9/585mMD1 vector on the other hand, the vg/ip ratio was 2.91E+05 (when the ICA was compared to the viral titer obtained via SV40 qPCR) and 5.59E+05 (when the ICA was compared to the viral titer obtained via ITR2 free qPCR). This means 1 infectious particle was detected amongst E+05 physical vector genomes. The AAV9/585mMD1 was '10 fold less infectious' than AAV9/mMD1 vector. This may be due to the larger size genome carried by AAV9/585mMD1 which is beyond the 5kb packaging capacity of AAV, especially for viral genomes packaged in AAV9 (unpublished data from Dr Caroline Le Guiner). Larger sized genomes that cannot 'fit' into the AAV capsid can potentially be truncated and this affects the infectivity of the virus (discussed in Section 5.3).

5.2.4 Generation of minimised versions of mMD1 and 585mMD1 constructs that are within the AAV packaging capacity

The ICA showed that packaging genome exceeding the packaging capacity of wt-AAV of ~4.7kb is detrimental to the infectivity of the virus particles, specifically for AAV serotype 9. It was essential for us to minimize the gene expression cassettes to be within the packaging capacity of wt-AAV (~4.7kb), especially for 585mMD1 which was ~5.2kb long. To enable side-by-side comparison, mMD1 expression cassette, which was ~4.6kb was also minimised exactly as 585mMD1 (Figure 5.11). The work to minimise the AAV expression cassettes was initiated both at Royal Holloway and University of Nantes. The attempt of minimising the mMD1 construct was successfully done by our collaborators in University of Nantes, France: Dr Audrey Bourdon and Dr Caroline Le Guiner. The minimisation of mMD1 was performed by a series of fragment synthesis and cloning workflows to remove linker sequences found in between the components of the gene expression cassette (Figure 5.11). In addition, the 125 bp SV40 polyA signal was also replaced by a shorter, highly efficient synthetic polyA signal called pCl NeO-pA which is 49 bp in length (Levitt et al, 1989; Himeda, Chen & Hauschka, 2011; Hakim et al, 2017). These strategies brought the mMD1 cassette length down to 4.2 kb which is called mini MD1.

The next step of generating minimized 585mMD1 was done here in our lab at Royal Holloway, and this involved a fragment synthesis which included 585 bp R6K-RNA-OUT to be cloned into mini MD1. The fragment synthesis was essential as many single cutter restriction enzyme sites were lost in the minimisation process. The cloning of 585 bp R6K-RNA-OUT intron into mini MD1 plasmid was done by GenScript, following synthesis of the fragment covering regions of the promoter, transgene and the entire R6K-RNA-OUT in the middle. These strategies brought the 585mMD1 cassette length down to 4.8 kb which is called mini 585MD1. Full details of the fragment synthesis and cloning strategies can be found in Chapter 2: Materials and Methods.

Two new plasmids were generated following the minimisation:

p-rAAV-Spc5.12-mMD1-pClNeOpA
(also called p-mini MD1 **OR** mini MD1 plasmid)

p-rAAV-Spc5.12-585R6KRNAOUT-mMD1- pClNeOpA
(also called p-mini 585MD1 **OR** mini 585MD1 plasmid)

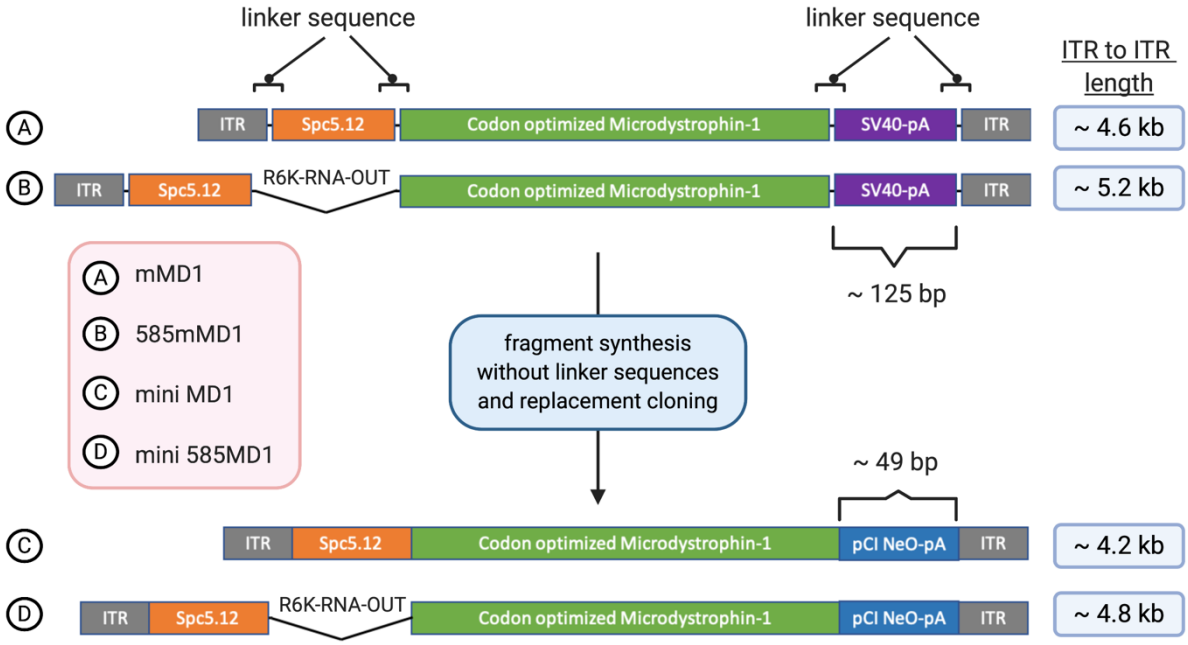

Figure 5.11 **Minimisation strategy of p-mMD1 and p-585mMD1 to produce p-mini MD1 and p-mini 585MD1 respectively.** A-D: Transcription units of p-mMD1, p-585mMD1, p-mini MD1 and p-mini 585MD1 respectively. The ITR to ITR lengths of p-mMD1 and p-585mMD1 are ~4.6kb and 5.2kb respectively. The original plasmid sequences contain 'linker sequences' that originated from previous cloning reactions to assemble the gene expression cassette. To remove the linker sequences, DNA fragments covering the gene expression casettes were synthesised, eliminating the linker sequences in the synthesis. The synthesised fragments were then used to replace the existing sequence using restriction site cloning, where a segment of the gene expression cassette with the linker sequence is removed by restriction digest; after which the fragment without linker sequence is inserted into the vector to replace the removed

sequence. Full details of the workflow can be found in Chapter 2: Materials and Methods. In addition, the 125 bp SV40 polyA was also replaced with a shorter synthetic 49bp polyA (Levitt et al, 1989; Himeda, Chen & Hauschka, 2011; Hakim et al, 2017) bringing the final ITR to ITR length of mini MD1 to 4.2kb (C). Next, cloning of R6K-RNA-OUT intron into (C) generated mini 585MD1 (D) which is within the packaging capacity of AAV9.

As described in Chapter 3, the ITR regions in AAV plasmids are prone to deletions due to the complex structure the DNA sequence acquires at the ITR regions and as such, an optimized protocol was used in plasmid propagation of p-mini MD1 and p-mini 585 MD1. To try to reduce such events, a recombination deficient bacterial strain: TOP10 cells (Wilmott et al, 2019) were used in this study. An optimized protocol was used in plasmid propagation where the AAV plasmids were produced in bacterial host cells growing at 32ºC instead of 37ºC; with a culture time between 14 and 16 hours (Wilmott et al, 2019). Nevertheless, after every cycle of bacterial growth and plasmid preparation, a quality control step was necessary. Direct sequencing would be ideal, but routine Sanger sequencing is inadequate due to the high GC content and the secondary structure of the ITRs restricting the movement of DNA polymerase along the sequence. Alternatively, detailed restriction enzyme site evaluations targeting specific regions around the ITRs are often used routinely to confirm the integrity of these regions in the plasmids (Figure 5.12). Restriction digest profiles of the newly generated p-mini MD1 and p-mini 585MD1 plasmids revealed that the AAV gene expression cassettes within the plasmids appeared to be intact without any deletions detectable by these methods.

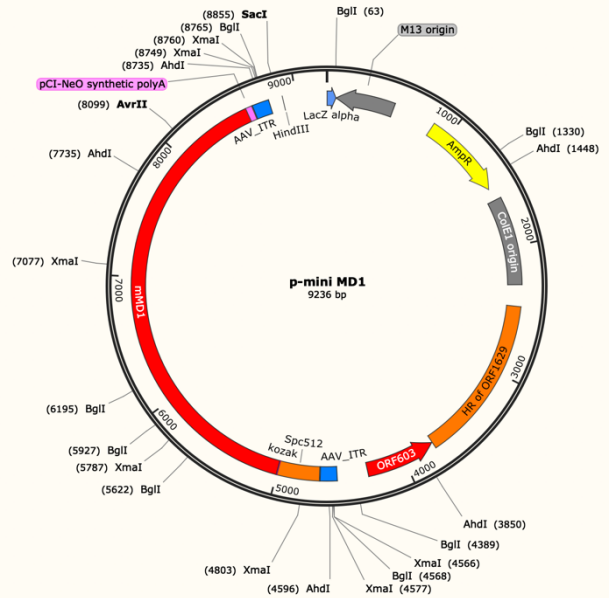

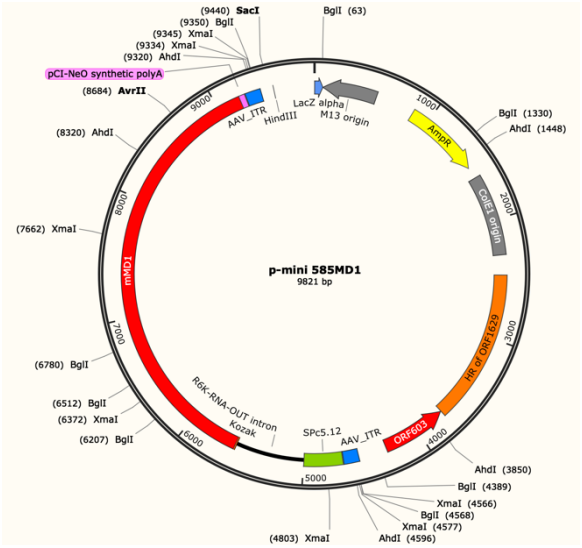

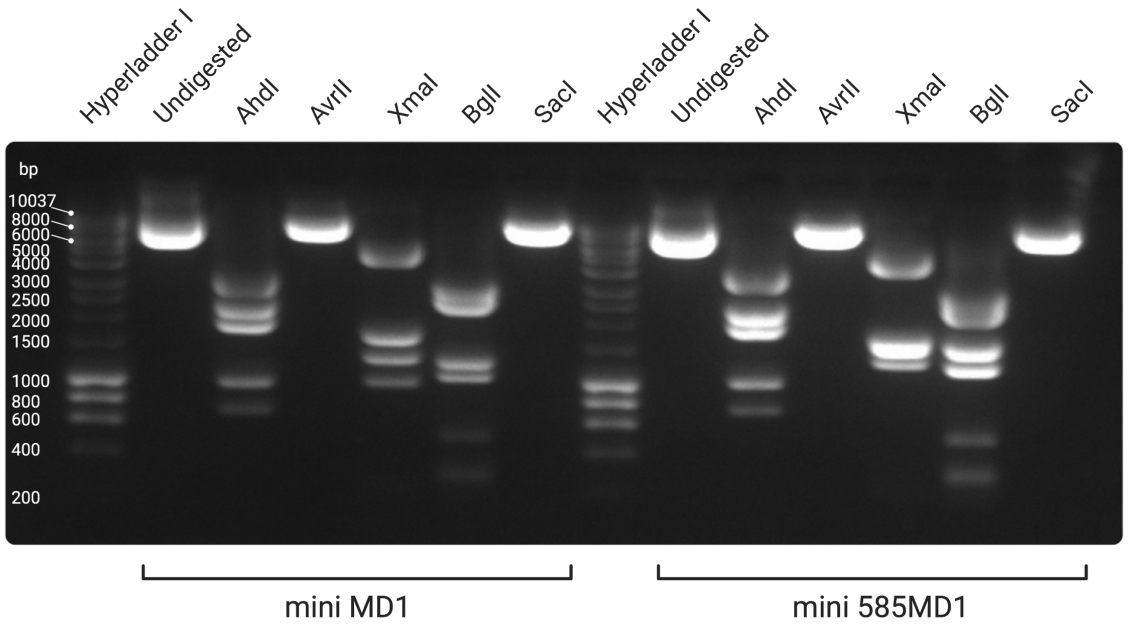

Restriction enzymes	Expected fragments (bp)
AhdI	746, 1000, 1949, 2402, 3139
AvrII	9236
XmaI	226, 984, 1290, 1672, 5042
BglI	179, 268, 305, 534, 1054, 1267, 2570, 3059
SacI	9236

Restriction enzymes	Expected fragments (bp)
AhdI	746, 1000, 1949, 2402, 3724
AvrII	9821
XmaI	226, 1290, 1569, 1672, 5042
BglI	179, 268, 305, 534, 1267, 1639, 2570, 3059
SacI	9821

plasmids.

[From previous page]

Plasmid maps with restriction sites mapped in are shown on the top (image generated using SnapGene). Numbers in round brackets next to restriction enzymes indicate positions of the cutting sites of the respective enzymes. Agarose gel images (middle) show the presence of all the expected bands confirming the integrity of the constructs. The expected fragment sizes in base pairs (bps) are shown on the respective tables (bottom). All restriction enzyme digests were performed using the recommended buffers supplied by New England Biolabs with the restriction enzymes, at respective optimal temperatures provided by the manufacturer. Larger images of the plasmid maps can be found in Section 5.4 Appendix.

5.2.5 Enhancement of microdystrophin expression *in vitro* following addition of engineered intron into mini MD1 cassette.

To evaluate the protein expression of the microdystrophin expressing AAV constructs, transient transfection experiments using mini MD1 and mini 585MD1 plasmids were carried out in HEK293T. The HEK293T cells were transfected with the optimised plasmid dose of 2 μg for 9.4 cm^2 growth area (well size of a 6-well plate) (data from Chapter 3) and harvested after 72 hours for total protein extraction, quantification and Western blotting immunological analyses. Extracted total protein was quantified using DC™ (detergent compatible) protein colorimetric assay measured at 750 nm and processed for SDS-PAGE. 50 μg of total protein extracts from HEK293T were loaded on NuPAGE Novex 3–8% Tris Acetate gels. Electrophoresis gels were run for 1 hour 15 minutes at 150V. The subsequent transfer of resolved protein bands over to nitrocellulose membrane was carried out at 30V for 2 hours. The nitrocellulose membrane was then blocked in 5% skim milk in PBS, 0.1% Tween-20 for 1 hour at room temperature. Following blocking, the membrane was cut using the protein ladder as guide to separate the antibody incubations to detect microdystrophin and the protein sample loading control, alpha-tubulin. The membrane was hybridized with MANEX 1011C (1:100 dilution), an anti-dystrophin antibody specific for exons 10 and 11 of the dystrophin protein (Glenn Morris; Le Guiner et al., 2017) and with a secondary goat anti-mouse antibody (1: 10000 dilution). For protein sample loading control, the membrane was hybridized with anti-alpha tubulin antibody raised in rabbit (1:2500 dilution) and with a secondary donkey anti-rabbit antibody (1: 10000 dilution). Complete details of the workflow including suppliers and manufacturers of the materials can be found in Chapter 2: Materials and Methods. Immunoblots were visualized by Odyssey CLx Imaging System (LI-COR) using fluorescence detection. Direct detection was possible as the secondary antibodies used were labelled with near-infrared fluorescent dyes. The secondary antibody used for detection of microdystrophin fluoresces at 800 nm channel (green signals on immunoblots) and for the protein loading control, the secondary antibody used for detection fluoresces at 700 nm channel (red signals on immunoblots).

A five-fold increase in transgene expression (Figure 5.13) was seen with the addition of 585 R6K-RNA-OUT intron in mini MD1.

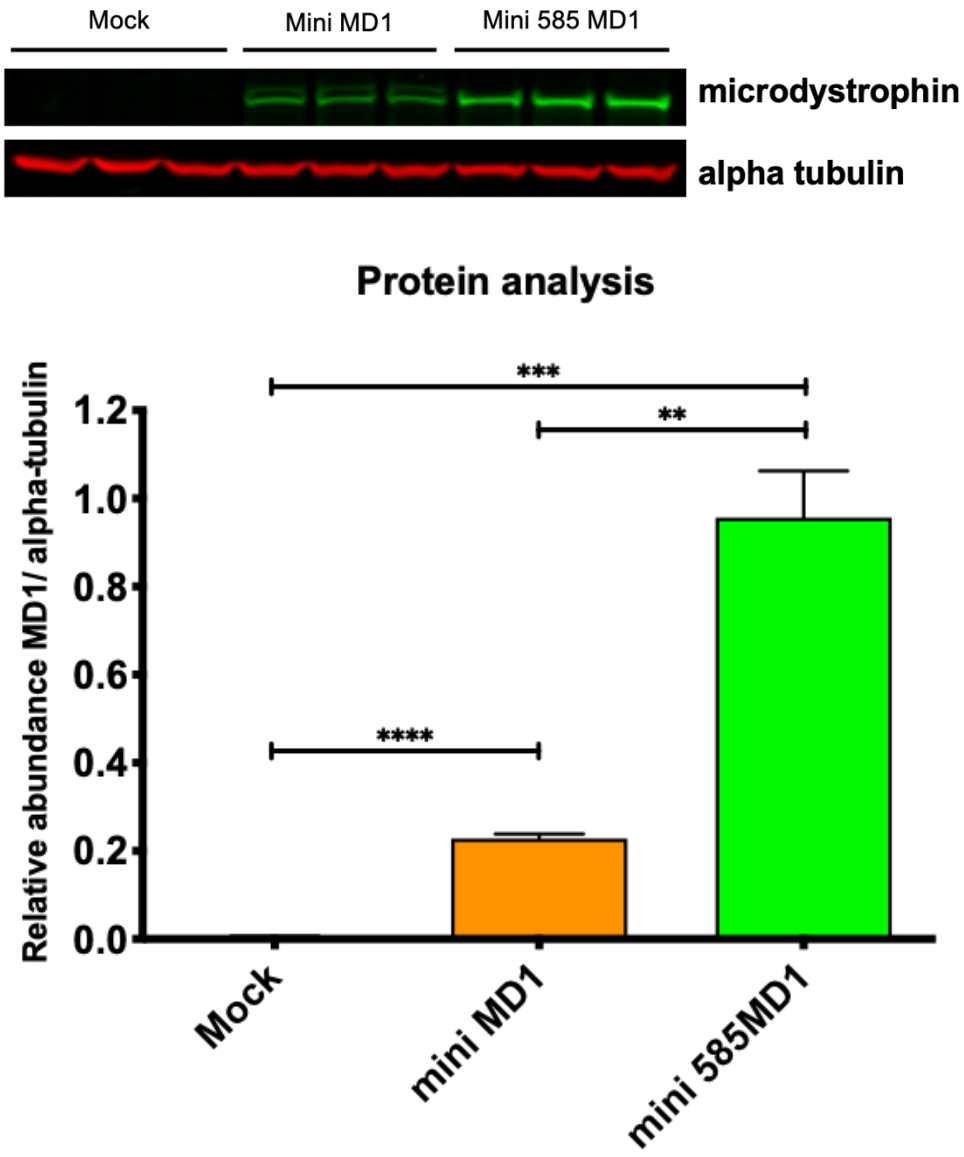

with mini MD1 and mini 585MD1 plasmids.

[From previous page]

HEK293T cells were transfected with either p-mini MD1 or p-mini 585MD1 at a plasmid dose of 2 μg for 9.4 cm^2 growth area (well size of a 6-well plate). 72-hours post transfection, total protein were extracted from the cultures and an SDS-PAGE Western blot assay was performed. The immunoblot membrane was hybridized with MANEX 1011C, a mouse anti-dystrophin antibody specific for exons 10 and 11 of the dystrophin protein and with a secondary goat anti-mouse antibody labelled with near-infrared fluorescent dyes that fluoresces at 800 nm channel (green signals on immunoblots) visualized by near infra-red imaging on an Odyssey CLx Imaging System (LI-COR). For protein sample loading control, the same membrane was hybridized with rabbit anti-alpha tubulin antibody and secondary donkey anti-rabbit antibody labelled with labelled with near-infrared fluorescent dyes that fluoresces at 700 nm channel (red signals on immunoblots) visualized by near infra-red imaging on an Odyssey CLx Imaging System (LI-COR). The fluorescence intensity of the bands (both microdystrophin and alpha-tubulin) were quantified using Image Studios software (LI-COR) and the background (noise values) were subtracted to obtain the intensity values. The ratio of MD1 fluorescence intensity value: α-tubulin fluorescence intensity value is a readout of relative abundance of MD1 protein following the treatment. All data represent mean ± SEM. (N, number of samples per treatment group=3). Statistical analysis was by one-way ANOVA. $^{**}P \leq 0.01$, $^{***}P \leq 0.001$, $^{****}P \leq 0.0001$.

A five-fold increase in transgene expression was observed in p-mini 585MD1 transfected samples compared to p-mini MD1 transfection (a four-fold increase in transgene expression was observed in the samples treated with the original non-miniaturised counterparts). This once again provided proof-on-principle *in vitro* that the addition of R6K-RNA-OUT in the microdystrophin expression cassette has the potential of elevating transgene expression level. The mini MD1 construct seems to produce another slightly larger band above the expected microdystrophin band in the Western blot (Figure 5.13) and the reason for this is not quite well understood, although we hypothesise that an alternative start site may have been generated following manipulations to the original mMD1 plasmid. This did not seem to have an effect on the gene expression construct as Dr Audrey Bourdon and Dr Caroline Le Guiner have performed multiple studies using this mini MD1 construct packaged into AAV (unpublished data from Dr Bourdon's PhD thesis; personal communication with Dr Caroline Le Guiner). This issue however was solved following cloning of 585 R6K-RNA-OUT into p-mini MD1 in between the promoter and the transgene. It is possible that the alternative start may have been abolished following this cloning to generate p-mini 585MD1. Nevertheless, the p-mini MD1 only serves as a construct for direct comparison to p-mini 585MD1 in this experiment. The mMD1 construct without minimisation (~4.6kb) is within the packaging capacity of AAV and therefore the mini MD1 construct will not be used for therapeutic purpose in the future.

Following the Western blot evaluation, we vectorised the minimised constructs for *in vivo* work in the *mdx* mice model. We produced rAAV9 vectors as described in section 5.2.1; production of eight roller bottles of AAV9/mini MD1 and eight roller bottles of AAV9/ mini 585MD1 have been completed. Future work utilising these vectors are discussed in detail in Chapter 6.

5.3 Discussion

The 585 R6K-RNA-OUT intron (Lu *et al.*, 2017) in AAV gene expression cassette 585mMD1 has been shown to enhance transgene expression by several folds; four-fold increase *in vitro* (Chapter 3). In Chapter 4, the functionality of p-mMD1 and p-585mMD1 was assessed to ensure the protein produced was functional. Western blot assay confirmed the presence of microdystrophin and immunohistochemistry assay confirmed the localisation of the protein to the sarcolemma. Following these observations, in this chapter, rAAV9 vectors carrying the therapeutic gene expression cassette mMD1 and 585mMD1 were produced and characterised.

After production of both the viral vectors AAV9/mMD1 and AAV9/585mMD1, quantification of the viral titers by qPCR revealed that there was not much difference in the yield of the virus (both titers were at 10^{13}vp/ml in a final volume of 400-500 μl) despite the differences in the genome size. Packaging inefficiencies are usually indicated by a difference of a log (Dong, Nakai & Xiao, 2010) or more in the viral titers. The viral titers were also verified by further qPCR assays performed in a different laboratory by our collaborators in University of Nantes, France. In the past, significant variability in titer values obtained by qPCR from both inter- and intralaboratory have been reported (D'Costa *et al.*, 2016) and as such, to ensure dosage harmonization, this verification step was carried out. No difference was found between the titer values reported at Royal Holloway and University of Nantes.

Following the production and characterisation of the therapeutic vectors, they were tested in *mdx* mice via intramuscular route of delivery to the TA muscles to evaluate the vector quality and transgene expression *in vivo*. A dose escalation study was performed, and the muscle tissues were harvested 3 months post treatment.

Western blot and immunohistochemistry analyses showed a dose dependent expression of microdystrophin in both the AAV9/mMD1 and AAV9/585mMD1 treated samples, however, the AAV9/585mMD1 treated samples did not result in elevated levels of protein production compared to AAV9/mMD1 treatment (at both doses). This could be partly due to the size of the genetic cargo of AAV9/585mMD1 which is 500 bp above the 4.7kb wild-type limit (discussed later in this section). Centronucleation was also apparent in all the treated samples, suggesting ongoing regeneration-degeneration cycles which is common in *mdx* mice as they are ageing. H&E staining to further confirm this event, indicated that the many hallmarks of regeneration were present in all the treated samples except AAV9/mMD1 high dose treatment, where improvements were seen: a huge number of nuclei have moved to the periphery (although centronucleation is still apparent) and regularly sized and shaped muscle fibers were seen. The best histological and functional outcome was seen in the AAV9/mMD1 treated samples. This shows that a higher dose is needed to improve muscle histology and the AAV9/MD1 has a potential in treating DMD. The overall conclusion that can be made based on the immunohistochemistry results is that AAV9/mMD1 high dose rescued the disease phenotype at the molecular level, whilst the other treatments including AAV9/mMD1 low dose did not seem to be therapeutically beneficial at the molecular level.

Functional outcome of the treatment was also assessed via electrophysiology of the TA muscles. The eccentric contraction data corresponded well with the protein level data indicated by the Western blot assay, except for AAV9/585mMD1 high dose treated samples, where the loss of force following eccentric contractions almost matched the level of saline treated samples. This indicates that the dystrophic phenotype was not rescued in the AAV9/585mMD1 high dose treated samples, despite the presence of microdystrophin. AAV9/mMD1 high dose successfully rescued the disease phenotype at the functional level. AAV9/mMD1 low dose and AAV9/585mMD1 low dose both performed similarly, and whilst this was not the expected results from our

hypothesis; based on the Western blot data, since the protein levels were similar in both the treatments, the functional outcome is sensible.

The 585mMD1 is an overexpressing construct, as such, there will be more microdystrophin produced in each transduced muscle fiber compared to the mMD1 construct. Whilst this is therapeutically relevant, it may be possible that a very elevated microdystrophin production over a long period of time could result in protein misfolding and essentially accumulation of toxic proteins in the cells (Hetz, 2012). It is also important to note the structural nature of microdystrophin protein and as such, it accumulates inside the cells instead of being secreted. There is a possibility that an imbalance exists between accumulation of faulty or misfolded microdystrophin due to the very high turnover induced by the 585mMD1 construct and proteosomal degradation. This could lead to stress signals released by such cells (Hetz, 2012) leading to degeneration, followed by regeneration, and as a result losing the therapeutic protein effect in the transduced muscle fibers. Based on the histology and immunohistochemistry results discussed in this chapter, AAV9/585mMD1 high dose treated samples showed muscle hypertrophy leading to fibre splitting and higher level of connective tissue presence around the muscle fibres. The AAV9/585mMD1 high dose treated samples also failed in functional rescue, despite the high level of microdystrophin present in Western blot and immunohistochemistry. More importantly, the AAV9/585mMD1 low dose treatment provided some level of protection at the functional level indicating the possible 'toxicity' at a higher dose.

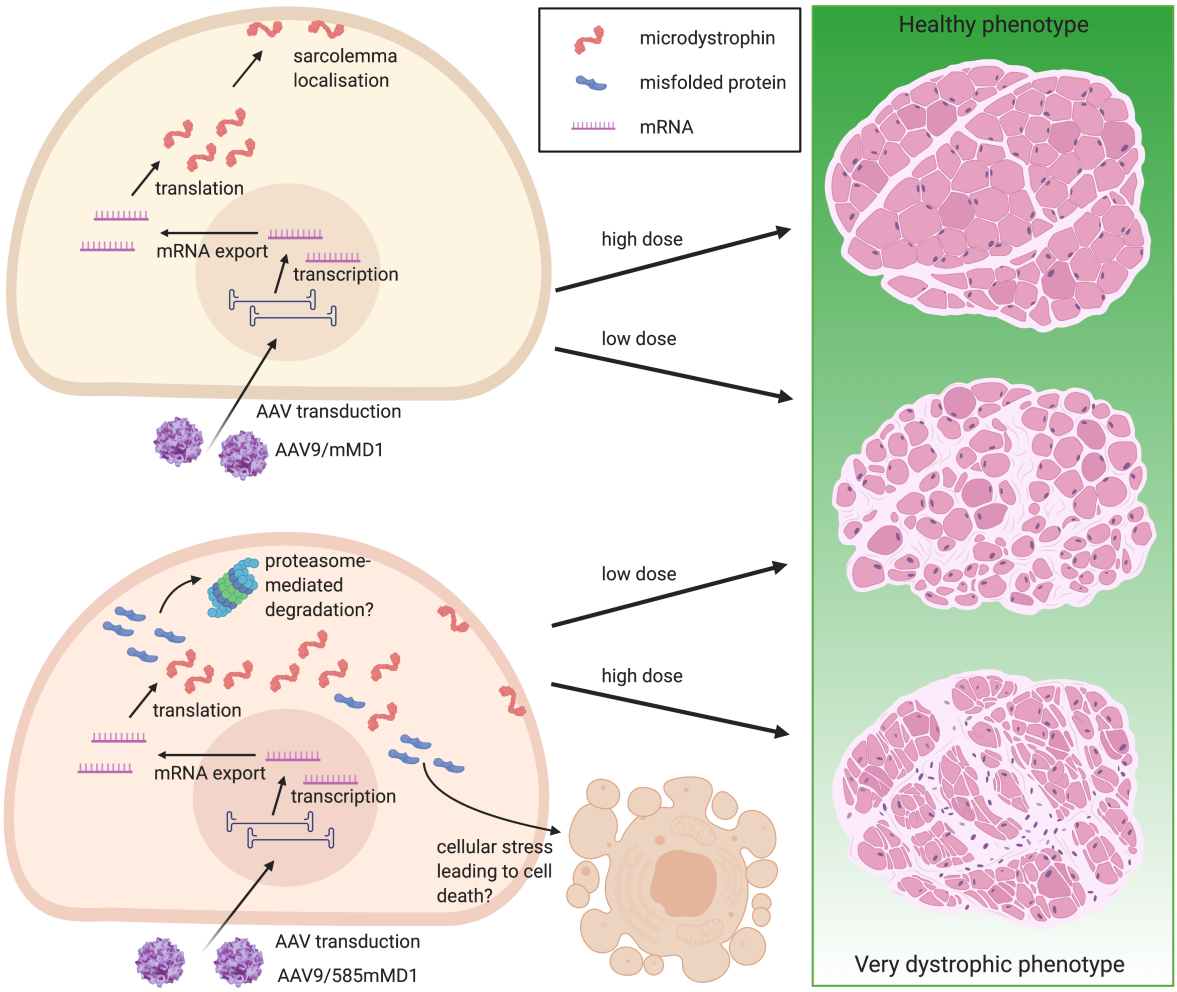

AAV9/mMD1 and AAV9/585mMD1 treated cells. The viral serotype is similar in both the treatments (AAV9); as such, theoretically, transduction of the muscle fibers by the two viruses (AAV9/mMD1 and AAV9/585mMD1) would not differ. From Chapter 3, it has been established that the addition of R6K-RNA-OUT does not affect level of mRNA production. The nucleocytoplasmic distribution of mRNA and mRNA stability are also unaffected by the presence of intron (Nott, Meislin and Moore, 2003). However, intron splicing has an effect on increasing translational yields compared to intronless transcripts (Nott, Meislin and Moore, 2003; Powell and Rivera-Soto, 2015). As a result, the 585mMD1 construct is capable of producing more microdystrophin protein per effective transduction. Whilst this could be beneficial in achieving therapeutic efficacy, this approach could also be counterproductive at a higher AAV9/585mMD1 dosage. This is because microdystophin is an intracellular protein and therefore, the protein product accumulates in the cell instead of being secreted. A high turnover of microdystrophin in

such a situation could mean cellular stress due to excessive production of the protein, especially when protein misfolding begin to happen (shown in blue) and proteasomal degradation could not catch up. Under extreme cellular stress, cell death could potentially happen, completely diminishing the therapeutic effect. This leads to the very dystrophic phenotype observed in the AAV9/585mMD1 high dose treated samples. On the other hand, AAV9/585mMD1 low dose treated samples showed a more moderate dystrophic phenotype.

An infectious centre assay (ICA) carried out to test the infectivity of the vectors also revealed a ten-fold reduction in infectivity of AAV9/585mMD1. This suggests that the packaging capacity of AAV9 is lower than 5.2kb and as such, truncated fragmentary genomes are possibly produced in the packaging process of 585mMD1. Whilst 'oversized' AAV vectors carrying genome above 4.7kb in length have successfully expressed full-length protein in some previous studies, it was found that such 'oversized' AAV vectors carried a highly heterogenous mixture of genomes of different sizes (Tornabene & Trapani, 2020). The truncated genomes are capable of reassembling to reconstitute the full-length expression cassette in the target cell nucleus, and thus enabling protein expression (Tornabene & Trapani, 2020).

The size of the genetic cargo of AAV9/585mMD1 is ~5.2kb, which is approximately 11% above the packaging capacity of wild-type AAV. Thus deletion in the 585mMD1 genome that extended beyond the 5′ ITR and into the Spc5.12 promoter (in the case of the plus strand) or SV40 polyA region (in the case of the minus strand) are possible (Figure 5.15). These deletions are unfavourable as they affect the vector performance especially when the ITRs or gene expression elements are deleted (Yan *et al.*, 2015). The route of delivery of the viral particles via intramuscular injection helps in this situation, where the AAVs are concentrated in the TA muscle. This increases the chances of recombination events that generate intact vector genomes, despite the truncated fragmentary genomes of 585mMD1 packaged into AAV9 (Figure 5.15). As such, the transcriptionally functional 585mMD1 genome could account for some of the

observations such as protein levels in the treatments and dystrophin positive fibers, however, these levels never exceeded the levels observed for the mMD1 treated samples. Despite similar amount of vectors injected per dose for the AAV9/mMD1 and AAV9/585mMD1, it is possible that the amount of intact vector genomes for AAV9/585mMD1 is actually lower than AAV9/mMD1. This provides a reasonable explanation to why the AAV9/585mMD1 treated samples did not result in elevated microdystrophin production compared to the AAV9/mMD1 treated samples at either dose.

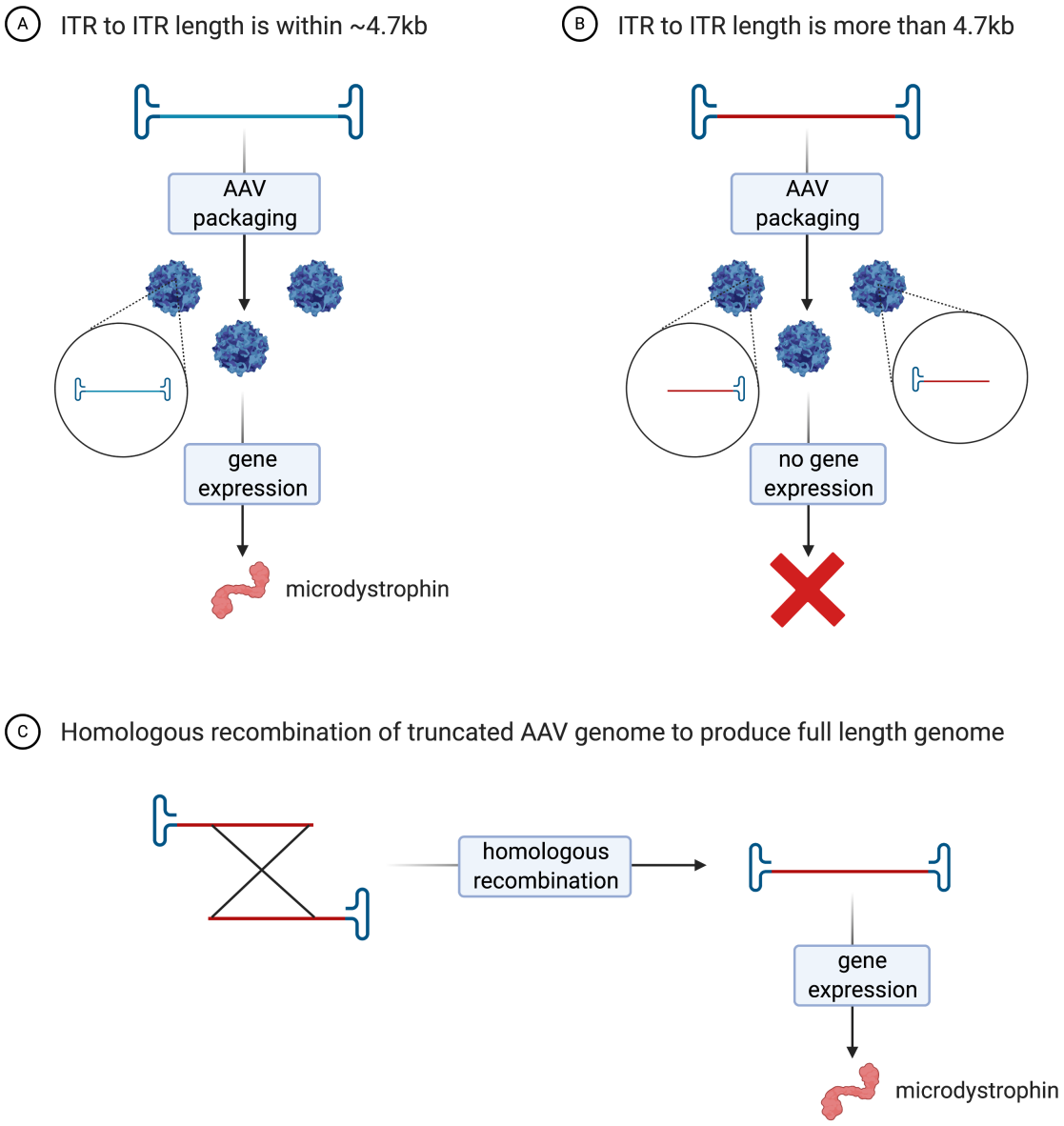

fragmentary vector genomes in oversized 585mMD1 construct. (A) For genetic cargo within 4.7 kb, packaging of AAV is efficient and as such, the gene expression is not affected. (B) For oversized genetic cargo (585mMD1), it is possible that the genome is truncated after ~4.7kb from the 3' end and as a result, fragmentary genomes are packaged in AAV. Whilst the gene expression can be rescued as shown in (C) via homologous recombination (Wu, Yang & Colosi, 2010), for the same amount of virus injected, the availability of intact genome is lower in the AAV9/585mMD1 treated samples.

Wild-type AAV has a packaging capacity of 4.7kb. The ITR to ITR length of gene expression cassettes mMD1 and 585mMD1 are 4.6 kb and 5.2 kb respectively. There was a debate on the packaging capacity of recombinant AAV and up to 5kb is generally accepted as the upper limit (Wu et al., 2010). However, this packaging capacity seems to differ from serotype to serotype and very recently, packaging genome up to 6 kb in AAV8 has been reported (Krooss et al., 2020). It is also worth noting that there is a possibility that the packaging capacity of AAV could also vary depending on the genetic cargo that is packaged in the AAV, as different nucleic acid sequences acquire different conformations, and as such different compaction is achieved. This was the reason we proceeded with the experiments involving AAV9/585mMD1 construct in this Chapter. However, as it became apparent that the genome size was an issue that affects packaging efficiency, we decided to minimise the 585mMD1 construct.

Following successful minimisation of the p-mMD1 construct by our collaborators in Nantes, France, we reduced the gene expression cassette size of 585mMD1 to 4.8 kb to ensure intact vector genomes being packaged into the AAV9 vectors. The successful cloning workflow was validated by sequencing and restriction enzyme profiles. The minimised constructs were able to express microdystrophin and the p-mini 585 MD1 transfected samples showed a five-fold elevated level of microdystrophin expression compared to p-mini MD1 transfected samples. We decided to proceed with vector production of these minimised constructs (AAV9/mini MD1 and AAV9/mini 585 MD1); which was complete at the point of writing this thesis. Further work to be conducted using these vectors are discussed in the next Chapter.

5.4 Appendix

5.4.1 Plasmid map of p-mini MD1 with restriction sites mapped

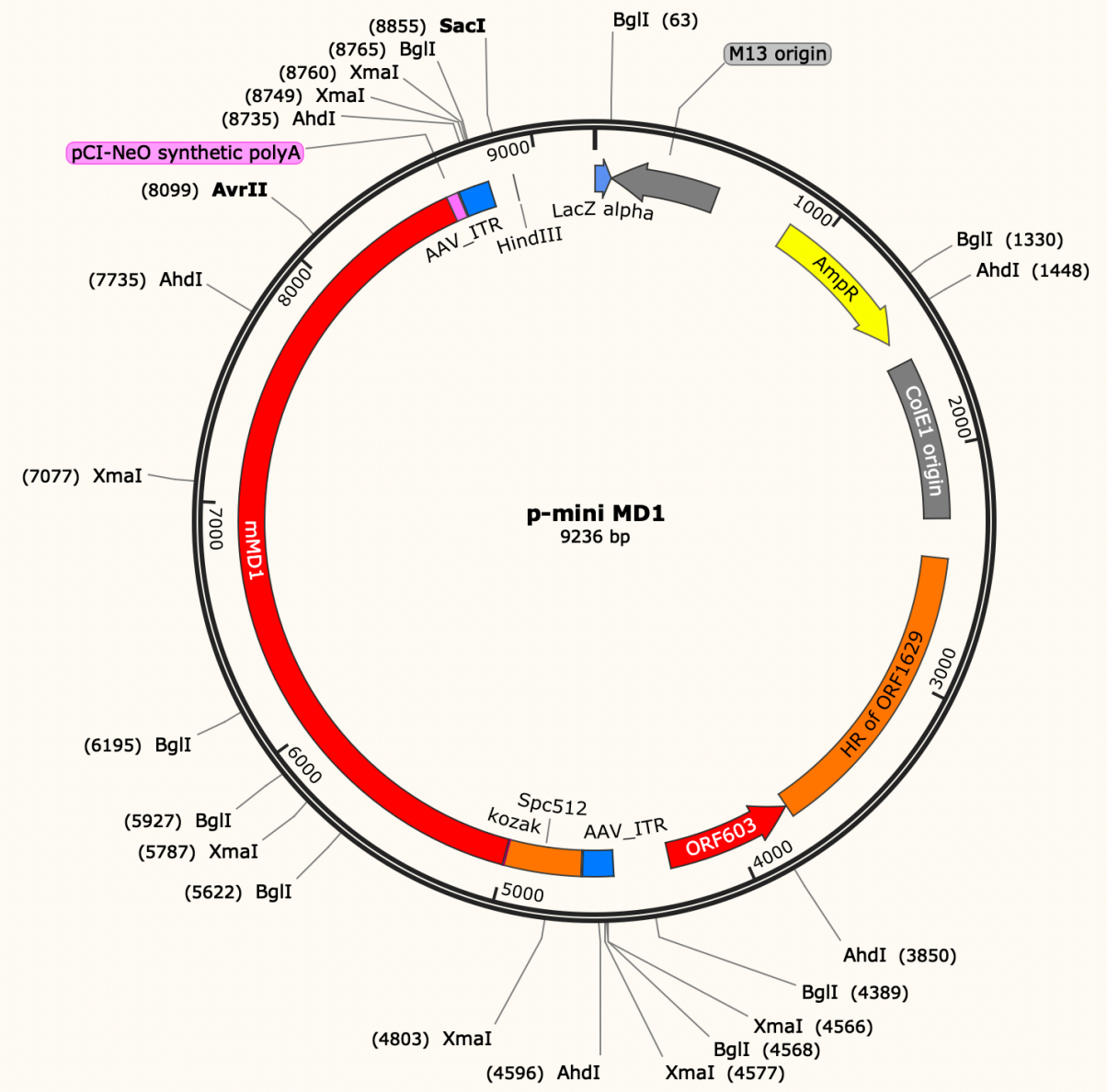

Plasmid map of p-mini 585MD1 with restriction sites mapped

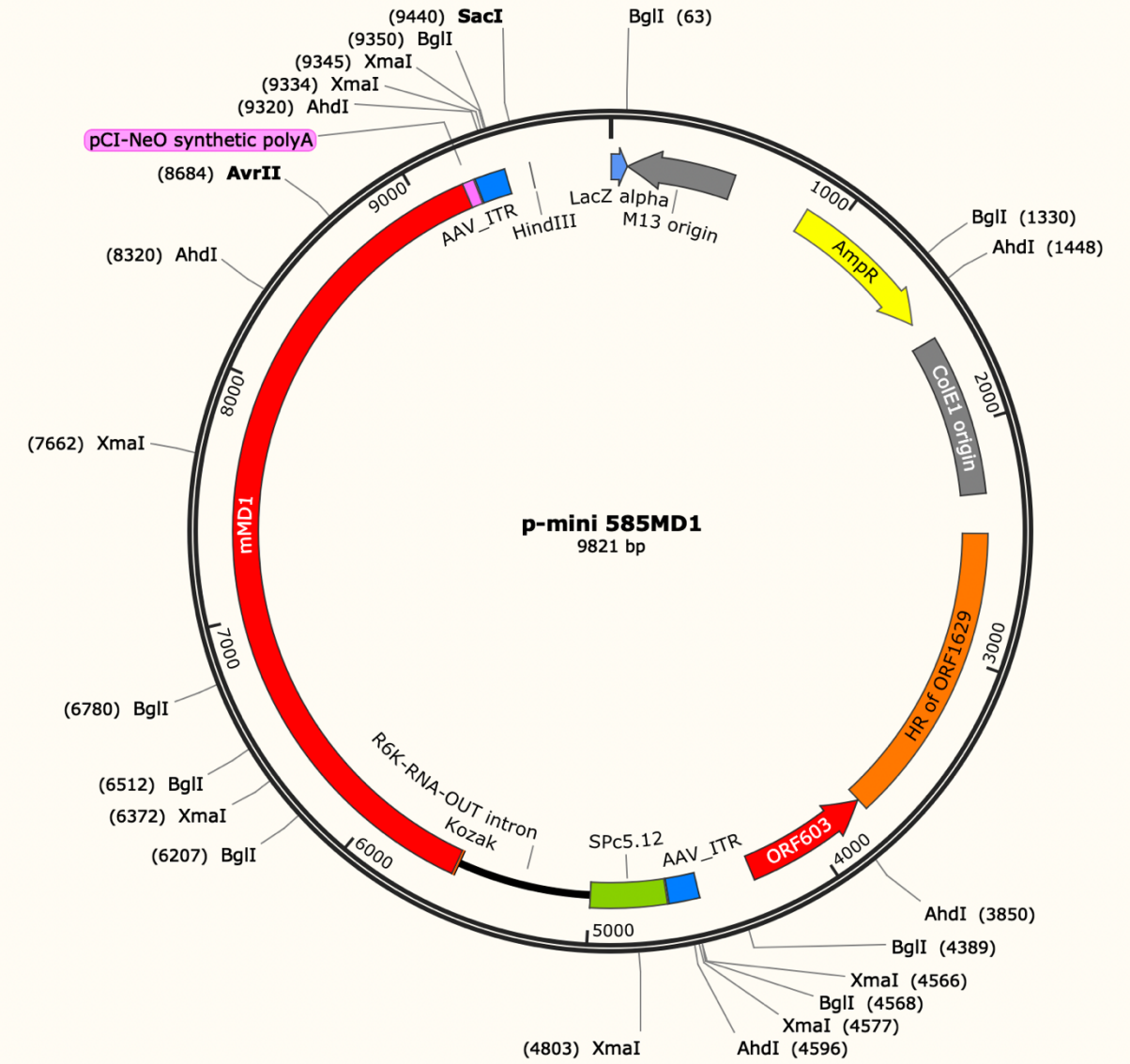

Chapter 6 Conclusion and future work

6.1 Summary of research findings

We initiated this study by engineering the MD1 expressing AAV cassettes, where we added an engineered intron R6K-RNA-OUT (Lu *et al.*, 2017) into the MD1 expressing cassettes in between the promoter and the transgene. Following successful cloning and characterisation of the plasmid construct, p-585 MD1 was generated. Our initial testing of these constructs in an *in vitro* model showed proof-of-principle that the R6K-RNA-OUT intron was indeed capable of enhancing transgene expression level. The constructs expressed the correct protein, with enhancement of translation rather than transcription; this observation is in agreement with other studies where transcription was not affected by the presence of introns (Nott, Meislin and Moore, 2003; Powell and Rivera-Soto, 2015). The mechanism behind this enhancement of translation was not very well understood but is thought to be related with splicing activity of introns as discussed in Chapter 3 (Powell and Rivera-Soto, 2015).

As we established the proof-of-principle *in vitro*, we furthered this work to a very well defined DMD animal model: the *mdx* mice. We started off with a relatively short-term electrotransfer protocol as this technique was readily available in our lab; where we delivered the plasmid constructs to the TA of the *mdx* mice and performed outcome studies two weeks later. This study was important to verify if the plasmid constructs were able to express the correct protein *in vivo* as *in vitro* studies often have limitations that may not capture exactly what is happening at the organismal level. This checkpoint was also passed and the aim of this workflow was to test for the presence of microdystrophin localised to the sarcolemma following delivery of the plasmid constructs, which we observed. We decided to perform isolated muscle function analyses as well, which unfortunately did not show any significant differences between the treatment groups and saline. This was, however, expected as gene delivery efficiency using electrotransfer is very low (Acsadi et al, 1991) and muscle damage occurs during the electrotransfer, which ultimately compromises functional recovery following expression of microdystrophin.

We then vectorised the p-mMD1 and p-585mMD1 constructs where we chose AAV9 as serotype of choice as this serotype has shown to efficiently transduce muscle and heart (Duan, 2015). We started off with a dose escalation IM injection study to evaluate vector quality and transgene expression levels in the TA muscle. The treatment duration was three months, which was enough time period for microdystrophin accumulation to occur to provide muscle protection against contraction induced damage. Isolated muscle function analyses were performed after three months and a dose dependent protection against loss of force following eccentric contractions were observed in the AAV9/mMD1 treated samples. However, the AAV9/585mMD1 treated samples did not show similar trend, where the low dose provided some level of protection against loss of force following eccentric contractions matching AAV9/mMD1 low dose while there was no significant difference observed between the AAV9/585mMD1 high dose and saline treated samples.

The reasons for this include the following:
i) The genome of 585mMD1 packaged into rAAV9 was 5.2kb in length, which is 500 bp above the 4.7kb wild-type packaging limit. This would have caused fragmentary genomes to be packaged into the rAAV9 which may not necessarily be harmful, because homologous recombination can rescue the formation of full-length genome (Wu, Yang & Colosi, 2010), but this can severely reduce the efficacy of the treatment. The efficacy would be further reduced if an intravenous (IV) route of delivery was employed, as the vectors would not be concentrated in a specific muscle as they would be when injected intramuscularly. This hypothesis corresponded well with the Western blot data that showed a dose dependent expression of microdystrophin in both the AAV9/mMD1 and AAV9/585mMD1 treated samples, however, the AAV9/585mMD1 treatment did not result in better functional outcome than AAV9/mMD1.

ii) The 585mMD1 construct is an overexpressing construct and as such, the level of protein production per successful virus transduction would be higher for AAV9/585mMD1. Whilst elevation of transgene expression up to 100-fold *in vivo* was shown in the liver (Lu *et al.*, 2017) following addition of an engineered

intron into the AAV gene expression cassette, it is worth noting that all the studies performed were on proteins that were secreted out of the cells. An intron certainly can be a very valuable gene expression regulatory element that can increase transgene expression (Powell et al, 2015) but so far, no such study that compared the effect of overexpression of a structural protein that is retained in the cell, especially in a skeletal muscle setting has been published. Therefore, whether to expect a 'toxic' effect following overexpression of an intracellular protein remain to be explored. This hypothesis corresponds to the observation where the AAV9/585mMD1 low dose treated samples provided better protection against loss of force following eccentric contractions compared to the AAV9/585mMD1 high dose.

We also learned from the AAV IM study that packaging genomes beyond the packaging capacity of AAV (~4.7kb) causes the infectivity of the virus to be compromised. This was evident from the infectious centre assay (ICA) where the AAV9/585mMD1 particles were 10 times less infectious than AAV9/mMD1 particles. We generated minimised constructs of p-mMD1 and p-585mMD1 called p-mini MD1 and p-mini 585MD1 respectively. This work was done in collaboration with Dr Audrey Bourdon and Dr Caroline Le Guiner (University of Nantes, France). We also performed some *in vitro* studies assessing the transgene expression levels of the constructs. The p-mini 585MD1 construct (with R6K-RNA-OUT intron) elevated transgene expression level by five-fold compared to p-mini MD1 in transfected HEK293T cells (the non-miniaturised p-585mMD1 elevated transgene expression level by four-fold compared to the non-miniaturised p-mMD1 in transfected HEK293T cells). We then vectorised these miniaturised constructs, packaging them in rAAV9. The production of AAV9/mini MD1 and AAV9/mini 585MD1 were complete. Future work using these vectors are discussed in Section 6.3.

6.2 Significance of this work

DMD is a lethal paediatric genetic disease and so far, there is no cure for this disease. Many therapeutic strategies are being tested in clinical trials but AAV gene therapy shows the most promising success so far (Table 1.4 in Chapter 1). AAV gene therapy also has the potential of treating 100% of the DMD patient population regardless of their mutations (provided they were not previously exposed to AAV infection, resulting in pre-existing immunity). As microdystrophin gene transfer using AAV has been proven to work in both preclinical and clinical models (Wang et al., 2000; Harper et al., 2002; Hakim et al., 2017; Le Guiner et al., 2017; Table 1.4), the focus of the research now is geared towards successfully translating this advanced therapy medicinal product (ATMP) from bench to bedside.

Several issues still remain to be tackled in AAV gene therapy and one such issue is potency and efficacy (Colella, Ronzitti and Mingozzi, 2017). The systemic nature of DMD that requires body-wide dystrophin restoration also means a high AAV dosage would be needed to cure this disease. Whilst AAV is a safe virus, it can still mount an immune response at a high dosage (Mingozzi and High, 2013). This would then reduce the efficacy of the treatment. A more potent gene expression cassette would mean less virus will be needed to achieve therapeutic effect. One way of enhancing gene expression is via addition of gene regulatory elements such as introns (Powell et al, 2015) into the gene expression cassette. Apart from making the therapy safer due to reduced chances of provoking the immune system, a more potent gene expression cassette would also contribute to solving the bottleneck in AAV manufacturing at a large scale, as less virus will be needed to treat each patient. This in turn will also bring the cost of therapy down as currently, even the 'cheapest' AAV gene therapy drug carry a six-digit price tag.

The AAV gene therapy field is expanding exponentially, and we are just at the beginning (Wang, Tai and Gao, 2019). The interdisciplinary nature of this field combines knowledge from the fields of molecular biology, bioinformatics,

epidemiology, structural biology, immunology, genomics and other biomedical disciplines to innovate life-changing therapies (Wang, Tai and Gao, 2019). The findings from this study will not just be relevant in the context of AAV gene therapy for DMD, but also for many other diseases utilising this viral vector.

6.3 Future work

The proof-of-principle *in vitro* that microdystrophin production is enhanced following addition of an engineered intron opens up numerous potential for utilising this intron in AAV gene therapy constructs. Studies *in vivo* provided several challenges, however, they were great learning opportunities. Here, we outline some further studies that will help us understand whether the R6K-RNA-OUT intron has the potential of elevating transgene expression level *in vivo* to provide therapeutic benefits in the treatment of DMD via gene transfer therapy.

Plasmid constructs are easily produced compared to viral vectors and as such, previously, we started *in vivo* work by conducting a plasmid electrotransfer study. Whilst this captured the protein production capability of the constructs tested, the therapeutic benefits of both the constructs were not revealed due to the muscle damage caused by the technique itself. As such, for the newly generated minimised constructs, the electrotransfer study was not performed. In addition, at the point of collaboration with Dr Audrey Bourdon and Dr Caroline Le Guiner (Nantes, France), the p-mini MD1 has already been vectorised and used in several studies by our collaborators (unpublished data and personal communication with Dr Caroline Le Guiner). The vectorised mini MD1 constructs were capable of producing microdystrophin at a level similar to the original mMD1 construct (unpublished data and personal communication with Dr Caroline Le Guiner). In our *in vitro* studies, the level of elevation of microdystrophin production of the p-mini 585MD1 construct versus p-mini MD1 was almost identical to the comparison between the original non-minimised respective plasmids. As such, the minimisation of the constructs did not compromise the gene expression strength or capabilities of the cassettes.

6.3.1 Evaluation of the infectivity of the minimised constructs

As the vector productions of AAV9/mini MD1 and AAV9/mini 585MD1 were complete at the point of writing this thesis, the next step would be to characterise the vectors in terms of infectivity. The infectious centre assay (ICA) is a valuable assay to characterise how the genome packaged into the vectors affect infectivity of the vectors. As both the genomes packaged into AAV9/mini MD1 and AAV9/mini 585MD1 are within the packaging capacity of AAV, the infectivity of both these vectors should be roughly the same. This would also be a decision-making point, whether or not to proceed with the *mdx* mice treatments if the infectivity of the viruses do not fall within the 'infectious threshold' described in Chapter 5.

The packaging capacity of wild-type AAV is ~4.7kb, however, there packaging capacity of rAAV remain a topic of debate as they seem to differ from serotype to serotype (Wu et al., 2010; Krooss et al., 2020). A very striking finding published recently by (Krooss et al., 2020) gained our attention where the authors claimed that AAV8 was capable of packaging genome up to 6 kb, which is well beyond the generally accepted threshold. As such, we produced rAAV8 vectors that packaged the transcriptional units mMD1 (~4.6kb) and 585mMD1 (~5.2kb); which were the non-minimized microdystrophin expressing constructs that was tested using AAV9 in this thesis. The infectivity of AAV9/585mMD1 was ten-fold lower compared to AAV9/mMD1 and whether this is true if the exact genomes were packaged in AAV8 is an interesting question to be answered. The ICA will provide answers to this. AAV8 is also a serotype of interest as several studies in muscle gene therapy have been performed using this serotype (Mack *et al*., 2017; Le Guiner *et al.*, 2017), including the AAV-microdystrophin human clinical trial recently initiated by Genethon in Europe (Trial number 2020-002093-27).

6.3.2 Systemic delivery of the AAV vectors to evaluate transgene expression level and tissue specificity

In this thesis, intramuscular injection was performed to deliver AAV vectors. This route of delivery was essential to assess the vector quality, transgene expression level and functional outcome. As the vectors were concentrated in one muscle (TA muscle in this case), a better assessment of protein production level could be performed as all the vectors are present in exactly the same location in all the treated samples without variability in distribution if delivered systemically. This was essential to establish proof-of-principle in this study. However, whether there were expression of the gene carried by AAV elsewhere in other tissues (for example, the liver) was not explored in this study.

It is important to note that this route of delivery is not therapeutically relevant in the context of DMD, where a body-wide transduction is required, which is only possible via intravascular (IV) mode of delivery. In addition, IV delivery is less immunogenic compared to IM delivery and as the vectors are in circulation, some leaky expression of the transgene in the liver could also possibly provide some immune tolerance towards the vectors (Verdera, Kuranda and Mingozzi, 2020). Thus, following the characterisation of infectivity of AAV9/mini MD1 and AAV9/mini 585MD1, an IV delivery of the vectors in *mdx* mice should be performed to study the distribution of the vectors and the level of protein expression in the more evenly transduced muscle fibres due to the systemic delivery. IV delivery would also result in transduction of the heart and diaphragm which are severely affected in DMD, and as such the therapeutic benefit of the treatment in those tissues could be assessed.

6.3.3 The use of dystrophin-deficient rat model to evaluate cardiac phenotype rescue

Respiratory management have extended the life expectancy of DMD patients, although historically, the leading cause of death in DMD was due to respiratory failure (Meyers and Townsend, 2019). As life expectancy is extended, cardiomyopathies are now one of the leading cause of morbidity and mortality in dystrophin-deficient patients and both DMD and BMD patients develop end-stage heart failure (Kamdar and Garry, 2016). As such, the assessment of the advanced therapy constructs in a suitable animal model to evaluate the rescue of cardiac phenotype is essential. The dystrophin deficient *mdx* mice only display limited muscle weakness and do not fully represent the human disease (Larcher et al, 2014), wheres the dystrophin-deficient rats (Dmd^{mdx}) closely resemble the pathological phenotype of DMD patients (Ouisse et al, 2019). Dmd^{mdx} also display a more severe cardiac phenotype mimicking the dilated cardiomyopathy observed in human patients (Larcher et al, 2014).

Following studies (discussed in 6.2.2) in *mdx* mice, if an enhancement of transgene expression is observed following addition of the engineered intron, this experiment should be carried out in Dmd^{mdx} as well to study the effects of the constructs in the heart. This is important to elucidate the efficacy of the treatment that is not just limited to skeletal muscles.

6.3.4 The hunt for a more muscle specific AAV serotype

Since rAAVs exhibited clinical promise more than 20 years ago, there have been constant pursuit to generate or isolate novel AAV capsids with new properties (Wang, Tai and Gao, 2019). As AAV gene therapy is actively moving into human clinical trials, there is a constant need and desire to improve the virus properties in terms of transduction efficiency, tissue tropism and immunogenicity (Zinn et al., 2015). In the case of DMD, an AAV serotype that is muscle-tropic and preferentially transfers gene into muscle cells would be ideal, especially because currently, a high dosage to achieve body-wide transduction is needed to treat DMD. Studies by (Gao et al, 2004) have shown that AAV sequences are widely distributed in both human and non-human primates. AAV sequences have also been successfully isolated from other animals such as pigs that showed good transduction profile in major organs of mice and were not neutralised by human antibodies (Bello *et al*., 2014).

Being a member of the Dependoparvovirus, AAV requires helper viruses such as Adenovirus to facilitate infection and replication (Wu, Asokan and Samulski, 2006). In the absence of helper viruses, AAV integrates its genome into a specific integration site in human chromosome 19 at a locus designated AAVS1; where the latent AAV genome remain quiescent until a favourable replication condition arises which is usually the encounter of helper viruses (Samulski et al. 2015). This nature of AAV can be exploited to isolate naturally occurring AAVs from multiple tissues from multiple species (Gao et al, 2004; Bello et al., 2014; Wang, Tai and Gao, 2019). This can be done using a PCR workflow targeting the AAV genome followed by characterisation of the isolated DNA sequence by Sanger sequencing which may lead to discovery of novel AAV sequences, which is a work in progress in our lab.

Previously, we have shown that AAV genomes can be found in human genomic DNA derived from muscle tissue with the frequency of detection of 18% ([Unpublished Master's Thesis] Elangkovan, 2017). The characterised AAVs were however, not novel (AAV9 was isolated). The chances of finding a novel

AAV serotype will increase with the number of samples analysed and therefore, this work is ongoing as we receive samples on a continuous basis when they become available. By isolating and characterising AAVs, there is a potential of finding novel AAV(s) which is/are muscle tropic. Delivering therapeutic constructs using muscle specific AAVs will improve the clinical outcome of the treatments. In addition, a lower dosage will be required for treatment, reducing potential immune response and also inevitably reducing the cost of treatment.

References

A Williams, J. (2014). Improving DNA vaccine performance through vector design. *Current Gene Therapy, 14*(3), 170-189.

Aartsma-Rus, A. and Krieg, A.M., 2017. FDA approves eteplirsen for Duchenne muscular dystrophy: the next chapter in the eteplirsen saga. *Nucleic acid therapeutics*, *27*(1), pp.1-3.

Aartsma-Rus, A., Fokkema, I., Verschuuren, J., Ginjaar, I., Van Deutekom, J., van Ommen, G.J. and Den Dunnen, J.T., 2009. Theoretic applicability of antisense-mediated exon skipping for Duchenne muscular dystrophy mutations. *Human mutation*, *30*(3), pp.293-299.

Abdul-Razak, H., Malerba, A. & Dickson, G. (2016) "Advances in gene therapy for muscular dystrophies", *F1000Research,* 5(F1000 Faculty Rev), 2030. doi: 10.12688/f1000research.8735.1

Acsadi, G., Dickson, G., Love, D.R., Jani, A., Walsh, F.S., Gurusinghe, A., Wolff, J.A. and Davies, K.E., 1991. Human dystrophin expression in mdx mice after intramuscular injection of DNA constructs. *Nature*, *352*(6338), pp.815-818.

Addgene (2020) *AAV Purification by Iodixanol Gradient Ultracentrifugation*. Available at: https://www.addgene.org/protocols/aav-purification-iodixanol-gradient-ultracentrifugation/ (Accessed 1 May 2021).

Agarwal, S., 2020. High-dose AAV gene therapy deaths. *Nat. Biotechnol*, *38*, p.910.

Akerstrom, T., Vedel, K., Needham, J., Hojman, P., Kontou, E., Hellsten, Y. and Wojtaszewski, J.F., 2015. Optimizing hyaluronidase dose and plasmid DNA

delivery greatly improves gene electrotransfer efficiency in rat skeletal muscle. *Biochemistry and Biophysics Reports*, *4*, pp.342-350.

Akerstrom, T., Vedel, K., Needham, J., Hojman, P., Kontou, E., Hellsten, Y. and Wojtaszewski, J.F., 2015. Optimizing hyaluronidase dose and plasmid DNA delivery greatly improves gene electrotransfer efficiency in rat skeletal muscle. *Biochemistry and Biophysics Reports*, *4*, pp.342-350.

Akkaraju, G. R., Huard, J., Hoffman, E. P., Goins, W. F., Pruchnic, R., Watkins, S. C., Cohen, J. B. and Glorioso, J. C. (1999) 'Herpes simplex virus vector-mediated dystrophin gene transfer and expression in MDX mouse skeletal muscle', *J Gene Med*, 1(4), pp. 280–289.

Al-Ali R, Gonzalez-Sarmiento R. (2016) Proximity of AUG sequences to initiation codon in genomic 5' UTR regulates mammalian protein expression. *Gene*. 594, 268–271.

Alberts, B., Johnson, A., Lewis, J., Raff, M., Roberts, K. and Walter, P., 2008. Molecular biology of the cell, 5th edn. Garland Science. *New York*.

Allard, B., 2006. Sarcolemmal ion channels in dystrophin-deficient skeletal muscle fibres. *Journal of Muscle Research & Cell Motility*, *27*(5-7), pp.367-373.

Allen, D.G., Whitehead, N.P. and Froehner, S.C., 2016. Absence of dystrophin disrupts skeletal muscle signaling: roles of Ca2+, reactive oxygen species, and nitric oxide in the development of muscular dystrophy. *Physiological reviews*, *96*(1), pp.253-305.

Angelini, C., 2009. Muscular dystrophy. In *Handbook of clinical neurology* (Vol. 95, pp. 477-488). Elsevier.

Arruda, V. R. and Xiao, W. (2007) 'It's all about the clothing: Capsid domination in the adeno-associated viral vector world', *Journal of Thrombosis and Haemostasis*, 5(1), pp. 12–15.

Atchison, R.W., Casto, B.C., Hammon, W.M. (1965) Adenovirus-associated defective virus particles. *Science*, 149, pp. 754-756.
Ayuso, E., Mingozzi, F. and Bosch, F., 2010. Production, purification and characterization of adeno-associated vectors. *Current gene therapy*, *10*(6), pp.423-436.

Bartlett, J. S., Wilcher, R. and Samulski, R. J. (2000) 'Infectious Entry Pathway of Adeno-Associated Virus and Adeno-Associated Virus Vectors', *J. Virol.,* 74(6), pp. 2777–2785.

Barton-Davis, E. R., Cordier, L., Shoturma, D. I., Leland, S. E. and Sweeney, H. L. (1999) 'Aminoglycoside antibiotics restore dystrophin function to skeletal muscles of mdx mice', *Journal of Clinical Investigation*, 104(4), pp. 375–381.

Bello, A. *et al.* (2014) Novel Adeno-associated Viruses Derived From Pig Tissues Transduce Most Major Organs in Mice. *Scientific Reports*. 4(6644), pp.1–11.

Berns, K.I., 2013. My life with adeno-associated virus: a long time spent studying a short genome. *DNA and cell biology*, *32*(7), pp.342-347.

Binks, M. (2019) Gene Therapy Trials: Pfizer. PPMD 2019 Annual Conference, 28 June 2019, Orlando Florida (Attended virtually).

Birnkrant, D. J., Bushby, K., Bann, C. M., Apkon, S. D., Blackwell, A., Brumbaugh, D., ... & Street, N. (2018). Diagnosis and management of Duchenne muscular dystrophy, part 1: diagnosis, and neuromuscular, rehabilitation, endocrine, and gastrointestinal and nutritional management. *The Lancet Neurology*, *17*(3), 251-267.

Blacklow, N.R., Hoggan, M.D. and Rowe, W.P., 1967. Isolation of adenovirus-associated viruses from man. *Proceedings of the National Academy of Sciences of the United States of America*, *58*(4), p.1410.

Blake, D.J., Weir ,A., Newey, S.E. and Davies, K.E. (2002) 'Function and genetics of dystrophin and dystrophin-related proteins in muscle.', *Physiol Rev*, 82, pp.291–329.

Bloquel, C., Fabre, E., Bureau, M.F. and Scherman, D., 2004. Plasmid DNA electrotransfer for intracellular and secreted proteins expression: new methodological developments and applications. *The Journal of Gene Medicine: A cross-disciplinary journal for research on the science of gene transfer and its clinical applications*, *6*(S1), pp.S11-S23.

Boisgerault, F. and Mingozzi, F., 2015. The skeletal muscle environment and its role in immunity and tolerance to AAV vector-mediated gene transfer. *Current gene therapy*, *15*(4), pp.381-394.

Boisgerault, F. and Mingozzi, F., 2015. The skeletal muscle environment and its role in immunity and tolerance to AAV vector-mediated gene transfer. *Current gene therapy*, *15*(4), pp.381-394.

Bruusgaard, J.C., Liestøl, K., Ekmark, M., Kollstad, K. and Gundersen, K., 2003. Number and spatial distribution of nuclei in the muscle fibres of normal mice studied in vivo. *The Journal of physiology*, *551*(2), pp.467-478.

Buchlis, G., Podsakoff, G. M., Radu, A., Hawk, S. M., Flake, A. W., Mingozzi, F. and High, K. a (2012) 'Brief report Factor IX expression in skeletal muscle of a severe hemophilia B patient 10 years after AAV-mediated gene transfer', *Blood*, 119(13), pp. 3038–3041.

Buchman, A. R., & Berg, P. (1988). Comparison of intron-dependent and intron-independent gene expression. *Molecular and Cellular Biology, 8*(10), 4395-4405.

Burns, D.P., Canavan, L., Rowland, J., O'Flaherty, R., Brannock, M., Drummond, S.E., O'Malley, D., Edge, D. and O'Halloran, K.D., 2018. Recovery of respiratory function in mdx mice co-treated with neutralizing interleukin-6 receptor antibodies and urocortin-2. *The Journal of physiology*, *596*(21), pp.5175-5197.

Bushby, K., Finkel, R., Birnkrant, D.J., Case, L.E., Clemens, P.R., Cripe, L., Kaul, A., Kinnett, K., McDonald, C., Pandya, S. and Poysky, J., 2010. Diagnosis and management of Duchenne muscular dystrophy, part 1: diagnosis, and pharmacological and psychosocial management. *The Lancet Neurology*, *9*(1), pp.77-93.

Bushby, K., Finkel, R., Wong, B., Barohn, R., Campbell, C., Comi, G.P., Connolly, A.M., Day, J.W., Flanigan, K.M., Goemans, N. and Jones, K.J., 2014. Ataluren treatment of patients with nonsense mutation dystrophinopathy. *Muscle & nerve*, *50*(4), pp.477-487.

Campellone, J. and Fetterman, A. (2017). *Types of Muscular Dystrophy and Neuromuscular Diseases - Health Encyclopedia - University of Rochester Medical Center*. [online] University of Rochester Medical Center. Available at: https://www.urmc.rochester.edu/encyclopedia/content.aspx?ContentTypeID=85&ContentID=P00792 [Accessed 25 Jan. 2017].

Carlson, C.G., 1998. The dystrophinopathies: an alternative to the structural hypothesis. *Neurobiology of disease*, *5*(1), pp.3-15.

Chamberlain, J.R. & Chamberlain, J.S. (2017) "Progress toward Gene Therapy for Duchenne Muscular Dystrophy", *Molecular Therapy,* 25(5), pp. 1125-1131.

Chamberlain, K., Riyad, J.M. & Weber, T. (2016) "Expressing transgenes that exceed the packaging capacity of adeno-associated virus capsids", *Human gene therapy methods*, vol. 27, no. 1, pp. 1-12.

Chan, S., Head, S.I. and Morley, J.W., 2007. Branched fibers in dystrophic mdx muscle are associated with a loss of force following lengthening contractions. *American Journal of Physiology-Cell Physiology*, *293*(3), pp.C985-C992.

Chandler, R. J. *et al.* (2015) Vector design influences hepatic genotoxicity after adeno-associated virus gene therapy. *J. Clin. Invest.* 125(2), pp.870–880.

Charleston, J.S., Schnell, F.J., Dworzak, J., Donoghue, C., Lewis, S., Chen, L., Young, G.D., Milici, A.J., Voss, J., DeAlwis, U. and Wentworth, B., 2018. Eteplirsen treatment for Duchenne muscular dystrophy: exon skipping and dystrophin production. *Neurology*, *90*(24), pp.e2146-e2154.

Chen, H. H., Mack, L. M., Kelly, R., Ontell, M., Kochanek, S. and Clemens, P. R. (1997) 'Persistence in muscle of an adenoviral vector that lacks all viral genes.', *Proceedings of the National Academy of Sciences of the United States of America*, 94(5), pp. 1645–50.

Chen, Z., He, C., Ehrhardt, A., & Kay, M. A. (2003). Minicircle DNA vectors devoid of bacterial DNA result in persistent and high-level transgene expression in vivo. *Molecular Therapy, 8*(3), 495-500.

Choi, J.H., Yu, N.K., Baek, G.C., Bakes, J., Seo, D., Nam, H.J., Baek, S.H., Lim, C.S., Lee, Y.S. and Kaang, B.K., 2014. Optimization of AAV expression cassettes to improve packaging capacity and transgene expression in neurons. *Molecular brain*, *7*(1), pp.1-10.

Colella, P., Ronzitti, G., & Mingozzi, F. (2017). Emerging issues in AAV-mediated in vivo gene therapy. *Molecular Therapy-Methods & Clinical Development,* 8, 87-104.

Conklin, L.S., Damsker, J.M., Hoffman, E.P., Jusko, W.J., Mavroudis, P.D., Schwartz, B.D., Mengle-Gaw, L.J., Smith, E.C., Mah, J.K., Guglieri, M. and Nevo, Y., 2018. Phase IIa trial in Duchenne muscular dystrophy shows vamorolone is a first-in-class dissociative steroidal anti-inflammatory drug. *Pharmacological research*, *136*, pp.140-150.

Crawford, G. E. *et al.* (2000) 'Assembly of the dystrophin-associated protein complex does not require the dystrophin COOH-terminal domain.', *J. Cell Biol.* 150(6), pp. 1399–1410.

d'Costa S, Blouin V, Broucque F, Penaud-Budloo M, Fçranois A, Perez IC, Le Bec C, Moullier P, Snyder RO, Ayuso E. Practical utilization of recombinant AAV vector reference standards: focus on vector genomes titration by free ITR qPCR. Molecular Therapy-Methods & Clinical Development. 2016 Jan 1;3:16019.

Dangain, J. and Vrbova, G., 1984. Muscle development in mdx mutant mice. *Muscle & Nerve: Official Journal of the American Association of Electrodiagnostic Medicine*, *7*(9), pp.700-704.

Darquet, A. M., Cameron, B., Wils, P., Scherman, D., & Crouzet, J. (1997). A new DNA vehicle for nonviral gene delivery: Supercoiled minicircle. *Gene Therapy, 4*(12), 1341.

Davies, K. E. and Nowak, K. J. (2006) 'Molecular mechanisms of muscular dystrophies: old and new players.', *Nature reviews. Molecular cell biology*, 7(10), pp. 762–773. doi: 10.1038/nrm2024.

Daya, S. and Berns, K. I. (2008) 'Gene therapy using adeno-associated virus vectors', *Clinical Microbiology Reviews*, 21(4), pp. 583–593.

Deconinck, N. *et al.* (1997) 'Expression of truncated utrophin leads to major functional improvements in dystrophin-deficient muscles of mice.', *Nature Med.* 3, pp. 1216–1221. doi:10.1038/nm1197-1216.

Dickson, G., Hill, V. and Graham, I.R., 2002. Screening for antisense modulation of dystrophin pre-mRNA splicing. *Neuromuscular Disorders*, *12*, pp.S67-S70.

Discovery Medicine (2018) *Generational changes of plasmid expression systems*. [ONLINE] Available at: http://www.discoverymedicine.com/Charles-H-Jones/files/2015/07/discovery_medicine_no_107_blaine_a_pfeifer_figure_3.png.jhtml?id=2|attachment_7. [Accessed 20 March 2018].

Dong B, Nakai H, Xiao W. Characterization of genome integrity for oversized recombinant AAV vector. Molecular therapy. 2010 Jan 1;18(1):87-92.

Doorenweerd, N., Mahfouz, A., van Putten, M., Kaliyaperumal, R., t'Hoen, P.A., Hendriksen, J.G., Aartsma-Rus, A.M., Verschuuren, J.J., Niks, E.H., Reinders, M.J. and Kan, H.E., 2017. Timing and localization of human dystrophin isoform expression provide insights into the cognitive phenotype of Duchenne muscular dystrophy. *Scientific reports*, *7*(1), pp.1-12.

Douar, A., Poulard, K., Stockholm, D. and Danos, O. (2001) 'Intracellular Trafficking of Adeno-Associated Virus Vectors : Routing to the Late Endosomal Compartment and Proteasome Degradation Intracellular Trafficking of Adeno-Associated Virus Vectors : Routing to the Late Endosomal Compartment and Proteasome Degra', *J. Virol.*, 75(4), pp. 1824–1833.

Douglas, A.G. and Wood, M.J., 2013. Splicing therapy for neuromuscular disease. *Molecular and Cellular Neuroscience*, *56*, pp.169-185.

Duan, D. (2016) Systemic delivery of adeno-associated viral vectors. *Curr. Opin. Virol.* 21, pp.16–25.
Duan, D. (2018). Micro-dystrophin gene therapy goes systemic in duchenne muscular dystrophy patients. *Human Gene Therapy*, DOI: 10.1089/hum.2018.012.

Duan, D., 2008. Myodys, a full-length dystrophin plasmid vector for Duchenne and Becker muscular dystrophy gene therapy. *Current opinion in molecular therapeutics*, *10*(1), pp.86-94.

Duan, D., 2015. Duchenne muscular dystrophy gene therapy in the canine model. *Human gene therapy Clinical development*, *26*(1), pp.57-69.

Duan, D., 2018. Systemic AAV micro-dystrophin gene therapy for Duchenne muscular dystrophy. *Molecular Therapy*, *26*(10), pp.2337-2356.

Duan, D., Goemans, N., Takeda, S. *et al.* (2021) Duchenne muscular dystrophy. *Nat Rev Dis Primers* **7,** 13. https://doi.org/10.1038/s41572-021-00248-3

Duan, D., Li, Q., Kao, A. W., Yue, Y., Pessin, J. E. and Engelhardt, J. F. (1999) 'Dynamin is required for recombinant adeno-associated virus type 2 infection.', *J. Virol.*, 73(12), pp. 10371–6.

Dunant, P., Walter, M. C., Karpati, G. and Lochmüller, H. (2003) 'Gentamicin fails to increase dystrophin expression in dystrophin-deficient muscle', *Muscle and Nerve*, 27(5), pp. 624–627.

Dunckley, M.G., Manoharan, M., Villiet, P., Eperon, I.C. & Dickson, G. (1998) "Modification of splicing in the dystrophin gene in cultured Mdx muscle cells by antisense oligoribonucleotides", *Human molecular genetics,* 7(7), pp. 1083-1090.

Eagle, M., Baudouin, S.V., Chandler, C., Giddings, D.R., Bullock, R. and Bushby, K., 2002. Survival in Duchenne muscular dystrophy: improvements in life expectancy since 1967 and the impact of home nocturnal ventilation. *Neuromuscular disorders*, *12*(10), pp.926-929.

Echigoya, Y., Nakamura, A., Nagata, T., Urasawa, N., Lim, K.R.Q., Trieu, N., Panesar, D., Kuraoka, M., Moulton, H.M., Saito, T., Aoki, Y., Iversen, P., Sazani, P., Kole, R., Maruyama, R., Partridge, T., Takeda, S. & Yokota, T. (2017) "Effects of systemic multiexon skipping with peptide-conjugated morpholinos in the heart of a dog model of Duchenne muscular dystrophy", *Proceedings of the National Academy of Sciences of the United States of America,* 114(16), pp. 4213-4218.

Edward Walford, 'Russell Square and Bedford Square', in *Old and New London: Volume 4* (London, 1878), pp. 564-572. *British History Online* http://www.british-history.ac.uk/old-new-london/vol4/pp564-572 [accessed 5 May 2020].

Elangkovan, N. (2017) Search for novel adeno-associated viruses (AAVs) in human muscle tissue (Unpublished Master's Thesis). Royal Holloway, University of London, United Kingdom.

Emery, A. E. (2002) 'The muscular dystrophies', *The Lancet*, 359(9307), pp. 687–695.

Emery, A.E. and Emery, M.L., 1993. Edward Meryon (1809-1880) and muscular dystrophy. *Journal of medical genetics*, *30*(6), pp.506-511.

Emery, A.E. and Emery, M.L., 2011. *The history of a genetic disease: Duchenne muscular dystrophy or Meryon's disease*. Oxford University Press.

England, S.B., Nicholson, L.V.B., Johnson, M.A., Forrest, S.M., Love, D.R., Zubrzycka-Gaarn, E.E., Bulman, D.E., Harris, J.B. and Davies, K.E., 1990. Very

mild muscular dystrophy associated with the deletion of 46% of dystrophin. *Nature*, *343*(6254), pp.180-182.

Ennen, J. P., Verma, M. and Asakura, A. (2013) 'Vascular-targeted therapies for Duchenne muscular dystrophy', *Skeletal Muscle*, 3(9), pp. 1–12.

Ervasti, J. M. , Ohlendieck, K. , Kahl, S. D. , Gaver, M. G. & Campbell, K. P. (1990) 'Deficiency of a glycoprotein component of the dystrophin complex in dystrophic muscle.', *Nature.* 345, pp. 315–319.

Ervasti, J.M. and Sonnemann, K.J., 2008. Biology of the striated muscle dystrophin–glycoprotein complex. *International review of cytology*, *265*, pp.191-225.

EU Clinical Trial Register (2021) *Clinical trial 2020-002093-27.* Available at: https://www.clinicaltrialsregister.eu/ctr-search/trial/2020-002093-27/FR (Accessed 1 May 2021).

Fabb, S. A., Wells, D. J., Serpente, P. & Dickson, G. (2002) 'Adeno-associated virus vector gene transfer and sarcolemmal expression of a 144 kDa micro-dystrophin effectively restores the dystrophin-associated protein complex and inhibits myofibre degeneration in nude/*mdx* mice.', *Hum. Mol. Genet.* 11(7), pp. 733–741.

Fairclough, R. J., Wood, M. J. and Davies, K. E. (2013) 'Therapy for Duchenne muscular dystrophy: renewed optimism from genetic approaches.', *Nature reviews. Genetics*. Nature Publishing Group, 14(6), pp. 373–8. doi: 10.1038/nrg3460.

Faust, S.M., Bell, P., Cutler, B.J., Ashley, S.N., Zhu, Y., Rabinowitz, J.E. and Wilson, J.M., 2013. CpG-depleted adeno-associated virus vectors evade immune detection. *The Journal of clinical investigation*, *123*(7), pp.2994-3001.

Fisher, R., Tinsley, J. M., Phelps, S. R., Squire, S. E., Townsend, E. R., Martin, J. E. and Davies, K. E. (2001) 'Non-toxic ubiquitous over-expression of utrophin in the mdx mouse', *Neuromuscular Disorders*, 11(8), pp. 713–721.

Flanigan, K.M., Dunn, D.M., Von Niederhausern, A., Soltanzadeh, P., Gappmaier, E., Howard, M.T., Sampson, J.B., Mendell, J.R., Wall, C., King, W.M. and Pestronk, A., 2009. Mutational spectrum of DMD mutations in dystrophinopathy patients: application of modern diagnostic techniques to a large cohort. *Human mutation*, *30*(12), pp.1657-1666.

Flotte, T. R. (2004) 'Gene Therapy Progress and Prospects: Recombinant adeno-associated virus (rAAV) vectors', *Gene Therapy*, 11(10), pp. 805–810.

Flotte, T., Carter, B., Conrad, C., Guggino, W., Reynolds, T., Rosenstein, B., Taylor, G., Walden, S. and Wetzel, R., 1996. A phase i study of an adeno-associated virus-cftr gene vector in adult cf patients with mild lung disease. Johns hopkins children's center, baltimore, maryland. *Human gene therapy*, *7*(9), pp.1145-1159.

Foster, H., Popplewell, L. & Dickson, G. (2012) "Genetic therapeutic approaches for Duchenne muscular dystrophy", *Human Gene Therapy,* 23(7), pp. 676-687.

Foster, H., Sharp, P. S., Athanasopoulos, T., Trollet, C., Graham, I. R., Foster, K., . . . Dickson, G. (2008). Codon and mRNA sequence optimization of microdystrophin transgenes improves expression and physiological outcome in dystrophic mdx mice following AAV2/8 gene transfer. *Molecular Therapy, 16*(11), 1825-1832.

Foy, H.M. and Grayston, J.T., 1976. Adenoviruses. In *Viral infections of humans* (pp. 53-69). Springer, Boston, MA.

François, A., Bouzelha, M., Lecomte, E., Broucque, F., Penaud-Budloo, M., Adjali, O., Moullier, P., Blouin, V. and Ayuso, E., 2018. Accurate Titration of Infectious AAV Particles Requires Measurement of Biologically Active Vector Genomes and Suitable Controls. *Molecular Therapy-Methods & Clinical Development*, *10*, pp.223-236.

Frank, D.E., Schnell, F.J., Akana, C., El-Husayni, S.H., Desjardins, C.A., Morgan, J., Charleston, J.S., Sardone, V., Domingos, J., Dickson, G. and Straub, V., 2020. Increased dystrophin production with golodirsen in patients with Duchenne muscular dystrophy. *Neurology*, *94*(21), pp.e2270-e2282.

Furger, A., O'Sullivan, J. M., Binnie, A., Lee, B. A., & Proudfoot, N. J. (2002). Promoter proximal splice sites enhance transcription. *Genes & Development, 16*(21), 2792-2799.

Gao, G., Vandenberghe, L. H., Alvira, M. R., Lu, Y., Calcedo, R., Zhou, X. and Wilson, J. M. (2004) 'Clades of Adeno-Associated Viruses Are Widely Disseminated in Human Tissues', *Journal of Virology*, 78(12), pp. 6381–6388.

Gao, G., Wilson, J.M. and Alvira, M. (2013) *EP 2341068 B1*. Paris, France: European Patent Office.

Gene Therapy Trials: Pfizer. PPMD 2019 Annual Conference; 28 June 2019; Orlando Florida.

Gene Therapy Trials: Sarepta. . PPMD 2019 Annual Conference; 28 June 2019; Orlando Florida.

Gene Therapy Trials: Solid Biosciences. . PPMD 2019 Annual Conference; 28 June 2019; Orlando Florida.

Gil-Farina, I., Fronza, R., Kaeppel, C., Lopez-Franco, E., Ferreira, V., D'avola, D., Benito, A., Prieto, J., Petry, H., Gonzalez-Aseguinolaza, G. and Schmidt, M.,

2016. Recombinant AAV integration is not associated with hepatic genotoxicity in nonhuman primates and patients. *Molecular Therapy*, *24*(6), pp.1100-1105.

Giraud, C., Winocour, E. and Berns, K. I. (1994) 'Site-specific integration by adeno-associated virus is directed by a cellular DNA sequence.', *Proceedings of the National Academy of Sciences of the United States of America*, 91(21), pp. 10039–10043.

Godfrey, C., Muses, S., McClorey, G., Wells, K.E., Coursindel, T., Terry, R.L., Betts, C., Hammond, S., O'Donovan, L., Hildyard, J. and El Andaloussi, S., 2015. How much dystrophin is enough: the physiological consequences of different levels of dystrophin in the mdx mouse. *Human molecular genetics*, *24*(15), pp.4225-4237.

Gollins, H., McMahon, J., Wells, K. E. and Wells, D. J. (2003) 'High-efficiency plasmid gene transfer into dystrophic muscle.', *Gene therapy*, 10(6), pp. 504–12.
Gowers, W.R., 1879. *Pseudo-hypertrophic muscular paralysis: a clinical lecture*. J. & A. Churchill.

Graham, Ian R., Vanessa J. Hill, Muthiah Manoharan, Gopal B. Inamati, and George Dickson. "Towards a therapeutic inhibition of dystrophin exon 23 splicing in mdx mouse muscle induced by antisense oligoribonucleotides (splicomers): target sequence optimisation using oligonucleotide arrays." *The Journal of Gene Medicine: A cross-disciplinary journal for research on the science of gene transfer and its clinical applications* 6, no. 10 (2004): 1149-1158.

Gray, S.J., Choi, V.W., Asokan, A., Haberman, R.A., McCown, T.J. and Samulski, R.J., 2011. Production of recombinant adeno-associated viral vectors and use in in vitro and in vivo administration. *Current protocols in neuroscience*, *57*(1), pp.4-17.

Grieger, J. C., & Samulski, R. J. (2005). Packaging capacity of adeno-associated virus serotypes: impact of larger genomes on infectivity and postentry steps. *Journal of virology*, *79*(15), 9933-9944.

Grieger, J. C., Choi, V. W., & Samulski, R. J. (2006). Production and characterization of adeno-associated viral vectors. *Nature Protocols, 1(3), 1412–1428.* doi:10.1038/nprot.2006.207

Grieger, J.C., Soltys, S.M. and Samulski, R.J., 2016. Production of recombinant adeno-associated virus vectors using suspension HEK293 cells and continuous harvest of vector from the culture media for GMP FIX and FLT1 clinical vector. *Molecular Therapy*, *24*(2), pp.287-297.

Grum, V. L., Li, D., MacDonald, R. I. & Mondragon, A. (1999) 'Structures of two repeats of spectrin suggest models of flexibility.', *Cell*, 98(4), pp. 523–535.

Guo, T., Jou, W., Chanturiya, T., Portas, J., Gavrilova, O. & McPherron, A.C. (2009) "Myostatin inhibition in muscle, but not adipose tissue, decreases fat mass and improves insulin sensitivity", *PloS one,* 4(3), pp. e4937.

Hakim, C. H., Wasala, N. B., Pan, X., Kodippili, K., Yue, Y., Zhang, K., ... & Schneider, J. S. (2017). A five-repeat micro-dystrophin gene ameliorated dystrophic phenotype in the severe DBA/2J-mdx model of Duchenne muscular dystrophy. *Molecular Therapy-Methods & Clinical Development*, *6*, 216-230.

Harper, S. Q. *et al.* (2002) 'Modular flexibility of dystrophin: implications for gene therapy of Duchenne muscular dystrophy.', *Nature Med.* 8, pp. 253–261.

Hauser, M.A., Robinson, A., Hartigan-O'Connor, D., Williams-Gregory, D., Buskin, J.N., Apone, S., Kirk, C.J., Hardy, S., Hauschka, S.D. and Chamberlain, J.S., 2000. Analysis of muscle creatine kinase regulatory elements in recombinant adenoviral vectors. *Molecular Therapy*, *2*(1), pp.16-25.

Hemmings, L., Kuhlman, P. A. & Critchley, D. R. (1992) 'Analysis of the actin-binding domain of α-actinin by mutagenesis and demonstration that dystrophin contains a functionally homologous domain.', *J. Cell Biol*. 116(6), pp. 1369–1380.

Hermonat, P.L. and Muzyczka, N., 1984. Use of adeno-associated virus as a mammalian DNA cloning vector: transduction of neomycin resistance into mammalian tissue culture cells. *Proceedings of the National Academy of Sciences*, *81*(20), pp.6466-6470.

Heslop, E., Turner, C., Irvin, A., Muntoni, F., Straub, V. and Guglieri, M., 2021. Gene therapy in Duchenne muscular dystrophy: Identifying and preparing for the challenges ahead. *Neuromuscular Disorders*, *31*(1), pp.69-78.

Hetz, C., 2012. The unfolded protein response: controlling cell fate decisions under ER stress and beyond. *Nature reviews Molecular cell biology*, *13*(2), pp.89-102.

Hilhorst, N., Spanoudi-Kitrimi, I., Goemans, N. and Morren, M.A., 2019. Injection site reactions after long-term subcutaneous delivery of drisapersen: a retrospective study. *European journal of pediatrics*, *178*(2), pp.253-258.

Himeda, C.L., Chen, X. and Hauschka, S.D., 2011. Design and testing of regulatory cassettes for optimal activity in skeletal and cardiac muscles. In *Muscle Gene Therapy* (pp. 3-19). Humana Press.

Hinderer, C., Katz, N., Buza, E.L., Dyer, C., Goode, T., Bell, P., Richman, L.K. and Wilson, J.M., 2018. Severe toxicity in nonhuman primates and piglets following high-dose intravenous administration of an adeno-associated virus vector expressing human SMN. *Human gene therapy*, *29*(3), pp.285-298.

Hoffman, E.P. and Kunkel L.M. (1989) 'Dystrophin abnormalities in Duchenne/Becker muscular dystrophy.', *Neuron*, 2, pp. 1019-1029. doi:10.1016/0896-6273(89)90226-2.

Hordeaux, J., Wang, Q., Katz, N., Buza, E.L., Bell, P. and Wilson, J.M., 2018. The neurotropic properties of AAV-PHP. B are limited to C57BL/6J mice. *Molecular Therapy*, *26*(3), pp.664-668.

Howard, M., Frizzell, R.A. and Bedwell, D.M., 1996. Aminoglycoside antibiotics restore CFTR function by overcoming premature stop mutations. *Nature medicine*, *2*(4), pp.467-469.

Hoy, S.M., 2019. Onasemnogene abeparvovec: first global approval. *Drugs*, *79*(11), pp.1255-1262.

Huard, J., Krisky, D., Oligino, T., Marconi, P., Day, C. S., Watkins, S. C. and Glorioso, J. C. (1997) 'Gene transfer to muscle using herpes simplex virus-based vectors', *Neuromuscular Disorders*, 7(5), pp. 299–313.

Ingram, D. (2019) Gene Therapy Trials: Sarepta. PPMD 2019 Annual Conference, 28 June 2019, Orlando Florida (Attended virtually).

Inuzuka, M. and Helinski, D.R., 1978. Replication of antibiotic resistance plasmid R6K DNA in vitro. *Biochemistry*, *17*(13), pp.2567-2573.

Jackson, M.F., Hoversten, K.E., Powers, J.M., Trobridge, G.D. and Rodgers, B.D., 2013. Genetic manipulation of myoblasts and a novel primary myosatellite cell culture system: comparing and optimizing approaches. *The FEBS journal*, *280*(3), pp.827-839.

Jiao, S., Williams, P., Berg, R.K., Hodgeman, B.A., Liu, L., Repetto, G. and Wolff, J.A., 1992. Direct gene transfer into nonhuman primate myofibers in vivo. *Human gene therapy*, *3*(1), pp.21-33.

Jo, B., & Choi, S. S. (2015). Introns: The functional benefits of introns in genomes. *Genomics & Informatics, 13*(4), 112-118.

Johnson, J. S. and Samulski, R. J. (2009) 'Enhancement of adeno-associated virus infection by mobilizing capsids into and out of the nucleolus.', *Journal of virology*, 83(6), pp. 2632–2644.

Kalia, M. and Jameel, S. (2011) 'Virus entry paradigms', *Amino Acids*, 41(5), pp. 1147–1157.

Kamdar, F. and Garry, D.J., 2016. Dystrophin-deficient cardiomyopathy. *Journal of the American College of Cardiology*, *67*(21), pp.2533-2546.

Kang, J.K., Malerba, A., Popplewell, L., Foster, K. & Dickson, G. (2011) "Antisense-induced myostatin exon skipping leads to muscle hypertrophy in mice following octa guanidine morpholino oligomer treatment", *Molecular therapy,* 19(1), pp. 159-164.

Kauss, M. A., Smith, L. J., Zhong, L., Srivastava, A., Wong, K. K. Jr., and Chatterjee, S. (2010) 'Enhanced long-term transduction and multilineage engraftment of human hematopoietic stem cells transduced with tyrosine-modified recombinant adeno-associated virus serotype 2.', *Human Gene Therapy*, 21(9), pp. 1129-1136.

Keeler, A.M. and Flotte, T.R., 2019. Recombinant adeno-associated virus gene therapy in light of Luxturna (and Zolgensma and Glybera): where are we, and how did we get here?. *Annual review of virology*, *6*, pp.601-621.

Keeling, K.M., Xue, X., Gunn, G. and Bedwell, D.M., 2014. Therapeutics based on stop codon readthrough. *Annual review of genomics and human genetics*, *15*, pp.371-394.

Keown A. Third Patient Dies In Audentes' Gene Therapy Study For Neuromuscular Disease | Biospace. 2020; Available at: https://www.biospace.com/article/third-pediatric-patient-dies-in-audentes-gene-therapy-study-for-rare-neuromuscular-disease/. Accessed 13 October, 2020.

Kochanek, S., Clemens, P. R., Mitani, K., Chen, H. H., Chan, S. and Caskey, C. T. (1996) 'A new adenoviral vector: Replacement of all viral coding sequences with 28 kb of DNA independently expressing both full-length dystrophin and beta-galactosidase.', *Proceedings of the National Academy of Sciences of the United States of America*, 93(12), pp. 5731–5736.

Koenig, M. *et al.* (1987) Complete cloning of the Duchenne muscular dystrophy (DMD) cDNA and preliminary genomic organization of the DMD gene in normal and affected individuals. *Cell,* **50**, 509–517.

Koenig, M., Beggs, A.H., Moyer, M., Scherpf, S., Heindrich, K., Bettecken, T., Meng, G., Müller, C.R., Lindlöf, M., Kaariainen, H. and De la Chapelle, A., 1989. The molecular basis for Duchenne versus Becker muscular dystrophy: correlation of severity with type of deletion. *American journal of human genetics*, *45*(4), p.498.

Koenig, M., Monaco, A. P. and Kunkel, L. M. (1988) 'The complete sequence of dystrophin predicts a rod- shaped cytoskeletal protein.', *Cell*, 53, pp. 219–226.

Koo, T., Athanasopoulos, T. and Dickson, G., 2008. Genetic and cell therapies: muscular dystrophy: the route to a cure. *BIOCHEMIST*, *30*(3), p.18.

Koo*, T., Okada, T., Athanasopoulos, T., Foster, H., Takeda, S. & Dickson, G. (2011) "Long-term functional adeno-associated virus-microdystrophin expression in the dystrophic CXMDj dog", *The journal of gene medicine,* 13(9), pp. 497-506.

Koo, T., Malerba, A., Athanasopoulos, T., Trollet, C., Boldrin, L., Ferry, A., Popplewell, L., Foster, H., Foster, K. & Dickson, G. (2011) "Delivery of AAV2/9-microdystrophin genes incorporating helix 1 of the coiled-coil motif in the C-terminal domain of dystrophin improves muscle pathology and restores the level of α1-syntrophin and α-dystrobrevin in skeletal muscles of mdx mice", *Human Gene Therapy*, vol. 22, no. 11, pp. 1379-1388.

Kornegay, J.N., Bogan, D.J., Bogan, J.R., Dow, J.L., Wang, J., Fan, Z., Liu, N., Warsing, L.C., Grange, R.W., Ahn, M. and Balog-Alvarez, C.J., 2016. Dystrophin-deficient dogs with reduced myostatin have unequal muscle growth and greater joint contractures. *Skeletal muscle*, *6*(1), p.14.

Kornegay, J.N., Childers, M.K., Bogan, D.J., Bogan, J.R., Nghiem, P., Wang, J., Fan, Z., Howard, J.F., Schatzberg, S.J., Dow, J.L. and Grange, R.W., 2012. The paradox of muscle hypertrophy in muscular dystrophy. *Physical Medicine and Rehabilitation Clinics*, *23*(1), pp.149-172.

Kornegay, J.N., Li, J., Bogan, J.R., Bogan, D.J., Chen, C., Zheng, H., Wang, B., Qiao, C., Howard, J.F. & Xiao, X. (2010) "Widespread muscle expression of an AAV9 human mini-dystrophin vector after intravenous injection in neonatal dystrophin-deficient dogs", *Molecular Therapy,* 18(8), pp. 1501-1508.

Kotin, R.M., Siniscalco, M., Samulski, R.J., Zhu, X.D., Hunter, L., Laughlin, C.A., McLaughlin, S., Muzyczka, N., Rocchi, M. and Berns, K.I., 1990. Site-specific integration by adeno-associated virus. *Proceedings of the National Academy of Sciences*, *87*(6), pp.2211-2215.

Kotterman, M. A. and Schaffer, D. V (2014) 'Engineering adeno-associated viruses for clinical gene therapy.', *Nature reviews. Genetics*. Nature Publishing Group, 15(7), pp. 445–51. doi: 10.1038/nrg3742.

Krooss, S. A., Dai, Z., Schmidt, F., Rovai, A., Fakhiri, J., Dhingra, A., ... & Srivaratharajan, S. (2020). Ex Vivo/In vivo Gene Editing in Hepatocytes Using "All-in-One" CRISPR-Adeno-Associated Virus Vectors with a Self-Linearizing Repair Template. *iScience*, *23*(1).

Kupatt, C., Windisch, A., Moretti, A., Wolf, E., Wurst, W. and Walter, M.C., 2021. Genome editing for Duchenne muscular dystrophy: a glimpse of the future?. *Gene Therapy*, pp.1-7.

Laforet, G. (2019) Gene Therapy Trials: Solid Biosciences. PPMD 2019 Annual Conference, 28 June 2019, Orlando Florida (Attended virtually).

Larcher, T., Lafoux, A., Tesson, L., Remy, S., Thepenier, V., François, V., Le Guiner, C., Goubin, H., Dutilleul, M., Guigand, L. and Toumaniantz, G., 2014. Characterization of dystrophin deficient rats: a new model for Duchenne muscular dystrophy. *PloS one*, *9*(10).

Le Guiner, C., Montus, M., Servais, L., Cherel, Y., Francois, V., Thibaud, J.L., Wary, C., Matot, B., Larcher, T., Guigand, L. and Dutilleul, M., 2014. Forelimb treatment in a large cohort of dystrophic dogs supports delivery of a recombinant AAV for exon skipping in Duchenne patients. *Molecular Therapy*, *22*(11), pp.1923-1935.

Le Guiner, C., Servais, L., Montus, M., Larcher, T., Fraysse, B., Moullec, S., ... & Koo, T. (2017). Long-term microdystrophin gene therapy is effective in a canine model of Duchenne muscular dystrophy. *Nature Communications*, *8*, 16105.

Le Hir, H., Izaurralde, E., Maquat, L.E. and Moore, M.J., 2000. The spliceosome deposits multiple proteins 20–24 nucleotides upstream of mRNA exon–exon junctions. *The EMBO journal*, *19*(24), pp.6860-6869.

Le, B.T., Adams, A.M., Fletcher, S., Wilton, S.D. and Veedu, R.N., 2017. Rational design of short locked nucleic acid-modified 2′-O-methyl antisense oligonucleotides for efficient exon-skipping in vitro. *Molecular Therapy-Nucleic Acids*, *9*, pp.155-161.

Levitt, N., Briggs, D., Gil, A. and Proudfoot, N.J., 1989. Definition of an efficient synthetic poly (A) site. *Genes & Development*, *3*(7), pp.1019-1025.

Levy, H. C., Bowman, V. D., Govindasamy, L., McKenna, R., Nash, K., Warrington, K., Chen, W., Muzyczka, N., Yan, X., Baker, T. S. and Agbandje-McKenna, M. (2009) 'Heparin binding induces conformational changes in Adeno-associated virus serotype 2', *Journal of Structural Biology*. Elsevier Inc., 165(3), pp. 146–156.

Li, X., Eastman, E. M., Schwartz, R. J., & Draghia-Akli, R. (1999). Synthetic muscle promoters: Activities exceeding naturally occurring regulatory sequences. *Nature Biotechnology, 17*(3), 241.

Li, Z.B., Kollias, H.D. & Wagner, K.R. (2008) "Myostatin directly regulates skeletal muscle fibrosis", *The Journal of biological chemistry,* 283(28), pp. 19371-19378.

Lim, K.R.Q., Yoon, C. and Yokota, T., 2018. Applications of CRISPR/Cas9 for the treatment of Duchenne muscular dystrophy. *Journal of personalized medicine*, *8*(4), p.38.

Lionarons, J.M., Hoogland, G., Hendriksen, R.G., Faber, C.G., Hellebrekers, D.M., Van Koeveringe, G.A., Schipper, S. and Vles, J.S., 2019. Dystrophin is

expressed in smooth muscle and afferent nerve fibers in the rat urinary bladder. *Muscle & nerve*, *60*(2), pp.202-210.

Liu, L., Parekh-Olmedo, H. and Kmiec, E. B. (2003) 'The development and regulation of gene repair.', *Nature reviews. Genetics*, 4(9), pp. 679–89.

Lo Cascio, C.M., Goetze, O., Latshang, T.D., Bluemel, S., Frauenfelder, T. and Bloch, K.E., 2016. Gastrointestinal dysfunction in patients with Duchenne muscular dystrophy. *PLoS One*, *11*(10), p.e0163779.

Long, C., Amoasii, L., Mireault, A.A., McAnally, J.R., Li, H., Sanchez-Ortiz, E., Bhattacharyya, S., Shelton, J.M., Bassel-Duby, R. and Olson, E.N., 2016. Postnatal genome editing partially restores dystrophin expression in a mouse model of muscular dystrophy. *Science*, *351*(6271), pp.400-403.

Long, C., McAnally, J.R., Shelton, J.M., Mireault, A.A., Bassel-Duby, R. and Olson, E.N., 2014. Prevention of muscular dystrophy in mice by CRISPR/Cas9–mediated editing of germline DNA. *Science*, *345*(6201), pp.1184-1188.

Loperfido, M., Jarmin, S., Dastidar, S., Di Matteo, M., Perini, I., Moore, M., Nair, N., Samara-Kuko, E., Athanasopoulos, T., Tedesco, F.S. and Dickson, G., 2016. piggyBac transposons expressing full-length human dystrophin enable genetic correction of dystrophic mesoangioblasts. *Nucleic acids research*, *44*(2), pp.744-760.

Lu-Nguyen, N., Malerba, A., Popplewell, L., Schnell, F., Hanson, G. & Dickson, G. (2017) "Systemic Antisense Therapeutics for Dystrophin and Myostatin Exon Splice Modulation Improve Muscle Pathology of Adult mdx Mice", *Molecular Therapy-Nucleic Acids,* 6, pp. 15-28.

Lu, J., Williams, J.A., Luke, J., Zhang, F., Chu, K. and Kay, M.A., (2017). A 5′ noncoding exon containing engineered intron enhances transgene expression from recombinant AAV vectors in vivo. *Human Gene Therapy*, *28*(1), pp.125-134.

Lu, J., Zhang, F., & Kay, M. A. (2013). A mini-intronic plasmid (MIP): A novel robust transgene expression vector in vivo and in vitro. *Molecular Therapy, 21*(5), 954-963.

Lu, Q. L., Liang, H.-D., Partridge, T. and Blomley, M. J. K. (2003) 'Microbubble ultrasound improves the efficiency of gene transduction in skeletal muscle in vivo with reduced tissue damage.', *Gene therapy*, 10(5), pp. 396–405.

Lu, Q.L., Cirak, S. and Partridge, T., 2014. What can we learn from clinical trials of exon skipping for DMD?. *Molecular Therapy-Nucleic Acids*, *3*.

Luke, J., Carnes, A. E., Hodgson, C. P., & Williams, J. A. (2009). Improved antibiotic-free DNA vaccine vectors utilizing a novel RNA based plasmid selection system. *Vaccine, 27*(46), 6454-6459.

Lynch, S.R. and Puglisi, J.D., 2001. Structural origins of aminoglycoside specificity for prokaryotic ribosomes. *Journal of molecular biology*, *306*(5), pp.1037-1058.

Mack, D.L., Poulard, K., Goddard, M.A., Latournerie, V., Snyder, J.M., Grange, R.W., Elverman, M.R., Denard, J., Veron, P. & Buscara, L. (2017) "Systemic AAV8-mediated gene therapy drives whole-body correction of myotubular myopathy in dogs", *Molecular Therapy,* 25(4), pp. 839-854.

Madeira, F., Park, Y.M., Lee, J., Buso, N., Gur, T., Madhusoodanan, N., Basutkar, P., Tivey, A.R., Potter, S.C., Finn, R.D. and Lopez, R., 2019. The

EMBL-EBI search and sequence analysis tools APIs in 2019. *Nucleic acids research*, *47*(W1), pp.W636-W641.

Mann, C.J., Anguela, X.M., Montane, J., Obach, M., Roca, C., Ruzo, A., Otaegui, P., Mir, L.M. and Bosch, F., 2012. Molecular signature of the immune and tissue response to non-coding plasmid DNA in skeletal muscle after electrotransfer. *Gene therapy*, *19*(12), pp.1177-1186.

Martino, A.T., Suzuki, M., Markusic, D.M., Zolotukhin, I., Ryals, R.C., Moghimi, B., Ertl, H.C., Muruve, D.A., Lee, B. and Herzog, R.W., 2011. The genome of self-complementary adeno-associated viral vectors increases Toll-like receptor 9–dependent innate immune responses in the liver. *Blood, The Journal of the American Society of Hematology*, *117*(24), pp.6459-6468.

Masri F, Cheeseman E, Ansorge S., 2019. Viral vector manufacturing: how to address current and future demands? Cell Gene Ther. Ins. 5(S5), 949–70.

Massopust, R.T., il Lee, Y., Pritchard, A.L., Nguyen, V.K.M., McCreedy, D.A. and Thompson, W.J., 2020. Lifetime analysis of mdx skeletal muscle reveals a progressive pathology that leads to myofiber loss. *Scientific Reports*, *10*(1), pp.1-16.

Matsuo, M. et al. (1991) 'Exon skipping during splicing of dystrophin mRNA precursor due to an intraexon deletion in the dystrophin gene of Duchenne muscular dystrophy kobe.', *J. Clin. Invest*. 87(6), pp. 2127–2131.

Matthews, E., Brassington, R., Kuntzer, T., Jichi, F. and Manzur, A.Y., 2016. Corticosteroids for the treatment of Duchenne muscular dystrophy. *Cochrane Database of Systematic Reviews*, (5).

McDonald, C.M., Campbell, C., Torricelli, R.E., Finkel, R.S., Flanigan, K.M., Goemans, N., Heydemann, P., Kaminska, A., Kirschner, J., Muntoni, F. and

Osorio, A.N., 2017. Ataluren in patients with nonsense mutation Duchenne muscular dystrophy (ACT DMD): a multicentre, randomised, double-blind, placebo-controlled, phase 3 trial. *The Lancet*, *390*(10101), pp.1489-1498.

McGreevy, J.W., Hakim, C.H., McIntosh, M.A. & Duan, D. (2015) "Animal models of Duchenne muscular dystrophy: from basic mechanisms to gene therapy", *Disease models & mechanisms,* 8(3), pp. 195-213.

McLenachan, S., Sarsero, J.P. and Ioannou, P.A., 2007. Flow-cytometric analysis of mouse embryonic stem cell lipofection using small and large DNA constructs. *Genomics*, *89*(6), pp.708-720.

McMahon, J.M., Signori, E., Wells, K.E., Fazio, V.M. and Wells, D.J., 2001. Optimisation of electrotransfer of plasmid into skeletal muscle by pretreatment with hyaluronidase–increased expression with reduced muscle damage. *Gene therapy*, *8*(16), pp.1264-1270.

Mendell JR, Al-Zaidy S, Shell R et al. (2017) Single-dose gene-replacement therapy for spinal muscular atrophy. *N Engl J Med*; 377:1713-1722.

Mendell, J. R., Campbell, K., Rodino-Klapac, L., Sahenk, Z., Shilling, C., Lewis, S., Bowles, D., Gray, S., Li, C., Galloway, G., Malik, V., Coley, B., Clark, K. R., Li, J., Xiao, X., Samulski, J., McPhee, S. W., Samulski, R. J. and Walker, C. M. (2010) 'Dystrophin Immunity in Duchenne's Muscular Dystrophy', *New England Journal of Medicine*, 363(15), pp. 1429–1437.

Mendell, J.R., Sahenk, Z., Lehman, K., Nease, C., Lowes, L.P., Miller, N.F., Iammarino, M.A., Alfano, L.N., Nicholl, A., Al-Zaidy, S. and Lewis, S., 2020. Assessment of systemic delivery of rAAVrh74. MHCK7. micro-dystrophin in children with Duchenne muscular dystrophy: a nonrandomized controlled trial. *JAMA neurology*, *77*(9), pp.1122-1131.

Mercuri, E. and Muntoni, F. (2013) 'Muscular dystrophies', *The Lancet*. Elsevier Ltd, 381(9869), pp. 845–860.

Meyers, T.A. and Townsend, D., 2019. Cardiac Pathophysiology and the Future of Cardiac Therapies in Duchenne Muscular Dystrophy. *International journal of molecular sciences*, *20*(17), p.4098.

Mingozzi, F. and High, K. A. (2011) 'Therapeutic in vivo gene transfer for genetic disease using AAV: progress and challenges', *Nature reviews.Genetics*, 12(5), pp. 341–355.

Mingozzi, F. and High, K. A. (2013) 'Immune responses to AAV vectors: Overcoming barriers to successful gene therapy', *Blood*, 122(1), pp. 23–36.

Mingozzi, F., & High, K. A. (2017). Overcoming the host immune response to adeno-associated virus gene delivery vectors: The race between clearance, tolerance, neutralization, and escape. *Annual Review of Virology,* 4, 511-534.

Mingozzi, F., Meulenberg, J. J., Hui, D. J., Basner-tschakarjan, E., Nicole, C., Edmonson, S. a, Hutnick, N. a, Betts, M. R., Kastelein, J. J., Erik, S., High, K. a, Hasbrouck, N. C. and Stroes, E. S. (2009) 'AAV-1mediated gene transfer to skeletal muscle in humans results in dose-dependent activation of capsid-specific T cells AAV-1 – mediated gene transfer to skeletal muscle in humans results in dose-dependent activation of capsid-specific T cells', *Blood*, 114(10), pp. 2077–2086.

Miraldi Utz, V., Coussa, R.G., Antaki, F. and Traboulsi, E.I., 2018. Gene therapy for RPE65-related retinal disease. *Ophthalmic genetics*, *39*(6), pp.671-677.

Mokri, B. & Engel, A. G. (1975) 'Duchenne dystrophy: electron microscopic findings pointing to a basic or early abnormality in the plasma membrane of the muscle fiber.', *Neurology*, 25, pp. 1111–1120.

Mokri, B. and Engel, A.G., 1998. Duchenne dystrophy: electron microscopic findings pointing to a basic or early abnormality in the plasma membrane of the muscle fiber. *Neurology*, *51*(1), pp.1-1.

Moore, M. (2018) *Genome Editing using Custom Endonucleases and Dystrophin cDNA Insertions Targeting Intron 1 of the Duchenne Muscular Dystrophy Gene*. PhD thesis. Royal Holloway, University of London. Available at: https://pure.royalholloway.ac.uk/portal/en/publications/genome-editing-using-custom-endonucleases-and-dystrophin-cdna-insertions-targeting-intron-1-of-the-duchenne-muscular-dystrophy-gene(6ded2453-f603-4f21-a337-8ca33940c82c).html (Accessed: 13 January 2021).

Moore, M., Vallese, D., Dickson, G. & Popplewell, L. (2015) "Exciting developments in CRISPR/Cas9-mediated genome engineering approaches for Duchenne Muscular Dystrophy", *Cell & Gene Therapy Insights*, 1(2), pp. 215-230.

Moorwood, C., Liu, M., Tian, Z. and Barton, E.R., 2013. Isometric and eccentric force generation assessment of skeletal muscles isolated from murine models of muscular dystrophies. *JoVE (Journal of Visualized Experiments)*, (71), p.e50036.

Morgan, J. E., Beauchamp, J. R., Pagel, C. N., Peckham, M., Ataliotis, P., Jat, P. S., . . . Partridge, T. A. (1994). Myogenic cell lines derived from transgenic mice carrying a thermolabile T antigen: A model system for the derivation of tissue-specific and mutation-specific cell lines. *Developmental Biology, 162*(2), 486-498.

Mueller, C., Chulay, J.D., Trapnell, B.C., Humphries, M., Carey, B., Sandhaus, R.A., McElvaney, N.G., Messina, L., Tang, Q., Rouhani, F.N. and Campbell-Thompson, M., 2013. Human Treg responses allow sustained recombinant adeno-associated virus–mediated transgene expression. *The Journal of clinical investigation*, *123*(12), pp.5310-5318.

Mullard A. Sarepta's DMD gene therapy falls flat. Nature reviews Drug discovery 2021;20(91).

Murach, K.A., Dungan, C.M., Peterson, C.A. and McCarthy, J.J., 2019. Muscle fiber splitting is a physiological response to extreme loading in animals. *Exercise and sport sciences reviews*, *47*(2), pp.108-115.

Murakami, T., Nishi, T., Kimura, E., Goto, T., Maeda, Y., Ushio, Y., Uchino, M. and Sunada, Y. (2003) 'Full-length dystrophin cDNA transfer into skeletal muscle of adult mdx mice by electroporation', *Muscle and Nerve*, 27(2), pp. 237–241.

Murray, E.L. and Schoenberg, D.R., 2007. A+ U-rich instability elements differentially activate 5′-3′ and 3′-5′ mRNA decay. *Molecular and cellular biology*, *27*(8), pp.2791-2799.

Nam, H.-J., Gurda, B. L., McKenna, R., Potter, M., Byrne, B., Salganik, M., Muzyczka, N. and Agbandje-McKenna, M. (2011) 'Structural Studies of Adeno-Associated Virus Serotype 8 Capsid Transitions Associated with Endosomal Trafficking', *Journal of Virology*, 85(22526), pp. 11791–1179944.

Nathwani, A.C., Reiss, U.M., Tuddenham, E.G., Rosales, C., Chowdary, P., McIntosh, J., Della Peruta, M., Lheriteau, E., Patel, N., Raj, D. and Riddell, A., 2014. Long-term safety and efficacy of factor IX gene therapy in hemophilia B. *New England Journal of Medicine*, *371*(21), pp.1994-2004.

Nature Technology (2013) *NTC7482 and NTC7485 Expression Vectors Instruction Manual*. [ONLINE] Available at: http://www.natx.com/assets/ntc7482-and-ntc7485-user-manual-3-0.pdf. [Accessed 27 March 2018].

NCT04240314. AAV9 U7snRNA Gene Therapy to Treat Boys With DMD Exon 2 Duplications. 2020; Available at: https://clinicaltrials.gov/ct2/show/NCT04240314. Accessed 20/03/2021.

Nelson, C.E., Hakim, C.H., Ousterout, D.G., Thakore, P.I., Moreb, E.A., Rivera, R.M.C., Madhavan, S., Pan, X., Ran, F.A., Yan, W.X. and Asokan, A., 2016. In vivo genome editing improves muscle function in a mouse model of Duchenne muscular dystrophy. *Science*, *351*(6271), pp.403-407.

Newlands, S., Levitt, L.K., Robinson, C.S., Karpf, A.C., Hodgson, V.R., Wade, R.P. and Hardeman, E.C., 1998. Transcription occurs in pulses in muscle fibers. *Genes & development*, *12*(17), pp.2748-2758.

Nicholson, L. V. (1993) 'The "rescue" of dystrophin synthesis in boys with Duchenne muscular dystrophy.', *Neuromuscul. Disord.* 3(5-6), pp. 525–531.

Nonnenmacher, M. and Weber, T. (2011) 'Adeno-associated virus 2 infection requires endocytosis through the CLIC/GEEC pathway', *Cell Host and Microbe*. Elsevier Inc., 10(6), pp. 563–576.

Nonnenmacher, M. and Weber, T. (2012) 'Intracellular transport of recombinant adeno-associated virus vectors', *Gene Therapy*. Nature Publishing Group, 19(6), pp. 649–658.

Nott, A., Le Hir, H. and Moore, M.J., 2004. Splicing enhances translation in mammalian cells: an additional function of the exon junction complex. *Genes & development*, *18*(2), pp.210-222.

Nott, A., Meislin, S.H. and Moore, M.J., 2003. A quantitative analysis of intron effects on mammalian gene expression. *Rna*, *9*(5), pp.607-617.

One Shot™ TOP10 Chemically Competent E. coli. 2020. *Thermofisher Scientific, 2020*. [online] Available at: <https://www.thermofisher.com/order/catalog/product/C404010#/C404010> [Accessed 3 December 2020].

Orefice, N.S., 2020. Development of new strategies using extracellular vesicles loaded with exogenous nucleic acid. *Pharmaceutics*, *12*(8), p.705.

Ostedgaard, L.S., Rokhlina, T., Karp, P.H., Lashmit, P., Afione, S., Schmidt, M., Zabner, J., Stinski, M.F., Chiorini, J.A. and Welsh, M.J., 2005. A shortened adeno-associated virus expression cassette for CFTR gene transfer to cystic fibrosis airway epithelia. *Proceedings of the National Academy of Sciences*, *102*(8), pp.2952-2957.

Ouisse, L.H., Remy, S., Lafoux, A., Larcher, T., Tesson, L., Chenouard, V., Guillonneau, C., Brusselle, L., Vimond, N., Rouger, K. and Péréon, Y., 2019. Immunophenotyping of a rat model of Duchenne's disease and demonstration of improved muscle strength after anti-CD45RC antibody treatment. *Frontiers in immunology*, *10*, p.2131.

Parent Project Muscular Dystrophy (2017) *Understanding Currently Recruiting Gene Therapy Studies*. [ONLINE] Available at: http://community.parentprojectmd.org/profiles/blogs/understanding-currently-recruiting-gene-therapy-studies. [Accessed 20 March 2018].

Pasquale, G. D. and Stacey, S. N. (1998) 'Adeno-Associated Virus Rep78 Protein Interacts with Protein Kinase A and Its Homolog PRKX and Inhibits CREB-Dependent Transcriptional Adeno-Associated Virus Rep78 Protein Interacts with Protein Kinase A and Its Homolog PRKX and Inhibits CREB- Dependent Tr', 72(10), pp. 7916–7925.

Pasternak, C., Wong, S. & Elson, E. L. (1995) 'Mechanical function of dystrophin in muscle cells.', *J. Cell Biol.* 128(3), pp. 355–361.

Pearce, M., Blake, D. J., Tinsley, J. M., Byth, B. C., Campbell, L., Monaco, A. P. and Davies, K. E. (1993) 'The utrophin and dystrophin genes share similarities in genomic structure', *Human Molecular Genetics*, 2(11), pp. 1765–1772.

Penaud-budloo, M., François, A., Clément, N. & Ayuso, E. (2018) Pharmacology of Recombinant Adeno-associated Virus Production. *Mol. Ther. Methods Clin. Dev.* **8,** 166–180.

Pereira, D. J., McCarty, D. M. and Muzyczka, N. (1997) 'The adeno-associated virus (AAV) Rep protein acts as both a repressor and an activator to regulate AAV transcription during a productive infection', *J Virol*, 71(2), pp. 1079–1088.

Petrof, B. J., Shrager, J. B., Stedman, H. H., Kelly, A. M. & Sweeney, H. L. (1993) 'Dystrophin protects the sarcolemma from stresses developed during muscle contraction.', *Proc. Natl Acad. Sci. USA.* 90(8), pp. 3710–3714.

Petrof, B.J., Shrager, J.B., Stedman, H.H., Kelly, A.M. and Sweeney, H.L., 1993. Dystrophin protects the sarcolemma from stresses developed during muscle contraction. *Proceedings of the National Academy of Sciences*, *90*(8), pp.3710-3714.

Pfizer (2018) A Study to Evaluate the Safety and Tolerability of PF-06939926 Gene Therapy in Duchenne Muscular Dystrophy. Retrieved from https://clinicaltrials.gov/ct2/show/record/NCT03362502 (ClinicalTrials.gov Identifier: NCT03362502).

Poongavanam, V., Madala, P.K., Højland, T. and Veedu, R.N., 2014. Computational investigation of locked nucleic acid (LNA) nucleotides in the

active sites of DNA polymerases by molecular docking simulations. *Plos one*, *9*(7), p.e102126.

Popplewell, L., Koo, T., Leclerc, X., Duclert, A., Mamchaoui, K., Gouble, A., Mouly, V., Voit, T., Pâques, F. & Cédrone, F. (2013) "Gene correction of a duchenne muscular dystrophy mutation by meganuclease-enhanced exon knock-in", *Human Gene Therapy,* 24(7), pp. 692-701.

Popplewell, L.J., Adkin, C., Arechavala-Gomeza, V., et al. (2010). Comparative analysis of antisense oligonucleotide sequences targeting exon 53 of the human DMD gene: Implications for future clinical trials. *Neuromuscul. Disord*. 20 (2), pp. 102–110.

Powell, S.K., Rivera-Soto, R. and Gray, S.J., 2015. Viral expression cassette elements to enhance transgene target specificity and expression in gene therapy. *Discovery medicine*, *19*(102), p.49.

Pozzoli, U., Sironi, M., Cagliani, R., Comi, G. P., Bardoni, A. and Bresolin, N. (2002) 'Comparative analysis of the human dystrophin and utrophin gene structures', *Genetics*, 160(2), pp. 793–798.

Prakash, V., Moore, M. & Yáñez-Muñoz, R.J. (2016) "Current progress in therapeutic gene editing for monogenic diseases", *Molecular Therapy,* 24(3), pp. 465-474.

Pramono, Z. A. et al. (1996) 'Induction of exon skipping of the dystrophin transcript in lymphoblastoid cells by transfecting an antisense oligodeoxynucleotide complementary to an exon recognition sequence.', *Biochem. Biophys. Res. Commun.* 226(2), pp. 445–449.

Prea, S. M., Chan, E. C., Dusting, G. J., Vingrys, A. J., Bui, B. V. and Liu, G. S. (2015) 'Gene therapy with endogenous inhibitors of angiogenesis for neovascular

age-related macular degeneration: Beyond anti-VEGF therapy', *Journal of Ophthalmology*. Hindawi Publishing Corporation, 2015. doi: 10.1155/2015/201726.

Provost-Craig, Rose and Hall. (2013) *Introduction to Anatomy and Physiology*. Goodheart Willcox Company.

QIAGEN[1] (2020) Removal Of Bacterial Endotoxins, Available at: https://www.qiagen.com/gb/service-and-support/learning-hub/technologies-and-research-topics/plasmid-resource-center/removal-of-bacterial-endotoxins/ (Accessed: 13 Jan 2021).

QIAGEN[2] (2020) EndoFree Plasmid Kits, Available at: https://www.qiagen.com/gb/products/discovery-and-translational-research/dna-rna-purification/dna-purification/plasmid-dna/endofree-plasmid-kits/?clear=true#orderinginformation (Accessed: 13 Jan 2021).

Rafael, J. A. *et al*. (1996) 'Forced expression of dystrophin deletion constructs reveals structure–function correlations.', *J. Cell Biol.* 134(1), pp. 93–102.

Rakowski, S.A. and Filutowicz, M., 2013. Plasmid R6K replication control. *Plasmid*, *69*(3), pp.231-242.

Ramos, J.N., Hollinger, K., Bengtsson, N.E., Allen, J.M., Hauschka, S.D. and Chamberlain, J.S., 2019. Development of novel micro-dystrophins with enhanced functionality. *Molecular Therapy*, *27*(3), pp.623-635.

Ramos, J.N., Hollinger, K., Bengtsson, N.E., Allen, J.M., Hauschka, S.D. and Chamberlain, J.S., 2019. Development of novel micro-dystrophins with enhanced functionality. *Molecular Therapy*, *27*(3), pp.623-635.

Rando, T. A. (2001) 'The dystrophin–glycoprotein complex, cellular signaling, and the regulation of cell survival in the muscular dystrophies.', *Muscle Nerve.* 24(12), pp. 1575–1594.

Rasowo, B., Shilpita, S., Ermira, S., Chuah, M. and Driessche, T.V., 2014. Development of novel muscle-specific adeno-associated viral vector constructs for gene therapy of Duchenne muscular dystrophy. *European Scientific Journal*, *10*(18).

Recht, M.I., Douthwaite, S. and Puglisi, J.D., 1999. Basis for prokaryotic specificity of action of aminoglycoside antibiotics. *The EMBO journal*, *18*(11), pp.3133-3138.

Riu, E., Grimm, D., Huang, Z., & Kay, M. A. (2005). Increased maintenance and persistence of transgenes by excision of expression cassettes from plasmid sequences in vivo. *Human Gene Therapy, 16*(5), 558-570.

Robinson-Hamm, J.N. and Gersbach, C.A., 2016. Gene therapies that restore dystrophin expression for the treatment of Duchenne muscular dystrophy. *Human genetics*, *135*(9), pp.1029-1040.

Rogers, G.L., Martino, A.T., Aslanidi, G.V., Jayandharan, G.R., Srivastava, A. and Herzog, R.W., 2011. Innate immune responses to AAV vectors. *Frontiers in microbiology*, *2*, p.194.

Romero, N.B., Braun, S., Benveniste, O., Leturcq, F., Hogrel, J.Y., Morris, G.E., Barois, A., Eymard, B., Payan, C., Ortega, V. and Boch, A.L., 2004. Phase I study of dystrophin plasmid-based gene therapy in Duchenne/Becker muscular dystrophy. *Human gene therapy*, *15*(11), pp.1065-1076.

Rosenberg, A.S., Puig, M., Nagaraju, K., Hoffman, E.P., Villalta, S.A., Rao, V.A., Wakefield, L.M. and Woodcock, J., 2015. Immune-mediated pathology in

Duchenne muscular dystrophy. *Science translational medicine*, *7*(299), pp.299rv4-299rv4.

Russell, D. W. & Grompe, M. (2015) Adeno-associated virus finds its disease. *Nat. Genet.* 47(10), pp.1104–1105.

Rybakova, I. N. & Ervasti, J. M. (1997) 'Dystrophin– glycoprotein complex is monomeric and stabilizes actin filaments in vitro through a lateral association.', *J. Biol. Chem*. 272(45), pp. 28771–28778.

Salvetti, A., Orève, S., Chadeuf, G., Favre, D., Cherel, Y., Champion-Arnaud, P., David-Ameline, J. and Moullier, P., 1998. Factors influencing recombinant adeno-associated virus production. *Human gene therapy*, *9*(5), pp.695-706.

Samulski, R. J., Salganik, M. and Hirsch, M. L. (2015) 'Adeno-associated Virus as a Mammalian DNA Vector', *Mobile DNA III*, 2(2), pp. 829–851. doi: 10.1128/microbiolspec.MDNA3-0052-2014.

Samulski, R.J., Chang, L.S. and Shenk, T., 1989. Helper-free stocks of recombinant adeno-associated viruses: normal integration does not require viral gene expression. *Journal of virology*, *63*(9), pp.3822-3828.

Sanlioglu, A. D., Karacay, B., Benson, P. K., Engelhardt, J. F. and Sanlioglu, S. (2004) 'Novel approaches to augment adeno-associated virus type-2 endocytosis and transduction', *Virus Research*, 104(1), pp. 51–59.

Sanlioglu, S., Benson, P. K., Yang, J., Atkinson, E. M., Reynolds, T. and Engelhardt, J. F. (2000) 'Endocytosis and nuclear trafficking of adeno-associated virus type 2 are controlled by rac1 and phosphatidylinositol-3 kinase activation.', *Journal of Virology*, 74(19), pp. 9184–96.

Sarcar, S., Tulalamba, W., Rincon, M.Y., Tipanee, J., Pham, H.Q., Evens, H., Boon, D., Samara-Kuko, E., Keyaerts, M., Loperfido, M. and Berardi, E., 2019. Next-generation muscle-directed gene therapy by in silico vector design. *Nature communications*, *10*(1), pp.1-16.

Sarepta Therapeutics I. A Randomized, Double-blind, Placebo-controlled Study of SRP-9001 for Duchenne Muscular Dystrophy (DMD). 2018; Available at: https://clinicaltrials.gov/ct2/show/NCT03769116.

Sarepta Therapeutics I. Systemic Gene Delivery Clinical Trial for Duchenne Muscular Dystrophy. 2017; Available at: https://clinicaltrials.gov/ct2/show/NCT03375164.

Schakowski, F., Gorschlueter, M., Buttgereit, P., Maerten, A., Lilienfeld-Toal, M. V., Junghans, C., . . . Strehl, J. (2007). Minimal size MIDGE vectors improve transgene expression in vivo. *In Vivo, 21*(1), 17-23.

Schek, N., Cooke, C. and Alwine, J.C., 1992. Definition of the upstream efficiency element of the simian virus 40 late polyadenylation signal by using in vitro analyses. *Molecular and Cellular Biology*, *12*(12), pp.5386-5393.

Schek, N., Cooke, C. and Alwine, J.C., 1992. Definition of the upstream efficiency element of the simian virus 40 late polyadenylation signal by using in vitro analyses. *Molecular and Cellular Biology*, *12*(12), pp.5386-5393.

Schwartz, L.M., 2019. Skeletal muscles do not undergo apoptosis during either atrophy or programmed cell death-revisiting the myonuclear domain hypothesis. *Frontiers in physiology*, *9*, p.1887.

Sherratt, T. G., Vulliamy, T., Dubowitz, V., Sewry, C. A. & Strong, P. N. (1993) 'Exon skipping and translation in patients with frameshift deletions in the dystrophin gene.', *Am J. Hum. Genet.* 53(5), pp. 1007–1015.

Shirley, M., 2021. Casimersen: First Approval. *Drugs*, pp.1-5.

SignaGen Laboratories. (2017) *Introduction to AAV*. [Online] Available from: http://signagen.com/Introduction-to-AAV [Accessed 26 June 2017].

Sipo, I., Fechner, H., Pinkert, S., Suckau, L., Wang, X., Weger, S. and Poller, W. (2007) 'Differential internalization and nuclear uncoating of self-complementary adeno-associated virus pseudotype vectors as determinants of cardiac cell transduction.', *Gene therapy*, 14(18), pp. 1319–1329.

Skuk, D., Goulet, M., Roy, B., Chapdelaine, P., Bouchard, J.P., Roy, R., Dugré, F.J., Sylvain, M., Lachance, J.G., Deschênes, L. and Senay, H., 2006. Dystrophin expression in muscles of duchenne muscular dystrophy patients after high-density injections of normal myogenic cells. *Journal of Neuropathology & Experimental Neurology*, *65*(4), pp.371-386.

Skuk, D., Roy, B., Goulet, M., Chapdelaine, P., Bouchard, J.P., Roy, R., Dugré, F.J., Lachance, J.G., Deschênes, L., Senay, H. and Sylvain, M., 2004. Dystrophin expression in myofibers of Duchenne muscular dystrophy patients following intramuscular injections of normal myogenic cells. *Molecular Therapy*, *9*(3), pp.475-482.

Smith, L. J., Ul-Hasan, T., Carvaines, S. K., Van Vliet, K., Yang, E., Wong, K. K., Agbandje-McKenna, M. and Chatterjee, S. (2014) 'Gene Transfer Properties and Structural Modeling of Human Stem Cell-Derived AAV', *Molecular Therapy*, 22(9), pp. 1625–1634.

Smith, R. H. (2008) 'Adeno-associated virus integration: virus versus vector.', *Gene therapy*, 15(11), pp. 817–822.

Sokołowska, E. and Błachnio-Zabielska, A.U., 2019. A Critical Review of Electroporation as A Plasmid Delivery System in Mouse Skeletal Muscle. *International journal of molecular sciences*, *20*(11), p.2776.

Solid Biosciences (2017) Microdystrophin Gene Transfer Study in Adolescents and Children With DMD (IGNITE DMD). Retrieved from https://clinicaltrials.gov/ct2/show/record/NCT03368742 (ClinicalTrials.gov Identifier: NCT03368742).

Song, L., Li, X., Jayandharan, G. R., Wang, Y., Aslanidi, G. V., Ling, C., Zhong, L., Gao, G., Yoder, M. C., Ling, C., Tan, M. and Srivastava, A. (2013) 'High-Efficiency Transduction of Primary Human Hematopoietic Stem Cells and Erythroid Lineage-Restricted Expression by Optimized AAV6 Serotype Vectors In Vitro and in a Murine Xenograft Model In Vivo', *PLoS ONE*, 8(3), pp. 1–12.

Sonntag, F., Bleker, S., Leuchs, B., Fischer, R. and Kleinschmidt, J. A. (2006) 'Adeno-associated virus type 2 capsids with externalized VP1/VP2 trafficking domains are generated prior to passage through the cytoplasm and are maintained until uncoating occurs in the nucleus.', *Journal of virology*, 80(22), pp. 11040–54.

Sonntag, F., Schmidt, K. and Kleinschmidt, J. A. (2010) 'A viral assembly factor promotes AAV2 capsid formation in the nucleolus.', *Proceedings of the National Academy of Sciences of the United States of America*, 107(22), pp. 10220–10225. doi: 10.1073/pnas.1001673107.

Strassburger, E., 1893. Ûber die Wirkungssphäre der kerne und die zellgrösse. *Histol Beitr*, *5*, pp.97-124.

Tabebordbar, M., Zhu, K., Cheng, J.K., Chew, W.L., Widrick, J.J., Yan, W.X., Maesner, C., Wu, E.Y., Xiao, R., Ran, F.A. and Cong, L., 2016. In vivo gene

editing in dystrophic mouse muscle and muscle stem cells. *Science*, *351*(6271), pp.407-411.

Tanaka, K., Watakabe, A. & Shimura, Y. (1994) 'Polypurine sequences within a downstream exon function as a splicing enhancer.', *Mol. Cell Biol.* 14(2), pp. 1347–1354.

Tarantal, A. F., Lee, C. C. I., Martinez, M. L., Asokan, A. & Samulski, R. J. (2017) Systemic and persistent muscle gene expression in rhesus monkeys with a liver de-targeted adeno-associated virus vector. *Human Gene Therapy*, 28(5), pp. 385-391.

Taylor-Weiner, H., Grigsby, C.L., Ferreira, D.M., Dias, J.M., Stevens, M.M., Ruas, J.L. and Teixeira, A.I., 2020. Modeling the transport of nuclear proteins along single skeletal muscle cells. *Proceedings of the National Academy of Sciences*, *117*(6), pp.2978-2986.

Taylor, N. P., 2020. *Astellas' Audentes reports 3rd death in gene therapy trial.* Available from: https://www.fiercebiotech.com/biotech/astellas-audentes-reports-third-death-gene-therapy-trial (Accessed 1 May 2021).

Terry, R. L., & Wells, D. J. (2016). *Histopathological Evaluation of Skeletal Muscle with Specific Reference to Mouse Models of Muscular Dystrophy. Current Protocols in Mouse Biology, 343–363.* doi:10.1002/cpmo.19

Thermo Fisher Scientific[1]. (2014) *TOPO™ TA Cloning™ Kit for Sequencing, with pCR™4-TOPO™ Vector, One Shot™ TOP10 Chemically Competent E. coli, and PureLink™ Quick Plasmid Miniprep Kit.* [Online]. Available from: https://www.thermofisher.com/order/catalog/product/K457502 [Accessed 30 June 2017].

Thermo Fisher Scientific[2]. (2014) *TOPO® TA Cloning® Kit for Sequencing User Guide.* [Online]. Available from: https://tools.thermofisher.com/content/sfs/manuals/topotaseq_man.pdf [Accessed 30 June 2017].

Tinsley, J. *et al.* (1998) 'Expression of full-length utrophin prevents muscular dystrophy in *mdx* mice.', *Nature Med.* 4, pp. 1441–1444. doi:10.1038/4033.

Tinsley, J. M., Blake, D. J., Roche, A., Fairbrother, U., Riss, J., Byth, B. C., Knight, A. E., Kendrick-Jones, J., Suthers, G. K. and Love, D. R. (1992) 'Primary structure of dystrophin-related protein.', *Nature*, 360(6404), pp. 591–593.

Tinsley, J. M., Potter, a C., Phelps, S. R., Fisher, R., Trickett, J. I. and Davies, K. E. (1996) 'Amelioration of the dystrophic phenotype of mdx mice using a truncated utrophin transgene.', *Nature*, 384(6607), pp. 349–353.

Tornabene P, Trapani I. (2020) Can Adeno-Associated Viral Vectors Deliver Effectively Large Genes?. Human Gene Therapy. Jan 9.

Uematsu, S. and Akira, S., 2007. Toll-like receptors and Type I interferons. *Journal of Biological Chemistry*, *282*(21), pp.15319-15323.

US National Library of Medicine. ClinicalTrials.gov https://www.clinicaltrials.gov/ct2/show/NCT02196467 (2020).

Valencia, P., Dias, A. P., & Reed, R. (2008). Splicing promotes rapid and efficient mRNA export in mammalian cells. *Proceedings of the National Academy of Sciences, 105*(9), 3386-3391.

van der Bent, M.L., da Silva Filho, O.P., van Luijk, J., Brock, R. and Wansink, D.G., 2018. Assisted delivery of antisense therapeutics in animal models of

heritable neurodegenerative and neuromuscular disorders: a systematic review and meta-analysis. *Scientific reports*, *8*(1), pp.1-12.

van Deutekom, J. C. T. and van Ommen, G.-J. B. (2003) 'Advances in Duchenne muscular dystrophy gene therapy.', *Nature reviews. Genetics*, 4(10), pp. 774–783.

Vandewalle, J., Luypaert, A., De Bosscher, K. and Libert, C., 2018. Therapeutic mechanisms of glucocorticoids. *Trends in Endocrinology & Metabolism*, *29*(1), pp.42-54.

Verdera, H.C., Kuranda, K. and Mingozzi, F., 2020. AAV vector immunogenicity in humans, a long journey to successful gene transfer. *Molecular Therapy*.

Verhaart, I.E. and Aartsma-Rus, A., 2019. Therapeutic developments for Duchenne muscular dystrophy. *Nature Reviews Neurology*, *15*(7), pp.373-386.

Wagner, K.R., 2020. The elusive promise of myostatin inhibition for muscular dystrophy. *Current opinion in neurology*, *33*(5), pp.621-628.

Waldrop, Megan, Michael Lawlor, Tatyana Meyers Vetter, Emma Frair, Margaret Beatka, Hui Meng, Megan Iammarino et al. "LATE BREAKING NEWS ORAL PRESENTATION: LBO 3 Expression of apparent full-length dystrophin in skeletal muscle in a first-in-human gene therapy trial using the scAAV9. U7-ACCA vector." *Neuromuscular Disorders* 30 (2020): S166-S167.

Wang, B., Li, J. & Xiao, X. (2000) 'Adeno-associated virus vector carrying human minidystrophin genes effectively ameliorates muscular dystrophy in *mdx* mouse model.', *Proc. Natl Acad. Sci. USA.* 97(25), pp. 13714–13719.

Wang, D., Tai, P.W. and Gao, G., 2019. Adeno-associated virus vector as a platform for gene therapy delivery. *Nature Reviews Drug Discovery*, *18*(5), pp.358-378.

Wang, Z., Tapscott, S. J., Chamberlain, J. S. and Storb, R. (2011) 'Immunity and AAV-mediated gene therapy for muscular dystrophies in large animal models and human trials', *Frontiers in Microbiology*, 2(SEP), pp. 1–6. doi: 10.3389/fmicb.2011.00201.

Wang, Z., Zhu, T., Qiao, C., Zhou, L., Wang, B., Zhang, J., Chen, C., Li, J. and Xiao, X., 2005. Adeno-associated virus serotype 8 efficiently delivers genes to muscle and heart. *Nature biotechnology*, *23*(3), pp.321-328.

Warner, L. E. *et al*. (2002) 'Expression of *Dp260* in muscle tethers the actin cytoskeleton to the dystrophin–glycoprotein complex and partially prevents dystrophy.', *Hum. Mol. Genet.* 11(9), pp. 1095–1105.

Watanabe, N., Nagata, T., Satou, Y., Masuda, S., Saito, T., Kitagawa, H., Komaki, H., Takagaki, K. and Takeda, S.I., 2018. NS-065/NCNP-01: an antisense oligonucleotide for potential treatment of exon 53 skipping in Duchenne muscular dystrophy. *Molecular Therapy-Nucleic Acids*, *13*, pp.442-449.

Watt, D.J., Lambert, K., Morgan, J.E., Partridge, T.A. and Sloper, J.C., 1982. Incorporation of donor muscle precursor cells into an area of muscle regeneration in the host mouse. *Journal of the neurological sciences*, *57*(2-3), pp.319-331.

Weinmann, J., Weis, S., Sippel, J., Tulalamba, W., Remes, A., El Andari, J., Herrmann, A.K., Pham, Q.H., Borowski, C., Hille, S. and Schönberger, T., 2020. Identification of a myotropic AAV by massively parallel in vivo evaluation of barcoded capsid variants. *Nature communications*, *11*(1), pp.1-12.

Welch, E.M., Barton, E.R., Zhuo, J., Tomizawa, Y., Friesen, W.J., Trifillis, P., Paushkin, S., Patel, M., Trotta, C.R., Hwang, S. and Wilde, R.G., 2007. PTC124 targets genetic disorders caused by nonsense mutations. *Nature*, *447*(7140), pp.87-91.

Whitehead, N.P., Yeung, E.W. and Allen, D.G., 2005. Muscle damage in mdx (dystrophic) mice: The role of calcium and reactive oxygen species. In *Proceedings of the Australian Physiological Society* (Vol. 36, pp. 111-117).

Wilmott, P., Lisowski, L., Alexander, I.E. and Logan, G.J., 2019. A User's Guide to the Inverted Terminal Repeats of Adeno-Associated Virus. *Human Gene Therapy Methods*, *30*(6), pp.206-213.

Wistuba, A., Kern, A., Weger, S., Grimm, D. and Kleinschmidt, J. A. (1997) 'Subcellular compartmentalization of adeno-associated virus type 2 assembly.', *Journal of Virology*, 71(2), pp. 1341–52.

Wolff, J.A., Malone, R.W., Williams, P., Chong, W., Acsadi, G., Jani, A. and Felgner, P.L., 1990. Direct gene transfer into mouse muscle in vivo. *Science*, *247*(4949), pp.1465-1468.

Wright, J.F., 2020. Codon Modification and PAMPs in Clinical AAV Vectors: The Tortoise or the Hare?. *Molecular Therapy*, *28*(3), pp.701-703.

Wu Z, Yang H, Colosi P. Effect of genome size on AAV vector packaging. Molecular Therapy. 2010 Jan 1;18(1):80-6.

Wu, X. *et al.* (2017) IAPP modulates cellular autophagy , apoptosis , and extracellular matrix metabolism in human intervertebral disc cells. *Cell Death Discovery*. 3(16107), pp.1–12.

Wu, Z., Asokan, A. and Samulski, R. J. (2006) 'Adeno-associated Virus Serotypes: Vector Toolkit for Human Gene Therapy', *Molecular Therapy*, 14(3), pp. 316–327. doi: 10.1016/j.ymthe.2006.05.009.

Wu, Z., Sun, J., Zhang, T., Yin, C., Yin, F., Van Dyke, T., Samulski, R.J. and Monahan, P.E., 2008. Optimization of self-complementary AAV vectors for liver-

directed expression results in sustained correction of hemophilia B at low vector dose. *Molecular Therapy*, *16*(2), pp.280-289.

Wu, Z., Yang, H. & Colosi, P. (2010) "Effect of genome size on AAV vector packaging", *Molecular Therapy*, vol. 18, no. 1, pp. 80-86.

Xie, Q., Bu, W., Bhatia, S., Hare, J., Somasundaram, T., Azzi, A. and Chapman, M. S. (2002) 'The atomic structure of adeno-associated virus (AAV-2), a vector for human gene therapy.', *Proceedings of the National Academy of Sciences of the United States of America*, 99(16), pp. 10405–10410.

Yan Z, Sun X, Feng Z, Li G, Fisher JT, Stewart ZA, Engelhardt JF. Optimization of recombinant adeno-associated virus-mediated expression for large transgenes, using a synthetic promoter and tandem array enhancers. Human gene therapy. 2015 Jun 1;26(6):334-46.

Ylä-Herttuala, S., 2012. Endgame: glybera finally recommended for approval as the first gene therapy drug in the European union. *Molecular Therapy*, *20*(10), pp.1831-1832.

Yoshida, M. & Ozawa, E. (1990) 'Glycoprotein complex anchoring dystrophin to sarcolemma.', *J. Biochem. (Tokyo)* 108(5), pp. 748–752.

Yoshioka, M.I.E.K.O., Okuno, T.A.K.E.H.I.K.O., Honda, Y.O.S.H.I.H.I.T.O. and Nakano, Y.O.S.H.I.H.I.S.A., 1980. Central nervous system involvement in progressive muscular dystrophy. *Archives of disease in childhood*, *55*(8), pp.589-594.

Yuasa, K. *et al.* (1998) 'Effective restoration of dystrophin-associated proteins *in vivo* by adenovirus-mediated transfer of truncated dystrophin cDNAs.', *FEBS Lett.* 425(2), pp. 329–336.

Yucel, N., Chang, A.C., Day, J.W., Rosenthal, N. and Blau, H.M., 2018. Humanizing the mdx mouse model of DMD: the long and the short of it. *NPJ Regenerative medicine*, *3*(1), pp.1-11.

Yue, Y. *et al.* (2015) Safe and bodywide muscle transduction in young adult Duchenne muscular dystrophy dogs with adeno-associated virus. *Human Molecular Genetics.* 24(20), pp.5880–5890.

Yue, Y., Ghosh, A., Long, C., Bostick, B., Smith, B.F., Kornegay, J.N. and Duan, D., 2008. A single intravenous injection of adeno-associated virus serotype-9 leads to whole body skeletal muscle transduction in dogs. *Molecular Therapy*, *16*(12), pp.1944-1952.

Zhang, G., Ludtke, J.J., Thioudellet, C., Kleinpeter, P., Antoniou, M., Herweijer, H., Braun, S. and Wolff, J.A., 2004. Intraarterial delivery of naked plasmid DNA expressing full-length mouse dystrophin in the mdx mouse model of duchenne muscular dystrophy. *Human gene therapy*, *15*(8), pp.770-782.

Zhao, J., Yue, Y., Patel, A., Wasala, L., Karp, J.F., Zhang, K., Duan, D. and Lai, Y., 2020. High-Resolution Histological Landscape of AAV DNA Distribution in Cellular Compartments and Tissues following Local and Systemic Injection. *Molecular Therapy-Methods & Clinical Development*, *18*, pp.856-868.

Zincarelli, C., Soltys, S., Rengo, G. and Rabinowitz, J.E. (2008) 'Analysis of AAV serotypes 1-9 mediated gene expression and tropism in mice after systemic injection.', *Mol Ther*, 16(6), pp. 1073–1080.

Zinn, E. and Vandenberghe, L. H. (2014) 'Adeno-associated virus: Fit to serve', *Current Opinion in Virology*. Elsevier B.V., 8, pp. 90–97. doi: 10.1016/j.coviro.2014.07.008.

Zinn, E. *et al.* (2015) In silico reconstruction of the viral evolutionary lineage yields a potent gene therapy vector. *Cell Rep.* 12, pp. 1056–1068.

Zolotukhin, S., Byrne, B.J., Mason, E., Zolotukhin, I., Potter, M., Chesnut, K., Summerford, C., Samulski, R.J. and Muzyczka, N., 1999. Recombinant adeno-associated virus purification using novel methods improves infectious titer and yield. *Gene therapy*, *6*(6), pp.973-985.